EXPERIMENTAL COMPARISON OF HEAT PIPES AND THERMOSYPHONS CONTAINING METHANOL AND ACETONE

by

Jana Strain E.I.T.
B.Eng., University of Victoria, 2015

A Thesis Submitted in Partial Fulfillment of the
Requirements for the Degree of

MASTER OF APPLIED SCIENCE

In the Department of Mechanical Engineering

EXPERIMENTAL COMPARISON OF HEAT PIPES AND THERMOSYPHONS CONTAINING METHANOL AND ACETONE

by

Jana Strain E.I.T.
B.Eng., University of Victoria, 2015

Supervisory Committee

Dr. Andrew Rowe	Department of Mechanical Engineering
Supervisor	
Dr. Peter Wild	Department of Mechanical Engineering
Departmental Member	
Dr. Phalguni Mukhopadhyaya	Department of Civil Engineering
Outside Member	

Abstract

The *cold chain* industry has a need for a standalone, electricity independent cooling unit that is used for both storage of warehouse product and on deliveries [1]. Mixed temperature fresh and frozen food deliveries are problematic without the distributor having specialized duel compartment refrigerated trucks [2]. These trucks permanently reduce the available capacity for payload delivery [2]. It would be valuable to the *cold chain* industry to have a passive, independent, storage unit that can be moved using a forklift and placed anywhere within a reefer or warehouse [1]. This versatile unit is a simple mechanical system, but presents a complicated thermal problem. One of the design challenges is to thermally isolate the load from the environment and to maintain thermal conditions for a specified length of time.

A proposed storage system uses heat pipes to connect the cargo compartment to a heat sink containing solid CO_2. Heat pipes are a simple, passive, and quiet way to transfer heat. Heat pipe design and theory is an active area of research with numerous papers in the literature; however, there is less reported about the actual process of manufacturing. This thesis investigates a new potential application of heat pipes, with a focus on the manufacturing process and experimental performance.

A total of four heat pipes and two thermosyphons are created using acetone and methanol as the working fluids, and copper and aluminum as the heat pipe housing. Performance is compared to an insulated copper tube with the same outer dimensions, where the primary performance metric is steady-state thermal resistance. In addition, transient performance is quantified as well as the temperature distribution along the outer in the evaporator, adiabatic and condenser regions.

Results show that the prototypes made out of copper reached steady-state faster than the aluminum pipes, while also having a smaller temperature differential between the evaporator and condenser. Methanol and acetone have similar performance over the temperature ranges of 198 K to 358 K. The best performing prototype is a copper thermosyphon containing methanol which achieves an effective thermal resistance of 2.0 K/W with an applied load of 40.7 W, when the condenser is cooled with dry ice in acetone. When cooled with ice water the copper thermosyphon achieves an effective thermal resistance of 0.5 K/W with a load of 40.7 W.

Table of Contents

List of Figures

List of Tables

List of Acronyms and Symbols

Symbol	Meaning	Units
α	Coefficient of thermal expansion	[1/K]
α	Contact angle of surface tension	[rad]
δ_g	Geometric parameter: 1 for a cylinder & 2 for a sphere	[X]
ε	Wick porosity	[X]
π	Constant of ratio of a circle's circumference to its diameter 3.14159	[X]
γ	Ratio of specific heats	[X]
λ	Latent heat of Vaporization	[J/kg]
ν	Poisson's ratio	[X]
μ	Absolute viscosity	[Ns/m^2]
ρ	Density	[kg/m^3]
Ψ	Angle heat pipe makes to horizontal	[deg]
σ	Surface tension	[N/m]
θ	Contact angle between working fluid and wick structure	[rad]
A	Area	[m^2]
A_w	Cross sectional area of the wick	[m^2]
B_v	Kraus and Bar-Cohen constant depending on passage shape and Reynolds #	[X]

Symbol	Meaning	Units
C_v	Constant dependent on the Mach number	[X]
D	Diameter	[m]
d_p	Outer diameter of the heat pipe	[m]
d_{pi}	Inner diameter of the heat pipe	[m]
d_v	Diameter of the vapor column	[m]
d_w	Screen wire diameter	[m]
E	Modulus of elasticity	[Pa]
g	Gravitational constant 9.81	[m/s^2]
h	Convection coefficient	[W/m^2 K]
h_{lv}	Latent heat of vaporization	[J/kg]
k_{eff}	Effective conductivity of the saturated wick	[W/m K]
k_l	Thermal conductivity of the working fluid in liquid phase	[W/m K]
k_s	Thermal conductivity of the shell material	[W/m K]
k_w	Thermal conductivity of the wick material	[W/m K]
K	Wick Permeability	[m^2]
l_a	Length of the adiabatic section	[m]
l_c	Length of the condenser	[m]
l_e	Length of the evaporator	[m]

Symbol	Meaning	Units
l_{eff}	Effective length of the heat pipe	[m]
l_i	Length of the interference fit	[m]
l_p	Length of the heat pipe	[m]
N	Mesh number	[1/m]
N_{wrap}	The number of wraps of a mesh screen wick structure	[x]
Δp	Pressure change from capillary, vapor, liquid, phase change and gravity	[Pa]
p_c	Maximum capillary pressure	[Pa]
p_{sat}	Saturated pressure	[Pa]
p_v	Vapor pressure	[Pa]
Q	Heat	[W]
Q_b	Heat transfer boiling limit	[W]
Q_c	Heat transfer capillary limit	[W]
Q_e	Heat transfer entrainment limit	[W]
Q_s	Heat transfer sonic limit	[W]
r_c	Capillary pumping radius	[m]
r_{hw}	Hydraulic radius	[m]
r_m	Mean wall radius	[m]

Symbol	Meaning	Units
r_n	Nucleation radius approximated at 2.54×10^{-7}	[m]
r_p	Outer radius of the pipe	[m]
r_{pi}	Inner radius of the pipe	[m]
R_1	Thermal resistance of the path where axial conduction is nil	[K/W]
R_2	Thermal resistance of the path for axial conduction	[K/W]
R_{HP}	Total thermal resistance of the heat pipe	[K/W]
R_i	Thermal resistance of the liquid vapor interface	[K/W]
R_s	Thermal resistance of the shell material at various locations within the pipe	[K/W]
R_v	Gas constant of the working vapor	[J/kg K]
R_v	Thermal resistance of the vapor	[K/W]
R_w	Thermal resistance of the wick at various locations within the pipe	[K/W]
s_h	Hoop stress	[Pa]
s_{th}	Thermal stress	[Pa]
S	Crimping factor	[X]
t_p	Thickness of the heat pipe shell	[m]
t_w	Thickness of the wick	[m]
t_{wall}	Wall thickness of pipe	[m]

Symbol	Meaning	Units
ΔT	Change is temperature	[K]
T_c	Temperature of the exterior heat pipe shell in the middle of the condenser	[K]
T_e	Temperature of the exterior heat pipe shell in the middle of the evaporator	[K]
T_v	Temperature of the vapor	[K]
V_f	Fill Volume ratio of working fluid	[%]
V_r	Actual volume of working fluid	[l]
V_t	Total internal volume of the cylinder	[l]

Acknowledgements

I thank Andrew Rowe for giving me the opportunity to study under his supervision as a graduate student. He introduced me to the concept of heat pipes and presented me the opportunity to work on this interesting project. This opportunity allowed me to expand my knowledge and experimental experience.

I thank Peter Evans for presenting Andrew with an interesting problem to solve and for helping to fund this research, along with the Mitacs Accelerate program. Peter, I admire your drive and persistence.

I thank Rodney Katz for his continuing mentorship and support. He inspired me to pursue design engineering, both personally and professionally.

I thank Dr. Paulo Trevizoli for his help in getting me over the finish line. He provided guidance and support with my experimental work, took photos for my experimental procedure, and created the figures of my experimental results.

I thank Dr. Armando Tura for encouraging me to pursue graduate school, and giving me guidance around the lab. I thank Theo Christiaanse for his kind words and helping me with LabVIEW. I thank my colleagues from the Cryofuels lab group and IESVic for sharing knowledge and giving advice in times of need.

I thank Pauline Shepherd and Sue Walton for their friendly smiles, eagerness to help and all of the administrative support their provided during my research.

I thank my family for believing in me and giving me support, love, and encouragement.

I thank my husband, Jerrett Strain, for understanding and supporting me on my academic journey. It has been a long road. I wouldn't be here today, if it wasn't for our incredible relationship and your ability to keep me engaged and challenged.

Chapter 1 Introduction

1.1 Background

ColdStar Solutions and CryoLogistics Refrigeration Technologies (CRT) approached the University of Victoria (UVic) with an idea that could benefit the *cold chain* industry but required further research and development. ColdStar Solutions is a warehousing and distribution company who deliver perishable food across British Columbia. CRT is working to develop solutions to problems with transportation refrigeration systems, and owns two patents on cooling refrigerated cargo containers using solid CO_2 snow [3], [4]. Cooling using CO_2 is beneficial because of the ability to achieve and maintain low temperatures even in warm climates, with low noise, while being less environmentally harmful than traditional mechanical refrigeration systems using hydrofluorocarbon (HFC) refrigerants[1]. In addition, the United States Environmental Protection Agency is implementing the phase-out of HFCs thereby forcing the *cold chain* industry to find and adopt new, greener, alternatives [5].

A refrigerated container that can hold a pallet of frozen product would be useful for both shipping and storage of perishable products [1]. Currently the food distribution industry must either have expensive reefers with multiple refrigerated compartments that can be set to different temperatures, or place all items at a single temperature and hope the frozen product does not melt and spoil before delivery [2].

The use of solid CO_2 for passive cooling in mobile systems has been proposed in various forms. Prior art in this field cools with sublimated CO_2 vapor in the cargo space, or uses electricity to power fans for temperature control. Flooding a compartment with CO_2 gas can present problems where human entry to the space is expected. An overview of relevant prior art is presented.

[1] In the cold-chain industry, a conventional refrigerated transport trailer is known as a *reefer*.

1.2 Prior Art

In 1990 and 1995, Thomsen patented designs for rail and truck shipping containers that use solid CO_2 as a refrigerant [3], [4]. The container is separated into an upper CO_2 storage bunker and a lower refrigerated space, displayed in Figure 1. The upper bunker is charged with CO_2 "snow" (solid CO_2 formed by flashing liquid CO_2 into the compartment), which is then used to cool the load. The CO_2 sublimes into vapor and flows downwards into the cargo hold where it cools the space and cargo without the use of electricity.

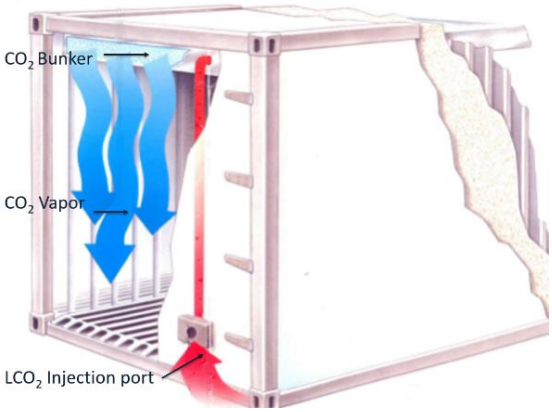

FIGURE 1: THOMSEN SHIPPING CONTAINER WITH A CO_2 BUNNKER [3].

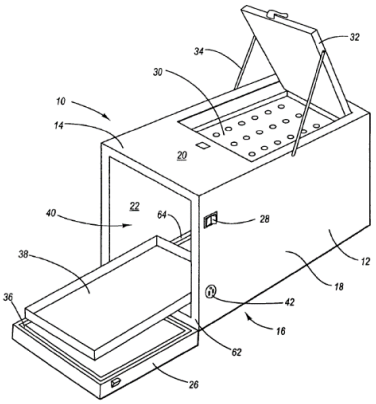

FIGURE 2: A SHIPPING CONTAINER INVENTED BY ARAGON [6].

In 2005 Aragon invented a self-contained, cryogenic shipping and storage container shown in Figure 2 [6]. The container has an upper bunker to hold solid CO_2, a slide out tray in the refrigerated section and does not require electricity. Cooling happens via sublimation and the vapor enters the cargo space. The container has desirable features such as recessed exterior features and a forklift compatible base. Optionally an electrical heat trace around the door can be included, to melt frost before opening the door at the cargo destination.

In 2012, Aragon improved his previous invention by designing a compartmentalized container with a control system that allows for each section to stay within user defined programmable limits, displayed in Figure 3 [7]. The control system is coupled to a fan which enhances heat transfer through forced convection when the system moves outside thermal tolerance. The container is powered using battery packs or by being plugged into a vehicle's 12-volt power supply.

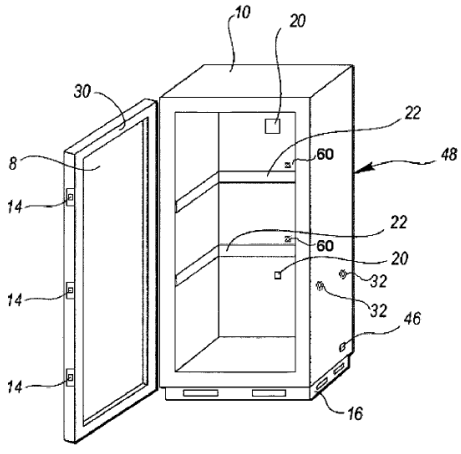

FIGURE 3: A THERMALLY CONTROLLED SHIPPING CONTAINER BY ARAGON [7].

Refrigerated pallet-sized containers were proposed using conventional vapor compression cycles in 2004 and 2012. In 2004 Broussard invented a temperature controlled shipping container that was large enough inside to contain an entire pallet, displayed in Figure 4 [8]. The container has both a cooling and heating unit that is in communication with the cargo space. A traditional vapor compression unit provides refrigeration and the temperature regulation unit includes a fan. The unit must be powered by an external source.

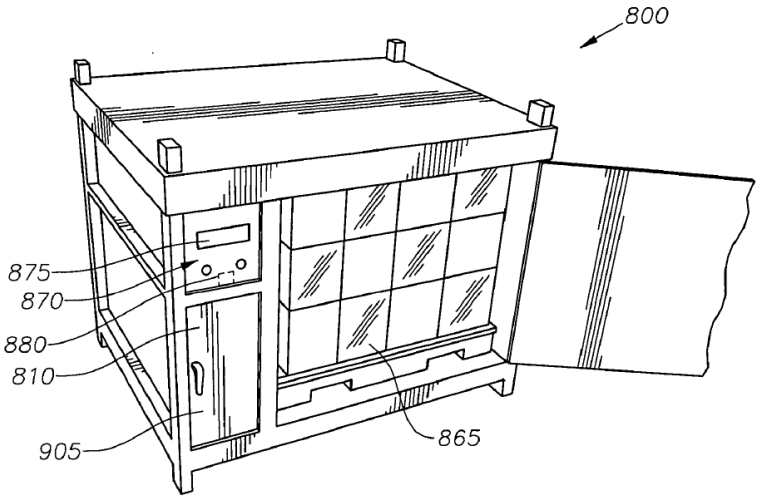

FIGURE 4: BROUSSARD'S PALLET-SIZED, TEMPERATURE CONTROLLED SHIPPING CONTAINER [8].

A 2012 invention by Harman and Taylor also allow for a pallet-sized shipment but with a focus on providing a container for lightweight aircraft shipping, displayed in Figure 5 [9].The cargo box adjoins to a hollow base with forklift tunnels. Located on the side of the container is a temperature control unit. The cargo container has both an electrical heater and vapor compression refrigeration. Onboard batteries provide power during shipping.

The five inventions listed do not keep CO_2 vapor out of the cargo area and many also require external power to function. The Thomsen patents can be improved on by separating vapor from the load and by limiting the thermal connection so that load temperature is controlled. The proposed solution uses heat pipes.

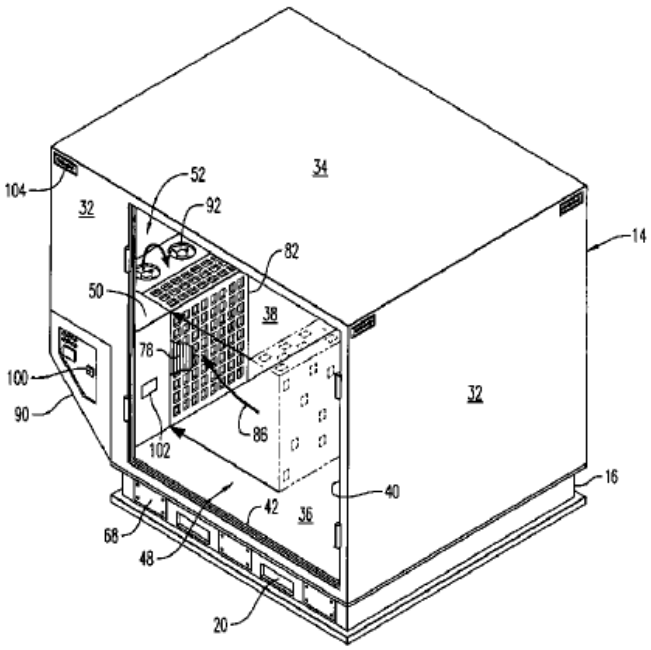

FIGURE 5: A PALLET SIZED SHIPPING CONTAINER BUILT FOR AIRCRAFTS [9].

1.3 OBJECTIVES

The first step towards building a passive refrigerated container is to make the thermal connection between the heat sink and the cargo. What type of heat pipe should be used since no commercially available heat pipes are sold specifically for this purpose? What type of working fluid should be used? What temperature range will the heat pipes operate in? How can the heat pipes be manufactured? What is the heat transport capacity? These questions have motivated the research contained in this thesis.

The objective of this thesis is to design, manufacture, and test the performance of heat pipes operating with solid CO_2 as the condenser thermal reservoir. This objective is reached using the following tasks:

1. Develop a passive heat transfer system with no requirement for forced convection.
2. Implement an analytic framework of screen wick heat pipes.
3. To theoretically determine the heat transfer limits.
4. Develop a novel way to fabricate heat pipes.
5. Fabricate various heat pipes that may satisfy the parameters and operating conditions.
6. Design and develop a testing apparatus to determine effective resistance.
7. Experimentally determine the thermal resistance, steady state evaporator temperature and transient thermal behavior of the manufactured heat pipes; and
8. Make a recommendation as to the best type of heat pipe to use for the specific application set out by my motivation.

1.4 SUMMARY

The thesis motivation and objectives were presented. The ultimate research goal of developing a technology allowing the *cold chain* industry to deliver and store cargo at various temperatures is approached by first analyzing the thermal connection between the cargo and heat sink. Eight specific objectives were identified to guide the research contained in this thesis.

The following chapters contain details about heat pipe theory and performance. A description of the iterative manufacturing process used to make prototype heat pipes is presented. Details about the creation of an evacuation and filling rig are given, as well as details about the system limits and losses encountered with the filling rig. An experimental testing apparatus is designed and built to thermally isolate the heat pipes from the surrounding environment. In the closing chapters, the experimental results are presented, analyzed and discussed.

Chapter 2 Heat Pipe Theory

In this chapter heat pipe theory and the associated physics are introduced. The heat transfer performance limits are discussed and the governing mathematical equations are presented.

Heat pipes are sealed, passive, two-phase heat transfer devices that absorb heat on one end of the pipe (the evaporator) and reject heat at the other (the condenser.) They come in a multitude of shapes and sizes and are commonly used in electronics for cooling [10], heat transfer for pipeline permafrost stability [11], and space applications [12]. Inside the heat pipe is a working fluid that exists in both liquid and vapor phases when in operation. In the evaporator heat is absorbed and the liquid vaporizes, at the other end of the pipe the vapor condenses as heat is rejected. Working fluid types include helium and nitrogen, for cryogenic temperatures, ammonia, water, acetone, and methanol for room temperatures, and liquid metal sodium and potassium for high temperature applications[2].

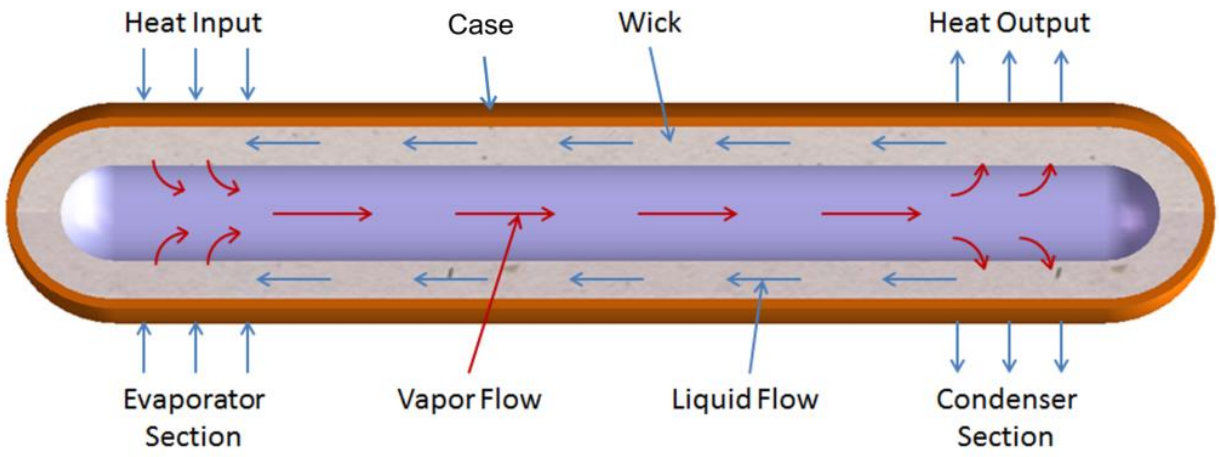

FIGURE 6: SCHEMATIC OF A HORIZONTIALLY ORIENTED HEAT PIPE ABSORBING HEAT IN THE EVAPORATOR AND REJECTING HEAT IN THE CONDENSER. VAPOR FLOWS THROUGH THE CENTER AND LIQUID FLOWS THROUGH THE WICK STRUCTURE [13].

Figure 6 displays the inner workings of a conventional cylindrical heat pipe with an external case (also referred to as a shell), an internal wick structure that lines the inner diameter of case, and a working fluid that exists in both vapor and liquid phases. Vapor flows from the

[2] Various working fluid types and their operational temperature ranges can be found in Appendix A.

evaporator to the condenser through the central void space. Liquid flows from the condenser to the evaporator through the wick structure.

A heat pipe without a wick is called a *thermosyphon*. Without a wick, gravity is the primary driver of liquid flow; thus, thermosyphons are usually limited to the orientation where the condenser is positioned above the evaporator as shown in Figure 7. Usually, thermosyphons contain a larger amount of working fluid compared to a heat pipe of similar proportions. The maximum heat transfer rates are shown experimentally to increase with the amount of working fluid up to a certain value [14].

Gravity moves condensate back to the evaporator where liquid pools on the bottom [15]. This dependence on gravity for liquid return to the evaporator is the single defining characteristic differentiating a thermosyphon from a heat pipe [15]. Heat, then, is absorbed in the evaporator where the liquid pool exists [14]. Vapor then rises through the adiabatic section and gives up its latent heat in the condenser section, before condensing into liquid and traveling down the walls of the thermosyphon.

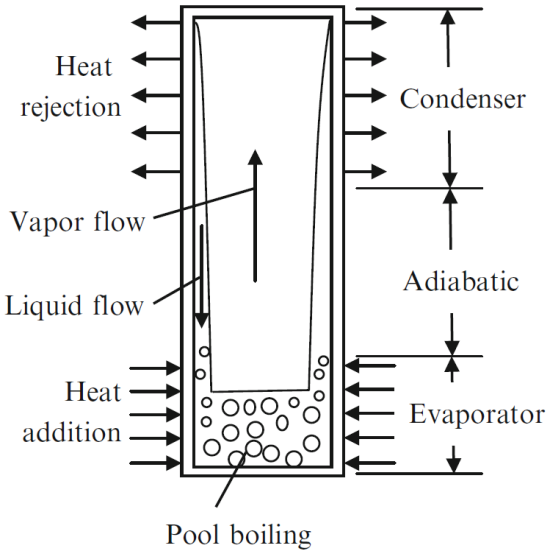

FIGURE 7: A THERMOSYPHON SCHEMATIC SHOWING A VERITICAL ORIENTATION, A WICKLESS STRUCTURE, AND A LIQUID POOL IN THE EVAPORATOR [17].

Due to two phase heat transfer, heat pipes do not have a set thermal conductivity like solid materials. Their effective thermal conductivity will change with total length, the amount of power being transferred, and with the sizes of the evaporator and condenser [11]. Comparing a heat pipe to a similar sized copper rod, the effective thermal conductivity of the heat pipe can be 10 to 10^4 times larger [16].

Figure 8 displays the temperature difference of a solid aluminum rod, a solid copper rod, and a copper and water heat pipe, that are 0.5 m long, 1.27 cm in diameter, and moving 20 W of thermal energy [15]. The temperature difference of the heat pipe from end to end is only 6ºC compared to 206 ºC for the copper rod and 460ºC for the aluminum rod. In this particular case, the effective thermal conductivity is 34 times greater than a copper rod.

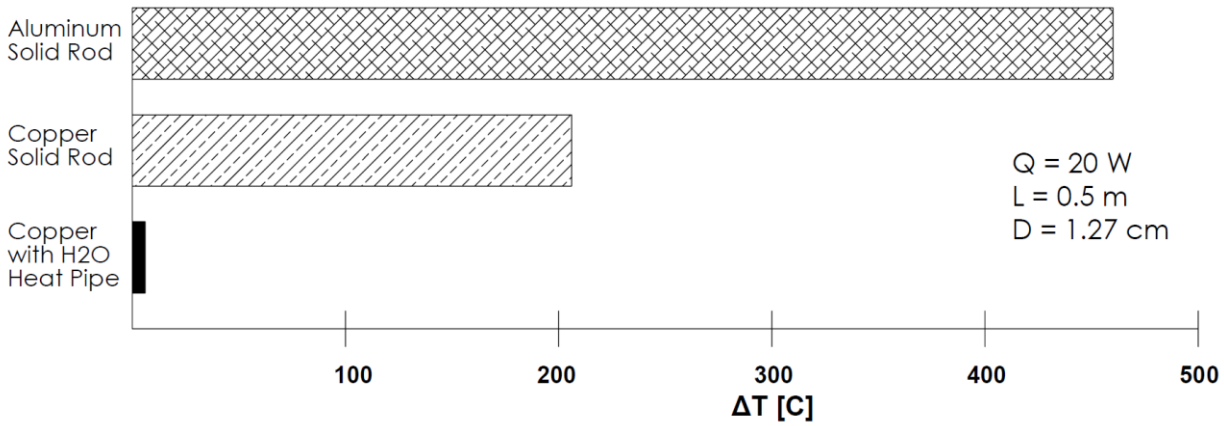

FIGURE 8: COMPARISON OF THE TEMPERATURE DIFFERENCE WITHIN A SOLID ALUMINUM AND COPPER ROD COMPARED TO A HEAT PIPE MADE OF COPPER AND FILLED WITH WATER. REDRAWN IN THE LIKENESS OF [15].

The benefits of heat pipes compared to other means of heat transfer include:

- Increased reliability.
- Rapid thermal response relative to solid conductors [15].
- Quiet operation.
- Reduced maintenance, on account of there being no moving parts.
- The ability to be fabricated in a multitude of shapes and sizes.
- Operation in any orientation including locating the evaporator above the condenser.

2.1 BASIC PHYSICS

The heat pipe functions as a small natural convection "engine" from a thermodynamic perspective [11], [17]. The forces required to maintain fluid circulation arise naturally as a result of the heat transfer process [11]. As the evaporator absorbs heat from the surroundings the fluid density decreases and vapor pressure increases, as the temperature rises. This results in vapor transfer to the condenser. At the condenser, the vapor gives up latent heat and condenses into liquid [11]. Frictional forces between the heat pipe surfaces and the fluid consume part of the thermal energy added to the evaporator [17]. Gravity assists the heat transfer process when the heat sink is located above the heat source [11]. External acceleration also influences heat transport. If the condensate is driven back to the evaporator as a result of acceleration then heat transport is enhanced, the opposite will reduce heat transport [11].

Displayed in Figure 9 for a generic heat pipe cycle in (a) is a representative heat transfer diagram and (b) is a temperature versus entropy diagram. At position "1" the working fluid is sub-

cooled liquid entering the evaporator. Adding heat to the system converts the saturated liquid to saturated vapor, bringing the cycle to position "2" Additional heating results in superheated vapor at 2'. The vapor moves to the condenser and rejects heat, eventually condensing to liquid at position "4", and then returns to the evaporator, thus driving the recirculating heat transfer process. Most of the temperature drop associated with heat pipes occurs as heat transfers through the wick and wall structure both into and out of the vapor space [11].

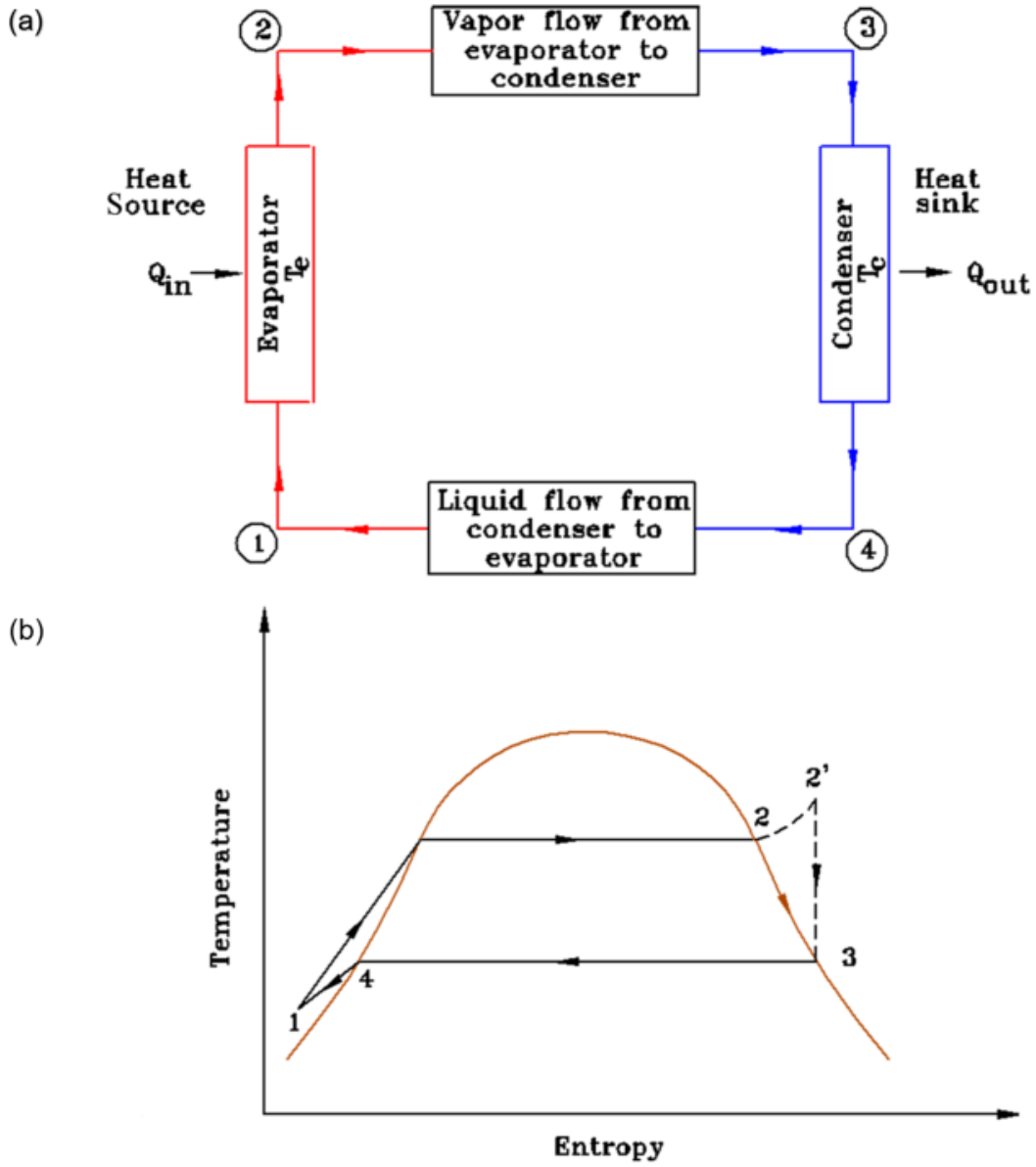

FIGURE 9: TEMPERATURE VERSUS ENTROPY GRAPH SHOWING THE THERMODYMANIC CYCLE UNDERGONE BY A CONVENTIONAL HEAT PIPE [14].

In a wicked heat pipe, fluid flow is linked to capillarity. Capillarity is the ability of the liquid vapor interface in a pore structure to withstand a pressure difference across it [11]. To describe capillarity an understanding of surface tension, contact angle and wettability are required. A meniscus is the interface between a liquid and vapor, and in the small region surrounding the meniscus the densities of both the liquid and vapor vary gradually [15]. Surface tension is equivalent to the energy required to break through the meniscus [18]. It arises from the attraction of liquid molecules to each other and the repulsion of liquid molecules to vapor molecules. The force acts perpendicularly and inwardly on the liquid, thereby decreasing the area and curving the surface [17]. This results in a liquid having a meniscus with the smallest surface area as possible at a liquid vapor interface [18]. An example is a drop of water having the shape of a sphere instead of another shape [18]. In addition, surface tension decreases with increasing temperature and a temperature variation results in fluid flowing due to shear stress at the liquid-vapor interface [11].

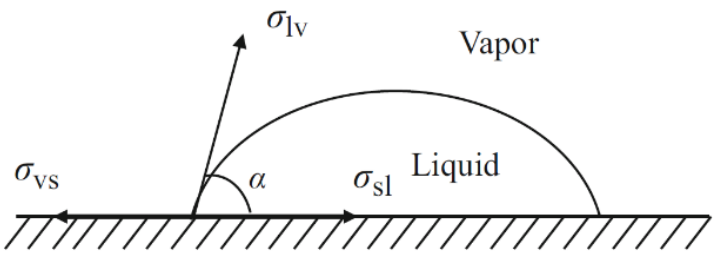

FIGURE 10: CONTACT ANGLE OF A LIQUID DROP ON A SOLID [17].

As shown in Figure 10, when a liquid drop sits on a solid surface the contact angle, α, is where the liquid-vapor interface meets the solid surface and is a result of the surface tension, σ. Figure 10 also displays the surface tension interactions between vapor and solid, σ_{vs}, between liquid and vapor, σ_{lv}, and between solid and liquid, σ_{sl}.

The contact angle is found by measuring from the solid surface, through the liquid and ending in the vapor region [15]. It is also used to describe the wettability of a liquid on a particular surface. If the contact angle is less than 90° then the surface is hydrophilic (absorbs liquid), an angle greater than 90° is called hydrophobic (repels liquid). The size of the contact angle is dependent on cohesion and adhesion forces. Cohesive forces bind the liquid molecules together and adhesive forces bind the liquid to the solid molecules [11]. Liquids used in heat pipes are generally hydrophilic [11].

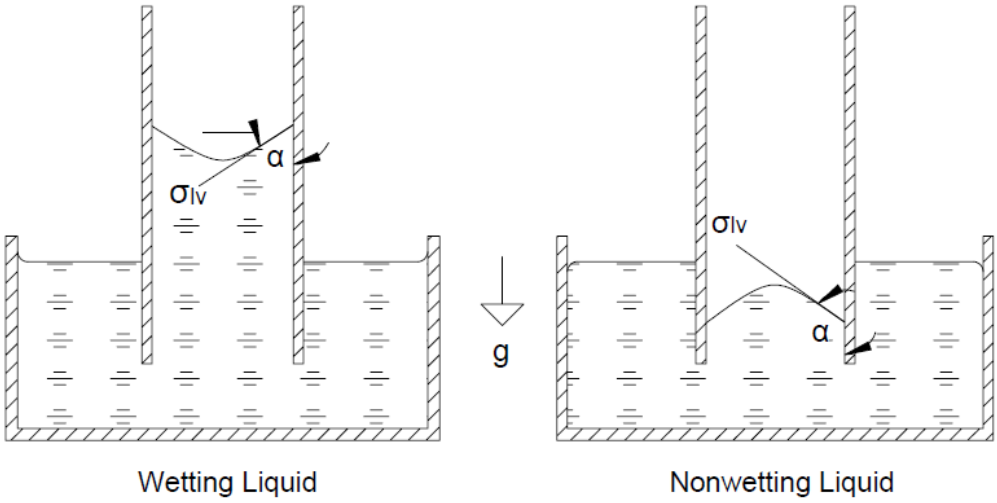

FIGURE 11: WETTING VERSUS NON WETTING LIQUIDS IN CAPILLARY TUBES.

When a pressure difference across a curved surface of a liquid exists, the ability to sustain that pressure is known as capillarity [11], which is dependent on fluid properties such as surface tension and fluid dependent properties such as contact angle. Capillarity can be visualized by placing a small tube inside a glass of liquid. Capillary forces cause a wetting liquid to rise inside the empty tube, as shown in the left of Figure 11, forming a concave-up mensicus. The adhesive forces between the liquid and the tube exceed that of the cohesive forces, such as surface tension, between the liquid molecules. The liquid rises in the tube until adhesive forces are balanced by the force of gravity [18]. Capillarity is maximized when the contact angle is close to 0 or 180 degrees and minimized when the angle is around 90 degrees [11]. Liquids with low surface tension will form a concave up meniscus and those with high surface tension having a convex meniscus [18]. Non-wetting surfaces will decrease in elevation as shown on the right of Figure 11.

A pressure gradient exists in the heat pipe as a result of vapor accumulation in the evaporator and depletion in the condenser, thus driving the vapor flow [11]. Heat is input on the evaporator side of the heat pipe and causes the liquid to boil and vaporize. At the beginning of the evaporator section the mass flow rate, velocity, and momentum of the vapor are zero and increase until a maximum is reached at the end of the evaporator [11]. Figure 12 displays a schematic of the pressure distribution for a conventional heat pipe [11]. The pressure scale is exaggerated. The vapor pressure drop is usually 1% or less at steady state, which results in near isothermal heat transport through the vapor space, but during start up can vary as much as 60% [11].

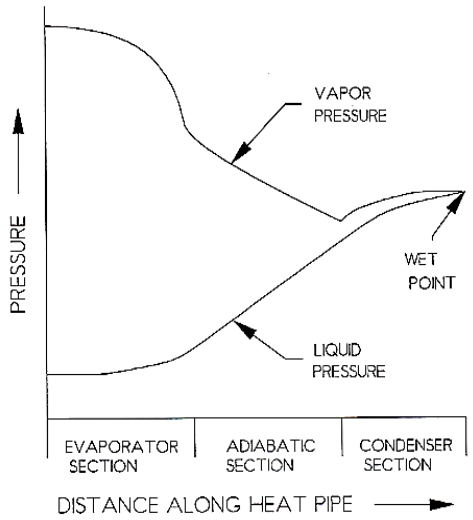

FIGURE 12: SCHEMATIC OF A CONVENTIONAL HEAT PIPE WITH THE PRESSURE VARIATION ALONG THE LENGTH DRIVING THE FLOW OF THE WORKING FLUID.

The concave down shape of the vapor pressure is caused by the frictional pressure drop, which increases with length [11]. Additionally, the increasing momentum also causes a pressure drop [11]. In the adiabatic region, the mass flow rate is constant and the only pressure drop is from friction which results in a linear decrease [11]. In the condenser, the mass flow rate, velocity, frictional pressure drop, and momentum decrease which causes a net pressure rise [11].

Vapor condenses into the wick as heat is rejected in the condenser. The coexistence of both liquid and vapor means the corresponding internal pressure is equivalent to the vapor pressure of the given heat pipe temperature [11]. The liquid flow rate increases in the condenser and decreases in the evaporator which results in a similar but opposite pressure curve profile to the vapor pressure because of the changing liquid frictional pressure drop [11]. The frictional pressure drop is dependent on the flow channel, therefore with an open channel the pressure drop will be small and for porous channels the opposite is true [11]. Momentum pressure is usually negligible in the liquid because of low velocity [11]. Gravity will increase the pressure difference when it assists the flow of condensate to the evaporator, because of the hydrostatic pressure difference [11]. Within the wick structure of the condenser liquid condensation causes flooding, resulting in a nearly flat meniscus [14], and evaporation within the evaporator causes the meniscus to recede into the pores of the wick [15], [14]. The menisci curvature difference causes a variation in the capillary pressure along the heat pipe [14].

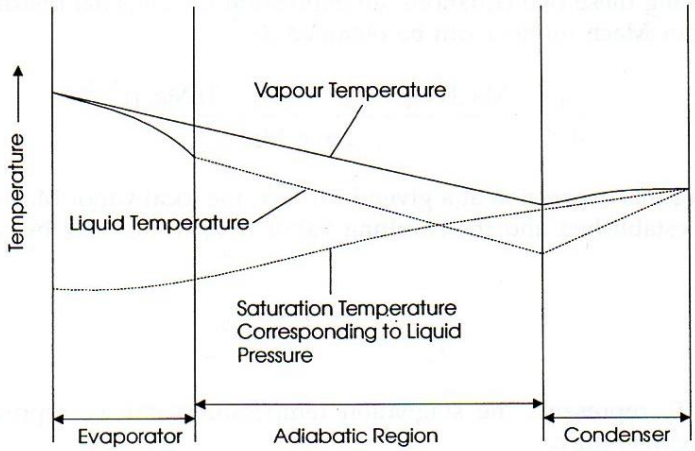

FIGURE 13: AXIAL VARIATION OF FLUID TEMPERATURES WITH AN OPERATING HEAT PIPE [15].

A typical temperature variation within an operating heat pipe is displayed in Figure 13 [15]. The vapor temperature decreases steadily from the evaporator through the adiabatic section because of decreasing vapor pressure and condensation of vapor at the liquid interface [15]. The temperature can increase in the condenser because of pressure recovery. The condensed liquid decreases in temperature until the end of the condenser then steadily rises in temperature until the evaporator because of heat transfer from the vapor flow [15]. A rapid increase in temperature occurs in the liquid at the evaporator section because external heat addition through the shell wall [15]. In the evaporator, the liquid pressure is below the vapor pressure because of capillary forces, which allows the liquid to evaporate into vapor [15].

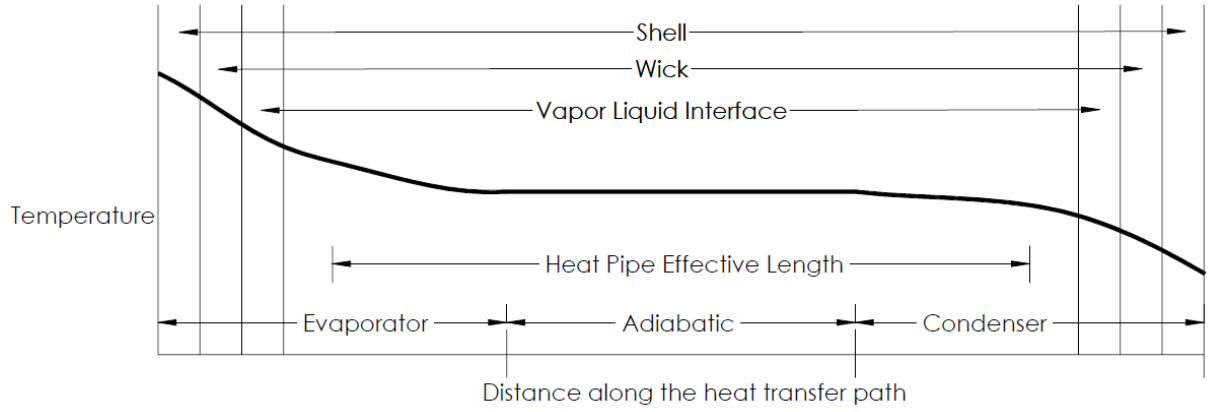

FIGURE 14: TEMPERATURE DISTRIBUTION ALONG THE HEAT TRANSFER PATH IN A HEAT PIPE [11].

During steady state operation, under normal operating conditions, the exterior temperature of the heat pipe is nearly constant through the adiabatic section, as depicted in Figure 14 [11]. There can be temperature drops across the wall, wick and liquid-vapor interface [11]. The thermal

losses across the liquid vapor interface can usually be neglected, except during high heat fluxes [11]. The majority of the temperature drops occur across the shell wall and wick of the heat pipe. The largest temperature drop will often occur in the shorter end, evaporator or condenser, depending on the design parameters [11]. A heat pipe that has equal heat input and output rates is considered to be in steady state [11].

2.2 Performance Limits

A number of transport phenomena can limit the heat transfer rate of a heat pipe. These limits arise due to design constraints, fluid properties, and operating conditions. The following sections describe the various ways that the heat flow can be constrained. Simplified methods for determining the associated maximum heat transfer rates for each phenomenon are presented.

2.2.1 Boiling Limit

The *boiling limit* occurs when the wick surface temperature becomes hotter then the saturated fluid temperature vapor bubbles get trapped in the wick and block the return of liquid to the evaporator, which causes reduced capillary pumping pressure, wick dry out, overheating and/or possibly a heat pipe meltdown [11]. The *boiling limit* is dependent on evaporator heat flux [10] and can be increased by increasing the vapor diameter [15].

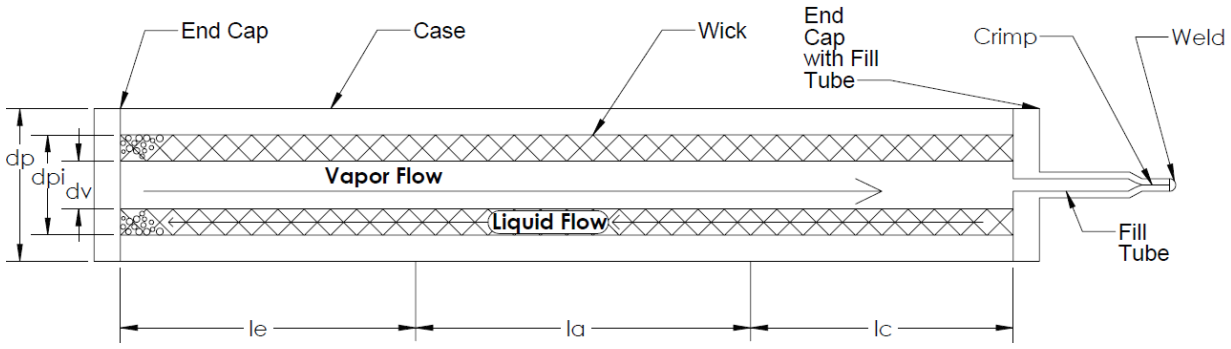

FIGURE 15: DISPLAY OF THE NUCLEATE BOILING WHEN THE *BOILING LIMIT* HAS BEEN REACHED.

$$Q_b = \frac{2\pi l_e k_{eff} T_v}{\lambda \rho_v \ln\left(\frac{d_{pi}}{d_v}\right)}\left[\frac{2\sigma}{r_n} - p_c\right] \tag{2.1}$$

The *boiling limit*, Q_b, as described by Equation (2.1) [15] depends on the length of the evaporator, l_e, effective conductivity of the saturated wick, k_{eff}, temperature of the vapor contained within the vapor column, T_v, surface tension, σ, maximum capillary pressure, p_c, latent heat of vaporization, λ, density of the vapor, ρ_v, inner diameter of the heat pipe, d_{pi}, diameter of the vapor column (the space in between the wick structure), d_v, and the nucleation radius which is approximated at 2.54 x 10^{-7}m [19], r_n.

$$k_{eff} = \frac{k_l[(k_l + k_w) - (1-\varepsilon)(k_l - k_w)]}{(k_l + k_w) + (1-\varepsilon)(k_l - k_w)} \tag{2.2}$$

The effective thermal conductivity of a wrapped screen wick is shown in Equation (2.2) [15], [17]. Thermal conductivities of the liquid and wick, k_l and k_w, and the wick porosity, $\boldsymbol{\varepsilon}$, are the parameters used to define the effective thermal conductivity.

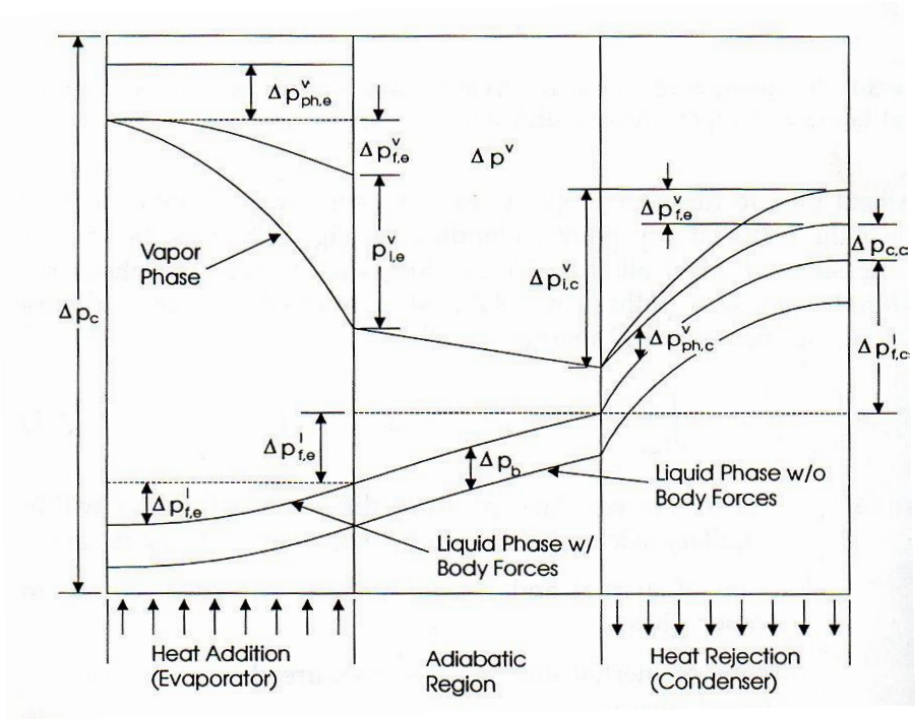

FIGURE 16: DISPLAY OF VARIOUS PRESSURE DROPS WITHIN A HEAT PIPE [15].

A graphical display of the pressure drops within a heat pipe is seen in Figure 16. The frictional, inertial and body force (gravity or acceleration) pressure drops are represented by Δp_f, Δp_i, and Δp_b. The inertial vapor pressure gradient is often small and therefore ignored [15].

$$\varepsilon = 1 - \frac{\pi S N d_w}{4} \tag{2.3}$$

The wick porosity shown in Equation (2.3) is dependent on the crimping factor constant, *S*, determined by Chi [20] to be equal to 1.05, the screen mesh number, *N*, and the screen wire diameter, d_w. The crimping factor accounts for the fact that screen wire wick structures are bent and woven in addition to being crossed [14]. A tightly wrapped wick will have a higher flow resistance that a loosely wrapped wick [21]. The screen mesh number is a measure of the number of openings per unit length. [15].

2.2.2 CAPILLARY LIMIT

The *capillary limit* occurs when the pumping pressure produced by liquid surface tension cannot overcome the sum of other pressure drops within the heat pipe. This occurs when the heat pipe is unable to return enough liquid from the condenser to the evaporator without the wick structure drying out and overheating [11]. Placing the evaporator below the condenser allows gravity to assist in the capillary pumping process. When the right-hand side of Equation (2.4) is equal to the left-hand side then the heat pipe is operating at its maximum heat transport capacity [11].

$$\Delta p_c \geq \Delta p_v + \Delta p_l + \Delta p_{ph} + \Delta p_{radial} + \Delta p_{axial} \tag{2.4}$$

These pressure differentials displayed in Figure 16 constitute the pressure drops defined in Equation (2.4). When the sum of all the system pressures from vapor, p_v, liquid, p_l, phase change, p_{ph}, and gravity dependent on the orientation of the pipe, p_{radial} and p_{axial}, is less than the capillary pumping limit, shown in Equation (2.4) [15], then the heat pipe is operating normally. Pressure changes arises during phase change as a result of the momentum from the molecules leaving the surface of the vapor and mixing with the surface liquid molecules [15]. When the sum of pressures equals the pumping pressure then this is the maximum capillary pumping pressure for the heat pipe system. When the pressure summation exceeds the capillary pumping pressure, this is the *capillary limit* then the heat pipe will no longer function. The capillary pumping pressure is also defined by Equation (2.5) [15]. Experimental values for the phase change pressures are small and considered to be negligible relative to other terms in Equation 2.4 [15].

$$\Delta p_c = \frac{2\sigma\cos\theta}{r_c} \tag{2.5}$$

The capillary pressure, shown in Equation (2.5), is dependent on contact angle between the working fluid and the wick structure, θ, and the capillary radius, r_c. defined by Equation (2.6) [15].

$$r_c = \frac{1}{2N} \tag{2.6}$$

TABLE 1: CONSTANTS ASSOCIATED WITH REYNOLDS AND MACH NUMBERS [15].

$\mathbf{Re_v}$	$\mathbf{Ma_v}$	$\mathbf{B_v}$	$\mathbf{C_v}$
< 2300	< 0.2	16	1
< 2300	> 0.2	16	$C_v = \left[1 + \frac{\gamma_v - 1}{2} Ma_v^2\right]^{-\frac{1}{2}}$
> 2300	< 0.2	$B_v = 0.0038\left(\frac{2r_h Q_c}{A_v \mu_v \lambda}\right)^{\frac{3}{4}}$	1
> 2300	> 0.2	$B_v = 0.0038\left(\frac{2r_h Q_c}{A_v \mu_v \lambda}\right)^{\frac{3}{4}}$	$C_v = \left[1 + \frac{\gamma_v - 1}{2} Ma_v^2\right]^{-\frac{1}{2}}$

Constants related to the vapor Reynolds, Re_v, and Mach number, Ma_v, are listed in Table 1 [15]. These constants are known as Kraus and Bar-Cohen constant, B_v, and a flow constant, C_v.

$$\Delta p_v = \left(\frac{2B_v C_v \mu_v}{d_v^2 A_v \lambda \rho_v}\right) l_{eff} Q \tag{2.7}$$

The vapor pressure drop shown in Equation (2.7) [15] is dependent on the absolute viscosity of the vapor, μ_v, effective length of the heat pipe, l_{eff}, heat transfer rate, Q, and the cross-sectional area of the vapor, A_v.

$$d_v = \mathrm{d_{pi}} \text{-} 4\mathrm{N}_{wrap}\mathrm{d_w} \tag{2.8}$$

The vapor diameter shown in Equation 2.8, is dependent on the number of wraps of the screen wick, N_{wrap}.

$$l_{eff} = 0.5l_e + l_a + 0.5l_c \tag{2.9}$$

The effective length, l_{eff}, of the heat pipe depends on the lengths of the evaporator, condenser and adiabatic sections of the heat pipe, l_e, l_c, and l_a as described in Equation (2.9) [15].

$$\Delta p_l = \left(\frac{\mu_l}{K A_w \lambda \rho_l} \right) l_{eff} Q \tag{2.10}$$

$$K = \frac{d_w{}^2 \varepsilon^3}{122(1-\varepsilon)^2} \tag{2.11}$$

The liquid pressure drop shown in Equation (2.10) [15] depends on the absolute viscosity of the liquid, μ_l, wick permeability, K, cross-sectional area of wick, A_w, and the density of the liquid, ρ_l. Equation (2.11) displays the wick permeability.

$$A_w = \frac{\pi}{4}(d_{pi}^2 - d_v^2) \tag{2.12}$$

The cross-sectional area of the wick for a cylindrical heat pipe is shown by Equation (2.12).

$$\Delta p_{axial} = \rho_l g l_p \sin\psi \tag{2.13}$$

$$\Delta p_{radial} = \rho_l g d_v \cos\psi \tag{2.14}$$

The axial and radial pressure changes are caused by body forces and the effects of gravity within the liquid and vapor [15]. The axial pressure change shown in Equation (2.13) [15] is dependent on the gravitational constant, g, the length of the heat pipe, l_p, and the angle heat pipe makes to horizontal, Ψ. The radial pressure change shown in Equation (2.14) [15]. The radial pressure drop only occurs in heat pipes were circumferential communication of the liquid within the wick is possible [15].

$$\mathrm{Re}_v = \frac{4Q}{\pi d_v \mu_v \lambda} \tag{2.15}$$

The Reynolds number of the vapor flow for a circular heat pipe is displayed in Equation (2.15) [15]. The Reynolds number is used to determine if the vapor flow is laminar or turbulent.

$$Ma_v = \frac{Q}{A_v \rho_v \lambda \sqrt{R_v T_v \gamma_v}} \tag{2.16}$$

The Mach number of the vapor flow is displayed in Equation (2.16) [15] and is dependent on the gas constant of the vapor, R_v, and the ratio of specific heats of the vapor, γ_v. The Mach number is used to determine if the flow is compressible or incompressible [15].

In order to solve for both the Reynolds and Mach number equations, the heat transport capacity is required, Q_c, which means the conditions of the vapor flow must be assumed [15]. An iterative process is followed to find the maximum heat transport capacity and then afterward the assumptions are validated by calculating the Reynolds and Mach numbers [15].

To find the value of the capillary heat transfer limit, Q_c, Equation (2.4) is solved to by equating the right and left hand sides and substituting in Equation (2.5) through (2.14). This value should then be substituted into the Reynolds and Mach number equations to validate the initial assumptions made about the vapor flow.

2.2.3 Entrainment Limit

Viscous shear forces arising from the opposite flow of liquid and vapor can impede the return of liquid to the evaporator. The opposing movements of higher velocity vapor and slower moving liquid results in a drag force that is balanced by surface tension [11].

Increased heat transport rates result in higher vapor velocities allowing for the vapor to pick up the liquid droplets and trap them [10]. If this persists, less liquid returning to the condenser will cause the evaporator to dry out. This is known as the *entrainment limit.* Entrainment initiates where fluid velocities are the highest at the evaporator exit [11] and can be increased by increasing the vapor diameter [15]. The drag on the liquid is determined by surface area which is proportional to wick pore size. As a result, the *entrainment limit* is an inverse function of wick pore size [11].

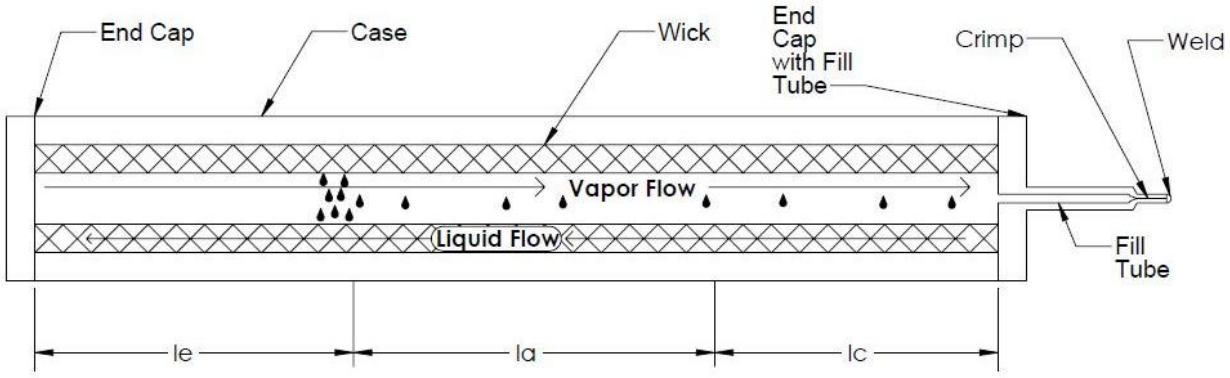

Figure 17: Display of the liquid and vapor streams when the *entrainment limit* has been reached. Liquid droplets are carried to the condenser by the vapor flow.

Figure 17 displays the *entrainment limit* when liquid droplets are entering into the vapor column at the evaporator exit. These droplets are then carried back to the condenser.

$$Q_e = A_v \lambda \left[\frac{\sigma \rho_v}{2 r_{hw}} \right]^{\frac{1}{2}} \tag{2.17}$$

$$r_{hw} = \frac{A_w}{\pi (d_v + d_{pi})} \tag{2.18}$$

The *entrainment limit*, Q_e, is given by Equation (2.17) where r_{hw} is the hydraulic radius [15].The hydraulic radius is defined by Equation (2.18) [15].

2.2.4 SONIC LIMIT

The *sonic limit* occurs at the evaporator exit where the vapor velocity has reached its highest value and the flow begins to choke. The vapor flow rate will not respond to the amount of heat added in the evaporator. The temperature of the heat pipe will rise and it will still function normally if it is within the operational limits. The *sonic limit* is usually encountered during startup. A condenser closely coupled to the heat sink enhances startup failure [11].

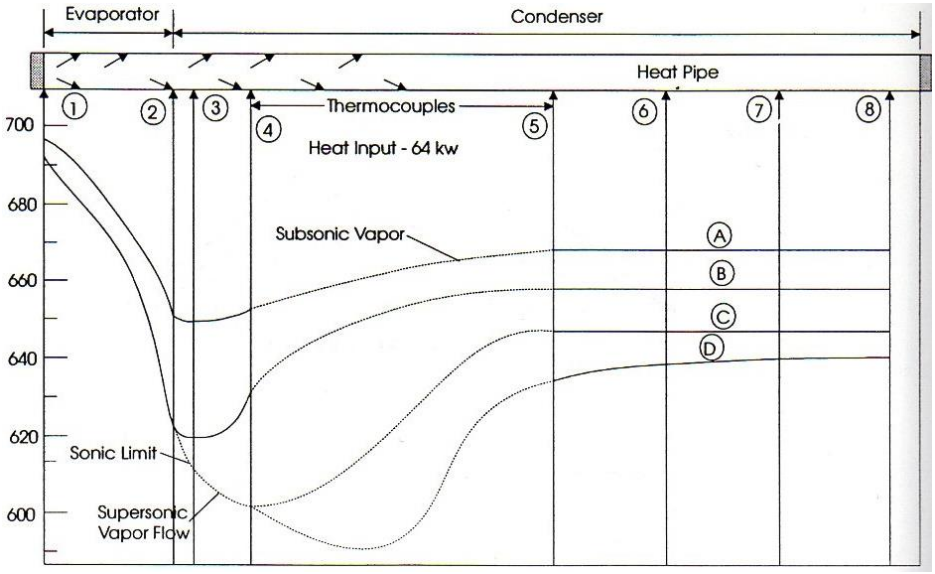

FIGURE 18: BEHAVIOUR OF VARIOUS VAPOR STREAMS FROM APPROACHING TO EXCEEDING THE *SONIC LIMIT* [15].

A temperature versus heat pipe axial position found in Figure 18 displays the behavior of multiple vapor streams from approaching the *sonic limit* to exceeding it. Curve A displays a partial pressure recovery during subsonic flow conditions [15]. Increasing the heat rejection rate and

lowering the condenser temperature for the remaining curves. The *sonic limit* is reached in Curve C [15]. At Curve D, the only noticeable change is a lowering of the condenser temperature [15].

$$Q_s = A_v \rho_v \lambda \left[\frac{\gamma_v R_v T_v}{2(\gamma_v + 1)} \right]^{\frac{1}{2}} \tag{2.19}$$

The *sonic limit*, Q_s, displayed in Equation (2.19) [15]. This equation assumes one dimensional vapor flow, that frictional effects are negligible, inertial effects dominate, and that the vapor behaves as an ideal gas [15].

2.2.5 Non-Condensable Gases

A practical consideration which can cause undesired heat pipe behavior is non-condensable gas trapped within the condenser. As depicted in Figure 19, in steady-state operation, non-condensable gas will accumulate at the condenser end of the heat pipe which can reduce the effective heat transfer area through the tube wall. Non-condensable gas is evident by sharp decreases in temperature within the condenser. This problem is reduced by proper cleaning and assembly procedures.

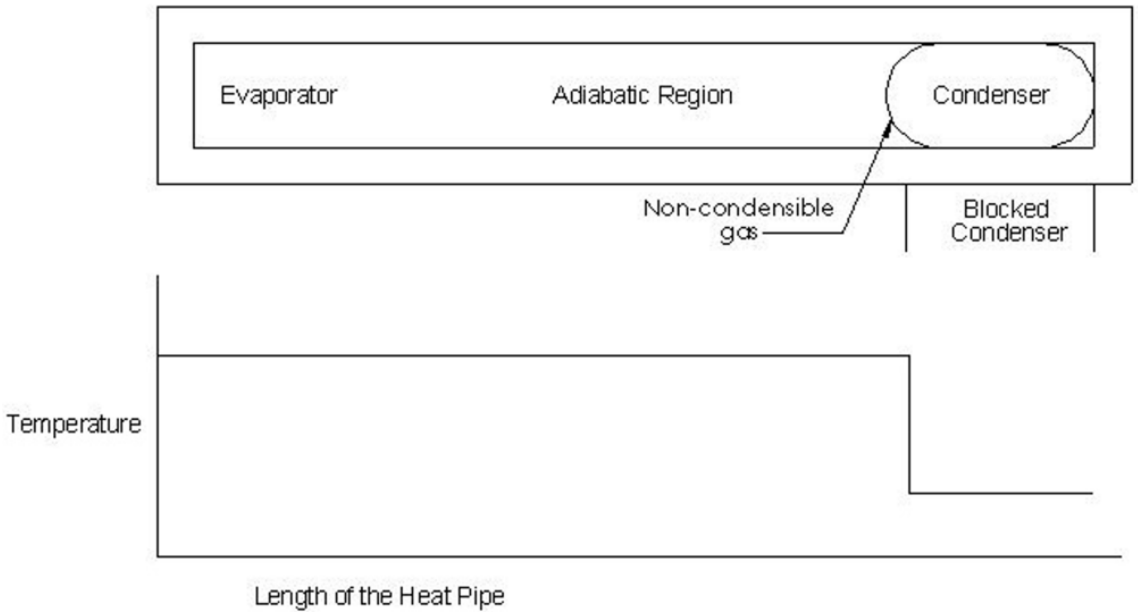

Figure 19: The effects on the temperaure profile of a heat pipe due to non-condensible gas formation in the condenser. Redrawn in the likeness of [15].

2.3 SUMMARY

This chapter described the general principles of heat pipes and thermosyphons. The main difference between a heat pipe and thermosyphon is that the latter does not have a wick. Because of this, the condenser must be above the evaporator so that gravity assists in the return of liquid to the evaporator.

Heat pipes function as small natural convection engines, absorbing heat in the evaporator and rejecting heat in the condenser. Thermal energy is used to move the working fluid within the heat pipe. Each heat pipe section has related temperature and pressure variations as a result of friction, momentum and fluid velocity. Fluid movement can be enhanced as a result of gravity, surface tension, capillarity, and the working fluid contact angle within the wick material.

Four phenomena limit the heat transport rate within a heat pipe:

- *Boiling Limit* - nucleate boiling occurs in the evaporator and leads to dry out.
- *Capillary Limit* - the total summation of pressures within the heat pipe is greater than the pumping pressure produced by the liquid surface tension in the wick. This leads to dry out and overheating.
- *Entrainment Limit* - liquid droplets are carried back to the condenser by the vapor, which leads to evaporator dry out.
- *Sonic Limit* - vapor flow becomes choked at the evaporator exit, and the heat pipe will no longer respond to increased heat addition in the evaporator.

Chapter 3 describes the design and manufacturing principles related to the fabrication of heat pipes. The shell, fill tube, and wick structures are examined more closely.

Chapter 3 Design and Manufacturing Principles

In Chapter 3 the components that make up a heat pipe are more thoroughly investigated. The end caps and shell, fill tube, wick, and working fluid, are discussed. The containment structures of conventional pipes are mechanically simple, but need to be built to withstand cyclical mechanical and thermal stress. These governing equations are presented. In addition, methodologies and equations for determining the optimal filling ratio are presented. The fill tube connects the heat pipe to the vacuum system and is also used to fill the heat pipe after assembly, cleaning and evacuation.

3.1 Design Considerations

Incident heat flux, geometric constraints, material type, heat transport limits, fabrication considerations, and structural integrity must all be considered when designing a heat pipe. The basic performance requirements such as operating temperatures and pressures are established in order to adequately design a heat pipe system. The freezing and critical temperature (temperature at the critical point [18]) of the working fluid defines the operating limits of the thermal environment. Material compatibility and working fluid degradation may occur when the upper pressure limits of the containment design are reached [22].

3.2 End Caps and Shell

The heat pipe shell and end caps must have the structural integrity to withstand internal pressure and temperature changes, as well as providing a leak free containment for the working fluid [10]. The container materials must be compatible with the working fluid[3] and the external environment. In addition, considering fabrication methods used, such as machining and welding. End caps are typically welded onto the shell.

The ability of a heat pipe to withstand internal pressure and wall temperature variations are the primary structural considerations that need to be evaluated. Thermal and mechanical stress can

[3] Appendix B lists a variety of fluid types and containment materials and their experimentally compatibility.

result in deformation and buckling of the heat pipe when the strength limitation of the containment material is exceeded.

3.2.1 Mechanical Stress

Hoop stress develops in thin-walled cylindrical objects that experience varying pressure on the inner and outer walls. A safety factor of four is recommended by B&K Engineering when comparing to the ultimate strength of the material [22]. The axial stress is one half of the hoop stress.

$$s_h = \frac{r_m}{t_{wall}} \Delta p \tag{4.18}$$

$$r_m = \frac{r_p + r_{pi}}{2} \tag{4.19}$$

The hoop stress displayed in Equation (4.18) [11] is dependent on the mean wall radius, r_m, the maximum pressure difference between the interior vapor pressure and exterior of the heat pipe shell, Δp, and the wall thickness of the heat pipe, t_{wall}. Equation (4.19) is dependent on the inner and outer radii of the heat pipe, r_{pi} and r_p.

3.2.2 Thermal Stress

A temperature differential across the heat pipe wall thickness will result in thermal stress. Compressive stress develops in the hotter inner wall of the condenser section and tensile stresses exist on the outer wall. The opposite is true at the evaporator section. The maximum thermal stress displayed in Equation (4.20) [11] occurs in the inner and outer radii of the tangential direction. The plus sign calculates the maximum compressive stress, occurring at the hottest surface, and the minus calculates the tensile stress, at the coolest surface. The stresses will be equal when the ratio of wall thickness to radius is much less than one [11].

$$s_{th} = \frac{\alpha E \Delta T_{wall}}{2(1-\nu)} \left[1 \pm \delta_g \frac{(r_p - r_{pi})}{3 r_{pi}} \right] \tag{4.20}$$

The thermal stress, s_{th}, is dependent on the coefficient of thermal expansion, α, modulus of elasticity, E, wall temperature difference, ΔT_{wall}, Poisson's ratio, ν, and the geometric parameter, δ_g. The geometric parameter used for a cylindrical heat pipe is equal to one.

3.3 FILL TUBE

Ideally, the fill tube inside diameter should be large to allow for reaching low vacuum pressures, and creating an easy pathway for working fluid to enter the heat pipe. Achieving low vacuum pressure means the majority of the impurities within the system have been removed.

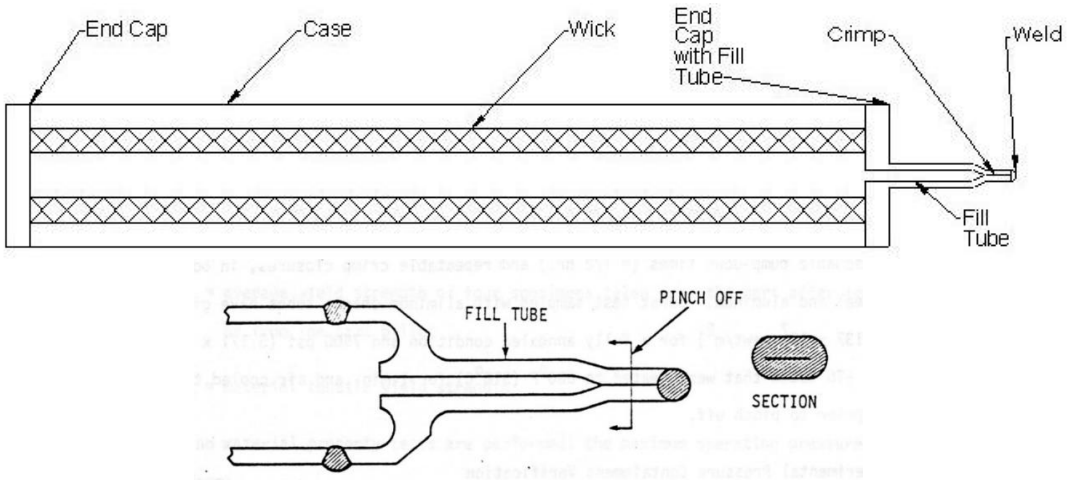

FIGURE 20: ABOVE A TYPICAL FILL TUBE WITH A CRIMP AND WELD TO ENSURE A FLUID TIGHT SEAL. BELOW IS A DETAILED CLOSE UP OF THE CRIMPED FILL TUBE [22].

As displayed in Figure 20, once charged, the fill tube is closed by pinching it off with a crimping tool and welding the pinched end shut. A thin wall is useful so as to allow for easy crimping. Getting a proper seal while crimping metal is a concern. There is a tradeoff between machinability and malleability. Softer materials are desirable for crimping, but that same material will be quite gummy when machined. Gumminess means that machining operations must be done slowly and with care and it is also likely that tools will grab and break. The fill tube is often welded into one of the end caps. Experimentation determines the maximum operating pressure of the fill tube, however because of its smaller size it usually exceeds that of the heat pipe [22].

3.4 WICK

The wick is a porous material that lines the inner structure of the heat pipe shell. Wicks constructed of a single material are call homogenous and one with multiple materials are composite [14]. Figure 21 displays multiple homogenous wicks and a composite wick. Each wick type has various advantages and disadvantages. The driving factor for selection is often cost and ease of manufacturability. Composite wick structures have the advantage of combining benefits of various structures. The key characteristics of the wick are permeability and the effective pumping radius

[22]. If the evaporator is placed above the condenser then this configuration requires a wick structure with a finer pore radius, resulting in a greater capillary force to overcome the force due to gravity [17].

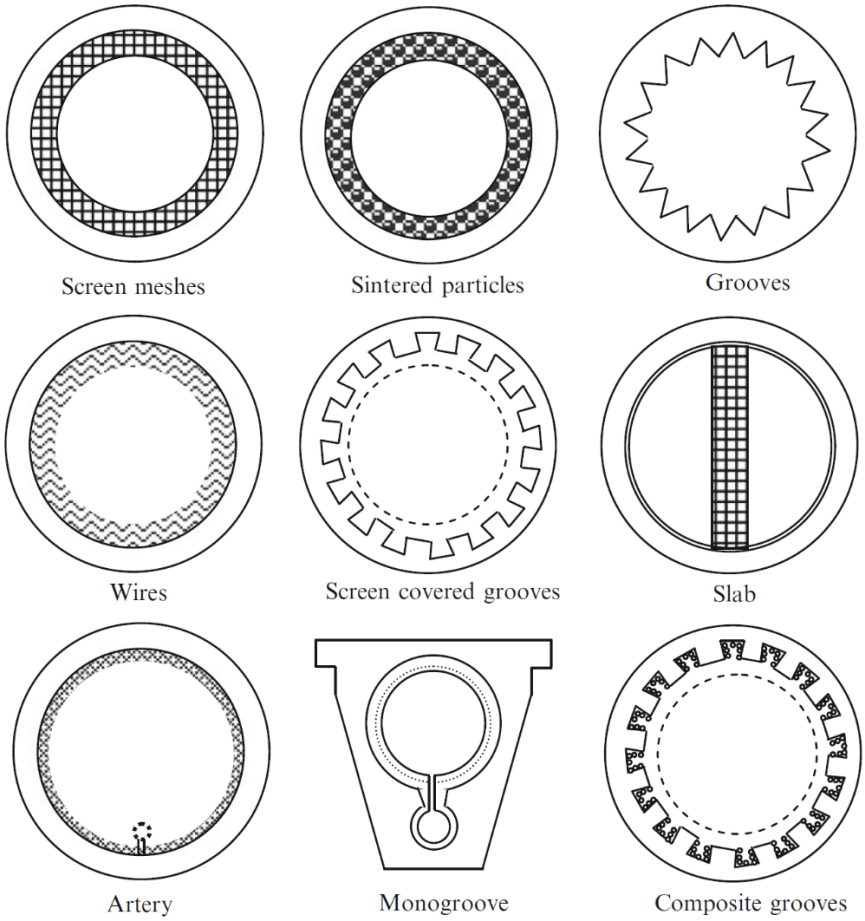

FIGURE 21: COMMON TYPES OF WICK STRUCTURES USED IN HEAT PIPES [17].

A small effective pore radius will result in a high capillary pumping pressure. A large effective pore radius will allow for higher flow rates and greater permeability. Therefore, a trade-off exists between pumping pressure and permeability. Creating a multilayered composite wicking structure allows for both high permeability and capillary pumping pressure [15]. To reduce wick and wall temperature drops and thermal stress, the wick should have a high thermal conductivity [14]. Using the same material for the heat pipe shell and wick is recommended in order to reduce the risk of impurities and non-condensable gases within the structure [11].

The most common and simple wick structure is the wrapped screen, which is often used because of the associated ease of installation. Changing the number of wraps, the tightness of the

wraps or the pores per unit area will change the effectiveness of the wick and impact the capillary limit [14]. Generally, screen wicks can have high permeability and capillary pressure; however, the effective thermal conductivity is low because of poor contact between the shell of the heat pipe and the screen [14].

3.5 WORKING FLUID

Operational temperature range, operating pressure, wicking capability, thermal conductivity, fluid compatibility, and stability help to determine the best working fluid for an application [22]. If the system operating temperature is between the freezing point and critical point of the working fluid, then the fluid is under saturated conditions [10] and the heat pipe will usually be operational.

Impurities in the working fluid from solids, liquids and non-condensable gases can detrimentally effect the operation or performance of a heat pipe [15]. Impurities from solids degrade the heat pipe performance by clogging the pores of the wick and also corroding inside the pipe [15]. Liquid impurities degrade performance by changing the viscosity of the working fluid and also changing the wetting angle. Impurity introduction is a result of improper cleaning, evacuation and charging procedures [14]. An example of an unstable combination is to use an aluminum wick and/or shell with water as the working fluid, as this will result in the creation of aluminum oxide and hydrogen. The hydrogen is a non-condensable gas that will occupy the vapor column and greatly reduce heat transport capacity [11].

3.6 FILLING RATIO

The filling ratio is one of the most important factors influencing heat transfer performance. Continuous circulation of vapor and liquid within the heat pipe or thermosyphon is required without the evaporator drying out or liquid being carried to the condenser [23].

$$V_f = \frac{V_r}{V_t} * 100 \tag{4.21}$$

$$V_t = \pi \frac{d_{pi}^2}{4} l_p \tag{4.22}$$

The governing equation for filing ratio is shown in Equation (4.21) [24]. V_f, is the filling ratio of the working fluid, V_r is the actual volume of the working fluid and V_t is the internal volume of the heat pipe as show in Equation (4.22).

A thermosyphon with large fill ratios can be subject to geyser boiling [14]. Geyser boiling occurs when a portion of working fluid is carried upward to the condenser by an expanding vapor bubble. At the end cap this bubble bursts and inner pipe wall is covered by a film of liquid. This will not affect heat transport of the system, but it may damage the end cap. For small fill volumes, a thermosyphon will have breaks in the liquid film returning to the evaporator and the heat transfer coefficient will decrease compared to a uniform falling film [14]. For very small fill volumes where there is no pool of liquid in the evaporator then dry out can occur, which results in a sudden spike in wall temperature [14].

3.7 SUMMARY

With an understanding of some of the key design considerations related to heat pipe construction, the next step is to quantify the thermal performance. Using the theory presented in Chapter 2, a generic thermal model of a heat pipe is described in Chapter 4. A simple resistance network describes the main components of a heat pipe and it is used to predict the end to end temperature differential various heat pipe configurations. With appropriate property data, and system constraints, the heat transfer performance limits of a various configurations are quantified.

Chapter 4 Heat Pipe Modeling

The most important metric quantifying the performance of a heat pipe is the effective thermal resistance between the outer surfaces of the condenser and evaporator. Unlike a simple solid, the effective heat transfer capacity is determined by a number of interrelated phenomena as described in Chapter 2. The following sections describe a steady-state resistive model of a heat pipe. This model is then used to determine the expected behavior of selected fluids for use with condenser temperatures set by solid CO_2. Specific heat pipe parameters are determined, and modeling is performed to determine the preferred heat pipe configuration for manufacturing. Once prototype heat pipes are manufactured an experiment will be set up to verify functionality. These experiments will help to meet the thesis objectives of determining the transient thermal response, steady state temperature differential, and the thermal resistance.

4.1 Modeling

To begin the process of designing a heat pipe the incident heat flux, geometric constraints and the type of heat sink and source are required. Initially a working fluid and compatible shell material are chosen. The fluid properties at various temperatures are required to solve the design equations. Geometric constraints of the system are applied and optimized. The optimal dimensions are determined using the heat transport equations that appear in Section 2.2. These limits also determine the performance within a specific temperature range. Once the geometry is finalized then the mechanical and thermal stress can be determined. Lastly the fill volume is determined. This iterative process occurs until the constraints are satisfied, then manufacturing can begin.

A heat pipe is considered to be at steady state when the temperature is constant and the rate of heat rejected equals the rate of heat addition. During a transient, there is an imbalance in the heat rate and a variation in the heat pipe temperature [11]. This condition occurs during startup and the process can result in reduced heat transfer rates or overheating when the opposite is true [11]. The minimum operating temperature can impact start-up behavior especially from a frozen or low vapor pressure states, because there, the heat transport capacity is negligible [14]. Modeling heat pipe startup is complex because of multi space dimensions with time variations, changing flow regimes, non-equilibrium expansion and phase changes [11]. The modeling of transient behavior will not be considered.

4.2 THERMAL RESISTANCE NETWORK

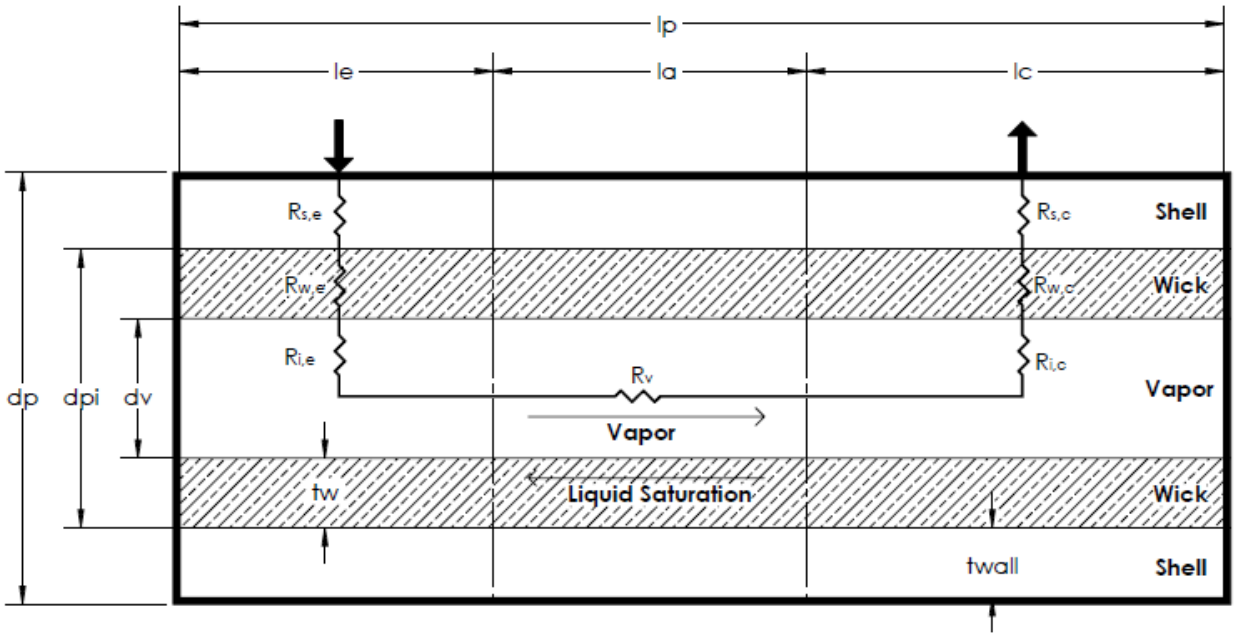

FIGURE 22: CYLINDRICAL HEAT PIPE THERMAL RESISTANCE DIAGRAM. ADAPTED IN THE LIKENESS OF [17].

The total thermal resistance, R_{hp}, of a cylindrical heat pipe can be defined in terms of a network as shown in Figure 22 [17],

$$R_{hp} = R_{s,e} + R_{w,e} + R_{i,e} + R_v + R_{i,c} + R_{w,c} + R_{s,c} \tag{4.1}$$

The main resistances considered include the shell, R_s, wick, R_w, interfacial, R_i, and vapor, R_v. The outer diameter of the heat pipe, d_p, total length of the pipe, l, lengths of the evaporator, l_e, adiabatic, l_a, and condenser, l_c, determine the values of the individual resistances.

$$R_{hp} = \frac{T_e - T_c}{Q} \tag{4.2}$$

The total thermal resistance is determined experimentally by measuring the average temperatures of the evaporator, T_e, and condenser, T_c as described in Equation (4.2) [17], [14].

$$R_{s,e} = \frac{\ln\left(\dfrac{d_p}{d_p - 2t_{wall,e}}\right)}{2\pi k_s l_e} \tag{4.3}$$

$$R_{s,c} = \frac{\ln\left(\frac{d_p}{d_p - 2t_{wall,c}}\right)}{2\pi k_s l_c} \tag{4.4}$$

$$R_{w,e} = \frac{\ln\left(\frac{d_p - 2t_{wall,e}}{d_v}\right)}{2\pi k_{eff} l_e} \tag{4.5}$$

$$R_{w,c} = \frac{\ln\left(\frac{d_p - 2t_{wall,c}}{d_v}\right)}{2\pi k_{eff} l_c} \tag{4.6}$$

The individual resistances of both the evaporator and condenser sections are a function of the thermal conductivity of the shell, k_s. These resistances are given by Equation (4.3) through Equation (4.6) [17], [25],

$$R_{i,e} = \frac{1}{\pi l_e d_v h_e} \tag{4.7}$$

$$R_{i,c} = \frac{1}{\pi l_c d_v h_c} \tag{4.8}$$

Heat transfer through the wall and wick structures is via conduction [17]. Upon reaching the inner wall of the wick at the wick and vapor interface, heat is transferred by thin film evaporation or condensation as described in Equation (4.7) and Equation (4.8) [17], [26]. The evaporation and condensation heat transfer coefficients, h_e and h_c, are required. The interfacial thermal resistance can often be neglected at low heat flux because the interfacial resistance tends to be much smaller than that of the wick [17].

$$R_v = \frac{\frac{T_{v,e}\Delta p_v}{h_{l,v}}\left(\frac{1}{\rho_v} - \frac{1}{\rho_l}\right)}{Q} \tag{4.9}$$

The thermal resistance of the vapor is defined by Equation (4.9) [17], where $T_{v,e}$ is the temperature of the vapor in the evaporator. The vapor pressure drop is usually 1% or less at steady state, resulting in nearly isothermal heat transport through the vapor space [11] and is often ignored.

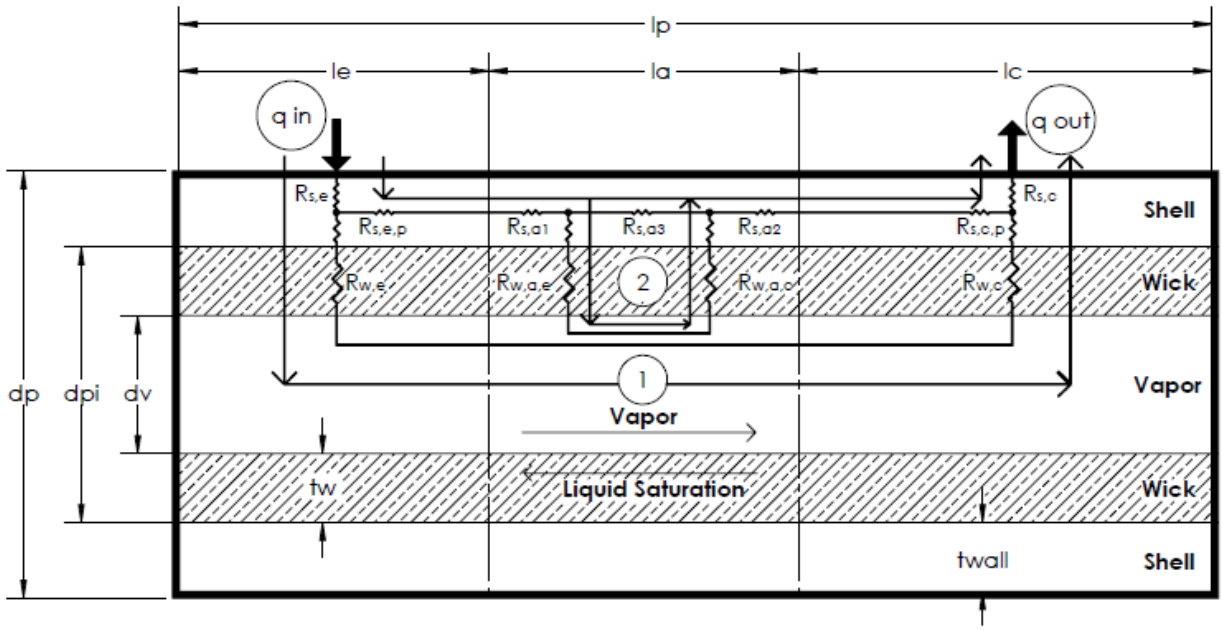

FIGURE 23: AN ALTERNATIVE THERMAL RESISTANCE NETWORK FOR A CLYINDRICAL HEAT PIPE THAT ACCOUNTS FOR AXIAL HEAT CONDUCTION [25].

The alternative model shown in Figure 23 considers the effect of axial heat conduction in the shell wall [25]. Axial heat conduction results in the evaporator and condenser having a larger surface area, therefore the circulation of working fluid follows shorter paths [25]. The consequences are reduced liquid pressure drops and the capillary limit increasing [25]. Figure 23 displays two distinct heat conduction paths between the shell of the evaporator and condenser.

$$R_1 = R_{w,e} + R_{w,c} \tag{4.10}$$

$$R_2 = R_{s,e,p} + R_{s,a1} + \frac{R_{s,a3}(2R_{w,a,e})}{R_{s,a3} + 2R_{w,a,e}} + R_{s,a2} + R_{s,c,p} \tag{4.11}$$

Path one is through the wick of the evaporator and condenser and is described by Equation (4.10) [25]. The second path considers axial conduction through the heat pipe wall and is described by Equation (4.11) [25].

$$R_{s,e,p} = \frac{l_e}{2\pi k_s \left(d_p^2 - \left(\frac{d_p + d_{pi}}{2} \right)^2 \right)} \tag{4.12}$$

$$R_{s,a1} = R_{s,a2} = \frac{l_a}{4\pi k_s \left(d_p^2 - \left(\frac{d_p + d_{pi}}{2} \right)^2 \right)} \tag{4.13}$$

$$R_{s,a3} = \frac{l_a}{2\pi k_s \left(d_p^2 - \left(\frac{d_p + d_{pi}}{2} \right)^2 \right)} \tag{4.14}$$

$$R_{w,a,e} = R_{w,a,c} = \frac{\ln \frac{d_{pi}}{d_v}}{\pi l_a k_{eff}} \tag{4.15}$$

$$R_{s,c,p} = \frac{l_c}{2\pi k_s \left(d_p^2 - \left(\frac{d_p + d_{pi}}{2} \right)^2 \right)} \tag{4.16}$$

The resistances that make up path two are determined by Equation (4.12) through Equation (4.16) [25]. Axial conduction has a significant effect in the wall when the pressure drop is more than 5% and will result in errors calculating the internal pressure drops and wall temperature distributions. [25]. When axial conduction is considered, then the total thermal resistance for the heat pipe becomes[4],

$$R_{hp} = R_{s,e} + \frac{R_1 R_2}{R_1 + R_2} + R_{s,c} \tag{4.17}$$

The experimental thermal resistance is predicted using both methods, with and without axial conduction. Since thermal conductivity of metals increases with temperature, thermal resistance should decrease with increased heat loads, resulting in higher evaporator temperatures.

4.3 MODELING PARAMETERS

To model the behavior of heat pipes some basic parameters are chosen including the working fluid, heat pipe shell material, size of the pipe, the type and size of wick structure and the

[4] Matlab code for solving the thermal resistance network is found in Appendix F.

temperature of the condenser. Numerical assumptions made during modeling are summarized below in Table 2. The lower temperature range is set by solid CO_2 and the upper ambient temperature range is set well above the upper temperature of a hot summer day in Canada. The theoretical heat pipe maximum temperature is set just below the maximum ambient temperature. To simplify the model, incompressible, laminar vapor, and liquid flow is assumed. This means assuming the Reynolds number is below 2300 and the Mach number below 0.2.

TABLE 2: ASSUMPTIONS MADE FOR NUMERICAL MODELING

Item	**Numerical Value**
Solid CO_2 sink temperature	195 K
Temperature of the condenser section	195 K
Ambient temperature maximum	353 K
Maximum heat pipe temperature	348 K
Maximum total length of heat pipe	254 mm
Outer diameter	19 mm
Shell thickness	1.6 mm
Laminar flow approximation	Re < 2300
Incompressible approximation	Ma < 0.2

The heat pipes are assumed to be vertically oriented heat pipes with the condenser located above the evaporator. The condenser temperature is assumed to be constant. The fill tube is neglected and a pure working fluid is assumed. Lastly, radiative heat transfer and contact resistance are negligible.

4.3.1 WORKING FLUID SELECTION

There are multiple fluids that have favorable behavior in the prescribed temperature range[5]. Acetone, ammonia, butane, ethane and freon-21 have all been experimentally tested and proven within 195 – 308 K. High pressures are an issue for ammonia and ethane at room temperature. Freon-21 is a phased out refrigerant because of environmental toxicity. Butane is quite flammable and therefore not an ideal choice for building a prototype. Acetone is the first choice for a working

[5] Appendix A displays various working fluids and their operational temperature range.

fluid. Methanol is a good choice for a second prototype working fluid because of favorable properties[6] at room temperature, such as low vapor pressure.

4.3.2 HEAT PIPE SHELL SELECTION

Aluminum is a suitable shell material for use with acetone because of chemical compatibility[7], machinability, and cost. Acetone is also compatible with copper. Methanol is incompatible [22] with an aluminum structure, therefore methanol heat pipes must use stainless steel or copper shells. Stainless steel is harder to machine, but simpler to weld. Copper is softer and easier to crimp.

TABLE 3: SUMMARY OF EXPERIMENTAL HEAT PIPE RESEARCH, DIMENSIONS AND RANGES

Temp	Q	Fluid	Wick	Mesh	Diameter [mm]		Length [mm]			Ref
[°C]	[W]			#	Outer	Inner	Evaporator	Adiabatic	Condenser	
0-80	0-15	Al2O3 nanofluids	Two layer screen	260	4	3	50	100	150	[27]
0-95	0-250	Al2O3 nanofluids	Three layer screen	100	12.5	11.5	100	50	150	[28]
20-80	0-100	Water	Sinter groove	-	8	7.44	50	100	50	[29]
35-80	0-160	Water	Screen 1mm thick	50	12	11	100	80	150	[30]
30-80	0-120	CuO nanofluids	Screen	100	12	?	100	80	150	[31]
?	30-70	Alcohol	Two layer ss screen	60	20	17.6	150	300	150	[32]
20-100	0-300	Water	Three layer screen	140	9.53	6.22	50.8	50.8	76.2	[33]

Table 3 summarizes cylindrical heat pipe experiments reported in the literature. This information is used as a guideline to set the lengths of the evaporator, adiabatic, and condenser sections. In all of the papers, none of the authors explain how the section lengths are determined. It appears many of the lengths are chosen based on the experimental equipment that is available.

[6] The various fluid properties for both acetone and methanol can be found in Appendix C & D.
[7] Appendix B shows working fluid and material compatibility charts.

None of the experiments use methanol or acetone. What is noticeable is the condenser is often longer than the other sections and the adiabatic and evaporator sections are often the same or similar lengths. Using these parameters as a guideline, with a maximum combined length and constant shell outer diameter and thickness, simulations are performed to find the heat transfer limits and to determine the prototype lengths.

4.4 ANALYSIS

The effect of the changing the wick structure is investigated[8]. As described in Chapter 2, heat pipe performance is strongly linked to the properties of the wick. Screen mesh wicks will be used for all simulations and manufacturing. Initially the wick mesh number is varied. As listed in Table 4, two commercially available screen mesh sizes are modeled for the aluminum heat pipes and three for the copper.

TABLE 4: SUMMARY OF DIFFERENT MESH SIZES USED IN ALUMINUM AND COPPER HEAT PIPES.

Mesh #	**Material**	
[1/m]	**Copper**	**Aluminum**
1969	Invalid Approximations: Turbulent Flow	Invalid Approximations: Turbulent Flow
3150	Invalid Approximations >228 K	
3937	Valid Approximations >228 K	
4724		Valid Approximations >208 K

The smaller mesh numbers did not comply with the assumptions[9]. The smallest mesh number (1969) means a larger wire diameter and results in higher heat transfer limits; however, the flow regime is turbulent therefore invalidating the initial laminar assumption. This was determined by checking the Reynolds number presented with Equation (2.18) and the Mach number in Equation (2.19). The midsized copper mesh presented some results that supported the flow regime assumptions, but the larger copper mesh performed better.

Using Table 3 as a guideline, the impacts of different section lengths and wick geometries on the operating limits are mapped. The key findings are shown in the following figures and

[8] MATLAB code for predicting the heat transfer limits is found in Appendix E.
[9] The complete data set for the varied mesh size is found in Appendix H.

discussed[10]. Based on the parametric analysis, a double wrapped screen is chosen for the heat pipe wick structure. This type of wick is easy to manufacture and does not appear to be a limiting factor for heat transfer.

With the wick defined, the impacts of varying section lengths are determined based on the total length being constant. Initially all section lengths are equal to create a baseline. Extending the length of the condenser increases the capillary limit, whereas a longer adiabatic section lowers the capillary limit. To allow for greater thermal contact in the condenser and also a higher capillary limit, the evaporator and adiabatic lengths are made equal and the condenser section is slightly longer. A summary of the main geometric features for the nominal heat pipe design are summarized in Table 5.

TABLE 5: PARAMETERS DETERMINED USING MATHEMATICAL MODELING.

Item	Numerical Value
Length of evaporator	76 mm
Length of adiabatic section	76 mm
Length of condenser	102 mm
Number of wick screen wraps	2
Mesh size for the aluminum wicks	4724 / m
Mesh size for copper wicks	3937 / m

The operational limits for the nominal design are numerically tested by varying the heat pipe operating temperature between 198-358K. Acetone and methanol are considered. The results for an aluminum heat pipe containing acetone are displayed in Figure 24. The results for a copper heat pipe containing acetone are displayed in Figure 25. The results for a copper heat pipe containing methanol are displayed in Figure 26.

[10] Detailed data is presented in Appendix I and J.

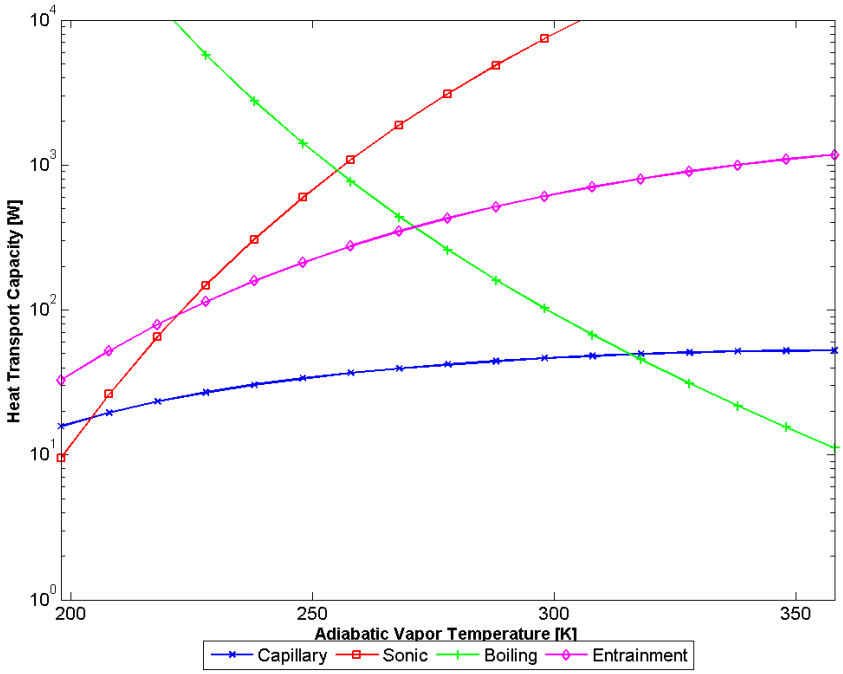

FIGURE 24: THE HEAT TRANSFER LIMITS OF A HEAT PIPE CONTAINING ACETONE IN AN ALUMINUM SHELL, 1.9 CM IN DIAMETER, WITH A #120 MESH, TWICE WRAPPED, ALUMINUM SCREEN WICK.

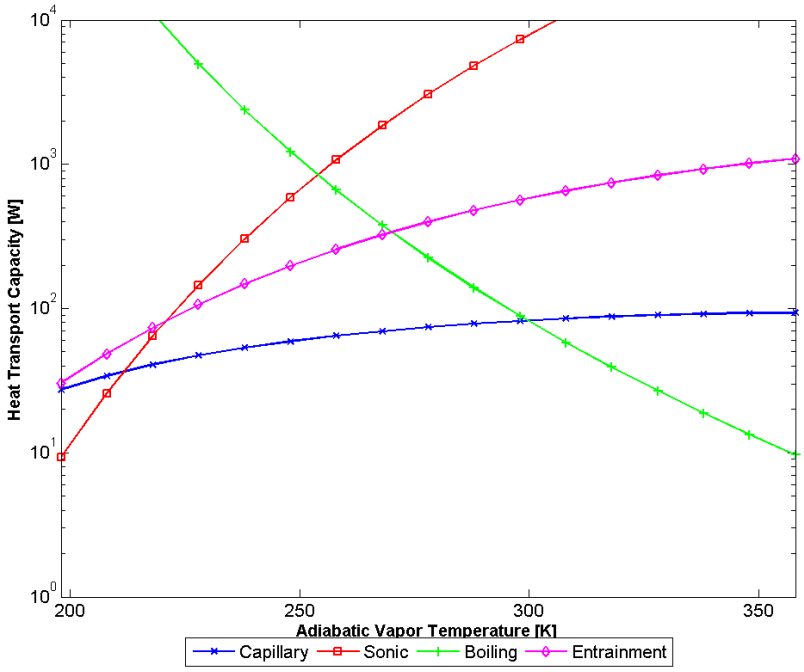

FIGURE 25: THE HEAT TRANSFER LIMITS OF A HEAT PIPE CONTAINING ACETONE IN A COPPER SHELL, 1.9 CM IN DIAMETER, WITH A #100 MESH, TWICE WRAPPED, COPPER SCREEN WICK.

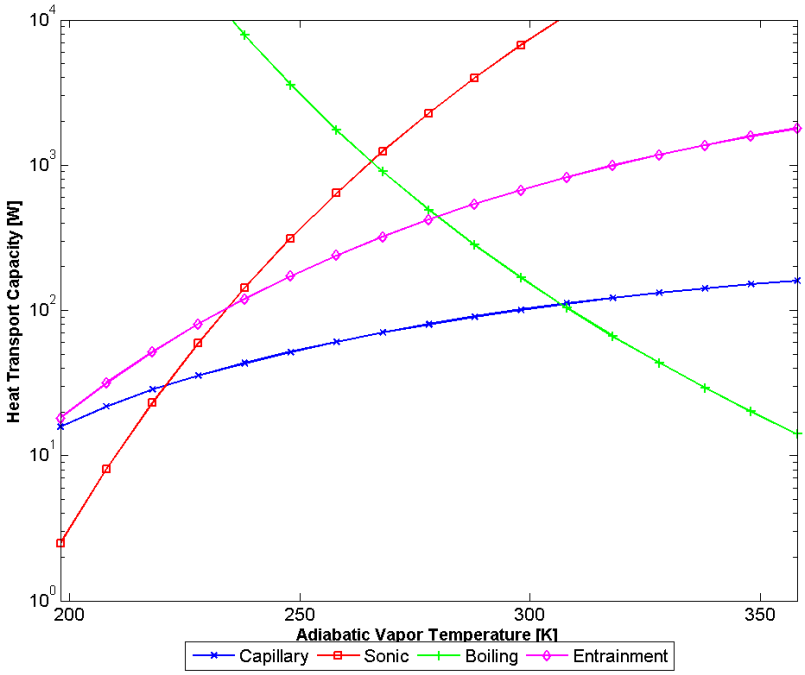

FIGURE 26: THE HEAT TRANSFER LIMITS OF A HEAT PIPE CONTAINING METHANOL IN A COPPER SHELL, 1.9 CM IN DIAMETER, WITH A #100 MESH, TWICE WRAPPED, COPPER SCREEN WICK.

It is evident from observing Figure 24 through Figure 26 that the capillary limit is the governing heat transfer limit for most of the operational temperature range. At low temperatures, the sonic limit dominates, however this limit could be increased by adding additional screen wraps to the wick structure. At higher temperatures, the boiling limit is governing the maximum heat transfer. Based on these results, the expected maximum heat transfer rate that can be obtained while still operating as standard heat pipes (two-phase) is less than 100 W.

The temperature of the evaporator is now determined using the thermal resistance network model described in Section 4.2 and Figure 23.[11] The following assumptions are made:

i. the condenser wall temperature is constant and equal to 195 K.
ii. heat input is prescribed from 10 – 60 W with increments of 10 W.
iii. the heat pipe is in steady-state (heat output is equal to heat input.)

Temperature is calculated with and without the effects of axial conduction in the shell wall. Calculated evaporator temperatures are summarized in Table 6 .

[11] The MATLAB code for solving this network is found in Appendix F.

TABLE 6: TEMPERATURES OF THE EVAPORATOR CALCULATED USING A THERMAL RESISTANCE NETWORK. TEMPERATURES ARE DISPLAYED FOR BOTH CASES EXCLUDING AND INCLUDING AXIAL CONDUCTION. AXIAL CONDUCTION IS VALID FOR THE SPECIFIC GEOMETRY AND COMPONENTS. THE CONDENSER TEMPERATURE IS ASSUMED TO BE CONSTANT AT 195 K.

Heat Applied	Copper Methanol [K]		Copper Acetone [K]		Aluminum Acetone [K]	
[W]	T_e	$T_{e \text{ with axial conduction}}$	T_e	$T_{e \text{ with axial conduction}}$	T_e	$T_{e \text{ with axial conduction}}$
10	203.2	201.3	205.5	202.7	205.5	203.7
20	211.3	207.6	216.4	210.6	216.1	212.5
30	220.3	214.4	227.2	218.3	227.2	221.7
40	228.7	220.9	237.9	226.1	237.9	230.5
50	238.3	228.1	249.7	234.5	249.8	240.2
60	247.0	234.7	260.7	242.4	260.7	249.2

For this particular case, axial conduction through the shell wall does have a significant effect on the evaporator temperature. In the worst case, with a maximum heat input of 60 W, the temperature of the evaporator varies by 18 K when axial conduction is considered. The impacts of axial conduction have a lesser effect at lower heat inputs.

TABLE 7: THE PREDICTED EXPERIMENTAL THERMAL RESISTANCE VALUES.

Heat Applied	Copper Methanol [W/K]		Copper Acetone [W/K]		Aluminum Acetone [W/K]	
[W]	R	$R_{\text{with axial conduction}}$	R	$R_{\text{with axial conduction}}$	R	$R_{\text{with axial conduction}}$
40	0.87	0.66	1.09	0.79	1.05	0.87

The key result in represented by the temperatures in Table 6 is the effective thermal resistance, *R*, of the heat pipes. The calculated values are summarized in Table 7. The *R* value equations in Equation (4.3) to Equation (4.6), and Equation (4.10) to Equation (4.17) are dependent on geometric properties and thermal conductivity. Since the thermal conductivity of aluminum, copper and the working fluids are fairly constant over the operational temperature range, the *R* values are assumed to be similar at varying heat inputs. The predicted resistance is on the order 1 K/W, which is predicted to decrease with increasing wall temperature in the evaporator. For lower temperatures, the opposite is true. These results will be the basis for validating the model against experimental measurements described later.

Internal pressures can vary significantly depending on the fluid properties and operating temperature. The safety factors for the nominal design are checked with variations in wall thickness and tube material. These variations represent possible ranges due to machining operations and are summarized in Table 8. Five different tube thicknesses with three different tube

materials are analyzed for mechanical and thermal stresses using the theory presented in Section 3.2.[12] The ideal factor of safety for each type of stress is three or more when compared to the yield strength of the material [22]. All of the pipe thicknesses for both material types and outer diameters meet that requirement.

TABLE 8: VARIATION IN WALL THICKNESS FOR VARIOUS HEAT PIPE SHELLS FOR STRESS TESTING.

Iter-ation	Original Wall thickness [mm]	Machining Operation	Resulting wall thickness [mm]
1	1.6	Turn down 1 mm off the outer diameter (0.5 mm off each side).	1.1
2	3.2	Turning 1mm off the outer diameter, plus putting an O-ring groove with a depth of 1.27 mm.	1.4
3	1.6		1.6
4	3.2	Removing 1 mm off the outer diameter.	2.7
5	3.2		3.2

4.5 SUMMARY

A nominal heat pipe design is set using the theory presented in Chapter 2. A thermal network model is described which is used to estimate temperature difference between the evaporator and condenser for prescribed heat transfer rates. Thermal performance limits and effective resistance are modeled. A parametric study is performed using different screen mesh sizes, the number of screen wraps, and varying the heat pipe section lengths. The nominal design is found to satisfy safety factor criteria. Chapter 5 details the heat pipe manufacturing process. A new way of assembling heat pipes is presented that does not require welding the end caps to the shell.

[12] The MATLAB code is in Appendix G and the complete data set in Appendix K.

Chapter 5 Heat Pipe Manufacturing

This chapter examines the complete manufacturing process of heat pipes. A new method of assembly is used, therefore avoiding the traditional welding of end caps. Methods of cleaning, assembling, evacuation and charging are presented. The working fluid ratio is determined for both the prototype heat pipes and thermosyphons. The manufacturing process of heat pipes can be broken down into a series of steps as shown by the block diagram in Figure 27.

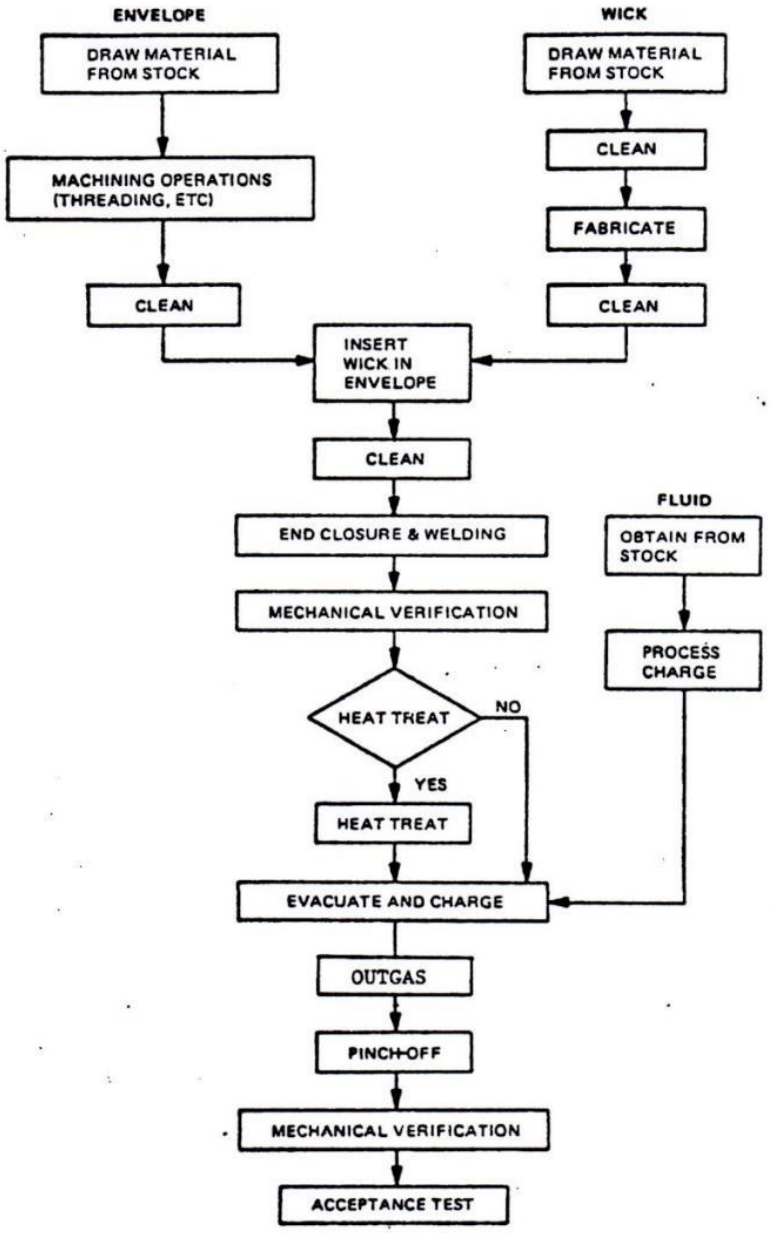

FIGURE 27: HEAT PIPE MANUFACTURING BLOCK DIAGRAM [22].

The process of can be simplified into seven distinct steps:

1. Selecting the appropriate working fluid, shell and wick structure.
2. Machining the shell, end caps, fill tube and forming the wick structure.
3. Cleaning all the components.
4. Assembling the components using brazing or welding.
5. Checking the heat pipe for leaks.
6. Evacuating the heat pipe and charging with working fluid.
7. Sealing the heat pipe using a crimping tool and welding the fill tube shut.

The following sections provide a detailed description of the methods for manufacturing, cleaning, assembly and filling.

5.1 MACHINING

Manufacturing challenges include attaching the end caps to the heat pipe, ensuring the heat pipe can hold pressure, getting a proper seal on the crimped fill tube, and designing an evacuation and charging system to fill the heat pipes. All of the literature reviewed on manufacturing of heat pipes recommends welding the end caps, crimping the fill tube, and then welding the crimped end. Welding a heat pipe filled with acetone or methanol is a safety concern because there is a risk of explosion. Welding the end caps is also a concern because the wall of the heat pipe is thin and, therefore, accuracy is challenging. To avoid these issues, an alternative to welding is determined for building the prototype heat pipes.

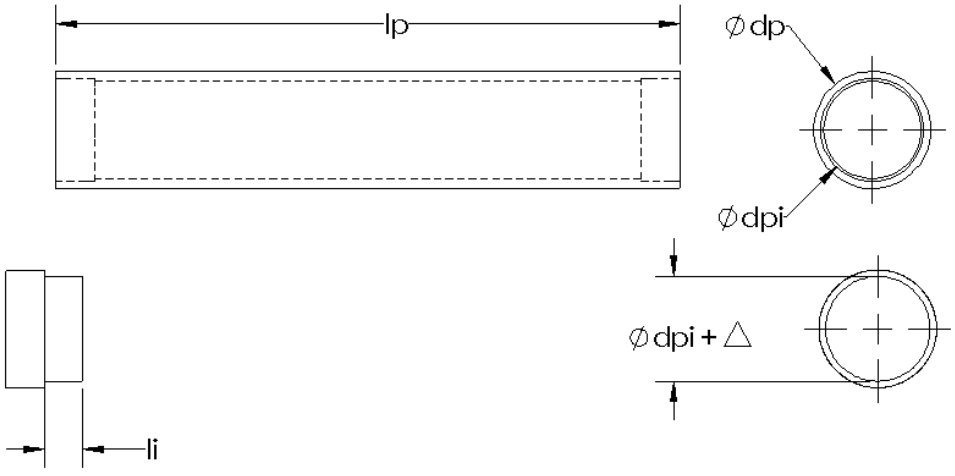

FIGURE 28: INTERFERENCE FIT OF THE SHELL (ON TOP) AND THE END CAPS (ON BOTTOM).

A first prototype heat pipe was constructed using an interference fit between the end cap and the pipe body as specified in Table 9 and shown in Figure 28. Aluminum tube was used for the shell and internally bored on a lathe until concentric at d_{pi}. Then two end caps were turned to have a larger diameter, Δ, for a set length, l_i, within the heat pipe shell. One end cap had a ¼" NPT female thread which was used for pressure testing with compressed air. The end caps were press fit onto the body using a vice. When the prototype was tested using compressed air, leaking was immediate and one end cap came off.

TABLE 9: NUMERICAL VALUES USED FOR ITERATION ONE OF THE PROTOTYPE PRESSURE TESTING.

Item	Numerical Value	Units
Pipe diameter	19.05	mm
Interference fit delta	0.127	mm
Interference fit length	6.35	mm
Measured press fit pressure required	20684	kPa
Compressed air pressure	414	kPa

FIGURE 29: PROTOTYPE HEAT PIPE USED FOR PRESSURE TESTING. THE ENDCAP ON THE LEFT IS BARBED WITH AN O-RING TO CREATE A FLUID SEAL, THE BODY IN THE MIDDLE IS BARBED ON THE INSIDE TO INTERFERE WITH THE ENDCAP AND LASTLY THE ENDCAP ON THE RIGHT HAS AN NPT FEMALE THREAD TO CONNECT COMPRESSED AIR AFTER THE HEAT PIPE IS ASSEMBLED.

A second prototype was constructed in a similar way except the two end caps were turned to have a larger diameter, thereby increasing the interference fit. Pressure testing showed that the heat pipe still leaked, but this time the end cap stayed in place. A third prototype was made in a similar manner to the second, but with barbs on the end caps, as seen in Figure 29. While slower than prototype two, the heat pipe still leaked. A fourth prototype was built using barbs on the inner

diameter of the shell. Leaking was reduced, but still present. Using higher pressures resulted in the end caps staying in place even with multiple cycles. The numerical values for iterations two to four are found below in Table 10.

TABLE 10: NUMERICAL VALUES USED FOR ITERATIONS TWO TO FOUR FOR PRESSURE TESTING.

Item	Numerical Value	Units
Pipe diameter	19.05	mm
Interference fit delta	0.254	mm
Interference fit length	6.35	mm
Compressed air pressure	689	kPa

A fifth prototype was constructed using an O-ring and barbs on the end caps, in addition to barbs on the shell as shown in Figure 29. The pipe was pressurized to approximately 4.5 times the expected pressure when using acetone near 308 K. At the time of writing the heat pipe has maintained pressure for over eleven months indicating a successful seal was obtained. The numerical values are in Table 11 below.

TABLE 11: NUMERICAL VALUES USED FOR ITERATION FIVE OF THE PROTOTYPE PRESSURE TESTING.

Item	Numerical Value	Units
Pipe diameter	19.05	mm
Interference fit delta	0.254	mm
Interference fit length	6.35	mm
Acetone pressure at 308 K	46	kPa
Compressed air pressure	207	kPa
Pressure safety factor minimum	4.5	
O-Ring size	14	

With the end-cap sealing solved, the next sealing challenge was the fill tube. A crimping tool was purchased and tests were done on both copper and aluminum tubes. The copper tubes were successfully crimped and pressure tested; however, the aluminum tubes were more difficult and brittle fractures appeared on the exterior surface. Because both acetone and methanol are compatible with copper, the fill tube end caps were constructed out of copper for all prototypes.

FIGURE 30: PROCESS OF MACHINING THE COPPER HEAT PIPES. 1. BORING THE SHELL. 2. BARBING THE SHELL. 3. TURNING DOWN THE OUTER DIAMETER OF THE EVAPORATOR AND ADIABATIC SECTIONS. 4. ADDING GROOVE FOR THERMOCOUPLE LOCATIONS. 5. ADDING THE O-RING GROOVE TO THE END CAP. 6. ADDING BARBS TO THE END CAP. 7. COMPLETED HEAT PIPE COMPONENTS. 8. SOLDERING THE FILL TUBE INTO THE END CAP. 9. ASSEMBLED HEAT PIPE.

End cap manufacturing involved significant trial and error. Attempts to machine the fill tube end cap out of a single piece of copper resulted in multiple broken drill bits. This is because of the poor machinability of copper, the small internal diameter of the fill tube, and a small diameter drill bit which lacks strength. Sealing of the fill tubes was also a challenge. After numerous attempts, the method arrived at for sealing the fill tube involved an initial crimp and then using a small bead of solder on the opening.

Based on the experiences described above, four beta prototypes were designed and fabricated as shown in Figure 30[13]. Later the heat pipes were redesigned to be slightly shorter than the originals with external grooves for thermocouple placement, and six 2nd generation beta prototypes were manufactured.

5.2 CLEANING

The cleaning process can be broken down into three stages: (1) an initial cleaning to remove debris and metal filings, (2) a chemical cleaning removing oil, water and films, and, (3) a final rinse removing solvents and etchants [17]. Proper cleaning procedures can help to reduce the presence of both impurities and non-condensable gases within the heat pipe [14].

Each type of metal has a recommended cleaning procedure. Initially, the methods described by Peterson were used [15]. For one step, he suggests soaking in a 50% nitric and 50% phosphoric acid mix, which proved to be destructive; therefore, the pipes were remade and the cleaning procedure for both aluminum and copper was altered to remove the use of acid. The final cleaning process for the aluminum heat pipes is as follows:

1. Scrub components with a wire brush using dish soap.
2. Scrub components with a wire brush using degreaser and soak for thirty minutes.
3. Rinse in working fluid (acetone) and soak for one hour.
4. Rinse again in working fluid (acetone).
5. Rinse with anhydrous isopropyl alcohol.
6. Dry with compressed air.

[13] Using the drawings found in Appendix L

The procedure for the copper heat pipes is similar:

1. Scrub components with a wire brush using dish soap.
2. Scrub components with a wire brush using degreaser soak for thirty minutes.
3. Soak copper components in acetone for one hour to remove oil and grease.
4. Rinse in working fluid (methanol or acetone) and soak for one hour.
5. Rinse again in working fluid (methanol or acetone) and dry with compressed air.

Upon completion of cleaning, the assembly of the heat pipes can begin. This process is described in the following section.

5.3 ASSEMBLY

FIGURE 31: VARIOUS PRESS FITTING METHODS. ON THE LEFT ARE THREE DIFFERENT DEVICES USED TO PERFORM THE PRESSFIT; 1. A VICE, 3. A HYDRAULIC PRESS AND 5. A LATHE. ON THE RIGHT THE RESULTING PROBLEMS WITH THE FIRST TWO METHODS, 2. AND 4. AND THE FINAL ASSEMBLED 2ND GENERATION BETA PROTOTYPES AT 6.

The assembly process was also iterative to find the most reliable way to press fit the end caps into the shell. Attempting a press fit using a vice resulted in misalignment, as shown in Figure 31 Photo 2. This happened because the vice was only applying pressure to the bottom half of the end cap. Next press fitting was attempted using a hydraulic press, as shown in Figure 31 Photo 3. The initial test was successful. However, this method applied excessive force resulting in a sharp lip and visible stress fractures, as seen in Figure 31 in Photo 4.

Press fits were then attempted using a lathe. This method allowed for moderately applied force and inherent alignment between the lathe and drill chucks, as shown in Figure 31 Photo 5. A total of six 2nd generation beta prototypes were assembled; four copper and two aluminum. The aluminum pipes contain acetone, one is a heat pipe and the other a thermosyphon. The copper pipes consist of a methanol thermosyphon, and three heat pipes; two containing methanol and the other acetone. The final assembled pipes are shown in Figure 31 Photo 6.

5.4 Evacuation and Charging

Heat pipe charging systems vary depending on the working fluid and operational temperature of the heat pipes. The charging rigs can be simple, as seen on the left of Figure 32 or more complicated, as seen on the right.

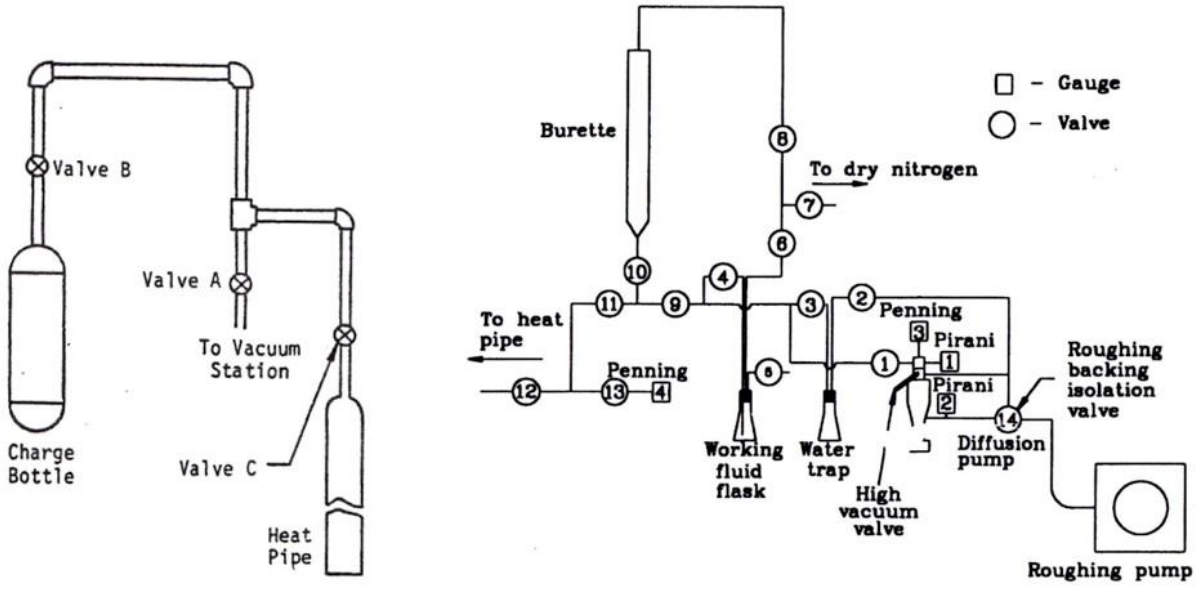

FIGURE 32: HEAT PIPE CHARGING RIGS; SIMPLE ON THE LEFT [22] AND COMPLEX ON THE RIGHT [15].

For heat pipes that are in the low temperature and room temperature operational range, a general filling procedure is outlined as follows:

1. Mount the heat pipe to a filling rig equipped with a high vacuum pump and evacuate for 24 hours or until a pressure of 1.33×10^{-5} Pa is reached [15].
2. Introduce a flush or purge working fluid charge into the heat pipe.
3. Evacuate the flush charge.
4. Introduce final working fluid charge.
5. Seal the heat pipe

A vacuum system was assembled using a combination of valves, KF, ISO and CF connections[14]. A burette was used to add working fluid into the heat pipe. A schematic of the vacuum and filling rig is shown in Figure 33.

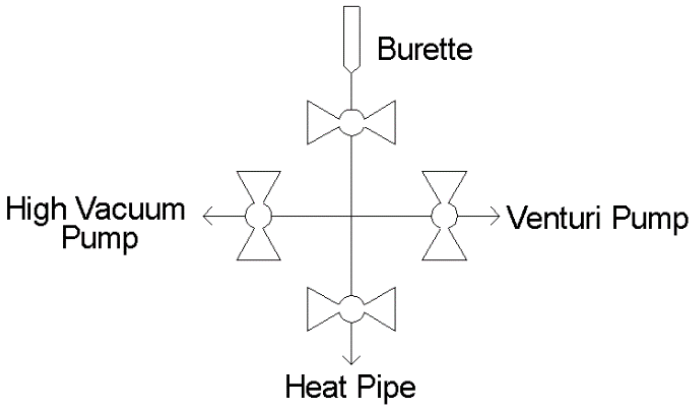

FIGURE 33: SIMPLIFIED EVACUTATION AND FILLING RIG SCHEMATIC.

The high vacuum system used was an Agilent TPS Mobile unit that was equipped with a TV551 NAV turbo molecular pump, a TS 600 dry scroll roughing pump, a XGS-600 gauge controller and a Varian ConvecTorr P-type gauge. An additional cold cathode gauge measures low pressures, a Leybold Vakuum GmbH, D-50968 Type PR25. A Vacoon JS-90M fixed venturi vacuum pump is used to remove the initial working fluid purge fill.

Two experiments were run to determine the lowest pressure attainable. The first experiment was run using the vacuum pump only. The second experiment used a heat gun at various intervals to accelerate the removal of vapor. Using heat and vacuuming for 19 hours resulted in lower

[14] The vacuum system building process can be seen in Appendix P.

pressures than 26 hours without heat. The pressure of each experiment was recorded for the first hour, before the purge charge was added, and then again before the filling of the final charge.[15]

A series of fill tests were performed on the beta heat pipe, HPB, and thermosyphon, TSB, (that were damaged by the acid cleaning process) to determine working fluid filling losses. The pipe was placed under deep vacuum for 20 mins before a 10 ml charge of methanol was added to the system. The charge was allowed two minutes to enter the pipe. The pipe was then removed and weighed and the rough pump used for 10 minutes to remove any remaining charge left in the vacuum system. The filling losses were greater for the thermosyphon tests. The results from these tests were used to predict the amount of fluid to add for the actual charging of the pipes. After each heat pipe or thermosyphon was filled the losses were recorded and used to get a better prediction for filling the next one.

The evacuation and charging procedure used on the 2nd generation beta pipes took approximately 24 hours and included an initial one hour vacuum, followed by a flush charge, then 22 hours under deep vacuum, and then the final working fluid charge was introduced.

5.5 Working Fluid Filling Ratio

A study by Lui et al. on closed loop pulsating heat pipes found the optimal filling ratio for water is 41% and ranges between 35% to 41% for methanol [34]. A study by Badran et al. using micro heat pipes found the optimal filling ratio is 5% and because they are orders of magnitude smaller than conventional heat pipes stated that this number aligned with the convention of filling to 10% for regular heat pipes [35]. Peterson suggests over filling heat pipes by 10-20% of the total volume of the arteries, grooves, etc. [15]. Based on this the heat pipes will be filled to a filling ratio of 10% over of the total inner volume of the wick structure, which is 6.1 ml, using the sample calculation of Equation (4.22).

$$V_t = 1.1\left(\frac{\pi l}{4}\left(d_{pi}^2 - d_v^2\right)\right) = \frac{\pi(0.254m)}{4}\left(0.0158^2 - 0.0149^2\right)\frac{1x10^6 ml}{m^3} = 6.06ml \qquad (5.1)$$

[15] See Appendix Q. The complete data set of all experiments is found in Appendix R.

A thermosyphon fill volume ratio study performed by Lin et al. found that the optimal fill volume for a thermosyphon ranged between 35-40% when working with water or alcohol [24]. Hussein et al. performed a study on cylindrical thermosyphons containing water and found the optimal filling ratio is 20% [36]. Noie found maximum heat transfer rates based on the aspect ratio of the evaporator length to the inner diameter maximized when the fill ratio is 60% for an aspect ratio of 11.8 when using distilled water as the working fluid [37]. Taking the average of the above studies results in a filling volume of the thermosyphons of 36.6%, which is 18.2 ml.

5.6 SUMMARY

An iterative design and manufacturing process was followed to ensure the prototypes could hold pressure and were fluid tight. As a result, the end caps were designed with an interference fit and an O-ring. All components were cleaned to remove debris, oils, films and other potential contaminants. The prototypes were press fit together on a lathe to ensure alignment.

TABLE 12: SUMMARY OF THE EVACUATION AND CHARGING OF THE BETA HEAT PIPES AND THERMOSYPHONS.

Pipe #	Material	Type	Fluid	Vacuum Pressure [Pa]	Charge Introduced [ml]	Fill Volume [ml]	Filling Losses [ml]	Ideal Fill [ml]	Error [%]	Filling Ratio [%]
HPB	Cu	HP	M	1.10E-02	10.7	7.73	2.97	6.1	26.7	14
TSB	Cu	TS	M	4.40E-01	25.3	19.81	5.49	20	-0.9	35.8
HP1	Cu	HP	M	1.10E-03	9.6	4.06	5.54	6.06	-33	7.3
TS2	Cu	TS	M	5.70E-02	24.6	17.1	7.5	18.23	-6.2	30.9
HP3	Cu	HP	M	6.90E-03	11.57	6.14	5.43	6.06	1.4	11.1
HP4	Cu	HP	A	7.30E-03	11.57	6.33	5.24	6.06	4.4	11.4
HP5	Al	HP	A	1.20E-02	11.5	5.44	6.06	6.06	-10.2	9.8
TS6	Al	TS	A	2.00E-02	25.73	19.4	6.33	18.23	6.4	35.1

The targeted filling ratio for the heat pipes and thermosyphons was 10% and 36% respectively. Table 12 displays a summary of the final vacuum pressure achieved before filling, the charge volume introduced, the charging losses and the resulting filling ratio and error associated with each fill.

Chapter 6 presents the testing apparatus and data acquisition system that will be used for heat transfer testing. The testing procedure is also outlined.

Chapter 6 Heat Pipe Testing

This chapter presents the heat transfer testing procedure, the testing apparatus, experimental equipment used, and the data acquisition system. The apparatus is designed so that a known heat load can be applied to the evaporator and the temperature distribution can be measured. This data is used to determine the effective thermal resistance as a function of load.

6.1 Testing Apparatus

The testing apparatus is designed to thermally isolate one heat pipe from the surroundings. This allows heat transfer limitations to be tested and compared to simulation results. The apparatus consists of six components; a heat sink, insulation, thermocouples, a DC heater, a fixture to hold the heater in place and a data acquisition system, all shown below in Figure 34.[16]

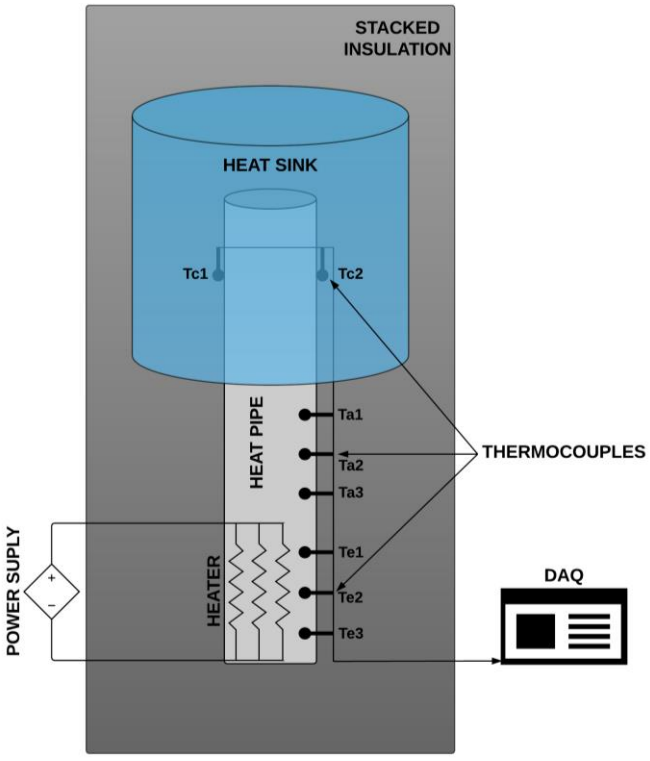

Figure 34: The thermally isolated heat pipe testing apparatus, consisting of insulation, heat sink, heat pipe, heater, heating fixtures thermocouples and DAQ system.

[16] Engineering drawings for the heat sink and insulation are found in Appendices M and N.

Surface-mount T-type thermocouples are placed on the heat pipes at six locations, three in both the evaporator (Te1, Te2 and Te3) and adiabatic sections (Ta1, Ta2, and Ta3). Two additional T-type thermocouples (Tc1 and Tc2) are used in the heat sink compartment, near the condenser section of the heat pipe. An Omega Kapton flexible resistance heater is wrapped around the evaporator section and provides up to 60W of heat using a XANTREX XPD 120-4.5 DC power supply. Thermal grease and a fixture are used to ensure good thermal contact and to prevent expansion away from the heat pipe surface during operation [14]. Artic Silver Ceramique thermal grease was used for all experiments. The heating fixture is a cylinder with a hole in the middle for the heat pipe and heater to fit into. As shown in Figure 38, 3 - 9, the fixture is cut vertically twice to create a removable section wherein the thermocouples are placed. The fixture is held together with zip ties that fit into three recessed pockets. [17]

The heat pipe must be thermally insulated from the surroundings to ensure the heat input is transferred through the heat pipe. At room temperature, insulation blankets made of fiberglass or ceramic wool are sufficient. Below room temperature condensation is an issue that can be minimized by using closed cell foam insulation [14]. Cryogenic heat pipes require vacuum chamber testing to prevent parasitic heat inputs from ambient [14]. Alternating layers of aluminum mylar and nylon netting are used for cryogenic insulation [14]. For the temperature range considered here, stackable closed cell polyethylene foam rubber insulation is used. This insulation was also chosen because it is safe to cut using a laser cutter, which is how all the stackable pieces were manufactured. Key insulation properties are found in Table 13.

TABLE 13: POLYETHYLENE INSULATION SPECIFICATIONS.

Heat flow rate (K Factor)	0.25
Temperature Range	72 - 372 K
Density Range	16-32 kg/m3
Sheet thickness	19 mm

The heat pipe condenser is immersed in a liquid acetone bath containing solid CO_2. The heat sink container is designed with alignment in mind, as shown in Figure 35. A simple post and

[17] Engineering drawings for the fixture are found in Appendix N.

plate method is used to compress the O-rings that seal the main compartment. As shown in pictures 1-4 of Figure 35, the main heat sink compartment is sealed with two plates, containing O-rings, by torqueing nuts located on the top and bottom of ready rod. As shown in 2 of Figure 35, four interior nuts are used to hold the ready rod in place on the bottom plate. Once the main compartment is assembled a heat pipe can be placed inside. The larger diameter condenser section of the heat pipe provides a lower stopping point in the heat sink chamber, because it will not fit through the container hole. The container is turned upside down and the heat pipe is held in position while the final sealing step is finished. An O-ring is placed over the evaporator section and slid up to the container base, shown in 5 of Figure 35. An additional lower O-ring plate is then used to sandwich the O-ring surrounding the heat pipe and create the final fluid seal between the heat sink compartment, shown in 6 of Figure 35. [18]

FIGURE 35: THE CONTAINER USED FOR THE HOLDING THE BATH OF ACETONE AND SOLID CO_2 USED AS THE EXPERIMENTAL HEAT SINK. 1. UPPER PLATE. 2. LOWER PLATE WITH HOLE FOR HEAT PIPE AND READY ROD HOLES FOR O-RING COMPRESSION. 3.SAME AS 2. WITH CONTAINER FOR HEAT SINK MATERIALS. 4. ASSEMBLED CONTAINER. 5. AN UPSIDE DOWN VIEW WITH THE HEAT PIPE INSERTED INTO THE BOTTOM AND DISPLAYING THE O-RING THAT WILL BE USED FOR SEALING. 6. COMPLETE ASSEMBLY WITH HEAT PIPE SEALED IN PLACE.

[18] Engineering drawings for the testing apparatus are found in Appendix M.

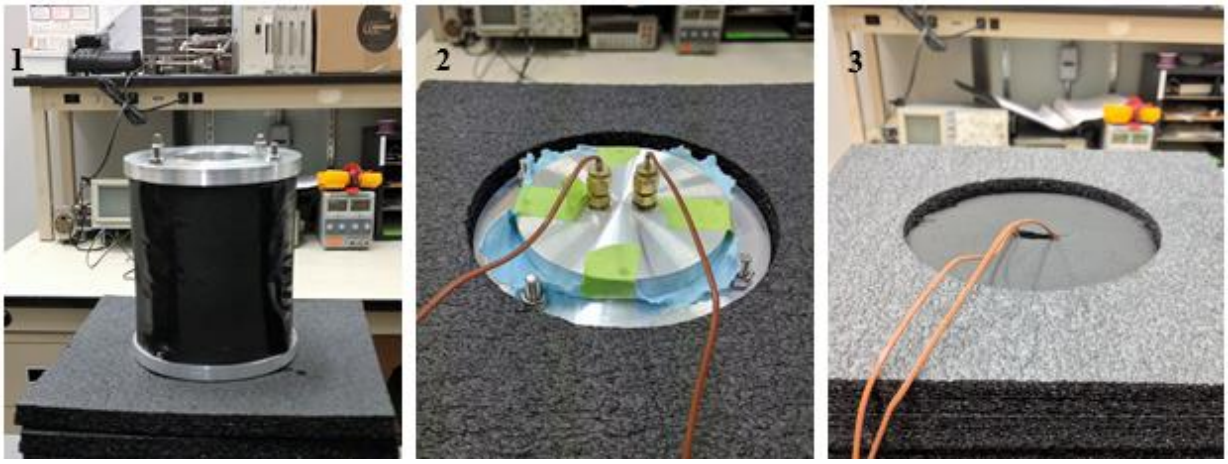

FIGURE 36: ADDING ADDITIONAL INSULATION TO THE TESTING APPARATUS AROUND THE HEAT SINK AND UPPER SEALING PLATE.

With the heat pipe mounted on the condenser bath, the testing apparatus is assembled using the following steps:

1. The O-ring surfaces are cleaned.
2. The heat sink is assembled, using two #149 O-rings and clamping together the plates using nuts and ready rod, as shown in Figure 35 in Pictures 2 to 4.
3. Insulation is wrapped around the heat sink, as shown in Figure 36, Picture 1.
4. Insulation is added around the upper sealing plate, as shown in Figure 36, Picture 3.
5. The heat pipe is mounted into the heat sink using a #115 O-ring. The O-ring plate compresses the O-ring using four screws, as shown in Figure 37, Picture 1.
6. One at a time the thermocouples are mounted onto the adiabatic section of the heat pipe and insulation is stacked over them. First the thermocouple is mounted to a piece of electrical tape, as shown in Figure 37, Picture 2. Then thermal paste is added in Picture 3. Then the three thermocouples are mounted, shown in Pictures 4 to 8.
7. The heater is covered in thermal paste, mounted to the evaporator section and the heating fixture placed on top, as shown in Figure 38, Pictures 1 – 3. Next, the three thermocouples and mounted and the fixture closed using zip-ties, shown in Pictures 5 and 9. The lower apparatus is placed into the lower polyethylene insulation sections and now rests on the stack of insulation and the heater leads are connected, shown in Picture 1 of Figure 39.

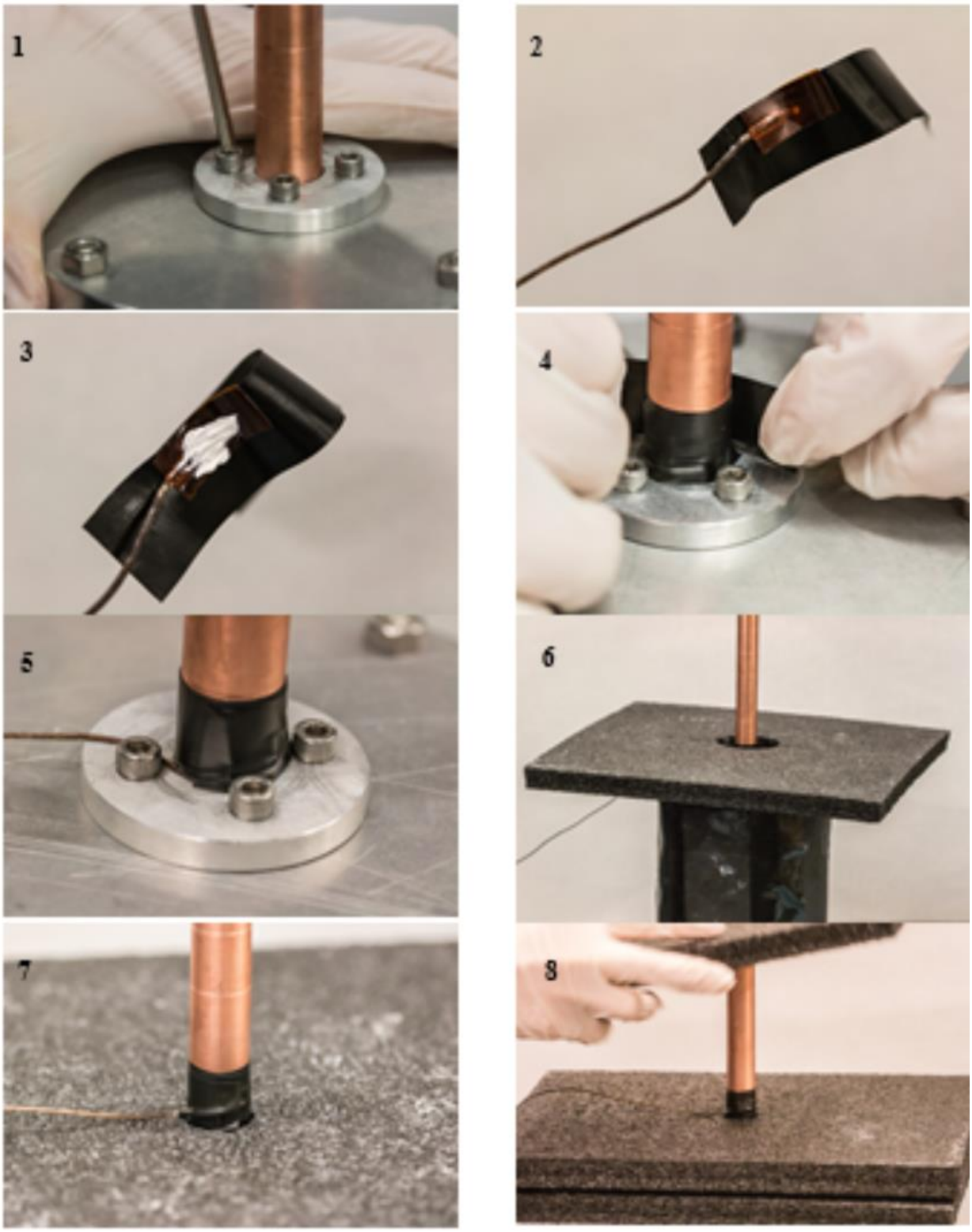

FIGURE 37: PHOTOS OF MOUNTING THE THERMOCOUPLES TO THE ADIABATIC SECTION.

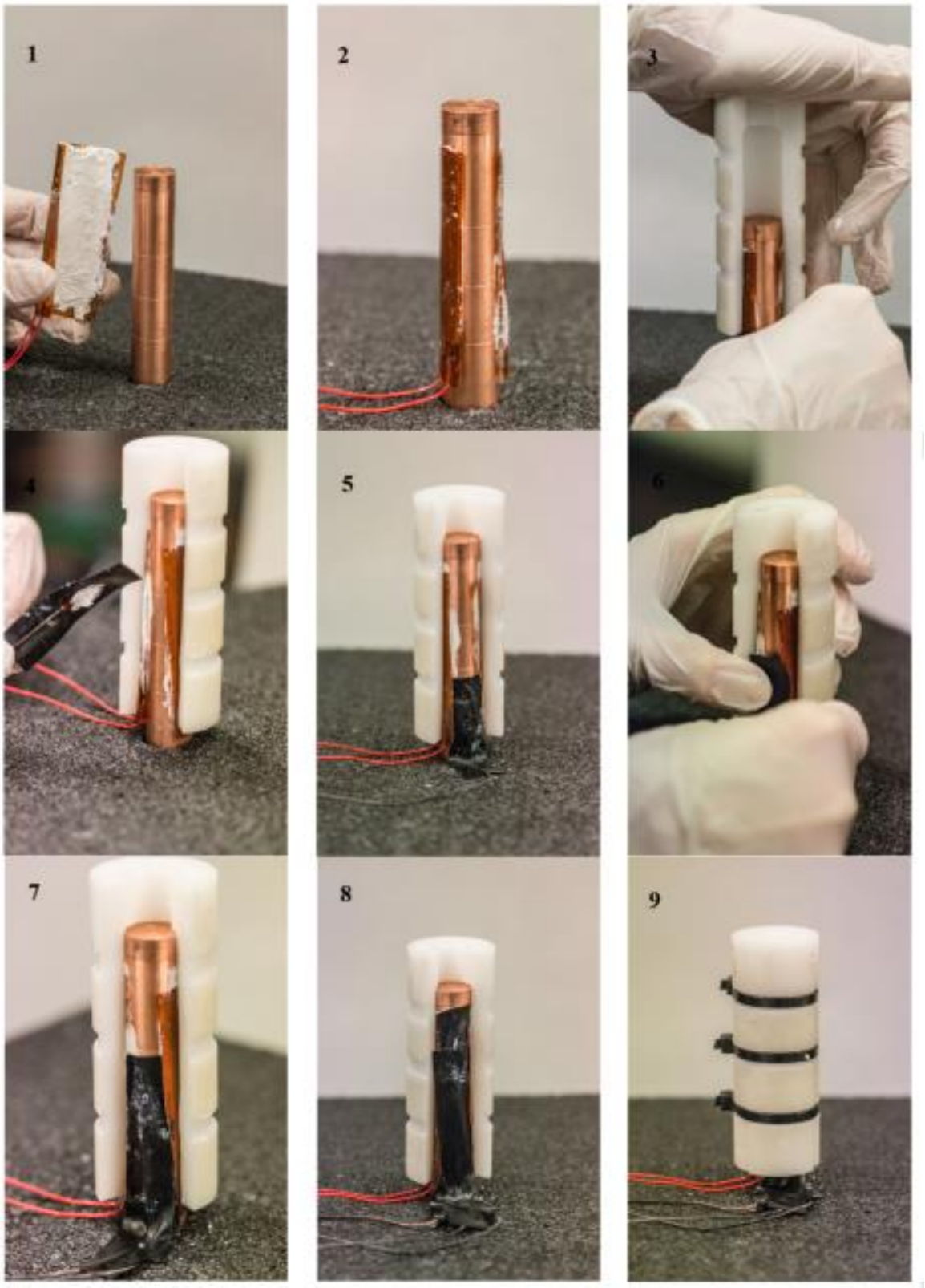

FIGURE 38: PHOTOS OF MOUNTING THE HEATER AND EVAPORATOR THERMOCOUPLES.

8. The heat sink chamber is filled with solid CO_2 and acetone, as shown in Figure 39, Picture 2. The last two thermocouples are mounted into the top of the heat sink fixture, where they will measure the temperature of the condenser.
9. The remaining insulation is stacked on top and a heavy object such as a book is placed on top to compress the layers of stacked insulation, as shown in Figure 39, Picture 3.
10. Testing is ready to begin.

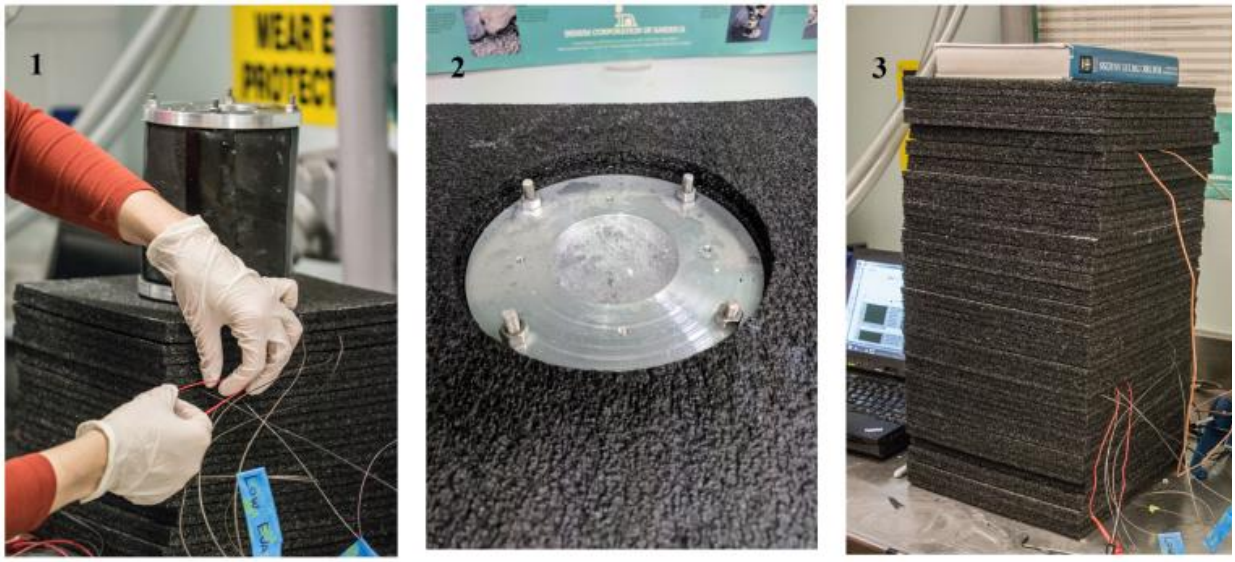

FIGURE 39: PHOTOS OF FINAL EXPERIMENTAL SET UP. PICTURE 2 DISPLAYS THE HEAT SINK FILLED WITH ACETONE AND SOLID CO_2.

6.2 DATA ACQUISITION

Data is collected using National Instruments signal conditioning equipment driven by a LabVIEW virtual instrument. During an experiment, each thermocouple collects data with a sampling rate of 1 Hz. For each 30 second sample window, data for each thermocouple is averaged and the resulting value is recorded in a separate excel file. The six average values of the adiabatic and evaporator thermocouples are recorded in an array within LabVIEW. Once 20 sets of data have been collected, then LabVIEW compares the new data set to the data set from 20 measurements ago. If there has been greater than or equal to 0.5 K change in any of the thermocouples, then data collection continues. If there is less than a 0.5 K change then LabVIEW will stop collecting data because steady state has been achieved.

Prior to setting 0.5 K as the tolerance for steady-state, scientific literature was reviewed. Do et al. [27] define steady state in their experimental work as a temperature change less that 0.1 K over a period of two minutes. Li et al. [29] used less than 0.1 K change over 30 seconds. Initial testing using Do's definition showed that 0.1 K was unsuitable for the laboratory environment. Instead, steady-state is defined based on less than a 0.5 K change in each of the adiabatic and evaporator thermocouples over a period of 10 minutes. Subsequent testing indicated that this criterion was sufficient.

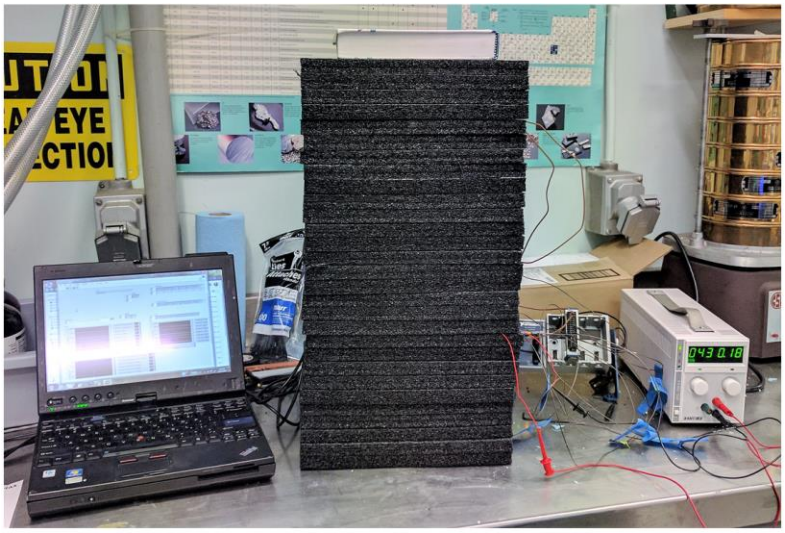

FIGURE 40: PHOTO OF EXPERIMENTAL SETUP.

Figure 40 displays a photo of the experimental set up during a test.

6.3 SUMMARY

A testing apparatus was built to thermally isolate a heat pipe from the environment. Eight T-type thermocouples measure the temperature in the condenser, adiabatic and evaporator sections. A flexible Kapton heater wrapped around the evaporator section supplies up to 60 W thermal load. Cooling in the condenser is either from a dry ice and acetone mix, or from ice water.

Chapter 7 presents the results of the manufacturing process and the heat transfer testing. Multiple figures display the difference is steady state temperature and thermal resistance. Displayed side by side are prototypes with different filling ratios, different case materials, different working fluids and finally comparing heat pipe, to a thermosyphon, and an insulated copper tube.

Chapter 7 Results

Representative experimental results are displayed in this chapter. Heat loads of up to 60 W are applied and the experiments are run until steady state is achieved. Example data plots showing the evolution of temperature during an experiment i.e. transient results, are presented. The behaviour of heat pipes is compared to a copper shell with no charge fluid. Finally, the steady-state temperature distributions are shown. Results are discussed in more detail in Chapter 8.

The characteristics of the two beta and six final prototypes are summarized again in Table 14 as reminder of the differences between them. The data are referred to using a naming convention consisting of the "Type" column and the "Pipe #" column. Hence, pipe 2 does not have a wick, therefore, it is a thermosyphon and the label "TS2" is used. Likewise, pipe number 5 would be "HP5". The inert copper shell is referred to as "CR". Finally, a dash after the name is followed by the heat load conditions; thus, pipe number 2 operating with a 4 W load would be "TS2-4W".

TABLE 14: SUMMARY OF THE EVACUATION AND CHARGING OF PIPES.

Pipe #	Material	Type	Fluid	Vacuum Pressure [Pa]	Charge Introduced [ml]	Filling Losses [ml]	Ideal Fill [ml]	Error [%]	Filling Ratio [%]
HPB	Cu	HP	M	1.10E-02	10.7	2.97	6.1	26.7	14
TSB	Cu	TS	M	4.40E-01	25.3	5.49	20	-0.9	35.8
HP1	Cu	HP	M	1.10E-03	9.6	5.54	6.06	-33	7.3
TS2	Cu	TS	M	5.70E-02	24.6	7.5	18.23	-6.2	30.9
HP3	Cu	HP	M	6.90E-03	11.57	5.43	6.06	1.4	11.1
HP4	Cu	HP	A	7.30E-03	11.57	5.24	6.06	4.4	11.4
HP5	Al	HP	A	1.20E-02	11.5	6.06	6.06	-10.2	9.8
TS6	Al	TS	A	2.00E-02	25.73	6.33	18.23	6.4	35.1

7.1 TRANSIENT THERMAL RESPONSE

The figures presented in this section are representative of the data collected during a typical experiment. Figures are presented in side by side comparisons of similar configurations[19].

[19] The complete figure set for all experiments is found in Appendix T.

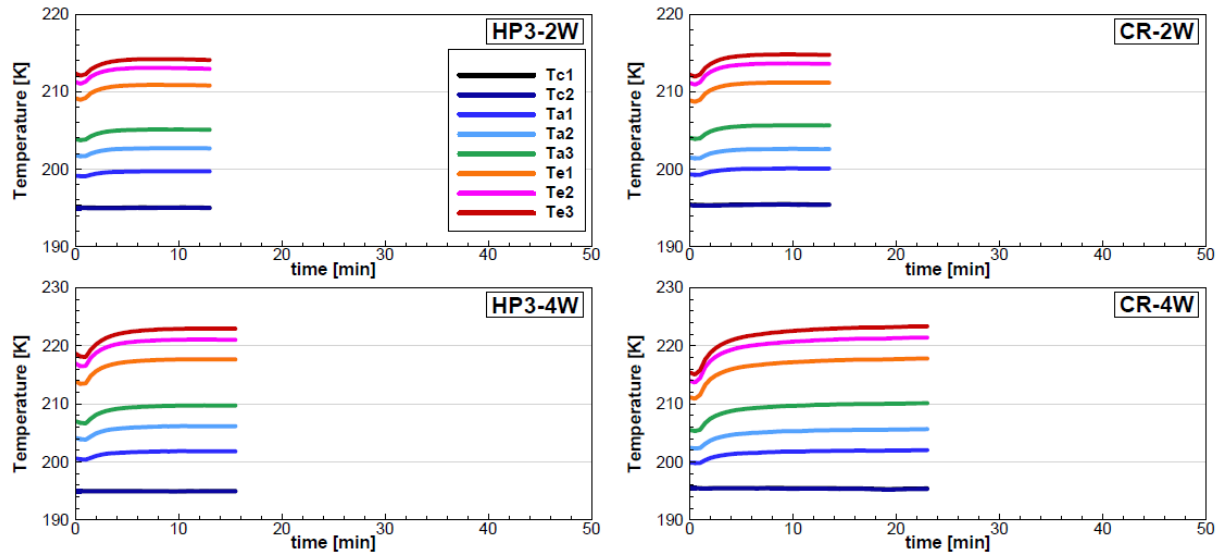

FIGURE 41: TRANSIENT THERMAL RESPONSE COMPARISON OF PERFORMANCE BETWEEN AN INSULATED COPPER ROD AND HP3. THE HEAT SINK CONTAINS DRY ICE AND ACETONE AND LOW HEAT LOADS ARE APPLIED.

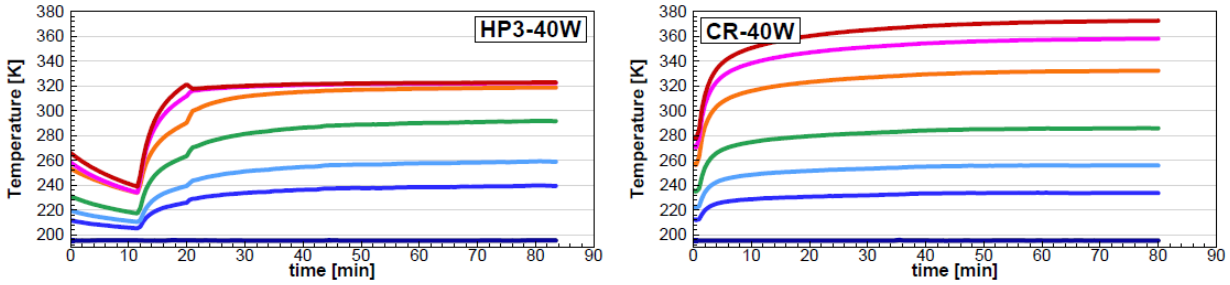

FIGURE 42: TRANSIENT THERMAL RESPONSE COMPARISON OF PERFORMANCE OF HP3 AND CR AT HIGH LOADS.

Figure 41 and Figure 42 compare HP3, a copper methanol heat pipe, to an insulated copper tube (CR), at low and high loads, when the condenser is cooled using a bath of acetone and dry ice. Heat inputs are varied from 2 W to 10 W in steps of 2 W for the low load testing. For the high load testing the heat input is varied from 10 W to 60 W in steps of 10 W. The minimum temperatures show when the experiment was started. Subsequently, the temperatures increase over time until steady state is achieved.

At low loads (2 and 4 W) HP3 has temperature distributions similar to the copper rod. This occurs because at low temperatures the heat pipe fluid has little heat transfer capacity and, the primary method of heat transfer is axial conduction. A key feature in Figure 42 for HP3 is the rapid change in temperatures throughout the heat pipes as the evaporator reaches 320K.

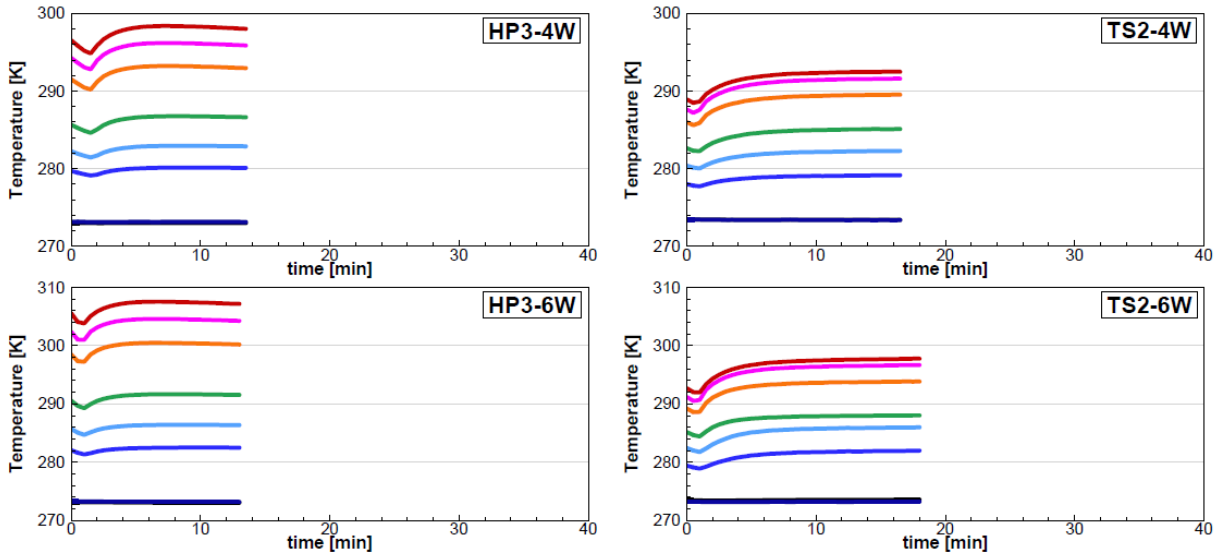

FIGURE 43: COMPARISON OF PERFORMANCE BETWEEN HEAT PIPE AND THERMOSYPHON IN A COPPER CASE WITH METHANOL AS THE WORKING FLUID. THE HEAT SINK CONTAINS ICE WATER AND LOW HEAT LOADS ARE APPLIED.

In addition to a dry-ice acetone bath, testing was done on HP3 and TS2 using ice water for cooling and representative comparisons are displayed in Figure 43 and Figure 44. The most noticeable difference seen when comparing the performance of HP3 in Figure 41 to Figure 43, is the higher overall temperatures. Comparing HP3 to TS2, one can see the temperature gradient is smaller for TS2 indicating the thermosyphon has a lower overall thermal resistance than HP3.

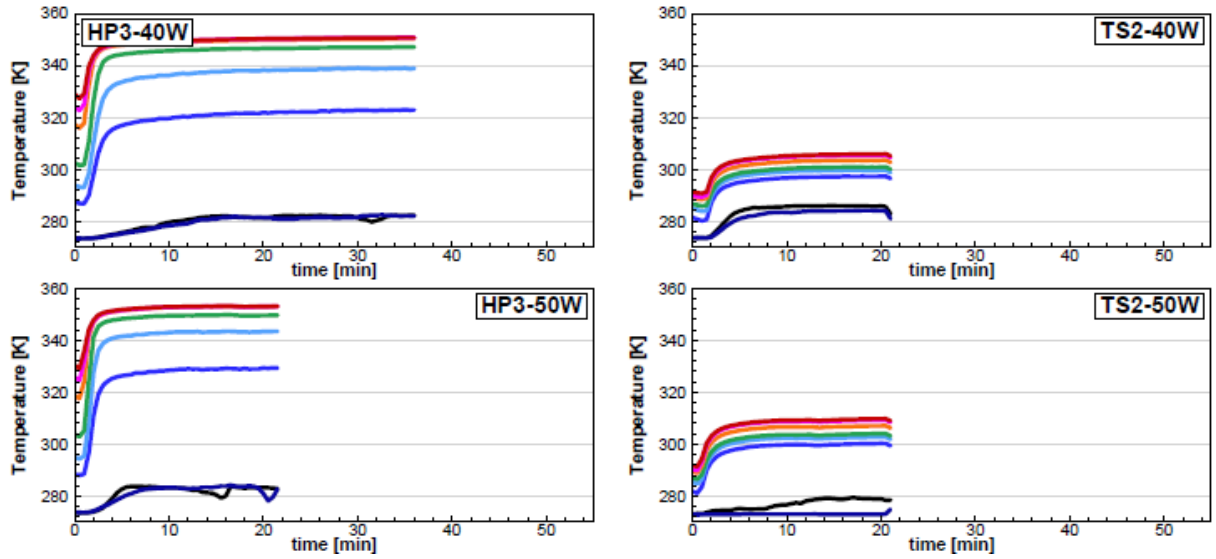

FIGURE 44: COMPARISON OF PERFORMANCE BETWEEN HEAT PIPE AND THERMOSYPHON IN A COPPER CASE WITH METHANOL AS THE WORKING FLUID. THE HEAT SINK CONTAINS ICE WATER AND HIGH HEAT LOADS ARE APPLIED.

Figure 44 shows the results for HP3 and TS2 when using an ice-water bath and higher heat loads. At these higher input loads, the temperature of the ice-water mixture around the condenser is less stable.

7.2 Steady State Temperature Distribution

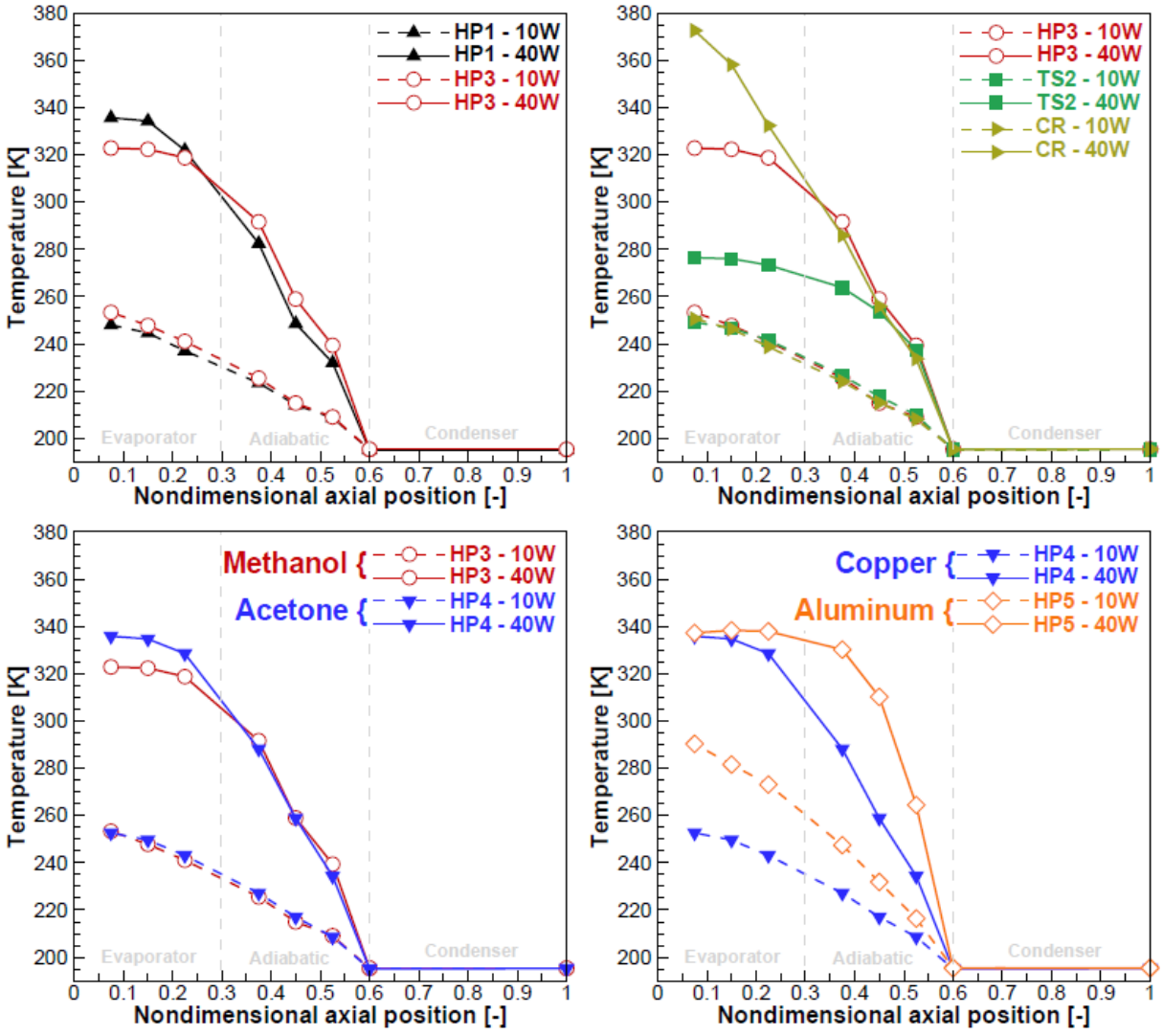

Figure 45: Steady state temperature differential comparisons at 10 W and 40 W applied load. The top left comparison shows the difference in heat pipes with different filling ratios. The top right compares a thermosyphon and heat pipe. The bottom left compares heat pipes with different workig fluids. The bottom right compares heat pipes with different case and wick materials.

The temperature distributions are displayed in Figure 45 where each plot shows the steady-state temperatures measured at each location along the heat pipes. The *x*-axis is normalized by the total length so that position varies between zero and one. The heater is wrapped around the

evaporator section, and the condenser is immersed in the cooling bath. The adiabatic section is surrounded by insulating material so that transverse heat transfer is prevented.

Testing done on CR displays the performance when axial conduction is the only method of heat transfer. The upper right graph in Figure 45 compares the copper tube, thermosyphon and heat pipe. At low loads (10 W), the temperature distribution in the evaporator section is nearly linear all which indicates the primary method of heat transfer is axial conduction. Axial conduction can be reduced by using a thinner tube wall. At 40 W, the temperature gradient in the copper tube is larger than the heat pipes, indicating the activity of the working fluid.

At high loads, the temperature distributions in the evaporator are flatter, indicating the heat pipes and thermosyphons are operational. This is seen for the 40 W loads in Figure 45. TS2 has constant temperature in the evaporator at 10W input load, while this behavior is not observed in HP3 and HP4 until 30 or 40 W input load. If the heat load were further increased, eventually the temperature distribution in the evaporator section would become linearly decreasing again, which is an indication of evaporator dry out and the capillary limit being reached [33]. Since this behavior did not appear, it can be concluded that the capillary limit was not reached for any of the experiments.

7.3 SUMMARY

Representative thermal response and steady state temperature distributions are presented. Time taken to achieve steady state, the final temperature distribution, and the behavior differences at low and high loads were presented. None of the pipes experienced the capillary limit or evaporator dry out during testing.

Chapter 8 is the discussion of the experimental process conducted while researching this thesis. Iterative design, cleaning, evacuation, and heat transfer testing is discussed in detail. The experimental behavior is explained with references to relevant literature.

Chapter 8 Discussion

Chapter 8 discusses the experimental results presented in Chapter 7. Observed behavior is interpreted and compared to the numerical predictions presented in Chapter 4.

8.1 Thermal Resistance

The effective thermal resistance of the heat pipes is the key performance metric. Once steady state is achieved an average temperature for the condenser, $T_{c(avg)}$, is determined using the two condenser thermocouples, and an average evaporator temperature, $T_{e(avg)}$, is calculated using the three evaporator thermocouples. With a prescribed heat load, Q, the thermal resistance, R, is determined using Equation 8.1.[20]

$$R = \frac{T_{e(avg)} - T_{c(avg)}}{Q} \tag{8.1}$$

Calculation uncertainties arise due to the measurement uncertainties summarized in Table 15. The total uncertainty is a function of the thermocouples and power supply. The heat input is determined by the voltage and current applied to the heater.

TABLE 15: UNCERTAINTY IN THE EXPERIMENTAL EQUIPMENT

Power Supply Meter Accuracy Voltage, *P* [38]	2 V
Power Supply Load Regulation Current, *I* [38]	0.006 A
T-Type Thermocouple, *T* [39]	1.0 K

The error bars within the thermal resistance calculations are determined using Equations 8.2 to 8.4. Equation 8.2 calculates the error in heat input (power supplied). Equation 8.3 calculates the uncertainty in the temperature difference between the average evaporator and condenser temperatures. Equation 8.4 calculates the error in the thermal resistance.

[20] Tables displaying the values for all configurations are found in Appendix T.

$$\xi_P = \sqrt{\left(\frac{\delta P}{\delta V}\omega_V\right)^2 + \left(\frac{\delta P}{\delta I}\omega_I\right)^2} \tag{8.2}$$

$$\xi_T = \sqrt{\sqrt{(\omega_{Te1})^2 + (\omega_{Te2})^2 + (\omega_{Te3})^2} + \sqrt{(\omega_{Tc1})^2 + (\omega_{Tc2})^2}} \tag{8.2}$$

$$\xi_R = \frac{T}{P}\sqrt{\left(\frac{\xi_T}{T}\right)^2 + \left(\frac{\xi_P}{P}\right)^2} \tag{8.2}$$

Figure 46 displays calculated *R* values as a function of heat load for HP3 and TS2 when using dry ice and acetone in the condenser (left) and using a water-ice bath (right). Both the heat pipe and thermosyphon show that thermal resistance is inversely proportional to heat input which agrees with standard heat pipe behavior [30]. The thermosyphon performs better than the heat pipe at high loads; however, at low loads the *R* values are similar, particularly for the acetone dry-ice bath. Increasing the condenser temperature by using ice-water for cooling, increases the performance for both HP3 and TS2, which is seen in the *R* values.

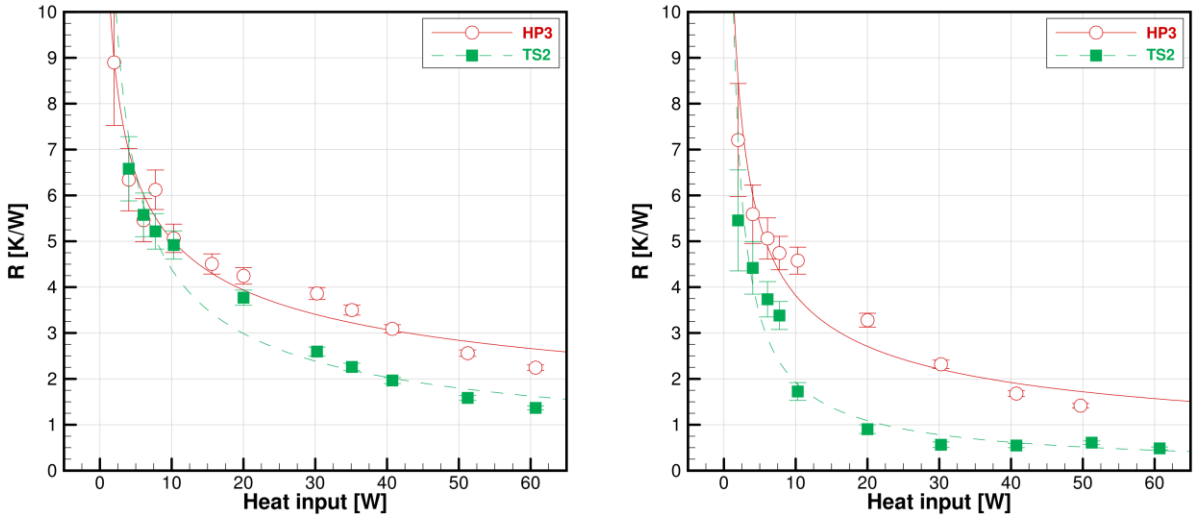

FIGURE 46: COMPARISON OF EXPERIMENTAL RESISTANCE VALUES BETWEEN TS2 AND HP3. BOTH ARE MADE OF COPPER WITH METHANOL AS THE WORKING FLUID, WITH DIFFERENT FILLING RATIOS. THE FIGURE ON THE LEFT HAD THE CONDENSER COOLED WITH DRY ICE AND ACEONE. THE FIGURE ON THE RIGHT, THE CONDENSER IS COOLED WITH ICE WATER.

Figure 47 summarizes thermal resistances for the other heat pipes and compares HP3 and TS2 to the copper tube (CR).

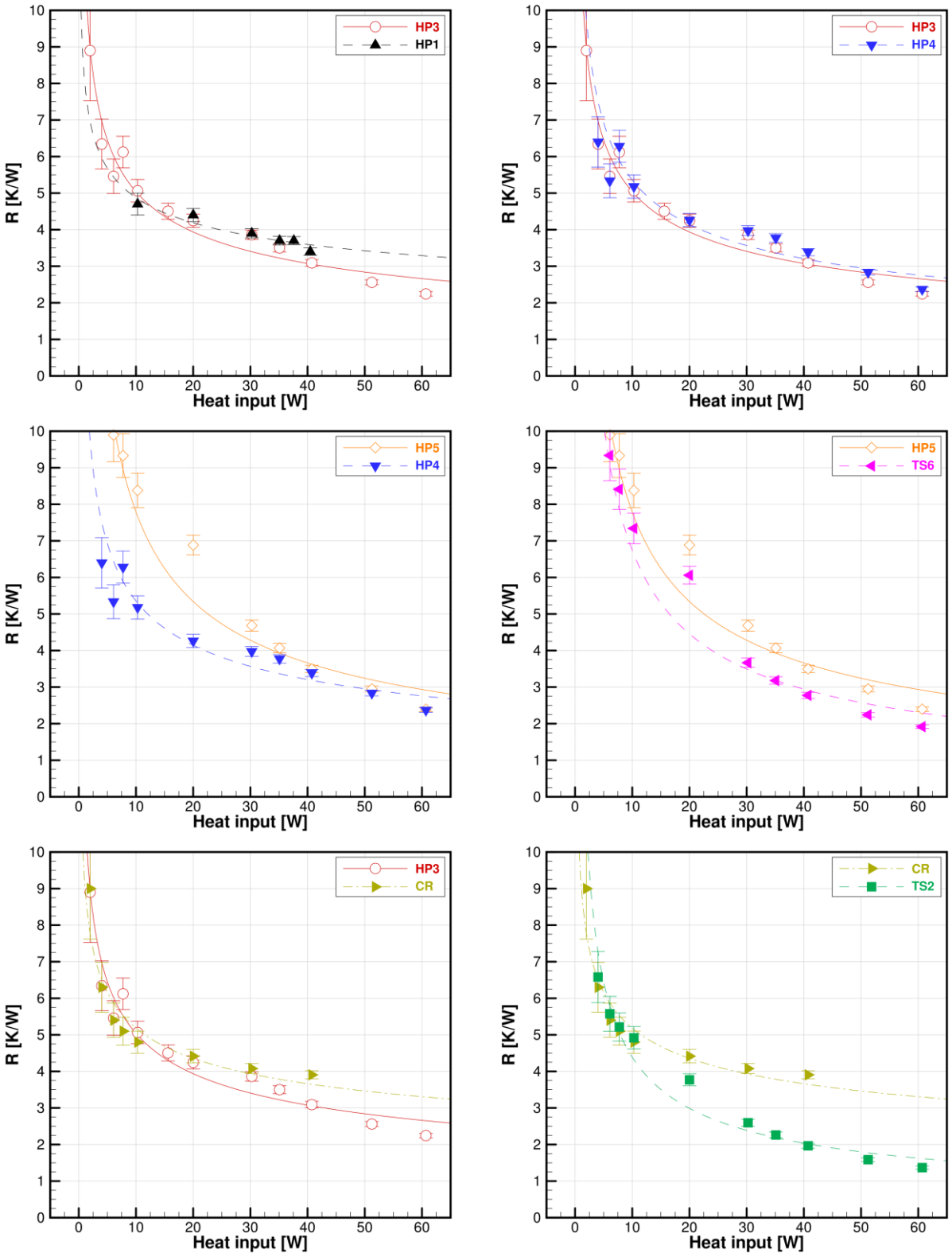

FIGURE 47: THERMAL RESISTANCE VALUE COMPARISONS FOR DIFFERENT FILLING RATIO, WORKING FLUID, SHELL MATERIAL, AND HEAT PIPE TO THERMOSYPHON AND A COPPER ROD, WITH THE CONDENSER COOLED BY A BATH OF ACETONE CONTAINING DRY ICE.

At low heat loads, the evaporator temperature is also low. Because of this, the vapor pressure in the heat pipes is low and a thick liquid film exists in the evaporator section. Both can cause high thermal resistance [32]. At higher heat loads, the evaporator temperature increases thereby increasing the vapor pressure. A thin liquid layer exists in the evaporator section [28], and a larger amount of working fluid is vaporized. These conditions result in lower thermal resistance [32]. In most low temperature applications, the majority of the thermal resistance within the heat pipe is attributed to the saturated wick structure in the evaporator and condenser regions [33].

The heat transfer characteristics of CR represent an ordinary conductor. The bottom left plot in Figure 47 compares HP3 to CR where the performance for both is similar up to 30 W. Thereafter, the slope begins to flatten out for CR, whereas the thermal resistance of the heat pipe continues to decrease. The bottom right graph compares TS2 to CR and there is a similar performance at low loads, and then a distinct departure at 10 W. The similar performance of HP3 and TS2 to the copper tube at low loads can be explained because the primary method of heat transfer is axial conduction.

TABLE 16: THERMAL RESISTANCE VALUE COMPARISIONS BETWEEN PREDICTED AND EXPERIMENTAL.

Heat Applied	Experimental Thermal Resistance Values									Predicted R Values		
[W]	HP1	TS2	TS2 (Ice)	HP3	HP3 (Ice)	HP4	HP5	TS6	CR	HP3	HP4	HP5
10	4.7	4.9	1.7	5.1	4.6	5.2	8.4	7.3	4.8			
20	4.4	3.8	0.9	4.2	3.3	4.3	6.9	6.1	4.4			
30	3.9	2.6	0.6	3.9	2.3	4.0	4.7	3.7	4.1			
40	3.4	2.0	0.5	3.1	1.7	3.4	3.5	2.8	3.9	0.9	1.1	1.1
50		1.6	0.6	2.6	1.4	2.8	2.9	2.2				
60		1.4	0.5	2.2		2.4	2.4	1.9				

Table 16 compares the experimental thermal resistances between 10 W and 60 W to the modeled values in Table 7. As can be seen, the experimental values are higher for the copper heat pipes. The copper thermosyphons have higher than predicted thermal resistance at low loads, and lower thermal resistance at high loads.

Some of the difference between experimental and modeled thermal resistance can be explained by a changing effective length within the heat pipe and thermosyphons. At low heat inputs the effective length is typically longer because the working fluid uses the entire wick

structure between the evaporator and condenser. As the temperature increases the effective lengths gets smaller because the hotter surface temperatures within the evaporator result in the working fluid vaporizing before reaching the evaporator end cap. This results in an increased thermal resistance at lower temperatures and the opposite is true for higher temperatures.

Non-condensable gas formation can also change the effective length of the heat pipe. As the temperature rises within the heat pipe the non-condensable gas will expand, thereby shortening the effective length of the heat pipe. There is a higher likelihood that impurities which cause non-condensable gas resided in the mesh screen of the heat pipes, which would lead to the heat pipes having higher thermal resistance compared to the thermosyphons.

The thermosyphon may also outperform the heat pipe because of poor thermal contact between the wick and shell, thereby increasing thermal resistance. In the model, the thermal resistance from the liquid vapor interface and the resistance of the vapor was neglected. This could impact the predictions, especially at higher heat inputs, causing greater thermal resistance.

The capillary limit was not reached for any heat pipe or thermosyphon. This is apparent because the thermal resistance continues to decrease with increasing temperature. When the capillary limit is exceeded, the thermal resistance will hit an absolute minimum and then begin to increase [40]. The minimum value is the capillary limit [40]. Increasing thermal resistance associated with increasing applied load after the capillary limit has been reached, is caused by the evaporator beginning to dry out and flooding occurring in the condenser [40].

8.2 Transient Thermal Response

8.2.1 Fill Ratio

HP1 and HP3 are methanol heat pipes and are the same except for the fill ratio. HP1 is under-filled by approximately 33% while HP3 is within 1% of the targeted charge. The transient thermal response of HP1 and HP3 are compared in Figure 48 for heat loads of 30 and 40 W. HP3 is shown on the left and HP1 on the right. While the steady-state thermal resistances are similar at both 30 W and 40 W, the response time of HP3 is shorter; similar results were reported by Kempers, et.al [33]. In the case of HP1 at 40 W, erratic temperature fluctuations are seen in the temperature traces once steady-state is reached.

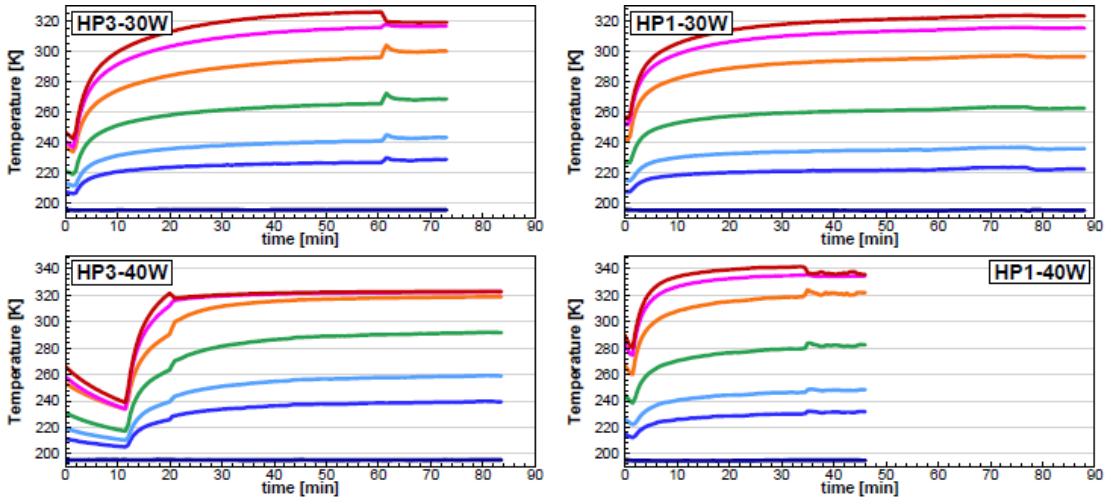

FIGURE 48: TRANSIENT THERMAL RESPONSE COMPARISON OF PERFORMANCE BETWEEN AN UNDERFILLED AND A PERFECTLY FILLED HEAT PIPE. HP1 IS UNDERFILLED. BOTH HEAT PIPES ARE MADE OF COPPER AND CONTAIN METHANOL. THE HEAT SINK CONTAINS DRY ICE AND ACETONE AND HIGH HEAT LOADS ARE APPLIED.

Erratic behaviour, characterized by a sudden drop in temperature is displayed when looking at Figure 48. Similar behavior is seen in the other heat pipes and thermosyphons[21]. A study by Farsi et.al found similar drops in temperature during transient tests. They called these *temperature excursions* and attributed the behavior to nucleation phenomenon [41]. By observing through a glass window, Farsi et. al saw many vapor bubbles in the evaporator and an increased liquid film thickness in the condenser and adiabatic sections [41].The boiling point of methanol at 1 atm is 337.8 K [42], and the temperature traces for HP1 become erratic when the evaporator temperature reaches this value. A jump in temperature occurs in HP3 when the evaporator temperature reaches ~320 K. Assuming residual gas contamination is the same, the differences between HP1 and HP3 must be due to liquid charge.

8.2.2 WORKING FLUID

Differences between working fluids can be seen by comparing HP3 (methanol) and HP4 (acetone) in Figure 49. From Figure 47, slightly lower thermal resistances are observed in the methanol heat pipe. The time to achieve steady state and the steady state temperatures are very similar between both working fluids. The steady state temperature for acetone at higher input loads is larger than in methanol, but overall, performance is similar.

[21] Appendix T displays the complete data set for heat transfer testing.

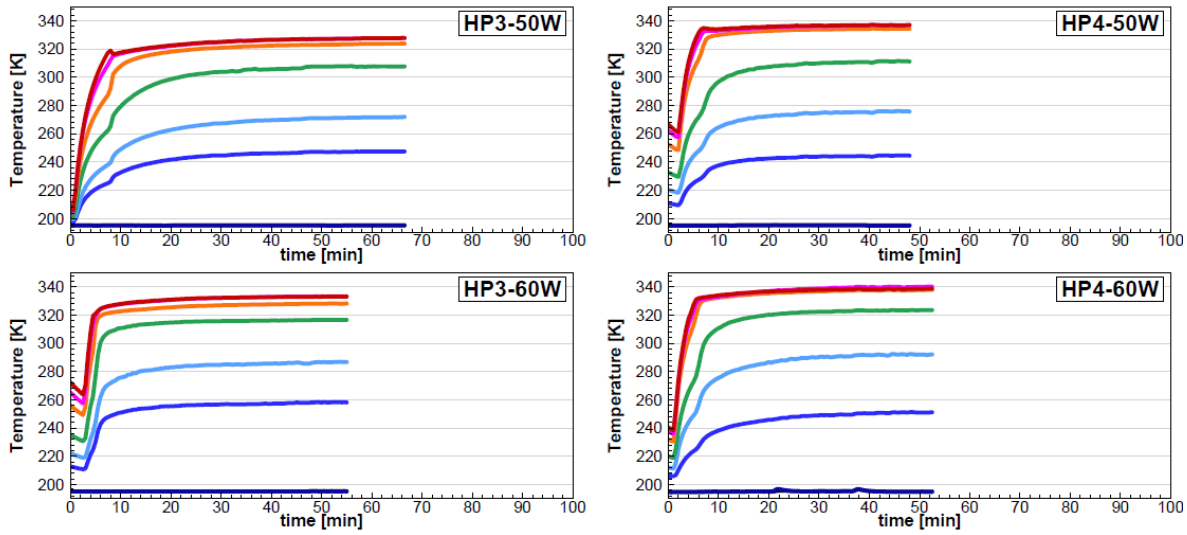

FIGURE 49: TRANSIENT THERMAL RESPONSE COMPARISON OF PERFORMANCE OF HP3 AND HP4 AT HIGH LOADS.

Different case and wick structures can be examined by comparing HP4 to HP5; both use acetone. HP4 is constructed of copper and HP5 is aluminum. As shown in Figure 50 and Figure 51, the heat pipe constructed of aluminum (HP5) takes longer to reach steady state. HP4 has a lower thermal resistance than HP5, as shown in the middle left graph displayed in Figure 47. This result is to be expected because copper is a better conductor than aluminum. The impact of wall conduction is most significant at low loads where the fluid resistance is high relative to the wall. This is clearly seen in Figure 50.

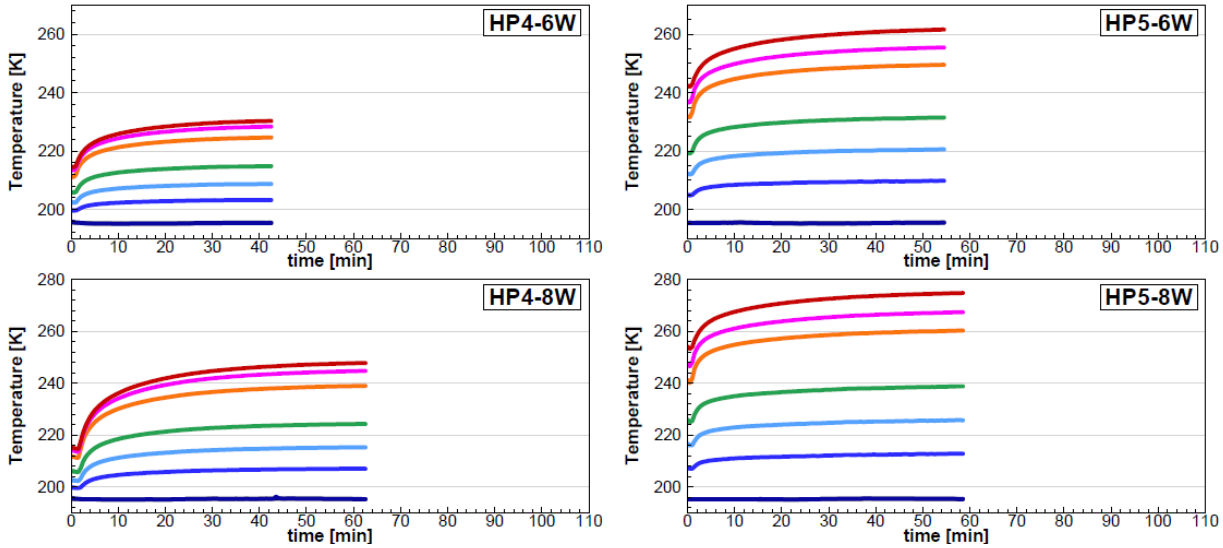

FIGURE 50: TRANSIENT THERMAL RESPONSE COMPARISON OF PERFORMANCE BETWEEN HEAT PIPES WITH DIFFERENT CASE MATERIALS. HP4 IS ENCASED IN COPPER AND HP5 IS ENCASED IN ALUMINUM. BOTH CONTAIN ACETONE AS THE WORKING FLUID. THE HEAT SINK CONTAINS DRY ICE AND ACETONE AND LOW LOADS APPLIED.

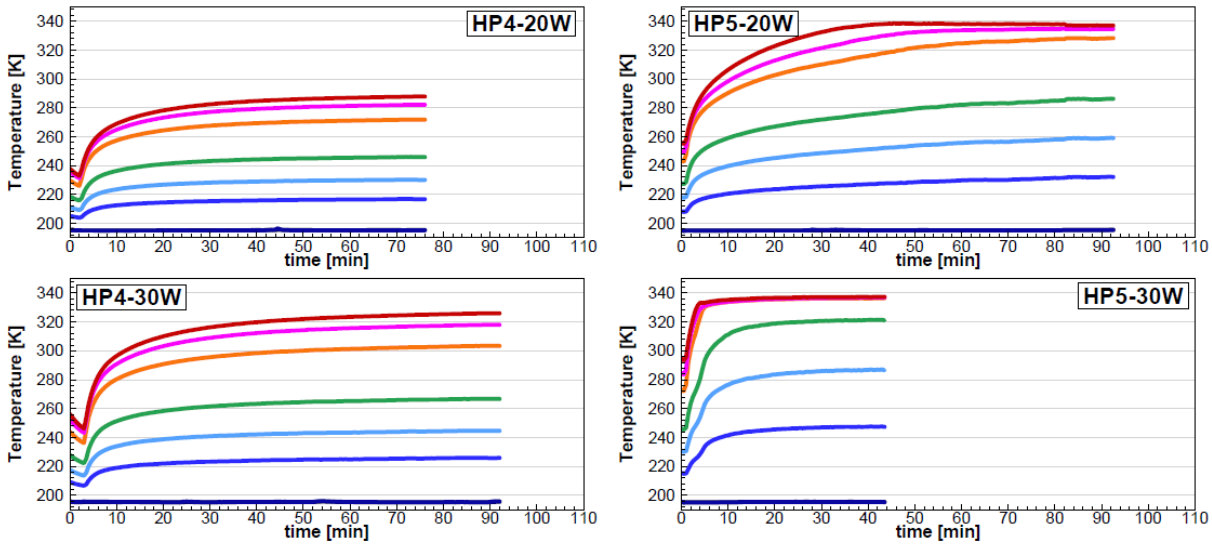

FIGURE 51: TRANSIENT THERMAL RESPONSE COMPARISON OF PERFORMANCE OF HP4 AND HP5 AT HIGH LOADS.

8.2.3 HEAT PIPE VERSUS THERMOSYPHON

Heat pipe and thermosyphon performance are compared using HP3 and TS2, which are constructed of copper and methanol. HP5 can be compared with TS6; both are constructed of aluminum and acetone.

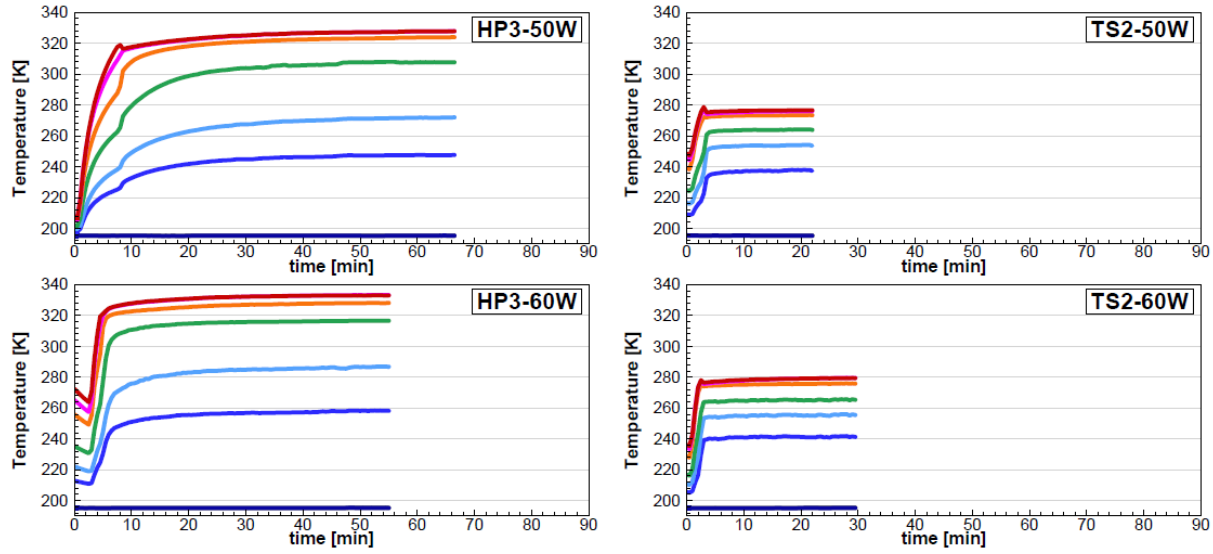

FIGURE 52: TRANSIENT THERMAL RESPONSE COMPARISON OF PERFORMANCE FOR HP3 AND TS2 AT HIGH LOADS.

As shown in Figure 46, the thermal resistance of HP3 is similar to TS2 at low heat inputs. At higher heat inputs the thermosyphon has a lower steady state temperature and achieves steady state more quickly, as shown in Figure 52. Kempers generally observed that heat pipes with larger

filling ratios have higher thermal resistance due to pooling liquid affecting [33]. From this it is predicted that TS2 should have a higher resistance than HP3, but the opposite is true. This is evidence of the high thermal resistance imposed by the wick structure of HP3.

The transient response of HP5 and TS6 are compared in Figure 53 and Figure 54. TS6 has lower thermal resistance values compared to HP5. The response time is similar at higher heat loads. At 8 W, HP5 is slower to reach steady state.

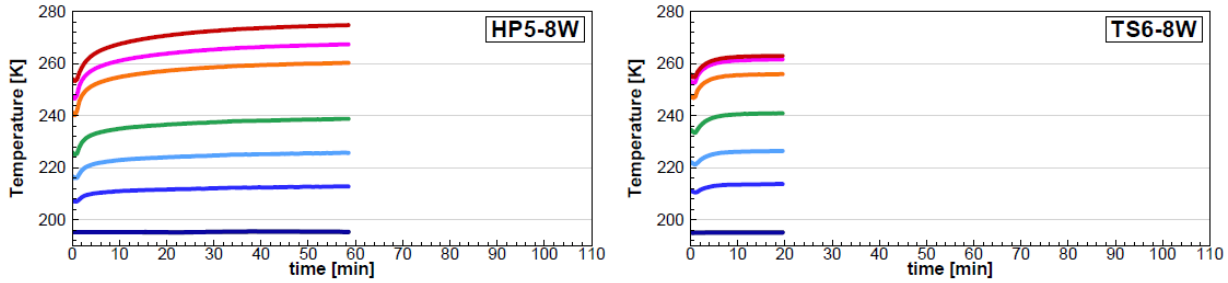

FIGURE 53: TRANSIENT THERMAL RESPONSE COMPARISON OF PERFORMANCE BETWEEN HEAT PIPE AND THERMOSYPHON IN AN ALUMINUM CASE WITH ACETONE AS THE WORKING FLUID. THE HEAT SINK CONTAINS DRY ICE AND ACETONE AND LOW HEAT LOADS ARE APPLIED.

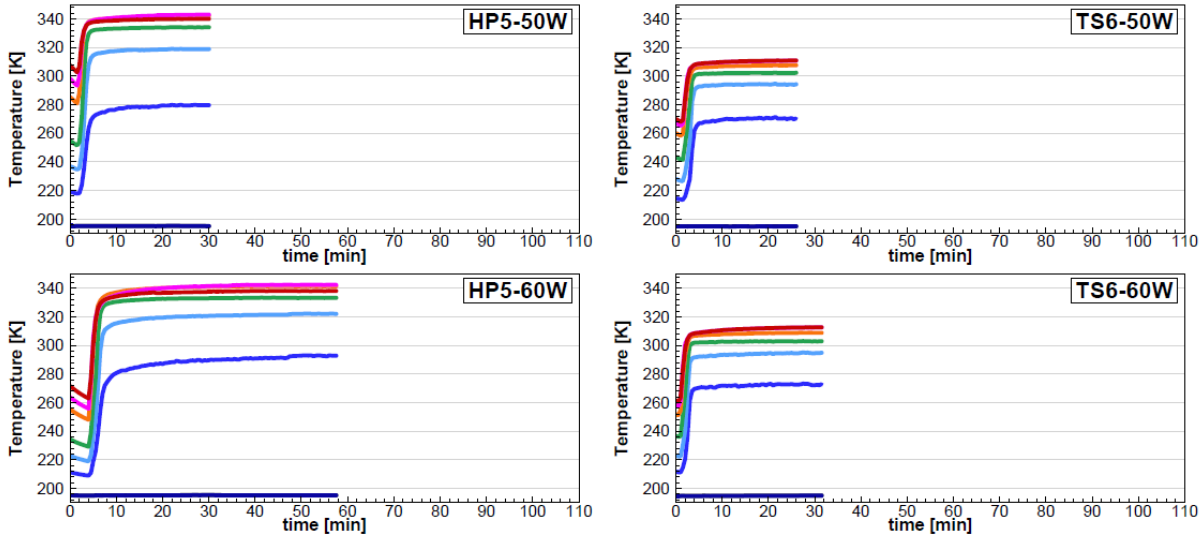

FIGURE 54: TRANSIENT THERMAL RESPONSE COMPARISON OF PERFORMANCE OF HP5 AND TS2 AT HIGH LOADS.

An experimental study by Ahmad and Yousif found that thermosyphons had smaller wall temperature variations between the evaporator and condenser, compared to a similarly constructed heat pipe [43], which corresponds to lower thermal resistance values.

8.2.4 COPPER TUBE

The transient response of TS2 is compared to the copper tube in Figure 55 and Figure 56.

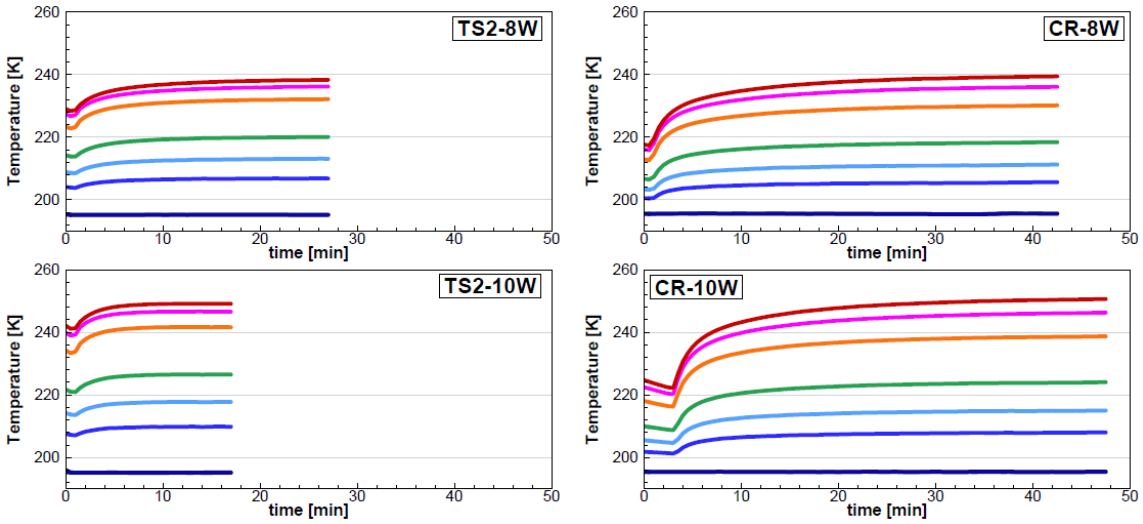

FIGURE 55: TRANSIENT THERMAL RESPONSE COMPARISON OF PERFORMANCE BETWEEN AN INSULATED COPPER ROD AND TS2. THE HEAT SINK CONTAINS DRY ICE AND ACETONE AND LOW HEAT LOADS ARE APPLIED.

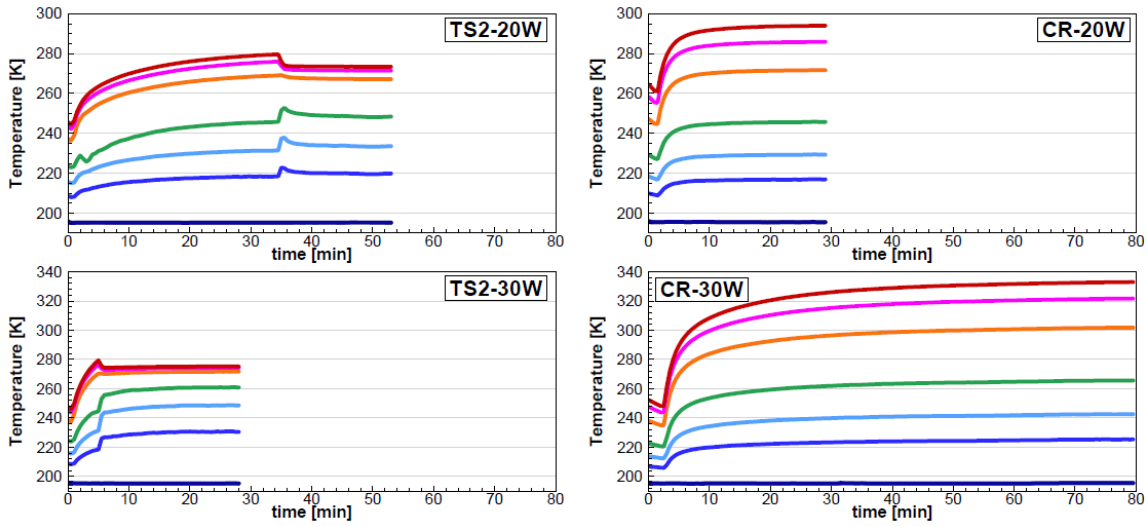

FIGURE 56: TRANSIENT THERMAL RESPONSE COMPARISON OF PERFORMANCE TS2 AND CR AT HIGH LOADS.

At low heat inputs (8 and 10 W) the temperature distributions are similar; however, CR takes longer to reach steady state. This indicates that axial conduction in the wall is the dominant heat transfer path. At higher loads (20 and 30 W), the thermosyphon temperatures jump when the evaporator temperature reaches ~275 K.

8.3 SUMMARY

The prototype with the best performance was the methanol thermosyphon, TS2. A thermal resistance of ~1.4 K/W is achieved with a 60 W load when the condenser is cooled by an acetone dry-ice bath. When cooled by an ice-water bath, the thermal resistance is ~0.5 K/W; this is ~8-10 times lower than the measured resistance of the copper shell. For comparison, the numerical model predicted thermal resistances on the order of 0.8-1 K/W for the heat pipes.

HP3 was the best performing heat pipe. At 40 W, the evaporator temperature is ~300 K, and the thermal resistance is 3 K/W which is a small improvement over the copper shell. One of the possible reasons for low performance is poor thermal contact of the wick structure within HP3. At low loads the steady state temperature of TS2 is ~245 K and heat transfer is due to axial conduction. For these conditions TS2, HP1, HP3 and HP4 all preform similarly.

Erratic behavior in the transient thermal response graphs is explained by nucleation phenomena. At that time, the heat pipe is approaching steady state, around the boiling point of the working fluid and there is an increase in the presence of vapor bubbles within the evaporator, as well as increased liquid film thickness in the condenser and adiabatic sections. To overcome this limitation and lower the steady state temperature within the heat pipe a different working fluid with a lower boiling point than methanol or acetone should be used.

Chapter 9 concludes this thesis and makes recommendations to improve the fabrication and testing of future heat pipes. The appendices contain additional information such as property tables, mathematical data, engineering drawings, and experimental data.

Chapter 9 Conclusions and Recommendations

A heat transfer system using heat pipes was proposed for a passive container using dry-ice for cooling. A simple model of wicked heat pipes was created and used to design prototypes containing methanol and acetone. The behavior of screen wick heat pipes was investigated and the theoretical heat transfer limits were determined. Four mesh wick heat pipes, two thermosyphons (wickless), and a hollow copper tube were fabricated and tested.

The heat pipes were manufactured and assembled using a press fit technique with O-rings for fluid sealing. A vacuum system was built and used to remove impurities before the working fluid was added to the pipes. Fluid losses lead to some variability between targeted filling ratios and those achieved.

The effects of filling ratio, working fluid, case and wick material, heat pipe, thermosyphon and copper tube, were experimentally investigated. Thermal resistance, transient thermal response and the steady temperature distributions were quantified and discussed for various heat pipe configurations. The heat pipe with the lowest thermal resistance operating with a condenser temperature set by an acetone-dry ice bath was the copper-methanol thermosyphon, TS2.

9.1 Fabrication, Cleaning and Assembly

The initial iterative design and testing process was successful given that each design change improved the heat pipe seal and allowed for greater air pressure to be held. These original prototypes were shorter and press fit together using a machine vice. However, when the first beta prototypes were assembled in this manner, alignment and force distribution was a major issue and the prototypes had to be remade. A few more iterative tests resulted in press fitting the 2nd generation beta prototypes using a lathe, which gave predictable results.

The fill tube provided another challenge. Initially the end caps containing the fill tube were attempted to be machined out of a single piece of stock material. Crimping the aluminum tubes was extremely difficult, and when successful stress fractures appeared on the exterior of the tube. As an alternative, the fill tube end caps for all prototypes were manufactured out of stock copper tube that was soldered into a machined end cap. Using copper, the crimp itself was still not fluid tight, but the addition of a bead of solder on the end created a satisfactory seal.

The literature recommended cleaning process involved an acid bath which resulted in removal of material and led to insufficient interference when press fitting the end caps into the shell. The original process is displayed in Figure 57. As a result, the cleaning process was modified to remove the use of acids and the prototypes were remade.

FIGURE 57: THE INITIAL CLEANING PROCESS USING ACID MIXES FOR THE COPPER COMPONENTS.

The appropriate sized wick was cut and rolled tightly over a delrin rod. This rod was then placed inside the shell, and the rod was used to smooth the wick to the sides of the shell. The wick structure was difficult to place inside the heat pipes. It often bent at the edges and got stuck requiring multiple attempts to get it inside the shell. The aluminum mesh (higher mesh number) was more difficult to install than the copper because it was softer. Gaps between the mesh wick and the shell were present resulting in poor thermal contact. Using precision ground tubes for any future shell structures may assist in ensuring better thermal contact. Also, a different method of inserting the mesh wick into the shell, or a different type of wick structure, should be considered.

9.2 EVACUATION AND CHARGING

Initial charging tests found an average of 5 ml of fluid lost per charge. These charges only had the pipe under vacuum pressure for 20 minutes before filling. Charging of the final prototypes resulted in even more fluid loss. Successive testing allowed for better predictions to be made regarding the filling losses so that an appropriate charge could be obtained in the final heat pipes.

Initially, the heat pipe charging process included a 24-hour vacuum before the purge charge was introduced, and then an additional 30 minutes at high vacuum followed, before the final charge was introduced. This process resulted in significantly less losses than any others. The vacuum process for the final prototypes began with a one-hour evacuation, followed by a flush charge, and then a 22-hour evacuation before the fill charge. The charge mass was determined by weighing the pipes with the crimping tool attached to the fill tube and using a large beaker to support the weight of the tool.

Charging of HP1 and TS2 resulted in less fluid than desired; however, the next heat pipe (HP3) was only 1.4% away from the design value. The remaining three pipes were all filled within 10% of the design value.

9.3 RECOMMENDATIONS

Recommendations for future work included modifications to the charging apparatus, use of fluids with lower boiling points, improved wick design and assembly, and testing with external heat sinks.

Previous researchers found that after 17,500 h acetone within an aluminum heat pipe will experience performance degradation. This decline was because of a self-reaction of acetone, which increased the boiling temperature from 329 K to 433 K [44]. This is an additional reason for choosing methanol over acetone as the working fluid.

The charging apparatus should be modified to minimize air contamination during the addition of working fluids. Indications of air contamination was the temperature of the heat pipes in the evaporator section at steady state, occurring close to atmospheric pressure.

Testing different working fluids in the future may results in better performance. Both pentane and propylene have lower boiling points than acetone or methanol and therefore may have better performance at lower temperatures. Pentane has a boiling point of 309.2 K [42]. Propylene has a boiling point of 225.6 K [42]. When testing HP3 and TS2 using ice water for cooling the condenser the thermal resistance decreased, as shown in Figure 46. This is evidence of superior performance at temperatures closer to the boiling point of the working fluid.

The next steps for improving on this research include additional testing of the 2nd generation beta prototypes to evaluate the thermal performance using only dry ice surrounding the

condenser and comparing the result to the acetone and dry ice bath. If the performance is severely affected, then using extended arrays attached to the condenser may result in improved thermal contact and performance.

If the test goes well, then a new testing apparatus should be built to see how the pipes cool using natural convection. This should be done individually and then with multiple pipes to investigate if a temperature variation exists within the container. The pulldown time required to freeze a bottle of water should be investigated and a small prototype container manufactured. This alpha prototype would be used to discover additional problems that need to be solved before designing and manufacturing of a prototype that CRT can use for demonstrations. Anticipated problems include frost formation around the exterior doors, means of filling the heat sink using liquid CO_2 that is flashed into solid, pressure regulation within the heat sink container from sublimating CO_2 gas, internal distribution of the solid CO_2, the shape of the solid CO_2 snow that provides the best heat transfer properties, and uneven cargo temperature distribution.

Additional research can be done on the heat pipes by manufacturing new heat pipes with a different wick structure. Since copper is the better choice for the heat pipes then the end caps can simply be soldered on instead of press fit. Thinner walled, precision ground, shell structures should be used to reduce heat loss through the shell as well as the impact of axial conduction.

References

[1] G. Schubak, "A Market Study of Cryogenic CO2 Refrigerated Containers for Cold Chain Logistics," Foresight Cleantech Accelerator Center, Vancouver, 2015.

[2] K. Hawes, Interviewee, *Cold Star Solutions C.E.O.*. [Interview]. 23 February 2016.

[3] V. E. Thomsen, "Refrigerated Shipping Container". USA Patent US5460013 A, 24 October 1995.

[4] V. E. Thomsen, "Refrigerated container". USA Patent US4891954 A, 09 January 1990.

[5] Environmental Protection Agency , "Protection of Stratospheric Ozone: Change of Listing Status for Certain Substitutes Under the Significant New Alternatives Policy Program; Final Rule," United States National Archives and Records Administration, Washington, 2015.

[6] D. M. Aragon, "Temperature Controlled Container". United States Patent US 2005/0188715 A1, 01 September 2005.

[7] D. M. Aragon, "Portable Active Cryo Container". United States Patent US 8,191,380 B2, 05 June 2012.

[8] K. W. Broussard, "Temperature Controlled Pallet-Sized Shipping Container". United States Patent US 2004/0226309 A1, 18 November 2004.

[9] D. E. Harman and K. M. Taylor, "Environment Controlled Cargo Container". United States Patent US 8,162,542 B2, 24 April 2012.

[10] G. Peterson, "Heat Pipes," in *Handbook of Heat Transfer*, United States of America, McGraw-Hill, 1998, pp. 12.1-12.20.

[11] C. C. Silverstein, Design and Technology of Heat Pipes for Cooling and Heat Exchange, Washington: Taylor & Francis , 1992.

[12] Thermacore, "Thermacore Thermal Management Solutions," [Online]. Available: http://www.thermacore.com/documents/common-questions-heat-pipes.pdf. [Accessed 05 July 2016].

[13] MHS, "My Heat Sinks," [Online]. Available: http://www.myheatsinks.com/docs/images/heat-pipe-solutions/hp_internal_view.png. [Accessed 12 June 2016].

[14] A. Faghri, Heat Pipe Science and Technology, Washington: Taylor & Francis, 1995.

[15] G. Peterson, An Introduction to Heat Pipes, New York: John Wiley & Sons, 1994.

[16] Thermacore, [Online]. Available: http://www.thermacore.com/documents/common-questions-heat-pipes.pdf. [Accessed 26 July 2016].

[17] H. Ma, Oscillating Heat Pipes, New York: Springer, 2015.

[18] J. C. Kotz, P. M. Treichel and J. R. Townsend, Chemistry & Chemical Reactivity, Belmont: Thomson Higher Education, 2009.

[19] P. D. Dunn and D. Reay, Heat Pipes 3rd ed., New York: Pergamon, 1982.

[20] S. Chi, Heat Pipe Theory and Practice, New York: McGraw-Hill, 1976.

[21] B. Zohuri, Heat Pipe Design and Technology: Modern Applications for Practical Thermal Management, Albuquerque: Springer, 2016.

[22] B&K Engineering, Heat Pipe Design Handbook, Maryland: National Techical Information Service, 1979.

[23] B. Jiao, L. Qiu and X. Zhang et al., "Investigation on the effect of filling ratio on the steady-state heat transfer performance of a vertical two-phase closed thermosyphon," *Applied Thermal Engineering,* no. 28, pp. 1417-1426, 2008.

[24] M.-C. Lin, L.-J. Chun, W.-S. Lee and S.-L. Chen, "Thermal performance of a two-phase thermosyphon energy storage system," *Science Direct,* no. 75, pp. 295-306, 2003.

[25] H. Shabgard and A. Faghri, "Performance characteristics of cylindrical heat pipes with multiple heat sources," *Applied Thermal Engineering,* no. 31, pp. 3410-3419, 2011.

[26] PSC Motors and Fans, [Online]. Available: http://pscmf.com/product/showproduct.php?id=196&lang=en. [Accessed 27 July 2016].

[27] K. H. Do, H. J. Ha and S. P. Jang, "Thermal resistance of screen mesh wick heat pipes using the water-based Al2O3 nanofluids," *International Journal of Heat and Mass Transfer,* no. 53, pp. 5888-5894, 2010.

[28] R. Ramachandra, K. Ganesan and M. Rajkumar et al., "Comparative study of the effect of hybrid nanoparticle on the thermal performance of cylindrical screen mesh heat pipe," *International Communications in Heat and Mass Transfer,* no. 76, pp. 294-300, 2016.

[29] Y. Li, S. Chen and B. He et al., "Effects of vacuuming process parameters on the thermal performance of composite heat pipes," *Applied Thermal Engineering,* no. 99, pp. 32-41, 2016.

[30] G. Kumaresan, S. Venkatachalapathy, L. Asirvatham and S. Wongwises, "Comparative study on heat transfer characteristics of sintered and mesh wick heat pipes using CuO nanofluids," *International Communications in Heat and Mass Transfer,* no. 57, pp. 208-215, 2014.

[31] S. Venkatachalapathy, G. Kumaresan and S. Suresh, "Performance analysis of cylindrical heat pipe using nanofluids – An experimental study," *International Journal of Multiphase Flow,* no. 72, pp. 188-197, 2015.

[32] R. Senthilkumar, S. Vaidyanathan and B. Sivaraman, "Comparative study on heat pipe performance using aqueous solutions of alcohols," *Heat Mass Transfer,* no. 48, pp. 2033-2040, 2012.

[33] R. Kempers, D. Ewing and C. Ching, "Effect of number of mesh layers and fluid loading on the performance of screen mesh wicked heat pipes," *Applied Thermal Engineering,* no. 26, pp. 589-595, 2006.

[34] X. Lui, Y. Chen and M. Shi, "Dynamic performance analysis on start-up of closed-loop pulsating heat pipes," *International Journal of Thermal Sciences,* vol. 65, pp. 224-233, 2013.

[35] B. Badran, F. Gerner and P. Ramadas et al., "Experimental Results for Low-Temperature Silicon Micromachined Micro Heat Pipe Arrays Using Water and Methanol as Working FLuids," *Experimental Heat Transfer,* vol. 10, pp. 253-272, 2007.

[36] H. Hussein, H. El-Ghetany and S. Nada, "Performance of wickless heat pipe flat plate solar collectors having different pipes cross sections geometries and filling ratios," *Energy Conversion and Management,* vol. 47, no. 11-12, pp. 1539-1549, 2006.

[37] S. Noie, "Heat transfer characteristics of a two-phase closed thermosyphon," *Applied Thermal Engineering,* no. 25, pp. 495-506, 2005.

[38] Ametek, "Sorensen XPD Series Programmable DC Power Supply Operation Manual," April 2009. [Online]. Available: http://www.programmablepower.com/dc-power-supply/XPD/downloads/XPD_Series_Operation_Manual_TM-PDOP-01XN_RvD.pdf. [Accessed 07 March 2017].

[39] Omega, "Revised Thermocouple Reference Tables," [Online]. Available: http://www.omega.ca/temperature/Z/pdf/z207.pdf. [Accessed 09 November 2016].

[40] A. Driss, S. Maalej and M. Zaghdoudi, "Experimentation and modeling of the steady-state and transient thermal performances of a helicoidally grooved cylindrical heat pipe," *Microelectronics Reliability,* vol. 62, pp. 102-112, 2016.

[41] H. Farsi, J. Joly and e. al, "An experimental and theoretical investigation of the transient behavior of a two-phase closed thermosyphon," *Applied Thermal Engineering,* vol. 23, pp. 1895-1912, 2003.

[42] NIST - National Institue of Standards and Technology, "Nist Chemistry WebBook," U.S. Secretary of Commerce , 2016. [Online]. Available: http://webbook.nist.gov/. [Accessed 07 January 2017].

[43] H. H. Ahmad and A. A. Yousif, "Comparison between a Heat Pipe and a Thermosyphon Performance with variable Evaporator Length," *Al-Rafadain Engineering Journal,* vol. 21, no. 2, p. Special section p1, 2013.

[44] X. Yang, Y. Yan and D. Mullen, "Recent developments of lightweight, high performance heat pipes," *Applied Thermal Engineering,* vol. 33, no. 34, pp. 1-14, 2012.

[45] Advanced Cooling Technologies, Inc., "Innovations in Action," 2017. [Online]. Available: https://www.1-act.com/operating-temperature-range/. [Accessed 22 February 2017].

[46] National Institute of Standards and Technology, "REFPROP: NIST Reference Fluid Properties (DLL version 9.1)," NIST, 2015.

[47] F. P. Incropera, D. P. Dewitt, T. L. Bergman and e. al., Principles of Heat and Mass Transfer, New York: John Wiley & Sons, 2013.

[48] Sigma-Aldrich, "Particle Size Conversion Table," [Online]. Available: http://www.sigmaaldrich.com/chemistry/stockroom-reagents/learning-center/technical-library/particle-size-conversion.html. [Accessed 21 March 2016].

[49] Global Digital Central, "Thermal-Fluids Central," [Online]. Available: https://www.thermalfluidscentral.org/encyclopedia/images/thumb/9/96/HPFig1.png/400px-HPFig1.png. [Accessed 24 July 2016].

[50] Aglient Technologies, "TPS-Mobile," Vacuum Products Division, Italy, 2011.

[51] Agilent Technologies, "TriScroll 600 Series Dry Scroll Vacuum Pump," Vacuum Products Division, Italy, 2010.

[52] Ideal Vacuum Products, [Online]. Available: http://www.idealvac.com/files/brochures/Varian_ConvecTorr_Gauges.pdf. [Accessed 24 May 2016].

[53] Leybold Vacuum, "Ideal Vacuum Products," [Online]. Available: http://www.idealvac.com/files/manuals/Leybold-PTR90-Gauge-Specs-Data-Manual.pdf. [Accessed 01 June 2016].

[54] Vacoon, "Vacuum Products," [Online]. Available: http://www.vaccon.com/perf-j-mid.aspx. [Accessed 07 July 2016].

[55] A. Mozumder, M. Chowdhury and A. Akon, "Characteristics of Heat Transfer for Heat Pipe and Its Correlation," *ISRN Mechanical Engineering*, vol. 2011, p. 7 pages, 2011.

[56] P. Couto and M. Mantelli, "Cryogenic Heat Pipes - A Review of the State of the Art," [Online]. Available: http://www.abcm.org.br/anais/encit/2000/arquivos/s14/s14p03.pdf. [Accessed 15 February 2017].

[57] R. Hajian, M. Layeghi and K. Sani, "Experimental study of nanofluid effects on the thermal performance with trsponse time of heat pipe," *Energy Conversion and Management*, vol. 56, pp. 63-68, 2012.

Appendix A: Working Fluid Temperature Ranges

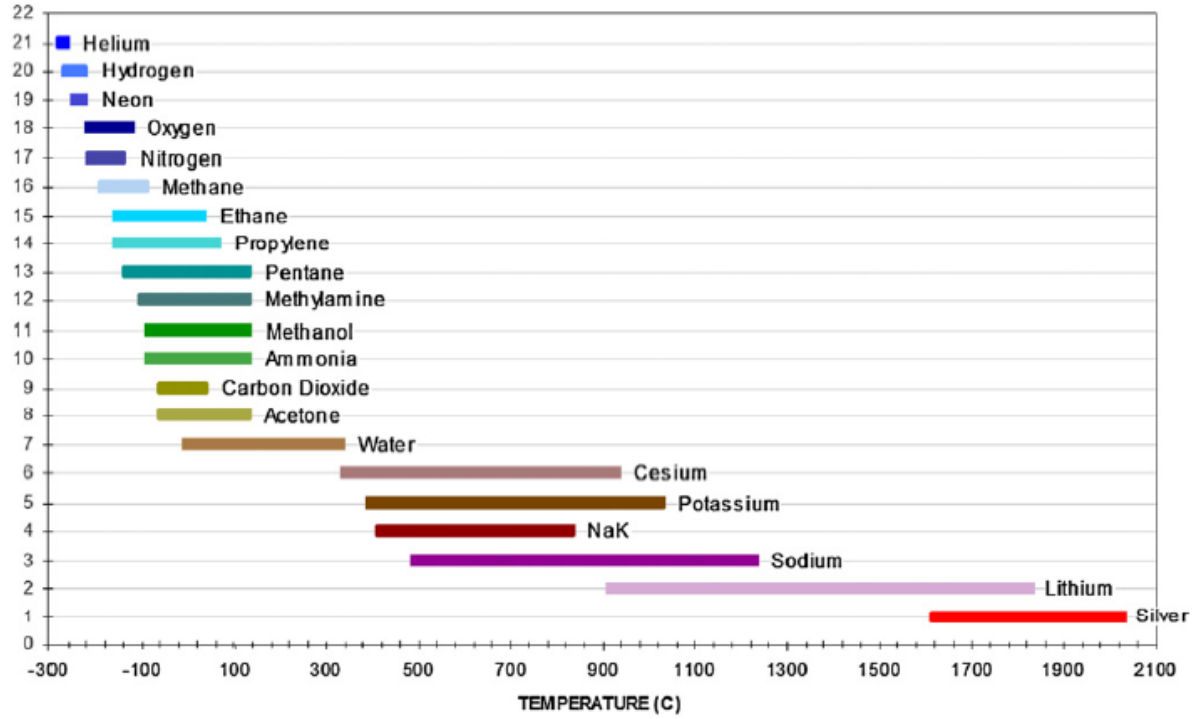

[44]

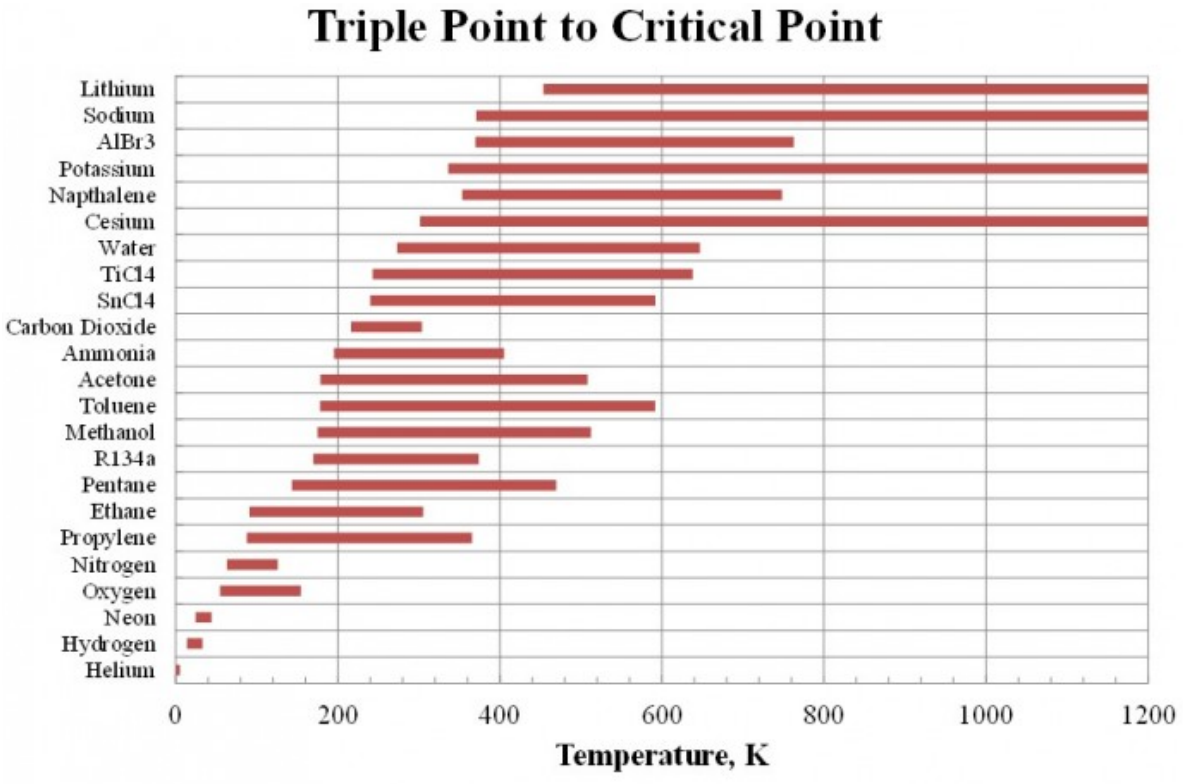

[45]

Appendix B: Compatibility of Case and Fluids

	Aluminum	Stainless Steel	Cold rolled steel	Iron	Copper	Brass	Silica	Nickel	Inconel	Tungsten	Tantalum	Molybdenum	Rhenium	Titanium	Niobium
Acetone	C	C			C	C	C								
Ammonia	C	C	C	C				C							
Benzene	C														
C_6F_6					C		C								
Cesium														C	C
DC 200	C	C			C			C							
DC 209					C										
Dimethyl Sulfide					C		C								
Dowtherm A		C			C		C								
Dowtherm E	I	C *	I		C	I									
Freon-11	C														
Freon-113	C														
Freon-21	C			C											
Indium		I						I	I	I	I	I			I
Lead		I						I	I	C	C			I	I
Lithium		I						I	I	C	C	C		I	C
Mercury		C #						I	I		I	I		I	I
Methanol	I	C		C	C	C	C	C							
Monsanto CP-32 (pyridene)	I				C										
Monsanto CP-34	I														
Monsanto CP-9					C		C								
n-butane	C														
n-heptane	C														
n-pentane	C	C													
Perchloroethylene					C		C								
Potassium								C						I	
Silver										C	C		I		
Sodium		C						C	C					I	C
Toluene	I														
Water	I	C *			C		C	C	I					C	

C = Compatible I = Incompatible * = Sensitive to Cleaning # = I with Austenitic SS [22]

Appendix C: Properties of Acetone

Temp	Pressure	Liquid Density	Vapor Density	Liquid Cp/Cv	Vapor Cp/Cv	Heat of Vapor.	Molar Mass	Liquid Therm Cond.	Vapor Therm Cond.	Liquid Viscosity	Vapor Viscosity	Surface Tension
[K]	[Pa]	[kg/m^3]	[kg/m^3]			[J/kg]	[g/mol]	[W/m K]	[W/m K]	[Pa s]	[Pa s]	[N/m]
198	27	892	9.67E-04	1.39	1.16	6.30E+05	5.81E+01	1.96E-01	7.67E-03	1.47E-03	5.33E-06	3.57E-02
208	79	881	2.66E-03	1.39	1.16	6.21E+05	5.81E+01	1.92E-01	8.19E-03	1.13E-03	5.59E-06	3.44E-02
218	205	871	6.57E-03	1.39	1.15	6.11E+05	5.81E+01	1.88E-01	8.75E-03	9.05E-04	5.86E-06	3.30E-02
228	481	860	1.48E-02	1.38	1.15	6.02E+05	5.81E+01	1.84E-01	9.32E-03	7.48E-04	6.13E-06	3.17E-02
238	1039	850	3.06E-02	1.38	1.15	5.92E+05	5.81E+01	1.80E-01	9.93E-03	6.33E-04	6.40E-06	3.04E-02
248	2088	839	5.91E-02	1.38	1.15	5.83E+05	5.81E+01	1.76E-01	1.06E-02	5.46E-04	6.67E-06	2.91E-02
258	3940	828	1.07E-01	1.38	1.15	5.73E+05	5.81E+01	1.72E-01	1.12E-02	4.77E-04	6.94E-06	2.78E-02
268	7034	818	1.85E-01	1.38	1.14	5.64E+05	5.81E+01	1.68E-01	1.19E-02	4.22E-04	7.21E-06	2.65E-02
278	11961	807	3.05E-01	1.38	1.14	5.54E+05	5.81E+01	1.63E-01	1.26E-02	3.77E-04	7.48E-06	2.53E-02
288	19479	796	4.82E-01	1.38	1.15	5.44E+05	5.81E+01	1.59E-01	1.34E-02	3.39E-04	7.75E-06	2.40E-02
298	30529	785	7.34E-01	1.38	1.15	5.34E+05	5.81E+01	1.55E-01	1.42E-02	3.07E-04	8.01E-06	2.27E-02
308	46244	774	1.08E+00	1.38	1.15	5.24E+05	5.81E+01	1.51E-01	1.50E-02	2.80E-04	8.28E-06	2.15E-02
318	67946	762	1.56E+00	1.39	1.15	5.14E+05	5.81E+01	1.47E-01	1.58E-02	2.56E-04	8.55E-06	2.02E-02
328	97151	750	2.18E+00	1.39	1.16	5.03E+05	5.81E+01	1.43E-01	1.66E-02	2.35E-04	8.82E-06	1.90E-02
338	135550	738	2.99E+00	1.39	1.16	4.92E+05	5.81E+01	1.39E-01	1.75E-02	2.17E-04	9.09E-06	1.78E-02
348	185030	726	4.01E+00	1.39	1.17	4.80E+05	5.81E+01	1.35E-01	1.85E-02	2.02E-04	9.36E-06	1.66E-02
358	247600	714	5.30E+00	1.40	1.18	4.68E+05	5.81E+01	1.31E-01	1.94E-02	1.87E-04	9.65E-06	1.54E-02

[46]

Appendix D: Properties of Methanol

Temp	Pressure	Liquid Density	Vapor Density	Liquid Cp/Cv	Vapor Cp/Cv	Heat of Vapor.	Molar Mass	Liquid Therm Cond.	Vapor Therm Cond.	Liquid Viscosity	Vapor Viscosity	Surface Tension
[K]	[Pa]	[kg/m^3]	[kg/m^3]			[J/kg]	[g/mol]	[W/m K]	[W/m K]	[Pa s]	[Pa s]	[N/m]
198	5	882	9.23E-05	1.25	1.24	1.29E+06	3.20E+01	2.52E-01	7.34E-03	4.84E-03	6.50E-06	3.20E-02
208	16	872	2.94E-04	1.25	1.23	1.28E+06	3.20E+01	2.44E-01	8.02E-03	3.46E-03	6.81E-06	3.07E-02
218	47	862	8.31E-04	1.24	1.22	1.27E+06	3.20E+01	2.38E-01	8.72E-03	2.59E-03	7.12E-06	2.96E-02
228	125	853	2.13E-03	1.24	1.21	1.26E+06	3.20E+01	2.31E-01	9.45E-03	2.01E-03	7.43E-06	2.85E-02
238	307	843	4.99E-03	1.24	1.21	1.25E+06	3.20E+01	2.26E-01	1.02E-02	1.59E-03	7.74E-06	2.75E-02
248	694	833	1.09E-02	1.23	1.20	1.24E+06	3.20E+01	2.20E-01	1.10E-02	1.29E-03	8.05E-06	2.65E-02
258	1466	824	2.21E-02	1.22	1.20	1.22E+06	3.20E+01	2.16E-01	1.18E-02	1.06E-03	8.36E-06	2.56E-02
268	2911	814	4.24E-02	1.22	1.21	1.21E+06	3.20E+01	2.11E-01	1.26E-02	8.81E-04	8.68E-06	2.47E-02
278	5476	805	7.71E-02	1.21	1.21	1.20E+06	3.20E+01	2.08E-01	1.35E-02	7.42E-04	8.99E-06	2.39E-02
288	9816	796	1.34E-01	1.21	1.22	1.18E+06	3.20E+01	2.04E-01	1.45E-02	6.33E-04	9.30E-06	2.30E-02
298	16849	786	2.23E-01	1.20	1.23	1.17E+06	3.20E+01	2.01E-01	1.54E-02	5.45E-04	9.62E-06	2.22E-02
308	27819	777	3.59E-01	1.20	1.24	1.15E+06	3.20E+01	1.98E-01	1.65E-02	4.73E-04	9.93E-06	2.13E-02
318	44348	767	5.58E-01	1.20	1.25	1.14E+06	3.20E+01	1.95E-01	1.76E-02	4.14E-04	1.02E-05	2.05E-02
328	68495	758	8.42E-01	1.20	1.26	1.12E+06	3.20E+01	1.92E-01	1.88E-02	3.66E-04	1.05E-05	1.96E-02
338	102800	748	1.24E+00	1.20	1.28	1.10E+06	3.20E+01	1.90E-01	2.01E-02	3.25E-04	1.08E-05	1.88E-02
348	150320	738	1.78E+00	1.21	1.30	1.08E+06	3.20E+01	1.88E-01	2.16E-02	2.90E-04	1.11E-05	1.79E-02
358	214680	727	2.50E+00	1.21	1.32	1.06E+06	3.20E+01	1.85E-01	2.32E-02	2.60E-04	1.14E-05	1.70E-02

[46]

Appendix E: Matlab Heat Pipe Operational Limits

```
%This is used to calculate the operational heat transfer limits of a heat pipe
% In Steady State modeling for acetone in aluminum
close all
clear all
clc

% Variable definitions
g=9.81;% Gravitational Acceleration [m/s^2]
R=8.314; % Universal Gas Constant [J/mol K]
rn=2.54E-7; %Nucleation site radius pg 98 Peterson. varies from 2.54E-5-2.54E-7 for metallic materials
S=1.05; % Crimping factor (Chi, 1976) pg 61
psi=pi/2; % HP Angle wrt horizontal [deg]
 % m=[]; %matrix to store values of the iterations
i=1; %Iteration number

% Parameters to Vary
%In Imperial Units
   material='Aluminum';
   lc=4; %Length of the condenser [in]
   la=3; %Length of the adiabatic region [in]
   le=3; %Length of the evaporator [in]
   dp=.75; %diameter of the pipe
   tp=0.063;
   dpi=dp-(2*tp); %Inner Pipe Diameter
   Nwrap=2; % Number of wraps of the screen wick

%Wick Parameters Assume a 2 layer mesh
   N=120; %% N Screen Mesh # [1/in] pg 73
   dw=0.004; %Wire Diameter p73 [in]
   kw=205; %Thermal Conductivity [W/m K]

% Calculated Values
   dp=dp*0.0254; %Converting diameter of the HP to metric [m]
   dpi=dpi*0.0254; %Converting diameter of the HP to metric [m]
   rpi=dpi/2; %Inner pipe radius
   lc=lc*0.0254; %Length of the condenser [m]
   la=la*0.0254; %Length of the adiabatic section [m]
   le=le*0.0254;
   N=N*39.37; %% N Screen Mesh # [1/m]
   dw=dw*0.0254; %Convert wire diamter to metric
% For Acetone
Prop=[
198.00  27.411  892.14  0.00096730  1.3902  1.1596  630130. 58.079  0.19559 0.0076679   0.0014663
0.0000053255   0.035698
208.00  79.214  881.47  0.0026618   1.3873  1.1565  620560. 58.079  0.19178 0.0081943   0.0011296
0.0000055905   0.034366
218.00  204.73  870.86  0.0065673   1.3852  1.1536  611070. 58.079  0.18788 0.0087452   0.00090525
0.0000058574   0.033041
228.00  480.68  860.27  0.014755    1.3837  1.1510  601630. 58.079  0.18390 0.0093224   0.00074812
0.0000061258   0.031724
```

```
238.00  1038.6  849.68  0.030580    1.3826  1.1487  592230. 58.079  0.17986 0.0099270    0.00063312
0.0000063954    0.030414
248.00  2087.7  839.07  0.059094    1.3819  1.1468  582820. 58.079  0.17578 0.010560    0.00054575
0.0000066656    0.029112
258.00  3939.9  828.40  0.10745 1.3815  1.1455  573360. 58.079  0.17167 0.011221    0.00047724  0.0000069362
0.027817
268.00  7034.4  817.67  0.18528 1.3814  1.1448  563820. 58.079  0.16753 0.011911    0.00042213  0.0000072065
0.026531
278.00  11961.  806.84  0.30493 1.3816  1.1447  554170. 58.079  0.16341 0.012630    0.00037686  0.0000074763
0.025254
288.00  19479.  795.89  0.48176 1.3821  1.1453  544350. 58.079  0.15931 0.013377    0.00033904  0.0000077452
0.023985
298.00  30529.  784.80  0.73422 1.3830  1.1467  534340. 58.079  0.15522 0.014151    0.00030704  0.0000080134
0.022726
308.00  46244.  773.54  1.0840  1.3843  1.1489  524100. 58.079  0.15115 0.014954    0.00027965  0.0000082809
0.021476
318.00  67946.  762.08  1.5563  1.3860  1.1521  513590. 58.079  0.14712 0.015784    0.00025600  0.0000085484
0.020236
328.00  97151.  750.40  2.1796  1.3883  1.1563  502770. 58.079  0.14313 0.016644    0.00023543  0.0000088169
0.019006
338.00  135550. 738.46  2.9864  1.3912  1.1616  491600. 58.079  0.13919 0.017533    0.00021742  0.0000090880
0.017788
348.00  185030. 726.22  4.0137  1.3949  1.1682  480020. 58.079  0.13530 0.018456    0.00020155  0.0000093638
0.016580
358.00  247600. 713.64  5.3034  1.3993  1.1764  467980. 58.079  0.13146 0.019416    0.00018749  0.0000096472
0.015385];

% Iterates thorough the table varying the vapor temperature of the HP to
% find the heat transfer limits and create a new table of important values
   MAX=size(Prop,1)

   for i=1:MAX
      m(i,1)=dp;
      % m(i,2)=le;
      Tp=Prop(i,1); %Temperature of the HP
      m(i,2)=Tp;
      m(i,11)=N;
      psat=Prop(i,2); % Saturation Pressure [Pa]
      m(i,10)=psat;
      rhol=Prop(i,3); %Density of the liquid [kg/m^3]
      rhov=Prop(i,4); %Density of the vapor [kg/m^3]
      gammav=Prop(i,6); % ratio of vapor cp/cv
      lambda=Prop(i,7); % Latent Heat of Vaporization [J/kg]
      kl=Prop(i,9); %Thermal Conductivity of the liquid[W/m K]
      mul=Prop(i,11);% Absolute viscosity [N s/m^2]
      muv=Prop(i,12);% Absolute viscosity [N s/m^2]
      sigma=Prop(i,13); % Surface Tension [N/m]
      M=Prop(i,8); %Molar mass [g/mol]
      Rgc=R*1000/M; %Vapor gas constant [J/kg K]

      % fprintf('The calculated Wick Porosity')
      epsilon=1-(pi*S*N*dw/4); % Wick Porosity
      % fprintf('The calculated Wick Permeability [m^2]')
      K=dw^2*epsilon^3/(122*(1-epsilon)^2); % Wick Permeability [m^2]
      rc=1/(2*N); %Capillary Radius
```

```
fprintf('The maximum Capillary Pumping Pressure [Pa]')
pcmax=2*sigma/rc
% m(i,5)=Pcmax;
dv=dpi-(Nwrap*(4*dw));
rv=dv/2;
% fprintf('The vapor area is [m^2]')
Av=pi*(dv^2)/4;
% fprintf('The liquid flow area is [m^2]')
Aw=pi*(dpi^2 - dv^2)/4;
lp=le+la+lc; %Total length of Pipe
leff=(0.5*le)+la+(0.5*lc); %Effective length of pipe
fprintf('The maximum axial Pressure Gradient [Pa]')
paxial=-rhol*g*lp*sin(psi) % Max pressure from gravity and orientation
ppm=pcmax-paxial; %Maximum effective pumping pressure
fprintf('Now assuming 1D, laminar, incompressible flow,\n')
fprintf('Take the pressure equation and solve for q [W].')
%Assumptions Rev<2300 & Mav<0.2
%From Iteration MA >0.2
% Ma=0.2293;
Cv=1;
Bv=16;
q=(pcmax-paxial)/(leff*((Cv*Bv*muv/(2*(dv/2)^2*Av*rhov*lambda))+(mul/(K*Aw*lambda*rhol))))
fprintf('A positive number means that the system will pump\n')
fprintf('Now to check the laminar and incompressible assumptions\n')
Re=4*q/(pi*dv*muv*lambda)
m(i,3)=Re;
fprintf('Since Re<2300 then the flow is laminar\n')
Ma=4*q/((lambda*pi*(dv)^2*rhov)*(gammav*(1000*R/M)*Tp)^0.5)
m(i,4)=Ma;
fprintf('since Ma<0.2then the flow is incompressible\n\n')
pv=(Cv*Bv*muv/(2*(dv/2)^2*Av*rhov*lambda))*leff*q;
pl=(mul/(K*Aw*lambda*rhol))*leff*q;
m(i,5)=q;

fprintf('Now to calculate the boiling, entrainment and sonic limits\n')
keff=(kl*((kl+kw)-(1-epsilon)*(kl-kw)))/((kl+kw)-(1+epsilon)*(kl-kw));
% Effective thermal conductivity of the saturated wick structure
rvh=0.5*dv;
Fv=(Bv*muv)/(2*Av*(rvh^2)*rhov*lambda); %[N/m^3 W] Vapor Frictional Coefficient
qcmL=q*leff; %[W m]
Fe=mul/(K*Aw*rhol*lambda); %[N/(m^3 W)] Liquid Frictional Coefficient
pc=Fe*leff*q+Fv*leff*q+paxial
qtest=ppm/(Fe+Fv); %[W m]

% Sonic Limit
fprintf('The sonic limit is')
qs=Av*rhov*lambda*((gammav*Rgc*Tp)/(2*(gammav+1)))^0.5
m(i,6)=qs;
%rho should be the stagnation density, but I do not know what that is

% Boiling Limit
fprintf('The boiling limit is')
qb=(2*pi*le*keff*Tp/(lambda*rhov*log(rpi/rv)))*((2*sigma/rn)-pcmax)
m(i,7)=qb;
```

```
        % Entrainment Limit
        rhw=Aw/(pi*(dv+dpi)); %hydralic radius of the wick
        fprintf('The entrainment limit is')
        qe=Av*lambda*(sigma*rhov/(2*rhw))^0.5
        m(i,8)=qe;

        %Checks to see if the inertial pressure gradient is neglible compared
        %to Pc. If it is not then it make be subtracted from Pc.
        Vv=q/(rhov*Av*lambda); %Mean vapor velocity
        pinertial=(rhov*(Vv)^2/(2*g))*((28/9)-(0.68*Re/((29*le/dv)+Re)))
        m(i,12)=le;
        m(i,13)=la;
        m(i,14)=lc;
        i=i+1;
    end

figure;

plotStyle = {'-bx', '-rs', '-g+', '-md', '-ko'};
for it=5:8
    plot(it)=semilogy( m(1:MAX,2), m(1:MAX,it), plotStyle {it-4}, 'LineWidth',1.5, 'MarkerSize', 7);
    hold on;
end

handle=gca;
set(handle, 'FontName','Arial','FontSize', 10)
ylabel('Heat Transport Capacity [W]','FontName','Arial Bold', 'FontSize', 9)
xlabel('Adiabatic Vapor Temperature [K]','FontName','Arial Bold', 'FontSize', 9)
stringTitle = ['Limits of an '  material ', 19 mm Diameter Heat Pipe containing Acetone'];
title (stringTitle ,'FontName','Arial Bold', 'FontSize', 12)
axis([m(1,2) m(MAX,2) 10^0 10^4])

legend('Capillary', 'Sonic', 'Boiling', 'Entrainment',...
    'Location', 'Southoutside', 'Orientation', 'horizontal')
% print(gcf, './Test Figure','-dpng')
% Moves the postition of the graph and resizes it
set(gcf, 'position', [800 100 1100 600]);
set(gcf, 'PaperPosition', [800 100 1100/100 600/100]);
%Saves the figure to the current folder
print(gcf, '-dpng', '-r100', ['./Acetone in .75 Aluminum Tube.png']);
```

Appendix F: Matlab Thermal Resistance Network

```
% Used to calculate the thermal resistance Network of the heat pipe.
%Working backwards from the known temperature of the condenser.
clc
clear all
%Parameters to Vary
   Tc=195; %Temperature of the condenser [K]
   dp=0.75; %diameter of the pipe
   dp=dp*0.0254; %Converting diameter of the HP to metric [m]
   dpe=0.715; %diameter of the pipe
   dpe=dpe*0.0254; %Converting diameter of the HP to metric [m]
   tp=0.0635; % Thickness of the pipe
   tp=tp*0.0254; %Converting pipe thickness to metric [m]
   dw=0.0045;%Thickness of wick (wrapped twice) 100 Mesh Number
   dw=dw*0.0254; %Convert to metric
   N=100; %% N Screen Mesh # [1/in]
   N=N*39.37; %% N Screen Mesh # [1/m]
   S=1.05; % Crimping factor (Chi, 1976)
   ks=386; %thermal conductivity of the copper pipe
   kw=386; %thermal conductivity of the copper wick
   kl=0.2375; %%Thermal Conductivity of methanol at 218K [W/m K]
   epsilon=1-(pi*S*N*dw/4); % Wick Porosity
   keff=(kl*((kl+kw)-(1-epsilon)*(kl-kw)))/((kl+kw)-(1+epsilon)*(kl-kw));
   q=10%[w]

   le=3; %Length of evaporator
   le=le*0.0254; %Length of the evaporator [m]
   la=3; % Length of the adiabatic section [in]
   la=la*0.0254; %Length of the condenser [m]
   lc=4; %Length of condenser
   lc=lc*0.0254; %Length of the condenser [m]

   %Calculated Values
   dpi=dp-(2*tp); %Inner Pipe Diameter
   dv=dpi-(4*dw); %inner diameter of the wick (AKA vapor column) [m]

   for i=1:6

      %Thermal Resistors %First finding the resistance of the heat pipe casing in the condenser
      Rsc=log(dp/dpi)/(2*pi*lc*ks);
      Rwc=log(dpi/dv)/(2*pi*lc*keff);
      Rwe=log(dpi/dv)/(2*pi*le*keff);
      Rse=log(dpe/dpi)/(2*pi*le*ks);

      %Used to determine if axial conduction will affect the HP

      R1=Rwe+Rwc;
      Rsep = le/(2*pi*ks*(dpe^2-((dpe+dpi)/2)^2));
      Rsa1 = la/(4*pi*ks*(dpe^2-((dpe+dpi)/2)^2));
      Rsa2 = la/(4*pi*ks*(dpe^2-((dpe+dpi)/2)^2));
      Rsa3 = la/(2*pi*ks*(dpe^2-((dpe+dpi)/2)^2));
      Rwae = log(dpi/dv)/(pi*la*keff);
      Rwac = log(dpi/dv)/(pi*la*keff);
```

```
    Rscp = lc/(2*pi*ks*(dp^2-((dp+dpi)/2)^2));
    R2=Rsep+Rsa1+(Rsa3*2*Rwae/(Rsa3+2*Rwae))+Rsa2+Rscp;
    R2/R1

    Rhp=Rse+R1+Rsc;
    Te = Rhp*q+Tc
    M(i,1)=q;
    M(i,2)=Te;
    Rhpconduction=Rse+(R1*R2/(R1+R2))+Rsc; %Rse+Rwe+Rie+Rv+Ric+Rwc+Rsc;
    Teconducation = Rhpconduction*q+Tc %Temp of the evaporator
    M(i,3)=Teconducation;

    q=q+10;
    i=i+1;
end
```

Appendix G: Matlab Stress Calculations

```
% This code is to calculate the maximum thermal and mechanical stress contained within different HP types under
% extreme conditions. This is for a heat pipe at 308K with 298K environmental  temp and containing acetone
clear all
clc
%Parameters to Vary
   Pi=46244; % Internal heat pipe pressure
   T3=255.6; %Temperature of the interior of the HP [K]
   T1=253.9; %Temperature of the exterior of the HP [K]
   dp=.75; %diameter of the pipe
   dp=dp*0.0254; %Converting diameter of the HP to metric [m]
   tp=[1/16]; % Thickness of the pipe
   tp=tp*0.0254; %Converting pipe thickness to metric [m]
   i=1;
   N=length(tp);

% %Standards for Aluminum
%    Po=101325; %External Pressure[Pa]
%    v=0.334; %Poissons Ratio Al
%    sy=95*10^6; %yield Strength of Aluminum at room temperature
%    dg=1; %Geometric parameter for cylinder is equal to 1

%Standards for Copper
   Po=101325; %External Pressure[Pa]
   v=0.355; %Poissons Ratio
   sy=70*10^6; %yield Strength at room temperature
   dg=1 %Geometric parameter for cylinder is equal to 1

% %Standards for Stainless Steel
%    Po=101325; %External Pressure[Pa]
%    v=0.305; %Poissons Ratio
%    sy=502*10^6; %yield Strength of SS at room temperature
%    dg=1 %Geometric parameter for cylinder is equal to 1

while i < N+1;
      %Calculated Values
      dpi=dp-(2*tp(i)); %Inner Pipe Diameter
      tpm=tp(i); %Converting pipe thickness to metric [m]
      R(i,1)=tpm;
      rpi=dpi/2; %Inner pipe radius
      ro=dp/2; %Outer Pipe diameter
      rm=(rpi+ro)/2; %Mean wall radius

   %Standards for Aluminum
      %Calculating the Youngs Modulus and Linear expansion at Twall
      MAl=[7.77E+01   -4.13E+02
      1.03E-02    -3.04E-01
      -2.92E-04   8.77E-03
      8.99E-07    -9.98E-06
      -1.07E-09   0]
     %Change Mal into the correct units
      x=1;
      while x<6;          MAl(x,1)=MAl(x,1)*10^9;
```

```
        MAl(x,2)=MAl(x,2)*10^5;
        x=x+1;
      end
      MAl;
       E=MAl(1,1)+ MAl(2,1)*T3 + MAl(3,1)*T3^2 + MAl(4,1)*T3^3 + MAl(5,1)*T3^4;
      %alpha=MAl(1,2)+ MAl(2,2)*Tp + MAl(3,2)*Tp^2 + MAl(4,2)*Tp^3 + MAl(5,2)*Tp^4
      alpha=23.6E-6;

%     %Standards for Copper
%        E=117E9;
%        alpha=16.6E-6;

%     %Standards for Stainless Steel
%        %Calculating the Youngs Modulus and Linear expansion at Twall
%        MAl=[2.10E+02 -2.96E+02
%        1.53E-01  -3.98E-01
%        -1.62E-03 9.27E-03
%        5.12E-06  -2.03E-05
%        -6.15E-09 1.71E-08]
%        %Change Mal into the correct units
%        x=1;
%        while x<6;
%           MAl(x,1)=MAl(x,1)*10^9;
%           MAl(x,2)=MAl(x,2)*10^5;
%           x=x+1;
%        end
%        MAl
% %        E=MAl(1,1)+ MAl(2,1)*T3 + MAl(3,1)*T3^2 + MAl(4,1)*T3^3 + MAl(5,1)*T3^4
%        %alpha=MAl(1,2)+ MAl(2,2)*Tp + MAl(3,2)*Tp^2 + MAl(4,2)*Tp^3 + MAl(5,2)*Tp^4
%        alpha=17.3E-6;

    fprintf('The hoop stress is [Pa]')
    sh=rm*(Po-Pi)/tpm
    R(i,2)=sh;
    fprintf('If the hoop stress is negative then it is tensile\n')
    fprintf('The Safety factor using the yield strength as the upper limit is [X]')
    safetyfactor=sy/abs(sh)
    R(i,3)=safetyfactor;

    fprintf('The compressive thermal stress is[Pa]')
    sthc=(alpha*E*(T1-T3)/(2*(1-v)))*(1+(dg*(ro-rpi)/(3*rpi)))
    R(i,4)=sthc;
    fprintf('The Safety factor using the yield strength as the upper limit is [X]')
    safetyfactorthc=sy/abs(sthc)
    R(i,5)=safetyfactorthc;

    fprintf('The tensile thermal stress is[Pa]')
    stht=(alpha*E*(T1-T3)/(2*(1-v)))*(1-(dg*(ro-rpi)/(3*rpi)))
    R(i,6)=stht;
    fprintf('The Safety factor using the yield strength as the upper limit is [X]')
    safetyfactortht=sy/abs(stht)
    R(i,7)=safetyfactortht;

    i=i+1;
end
```

Appendix H: Modeling Data: Varied Mesh size

Heat Transfer Limits of an Aluminum Heat Pipe containing Acetone Varying Mesh Number

	Pipe Diameter [m]	Temperature of HP [K]	Reynolds Number [X]	Mach Number [X]	Capillary Limit [W]	Sonic Limit [W]	Boiling Limit [W]	Entrainment Limit [W]	Viscous Limit [W]	Saturation Pressure [Pa]	Mesh # [1/m]	Evaporator Length [m]	Adiabatic Length [m]	Condenser Length [m]
120 Mesh using a twice wrapped screen	0.019	198	396	0.800	16	9	86906	33	17	27	4724	0.076	0.076	0.102
	0.019	208	477	0.359	20	26	31799	52	21	79	4724	0.076	0.076	0.102
	0.019	218	552	0.172	23	65	12921	79	25	205	4724	0.076	0.076	0.102
	0.019	228	620	0.088	27	147	5741	115	29	481	4724	0.076	0.076	0.102
	0.019	238	680	0.048	30	307	2754	159	33	1039	4724	0.076	0.076	0.102
	0.019	248	733	0.027	34	596	1412	213	36	2088	4724	0.076	0.076	0.102
	0.019	258	780	0.016	37	1086	766	276	40	3940	4724	0.076	0.076	0.102
	0.019	268	822	0.010	39	1877	437	348	43	7034	4724	0.076	0.076	0.102
	0.019	278	858	0.007	42	3092	260	428	45	11961	4724	0.076	0.076	0.102
	0.019	288	889	0.004	44	4885	161	515	48	19479	4724	0.076	0.076	0.102
	0.019	298	916	0.003	46	7437	103	608	50	30529	4724	0.076	0.076	0.102
	0.019	308	939	0.002	48	10953	67	704	52	46244	4724	0.076	0.076	0.102
	0.019	318	957	0.002	50	15668	45	803	54	67946	4724	0.076	0.076	0.102
	0.019	328	970	0.001	51	21835	31	901	55	97151	4724	0.076	0.076	0.102
	0.019	338	979	0.001	52	29726	22	998	56	135550	4724	0.076	0.076	0.102
	0.019	348	984	0.001	52	39635	16	1091	57	185030	4724	0.076	0.076	0.102
	0.019	358	983	0.000	52	51870	11	1178	57	247600	4724	0.076	0.076	0.102
Smaller mesh #50 results in a much higher Reynolds number	0.019	198	4675	10.126	173	8	36362	19	187	27	1969	0.076	0.076	0.102
	0.019	208	5946	4.800	227	23	13305	30	246	79	1969	0.076	0.076	0.102
	0.019	218	7075	2.372	279	57	5406	46	302	205	1969	0.076	0.076	0.102
	0.019	228	8068	1.233	327	128	2402	66	355	481	1969	0.076	0.076	0.102
	0.019	238	8941	0.674	373	267	1152	92	404	1039	1969	0.076	0.076	0.102
	0.019	248	9711	0.387	415	518	591	123	450	2088	1969	0.076	0.076	0.102
	0.019	258	10391	0.233	455	944	321	160	493	3940	1969	0.076	0.076	0.102
	0.019	268	10995	0.146	492	1632	183	202	533	7034	1969	0.076	0.076	0.102
	0.019	278	11530	0.094	526	2689	109	248	570	11961	1969	0.076	0.076	0.102
	0.019	288	12003	0.063	557	4248	67	299	604	19479	1969	0.076	0.076	0.102

	0.019	298	12418	0.044	586	6466	43	352	634	30529	1969	0.076	0.076	0.102
	0.019	308	12777	0.031	611	9523	28	408	662	46244	1969	0.076	0.076	0.102
	0.019	318	13079	0.022	632	13622	19	465	685	67946	1969	0.076	0.076	0.102
	0.019	328	13323	0.016	650	18984	13	522	705	97151	1969	0.076	0.076	0.102
	0.019	338	13506	0.012	664	25845	9	579	720	135550	1969	0.076	0.076	0.102
	0.019	348	13626	0.009	674	34460	6	632	731	185030	1969	0.076	0.076	0.102
	0.019	358	13679	0.007	680	45097	5	683	737	247600	1969	0.076	0.076	0.102

Heat Transfer Limits of an Copper Heat Pipe containing Acetone Varying Mesh Number

	Temperature of HP [K]	Reynolds Number [X]	Mach Number [X]	Capillary Limit [W]	Sonic Limit [W]	Boiling Limit [W]	Entrainment Limit [W]	Viscous Limit [W]	Saturation Pressure [Pa]	Mesh # [1/m]	Evaporator Length [m]	Adiabatic Length [m]	Condenser Length [m]
100 Mesh using a twice wrapped screen	198	694	1.412	27	9	74923	30	30	27.411	3937	0.076	0.076	0.102
	208	839	0.636	34	26	27415	49	37	79.214	3937	0.076	0.076	0.102
	218	973	0.306	41	64	11139	74	44	204.73	3937	0.076	0.076	0.102
	228	1094	0.157	47	145	4950	107	51	480.68	3937	0.076	0.076	0.102
	238	1202	0.085	53	303	2375	148	58	1038.6	3937	0.076	0.076	0.102
	248	1298	0.049	59	588	1217	198	64	2087.7	3937	0.076	0.076	0.102
	258	1382	0.029	64	1072	661	257	70	3939.9	3937	0.076	0.076	0.102
	268	1457	0.018	69	1852	377	324	75	7034.4	3937	0.076	0.076	0.102
	278	1522	0.012	74	3051	224	398	80	11961	3937	0.076	0.076	0.102
	288	1580	0.008	78	4820	139	479	85	19479	3937	0.076	0.076	0.102
	298	1629	0.005	82	7336	89	566	89	30529	3937	0.076	0.076	0.102
	308	1671	0.004	85	10805	58	655	92	46244	3937	0.076	0.076	0.102
	318	1705	0.003	88	15457	39	747	95	67946	3937	0.076	0.076	0.102
	328	1731	0.002	90	21541	27	838	98	97151	3937	0.076	0.076	0.102
	338	1750	0.002	92	29326	19	928	99	135550	3937	0.076	0.076	0.102
	348	1759	0.001	93	39102	13	1015	100	185030	3937	0.076	0.076	0.102
	358	1760	0.001	93	51171	10	1095	101	247600	3937	0.076	0.076	0.102
Smaller mesh #50 results in a much higher Reynolds number	198	4675	10.126	173	8	36351	19	187	27.411	1968	0.076	0.076	0.102
	208	5946	4.800	227	23	13301	30	246	79.214	1968	0.076	0.076	0.102
	218	7075	2.372	279	57	5404	46	302	204.73	1968	0.076	0.076	0.102
	228	8068	1.233	327	128	2401	66	355	480.68	1968	0.076	0.076	0.102
	238	8941	0.674	373	267	1152	92	404	1038.6	1968	0.076	0.076	0.102
	248	9711	0.387	415	518	591	123	450	2087.7	1968	0.076	0.076	0.102
	258	10391	0.233	455	944	320	160	493	3939.9	1968	0.076	0.076	0.102
	268	10995	0.146	492	1632	183	202	533	7034.4	1968	0.076	0.076	0.102
	278	11530	0.094	526	2689	109	248	570	11961	1968	0.076	0.076	0.102

	288	12003	0.063	557	4248	67	299	604	19479	1968	0.076	0.076	0.102
	298	12418	0.044	586	6466	43	352	634	30529	1968	0.076	0.076	0.102
	308	12777	0.031	611	9523	28	408	662	46244	1968	0.076	0.076	0.102
	318	13079	0.022	632	13622	19	465	685	67946	1968	0.076	0.076	0.102
	328	13323	0.016	650	18984	13	522	705	97151	1968	0.076	0.076	0.102
	338	13506	0.012	664	25845	9	579	720	135550	1968	0.076	0.076	0.102
	348	13626	0.009	674	34460	6	632	731	185030	1968	0.076	0.076	0.102
	358	13679	0.007	680	45097	5	683	737	247600	1968	0.076	0.076	0.102
Smaller mesh #80 results in many invalid approximations	198	1316	2.713	51	9	60356	27	55	27.411	3149	0.076	0.076	0.102
	208	1602	1.230	64	25	22085	43	70	79.214	3149	0.076	0.076	0.102
	218	1864	0.595	77	63	8974	65	84	204.73	3149	0.076	0.076	0.102
	228	2101	0.305	90	141	3987	94	97	480.68	3149	0.076	0.076	0.102
	238	2312	0.166	101	295	1913	130	110	1038.6	3149	0.076	0.076	0.102
	248	2500	0.095	112	572	981	174	122	2087.7	3149	0.076	0.076	0.102
	258	2666	0.057	123	1043	532	226	133	3939.9	3149	0.076	0.076	0.102
	268	2814	0.035	132	1802	303	285	143	7034.4	3149	0.076	0.076	0.102
	278	2944	0.023	141	2968	181	351	153	11961	3149	0.076	0.076	0.102
	288	3058	0.015	149	4689	112	422	162	19479	3149	0.076	0.076	0.102
	298	3157	0.011	156	7138	71	498	169	30529	3149	0.076	0.076	0.102
	308	3242	0.007	163	10513	47	577	176	46244	3149	0.076	0.076	0.102
	318	3312	0.005	168	15039	32	657	182	67946	3149	0.076	0.076	0.102
	328	3367	0.004	173	20958	22	738	187	97151	3149	0.076	0.076	0.102
	338	3406	0.003	176	28533	15	817	191	135550	3149	0.076	0.076	0.102
	348	3430	0.002	178	38045	11	893	193	185030	3149	0.076	0.076	0.102
	358	3436	0.002	179	49788	8	964	194	247600	3149	0.076	0.076	0.102

Heat Transfer Limits of an Copper Heat Pipe containing Methanol Varying Mesh Number

	Temperature of HP [K]	**Reynolds Number [X]**	**Mach Number [X]**	**Capillary Limit [W]**	**Sonic Limit [W]**	**Boiling Limit [W]**	**Entrainment Limit [W]**	**Viscous Limit [W]**	**Saturation Pressure [Pa]**	**Mesh # [1/m]**	**Evaporator Length [m]**	**Adiabatic Length [m]**	**Condenser Length [m]**
100 Mesh using a twice wrapped screen	198	160	2.983	16	2	441482	18	17	4.7406	3937	0.076	0.076	0.102
	208	213	1.283	22	8	137199	32	24	15.823	3937	0.076	0.076	0.102
	218	268	0.584	28	23	47930	52	31	46.904	3937	0.076	0.076	0.102
	228	324	0.282	36	60	18528	80	39	125.47	3937	0.076	0.076	0.102
	238	382	0.145	43	142	7822	120	47	306.9	3937	0.076	0.076	0.102
	248	442	0.079	52	312	3567	172	56	694.17	3937	0.076	0.076	0.102
	258	505	0.045	61	641	1740	239	66	1465.5	3937	0.076	0.076	0.102
	268	569	0.027	70	1240	901	321	76	2910.7	3937	0.076	0.076	0.102
	278	634	0.017	80	2275	492	421	87	5476.1	3937	0.076	0.076	0.102

	288	700	0.011	90	3980	281	539	98	9816	3937	0.076	0.076	0.102
	298	765	0.007	101	6675	168	674	109	16849	3937	0.076	0.076	0.102
	308	830	0.005	111	10778	104	827	121	27819	3937	0.076	0.076	0.102
	318	893	0.003	122	16815	66	996	132	44348	3937	0.076	0.076	0.102
	328	955	0.002	132	25441	43	1179	143	68495	3937	0.076	0.076	0.102
	338	1014	0.002	142	37433	29	1375	154	102800	3937	0.076	0.076	0.102
	348	1071	0.001	151	53705	20	1579	163	150320	3937	0.076	0.076	0.102
	358	1126	0.001	159	75308	14	1787	173	214680	3937	0.076	0.076	0.102
Smaller mesh #50 results in a much higher Reynolds number	198	865	17.181	80	2	214194	11	87	4.7406	1968	0.076	0.076	0.102
	208	1357	8.700	130	7	66565	20	141	15.823	1968	0.076	0.076	0.102
	218	1852	4.301	184	20	23254	32	200	46.904	1968	0.076	0.076	0.102
	228	2335	2.169	241	53	8989	50	261	125.47	1968	0.076	0.076	0.102
	238	2815	1.140	300	125	3795	75	325	306.9	1968	0.076	0.076	0.102
	248	3300	0.627	362	275	1731	107	392	694.17	1968	0.076	0.076	0.102
	258	3795	0.361	428	565	844	149	464	1465.5	1968	0.076	0.076	0.102
	268	4298	0.217	498	1093	437	200	539	2910.7	1968	0.076	0.076	0.102
	278	4810	0.135	571	2005	239	262	618	5476.1	1968	0.076	0.076	0.102
	288	5324	0.087	646	3508	137	336	700	9816	1968	0.076	0.076	0.102
	298	5838	0.058	723	5883	81	420	783	16849	1968	0.076	0.076	0.102
	308	6346	0.040	800	9499	50	515	867	27819	1968	0.076	0.076	0.102
	318	6846	0.028	877	14819	32	620	950	44348	1968	0.076	0.076	0.102
	328	7334	0.020	952	22421	21	735	1031	68495	1968	0.076	0.076	0.102
	338	7807	0.015	1024	32989	14	857	1110	102800	1968	0.076	0.076	0.102
	348	8265	0.011	1093	47330	10	984	1184	150320	1968	0.076	0.076	0.102
	358	8705	0.008	1157	66369	7	1114	1253	214680	1968	0.076	0.076	0.102
Smaller mesh #80 results in many invalid approximations	198	294	5.563	29	2	355646	16	31	4.7406	3149	0.076	0.076	0.102
	208	402	2.453	41	8	110524	28	44	15.823	3149	0.076	0.076	0.102
	218	511	1.129	53	22	38611	45	58	46.904	3149	0.076	0.076	0.102
	228	622	0.550	67	58	14925	71	73	125.47	3149	0.076	0.076	0.102
	238	735	0.283	82	138	6301	106	89	306.9	3149	0.076	0.076	0.102
	248	853	0.154	98	304	2873	151	107	694.17	3149	0.076	0.076	0.102
	258	975	0.088	116	624	1402	210	125	1465.5	3149	0.076	0.076	0.102
	268	1100	0.053	134	1206	726	283	145	2910.7	3149	0.076	0.076	0.102
	278	1227	0.033	153	2213	396	371	166	5476.1	3149	0.076	0.076	0.102
	288	1356	0.021	173	3873	227	474	187	9816	3149	0.076	0.076	0.102
	298	1484	0.014	193	6495	135	593	209	16849	3149	0.076	0.076	0.102
	308	1610	0.010	213	10487	84	728	231	27819	3149	0.076	0.076	0.102
	318	1735	0.007	233	16361	53	876	253	44348	3149	0.076	0.076	0.102
	328	1856	0.005	253	24753	35	1038	274	68495	3149	0.076	0.076	0.102
	338	1973	0.003	272	36421	24	1210	295	102800	3149	0.076	0.076	0.102
	348	2085	0.003	290	52254	16	1389	314	150320	3149	0.076	0.076	0.102
	358	2193	0.002	306	73273	11	1573	332	214680	3149	0.076	0.076	0.102

Appendix I: Modeling Data: Varied Number of Mesh Screen Wraps

Heat Transfer Limits of an Aluminum Heat Pipe containing Acetone Varying the Screen Wraps

	Pipe Diameter [m]	Temperature of HP [K]	Reynolds Number [X]	Mach Number [X]	Capillary Limit [W]	Sonic Limit [W]	Boiling Limit [W]	Entrainment Limit [W]	Viscous Limit [W]	Saturation Pressure [Pa]	Mesh # [1/m]	Evaporator Length [m]	Adiabatic Length [m]	Condenser Length [m]
Single wrapped mesh, slightly reduced the Reynolds #	0.019	198	196	0.386	8	10	176129	49	9	27	4724	0.076	0.076	0.102
	0.019	208	236	0.173	10	28	64446	78	11	79	4724	0.076	0.076	0.102
	0.019	218	272	0.083	12	69	26186	118	13	205	4724	0.076	0.076	0.102
	0.019	228	306	0.042	14	155	11636	171	15	481	4724	0.076	0.076	0.102
	0.019	238	335	0.023	15	324	5582	237	17	1039	4724	0.076	0.076	0.102
	0.019	248	362	0.013	17	628	2861	318	18	2088	4724	0.076	0.076	0.102
	0.019	258	385	0.008	19	1146	1553	412	20	3940	4724	0.076	0.076	0.102
	0.019	268	405	0.005	20	1980	885	519	22	7034	4724	0.076	0.076	0.102
	0.019	278	423	0.003	21	3262	527	639	23	11961	4724	0.076	0.076	0.102
	0.019	288	439	0.002	22	5153	326	769	24	19479	4724	0.076	0.076	0.102
	0.019	298	452	0.001	23	7844	208	907	25	30529	4724	0.076	0.076	0.102
	0.019	308	463	0.001	24	11553	137	1051	26	46244	4724	0.076	0.076	0.102
	0.019	318	472	0.001	25	16527	92	1198	27	67946	4724	0.076	0.076	0.102
	0.019	328	479	0.001	26	23031	63	1345	28	97151	4724	0.076	0.076	0.102
	0.019	338	483	0.000	26	31355	44	1489	28	135550	4724	0.076	0.076	0.102
	0.019	348	485	0.000	26	41807	31	1627	29	185030	4724	0.076	0.076	0.102
	0.019	358	485	0.000	27	54711	23	1757	29	247600	4724	0.076	0.076	0.102
Double wrapped Screen: Increased Reynolds & Mach #'s and HT Limits	0.019	198	396	0.800	16	9	86906	33	17	27	4724	0.076	0.076	0.102
	0.019	208	477	0.359	20	26	31799	52	21	79	4724	0.076	0.076	0.102
	0.019	218	552	0.172	23	65	12921	79	25	205	4724	0.076	0.076	0.102
	0.019	228	620	0.088	27	147	5741	115	29	481	4724	0.076	0.076	0.102
	0.019	238	680	0.048	30	307	2754	159	33	1039	4724	0.076	0.076	0.102
	0.019	248	733	0.027	34	596	1412	213	36	2088	4724	0.076	0.076	0.102
	0.019	258	780	0.016	37	1086	766	276	40	3940	4724	0.076	0.076	0.102
	0.019	268	822	0.010	39	1877	437	348	43	7034	4724	0.076	0.076	0.102
	0.019	278	858	0.007	42	3092	260	428	45	11961	4724	0.076	0.076	0.102
	0.019	288	889	0.004	44	4885	161	515	48	19479	4724	0.076	0.076	0.102
	0.019	298	916	0.003	46	7437	103	608	50	30529	4724	0.076	0.076	0.102
	0.019	308	939	0.002	48	10953	67	704	52	46244	4724	0.076	0.076	0.102
	0.019	318	957	0.002	50	15668	45	803	54	67946	4724	0.076	0.076	0.102
	0.019	328	970	0.001	51	21835	31	901	55	97151	4724	0.076	0.076	0.102
	0.019	338	979	0.001	52	29726	22	998	56	135550	4724	0.076	0.076	0.102
	0.019	348	984	0.001	52	39635	16	1091	57	185030	4724	0.076	0.076	0.102
	0.019	358	983	0.000	52	51870	11	1178	57	247600	4724	0.076	0.076	0.102
Made it a triple	0.019	198	600	1.246	23	9	57158	25	25	27	4724	0.076	0.076	0.102
	0.019	208	724	0.560	29	25	20914	40	31	79	4724	0.076	0.076	0.102

wrapped screen: Increased Reynolds & Mach #'s and HT Limits	0.019	218	839	0.269	34	62	8498	61	37	205	4724	0.076	0.076	0.102
	0.019	228	942	0.138	40	139	3776	89	43	481	4724	0.076	0.076	0.102
	0.019	238	1034	0.075	45	291	1812	123	49	1039	4724	0.076	0.076	0.102
	0.019	248	1115	0.043	50	564	929	165	54	2088	4724	0.076	0.076	0.102
	0.019	258	1187	0.025	54	1028	504	213	59	3940	4724	0.076	0.076	0.102
	0.019	268	1250	0.016	58	1777	287	269	63	7034	4724	0.076	0.076	0.102
	0.019	278	1305	0.010	62	2928	171	331	67	11961	4724	0.076	0.076	0.102
	0.019	288	1353	0.007	66	4625	106	398	71	19479	4724	0.076	0.076	0.102
	0.019	298	1394	0.005	69	7040	68	470	74	30529	4724	0.076	0.076	0.102
	0.019	308	1428	0.003	71	10369	44	544	77	46244	4724	0.076	0.076	0.102
	0.019	318	1455	0.002	73	14833	30	621	80	67946	4724	0.076	0.076	0.102
	0.019	328	1476	0.002	75	20670	21	697	81	97151	4724	0.076	0.076	0.102
	0.019	338	1490	0.001	76	28141	14	771	83	135550	4724	0.076	0.076	0.102
	0.019	348	1497	0.001	77	37522	10	843	84	185030	4724	0.076	0.076	0.102
	0.019	358	1495	0.001	78	49104	7	910	84	247600	4724	0.076	0.076	0.102
Make a 4 x wrapped screen	0.019	198	808	1.726	30	8	42278	21	33	27	4724	0.076	0.076	0.102
	0.019	208	977	0.778	38	23	15470	33	41	79	4724	0.076	0.076	0.102
	0.019	218	1133	0.375	45	58	6286	50	49	205	4724	0.076	0.076	0.102
	0.019	228	1274	0.192	52	132	2793	73	57	481	4724	0.076	0.076	0.102
	0.019	238	1399	0.104	59	275	1340	101	64	1039	4724	0.076	0.076	0.102
	0.019	248	1509	0.059	65	533	687	135	71	2088	4724	0.076	0.076	0.102
	0.019	258	1606	0.035	71	972	373	175	77	3940	4724	0.076	0.076	0.102
	0.019	268	1691	0.022	77	1680	213	220	83	7034	4724	0.076	0.076	0.102
	0.019	278	1766	0.014	82	2767	127	271	89	11961	4724	0.076	0.076	0.102
	0.019	288	1830	0.010	86	4372	78	326	93	19479	4724	0.076	0.076	0.102
	0.019	298	1886	0.007	90	6654	50	385	98	30529	4724	0.076	0.076	0.102
	0.019	308	1932	0.005	94	9801	33	446	101	46244	4724	0.076	0.076	0.102
	0.019	318	1969	0.003	97	14020	22	508	105	67946	4724	0.076	0.076	0.102
	0.019	328	1997	0.002	99	19538	15	570	107	97151	4724	0.076	0.076	0.102
	0.019	338	2016	0.002	101	26599	11	632	109	135550	4724	0.076	0.076	0.102
	0.019	348	2025	0.001	102	35466	8	690	110	185030	4724	0.076	0.076	0.102
	0.019	358	2024	0.001	102	46414	5	745	111	247600	4724	0.076	0.076	0.102
Make a 5 x wrapped screen	0.019	198	1020	2.242	37	8	33346	17	40	27	4724	0.076	0.076	0.102
	0.019	208	1237	1.013	47	22	12201	28	50	79	4724	0.076	0.076	0.102
	0.019	218	1436	0.489	56	55	4958	42	60	205	4724	0.076	0.076	0.102
	0.019	228	1615	0.250	65	124	2203	61	70	481	4724	0.076	0.076	0.102
	0.019	238	1774	0.136	73	259	1057	85	79	1039	4724	0.076	0.076	0.102
	0.019	248	1915	0.077	81	503	542	114	87	2088	4724	0.076	0.076	0.102
	0.019	258	2038	0.046	88	917	294	147	95	3940	4724	0.076	0.076	0.102
	0.019	268	2146	0.029	95	1585	168	186	103	7034	4724	0.076	0.076	0.102
	0.019	278	2241	0.019	101	2611	100	229	109	11961	4724	0.076	0.076	0.102
	0.019	288	2323	0.012	106	4125	62	275	115	19479	4724	0.076	0.076	0.102
	0.019	298	2393	0.009	111	6280	39	325	120	30529	4724	0.076	0.076	0.102
	0.019	308	2452	0.006	116	9249	26	376	125	46244	4724	0.076	0.076	0.102
	0.019	318	2500	0.004	119	13230	17	429	129	67946	4724	0.076	0.076	0.102
	0.019	328	2535	0.003	122	18437	12	481	132	97151	4724	0.076	0.076	0.102

	0.019	338	2559	0.002	124	25101	8	533	134	135550	4724	0.076	0.076	0.102
	0.019	348	2570	0.002	125	33469	6	583	136	185030	4724	0.076	0.076	0.102
	0.019	358	2569	0.001	126	43799	4	629	136	247600	4724	0.076	0.076	0.102

Heat Transfer Limits of a Copper Heat Pipe containing Acetone Varying the Screen Wraps

	Pipe Diameter [m]	Temperature of HP [K]	Reynolds Number [X]	Mach Number [X]	Capillary Limit [W]	Sonic Limit [W]	Boiling Limit [W]	Entrainment Limit [W]	Viscous Limit [W]	Saturation Pressure [Pa]	Mesh # [1/m]	Evaporator Length [m]	Adiabatic Length [m]	Condenser Length [m]
Single wrapped mesh, slightly reduced the Reynolds #	0.019	198	344	0.679	14	10	152106	46	15	27	3937	0.076	0.076	0.102
	0.019	208	414	0.305	17	27	55656	73	19	79	3937	0.076	0.076	0.102
	0.019	218	480	0.146	21	68	22615	111	22	205	3937	0.076	0.076	0.102
	0.019	228	539	0.075	24	154	10049	160	26	481	3937	0.076	0.076	0.102
	0.019	238	592	0.041	27	322	4821	222	29	1039	3937	0.076	0.076	0.102
	0.019	248	639	0.023	30	624	2471	298	33	2088	3937	0.076	0.076	0.102
	0.019	258	681	0.014	33	1138	1341	386	35	3940	3937	0.076	0.076	0.102
	0.019	268	717	0.009	35	1967	765	487	38	7034	3937	0.076	0.076	0.102
	0.019	278	750	0.006	38	3240	455	599	41	11961	3937	0.076	0.076	0.102
	0.019	288	778	0.004	40	5119	281	720	43	19479	3937	0.076	0.076	0.102
	0.019	298	802	0.003	42	7792	180	849	45	30529	3937	0.076	0.076	0.102
	0.019	308	823	0.002	43	11477	118	984	47	46244	3937	0.076	0.076	0.102
	0.019	318	840	0.001	45	16418	79	1122	48	67946	3937	0.076	0.076	0.102
	0.019	328	852	0.001	46	22880	55	1259	49	97151	3937	0.076	0.076	0.102
	0.019	338	861	0.001	47	31149	38	1394	50	135550	3937	0.076	0.076	0.102
	0.019	348	866	0.001	47	41532	27	1524	51	185030	3937	0.076	0.076	0.102
	0.019	358	867	0.000	47	54352	20	1645	51	247600	3937	0.076	0.076	0.102
Double wrapped Screen: Increased Reynolds & Mach #'s and HT Limits	0.019	198	694	1.412	27	9	74923	30	30	27	3937	0.076	0.076	0.102
	0.019	208	839	0.636	34	26	27415	49	37	79	3937	0.076	0.076	0.102
	0.019	218	973	0.306	41	64	11139	74	44	205	3937	0.076	0.076	0.102
	0.019	228	1094	0.157	47	145	4950	107	51	481	3937	0.076	0.076	0.102
	0.019	238	1202	0.085	53	303	2375	148	58	1039	3937	0.076	0.076	0.102
	0.019	248	1298	0.049	59	588	1217	198	64	2088	3937	0.076	0.076	0.102
	0.019	258	1382	0.029	64	1072	661	257	70	3940	3937	0.076	0.076	0.102
	0.019	268	1457	0.018	69	1852	377	324	75	7034	3937	0.076	0.076	0.102
	0.019	278	1522	0.012	74	3051	224	398	80	11961	3937	0.076	0.076	0.102
	0.019	288	1580	0.008	78	4820	139	479	85	19479	3937	0.076	0.076	0.102
	0.019	298	1629	0.005	82	7336	89	566	89	30529	3937	0.076	0.076	0.102
	0.019	308	1671	0.004	85	10805	58	655	92	46244	3937	0.076	0.076	0.102
	0.019	318	1705	0.003	88	15457	39	747	95	67946	3937	0.076	0.076	0.102
	0.019	328	1731	0.002	90	21541	27	838	98	97151	3937	0.076	0.076	0.102
	0.019	338	1750	0.002	92	29326	19	928	99	135550	3937	0.076	0.076	0.102
	0.019	348	1759	0.001	93	39102	13	1015	100	185030	3937	0.076	0.076	0.102
	0.019	358	1760	0.001	93	51171	10	1095	101	247600	3937	0.076	0.076	0.102
	0.019	198	1050	2.203	40	9	49188	23	43	27	3937	0.076	0.076	0.102

Made it a triple wrapped screen: Increased Reynolds & Mach #'s and HT Limits	0.019	208	1274	0.996	50	24	17998	37	54	79	3937	0.076	0.076	0.102
	0.019	218	1480	0.480	60	60	7313	57	65	205	3937	0.076	0.076	0.102
	0.019	228	1665	0.246	70	137	3250	82	76	481	3937	0.076	0.076	0.102
	0.019	238	1831	0.134	79	285	1559	114	85	1039	3937	0.076	0.076	0.102
	0.019	248	1977	0.076	87	552	799	152	95	2088	3937	0.076	0.076	0.102
	0.019	258	2106	0.046	95	1007	434	197	103	3940	3937	0.076	0.076	0.102
	0.019	268	2220	0.028	103	1740	247	249	111	7034	3937	0.076	0.076	0.102
	0.019	278	2320	0.018	109	2867	147	306	118	11961	3937	0.076	0.076	0.102
	0.019	288	2408	0.012	115	4529	91	368	125	19479	3937	0.076	0.076	0.102
	0.019	298	2483	0.008	121	6894	58	434	131	30529	3937	0.076	0.076	0.102
	0.019	308	2547	0.006	126	10154	38	503	136	46244	3937	0.076	0.076	0.102
	0.019	318	2599	0.004	130	14525	26	573	141	67946	3937	0.076	0.076	0.102
	0.019	328	2639	0.003	133	20242	18	643	144	97151	3937	0.076	0.076	0.102
	0.019	338	2667	0.002	135	27558	12	712	147	135550	3937	0.076	0.076	0.102
	0.019	348	2682	0.002	137	36744	9	778	148	185030	3937	0.076	0.076	0.102
	0.019	358	2683	0.001	138	48086	6	840	149	247600	3937	0.076	0.076	0.102
Make a 4 x wrapped screen	0.019	198	1411	3.056	52	8	36314	19	56	27	3937	0.076	0.076	0.102
	0.019	208	1719	1.388	66	23	13288	30	71	79	3937	0.076	0.076	0.102
	0.019	218	2002	0.671	79	57	5399	46	85	205	3937	0.076	0.076	0.102
	0.019	228	2255	0.345	92	128	2399	66	99	481	3937	0.076	0.076	0.102
	0.019	238	2481	0.187	103	267	1151	92	112	1039	3937	0.076	0.076	0.102
	0.019	248	2680	0.107	115	518	590	123	124	2088	3937	0.076	0.076	0.102
	0.019	258	2855	0.064	125	944	320	160	135	3940	3937	0.076	0.076	0.102
	0.019	268	3010	0.040	135	1632	183	202	146	7034	3937	0.076	0.076	0.102
	0.019	278	3146	0.026	144	2689	109	248	156	11961	3937	0.076	0.076	0.102
	0.019	288	3265	0.017	152	4248	67	299	164	19479	3937	0.076	0.076	0.102
	0.019	298	3367	0.012	159	6466	43	352	172	30529	3937	0.076	0.076	0.102
	0.019	308	3454	0.008	165	9523	28	408	179	46244	3937	0.076	0.076	0.102
	0.019	318	3524	0.006	170	13622	19	465	185	67946	3937	0.076	0.076	0.102
	0.019	328	3579	0.004	175	18984	13	522	189	97151	3937	0.076	0.076	0.102
	0.019	338	3616	0.003	178	25845	9	579	193	135550	3937	0.076	0.076	0.102
	0.019	348	3637	0.003	180	34460	6	632	195	185030	3937	0.076	0.076	0.102
	0.019	358	3638	0.002	181	45097	5	683	196	247600	3937	0.076	0.076	0.102
Make a 5 x wrapped screen	0.019	198	1775	3.974	63	8	28585	16	69	27	3937	0.076	0.076	0.102
	0.019	208	2175	1.815	80	21	10459	25	87	79	3937	0.076	0.076	0.102
	0.019	218	2539	0.880	97	53	4250	38	105	205	3937	0.076	0.076	0.102
	0.019	228	2865	0.452	112	120	1888	56	122	481	3937	0.076	0.076	0.102
	0.019	238	3153	0.246	127	250	906	77	138	1039	3937	0.076	0.076	0.102
	0.019	248	3408	0.140	141	485	464	103	153	2088	3937	0.076	0.076	0.102
	0.019	258	3632	0.084	154	884	252	134	167	3940	3937	0.076	0.076	0.102
	0.019	268	3829	0.052	166	1527	144	169	180	7034	3937	0.076	0.076	0.102
	0.019	278	4002	0.034	177	2516	86	208	191	11961	3937	0.076	0.076	0.102
	0.019	288	4154	0.023	187	3975	53	250	202	19479	3937	0.076	0.076	0.102
	0.019	298	4284	0.016	195	6051	34	295	212	30529	3937	0.076	0.076	0.102
	0.019	308	4394	0.011	203	8912	22	342	220	46244	3937	0.076	0.076	0.102
	0.019	318	4484	0.008	210	12748	15	390	227	67946	3937	0.076	0.076	0.102

	0.019	328	4553	0.006	215	17766	10	437	233	97151	3937	0.076	0.076	0.102
	0.019	338	4601	0.004	219	24187	7	484	237	135550	3937	0.076	0.076	0.102
	0.019	348	4627	0.003	222	32250	5	529	240	185030	3937	0.076	0.076	0.102
	0.019	358	4629	0.003	223	42204	4	571	241	247600	3937	0.076	0.076	0.102

Heat Transfer Limits of an Copper Heat Pipe containing Methanol the Varying Screen Wraps

	Pipe Diameter [m]	Temperature of HP [K]	Reynolds Number [X]	Mach Number [X]	Capillary Limit [W]	Sonic Limit [W]	Boiling Limit [W]	Entrainment Limit [W]	Viscous Limit [W]	Saturation Pressure [Pa]	Mesh # [1/m]	Evaporator Length [m]	Adiabatic Length [m]	Condenser Length [m]
Single wrapped mesh, slightly reduced the Reynolds #	0.019	198	81	1.459	8	3	896277	27	9	5	3937	0.076	0.076	0.102
	0.019	208	106	0.620	11	9	278536	47	12	16	3937	0.076	0.076	0.102
	0.019	218	133	0.280	14	25	97306	78	16	47	3937	0.076	0.076	0.102
	0.019	228	160	0.135	18	64	37614	121	20	125	3937	0.076	0.076	0.102
	0.019	238	188	0.069	22	151	15881	180	24	307	3937	0.076	0.076	0.102
	0.019	248	218	0.038	26	331	7241	258	28	694	3937	0.076	0.076	0.102
	0.019	258	249	0.022	31	681	3533	359	33	1466	3937	0.076	0.076	0.102
	0.019	268	280	0.013	36	1317	1830	483	39	2911	3937	0.076	0.076	0.102
	0.019	278	312	0.008	41	2416	999	632	44	5476	3937	0.076	0.076	0.102
	0.019	288	345	0.005	46	4228	571	809	50	9816	3937	0.076	0.076	0.102
	0.019	298	377	0.003	51	7090	341	1012	55	16849	3937	0.076	0.076	0.102
	0.019	308	409	0.002	57	11448	211	1242	61	27819	3937	0.076	0.076	0.102
	0.019	318	440	0.002	62	17861	134	1496	67	44348	3937	0.076	0.076	0.102
	0.019	328	470	0.001	67	27022	88	1771	73	68495	3937	0.076	0.076	0.102
	0.019	338	499	0.001	72	39760	59	2065	78	102800	3937	0.076	0.076	0.102
	0.019	348	527	0.001	77	57043	41	2371	83	150320	3937	0.076	0.076	0.102
Double wrapped Screen: Increased Reynolds & Mach #'s and HT Limits	0.019	198	160	2.983	16	2	441482	18	17	5	3937	0.076	0.076	0.102
	0.019	208	213	1.283	22	8	137199	32	24	16	3937	0.076	0.076	0.102
	0.019	218	268	0.584	28	23	47930	52	31	47	3937	0.076	0.076	0.102
	0.019	228	324	0.282	36	60	18528	80	39	125	3937	0.076	0.076	0.102
	0.019	238	382	0.145	43	142	7822	120	47	307	3937	0.076	0.076	0.102
	0.019	248	442	0.079	52	312	3567	172	56	694	3937	0.076	0.076	0.102
	0.019	258	505	0.045	61	641	1740	239	66	1466	3937	0.076	0.076	0.102
	0.019	268	569	0.027	70	1240	901	321	76	2911	3937	0.076	0.076	0.102
	0.019	278	634	0.017	80	2275	492	421	87	5476	3937	0.076	0.076	0.102
	0.019	288	700	0.011	90	3980	281	539	98	9816	3937	0.076	0.076	0.102
	0.019	298	765	0.007	101	6675	168	674	109	16849	3937	0.076	0.076	0.102
	0.019	308	830	0.005	111	10778	104	827	121	27819	3937	0.076	0.076	0.102
	0.019	318	893	0.003	122	16815	66	996	132	44348	3937	0.076	0.076	0.102
	0.019	328	955	0.002	132	25441	43	1179	143	68495	3937	0.076	0.076	0.102
	0.019	338	1014	0.002	142	37433	29	1375	154	102800	3937	0.076	0.076	0.102
	0.019	348	1071	0.001	151	53705	20	1579	163	150320	3937	0.076	0.076	0.102
	0.019	358	1126	0.001	159	75308	14	1787	173	214680	3937	0.076	0.076	0.102
	0.019	198	237	4.558	23	2	289838	14	25	5	3937	0.076	0.076	0.102

Made it a triple wrapped screen: Increased Reynolds & Mach #'s and HT Limits	0.019	208	321	1.991	32	8	90073	24	34	16	3937	0.076	0.076	0.102
	0.019	218	405	0.912	42	22	31467	40	45	47	3937	0.076	0.076	0.102
	0.019	228	492	0.443	52	56	12164	62	57	125	3937	0.076	0.076	0.102
	0.019	238	581	0.228	64	133	5135	92	69	307	3937	0.076	0.076	0.102
	0.019	248	673	0.124	76	293	2342	132	83	694	3937	0.076	0.076	0.102
	0.019	258	769	0.071	90	602	1143	183	97	1466	3937	0.076	0.076	0.102
	0.019	268	867	0.042	104	1165	592	247	112	2911	3937	0.076	0.076	0.102
	0.019	278	966	0.026	118	2138	323	323	128	5476	3937	0.076	0.076	0.102
	0.019	288	1066	0.017	134	3740	185	413	145	9816	3937	0.076	0.076	0.102
	0.019	298	1166	0.011	149	6273	110	517	162	16849	3937	0.076	0.076	0.102
	0.019	308	1265	0.008	165	10128	68	634	178	27819	3937	0.076	0.076	0.102
	0.019	318	1362	0.005	180	15802	43	764	195	44348	3937	0.076	0.076	0.102
	0.019	328	1455	0.004	195	23907	29	905	211	68495	3937	0.076	0.076	0.102
	0.019	338	1546	0.003	209	35176	19	1055	227	102800	3937	0.076	0.076	0.102
	0.019	348	1633	0.002	223	50467	13	1211	242	150320	3937	0.076	0.076	0.102
Make a 4 x wrapped screen	0.019	198	311	6.170	29	2	213979	11	31	5	3937	0.076	0.076	0.102
	0.019	208	428	2.743	41	7	66498	20	45	16	3937	0.076	0.076	0.102
	0.019	218	545	1.267	54	20	23231	32	59	47	3937	0.076	0.076	0.102
	0.019	228	664	0.617	68	53	8980	50	74	125	3937	0.076	0.076	0.102
	0.019	238	786	0.318	84	125	3791	75	91	307	3937	0.076	0.076	0.102
	0.019	248	912	0.173	100	275	1729	107	108	694	3937	0.076	0.076	0.102
	0.019	258	1041	0.099	117	565	844	149	127	1466	3937	0.076	0.076	0.102
	0.019	268	1174	0.059	136	1093	437	200	147	2911	3937	0.076	0.076	0.102
	0.019	278	1310	0.037	155	2005	239	262	168	5476	3937	0.076	0.076	0.102
	0.019	288	1446	0.024	175	3508	136	336	190	9816	3937	0.076	0.076	0.102
	0.019	298	1581	0.016	196	5883	81	420	212	16849	3937	0.076	0.076	0.102
	0.019	308	1715	0.011	216	9499	50	515	234	27819	3937	0.076	0.076	0.102
	0.019	318	1846	0.008	236	14819	32	620	256	44348	3937	0.076	0.076	0.102
	0.019	328	1974	0.005	256	22421	21	735	278	68495	3937	0.076	0.076	0.102
	0.019	338	2096	0.004	275	32989	14	857	298	102800	3937	0.076	0.076	0.102
	0.019	348	2214	0.003	293	47330	10	984	317	150320	3937	0.076	0.076	0.102
Make a 5 x wrapped screen	0.019	198	380	7.797	34	2	168434	9	37	5	3937	0.076	0.076	0.102
	0.019	208	534	3.538	50	7	52344	16	54	16	3937	0.076	0.076	0.102
	0.019	218	687	1.650	66	19	18286	27	72	47	3937	0.076	0.076	0.102
	0.019	228	841	0.807	84	49	7069	42	91	125	3937	0.076	0.076	0.102
	0.019	238	997	0.417	103	117	2984	63	111	307	3937	0.076	0.076	0.102
	0.019	248	1158	0.227	123	257	1361	90	133	694	3937	0.076	0.076	0.102
	0.019	258	1324	0.130	144	529	664	124	156	1466	3937	0.076	0.076	0.102
	0.019	268	1493	0.078	167	1023	344	168	181	2911	3937	0.076	0.076	0.102
	0.019	278	1666	0.048	191	1876	188	220	207	5476	3937	0.076	0.076	0.102
	0.019	288	1839	0.031	216	3283	107	281	234	9816	3937	0.076	0.076	0.102
	0.019	298	2012	0.021	241	5506	64	352	261	16849	3937	0.076	0.076	0.102
	0.019	308	2182	0.014	266	8889	40	431	288	27819	3937	0.076	0.076	0.102
	0.019	318	2349	0.010	291	13869	25	519	315	44348	3937	0.076	0.076	0.102
	0.019	328	2511	0.007	315	20982	17	615	342	68495	3937	0.076	0.076	0.102
	0.019	338	2667	0.005	339	30873	11	717	367	102800	3937	0.076	0.076	0.102

Appendix J: Modeling Data: Varied Section Lengths

Heat Transfer Limits of an Aluminum Heat Pipe containing Acetone Varying the Section Lengths

	Pipe Diameter [m]	Temperature of HP [K]	Reynolds Number [X]	Mach Number [X]	Capillary Limit [W]	Sonic Limit [W]	Boiling Limit [W]	Entrainment Limit [W]	Viscous Limit [W]	Saturation Pressure [Pa]	Mesh # [1/m]	Evaporator Length [m]	Adiabatic Length [m]	Condenser Length [m]
Equal lengths, 120 Mesh Twice Wrapped	0.019	198	396	0.800	16	9	86906	33	16	27	4724	0.076	0.0762	0.0762
	0.019	208	477	0.359	20	26	31799	52	20	79	4724	0.076	0.0762	0.0762
	0.019	218	551	0.172	23	65	12921	79	23	205	4724	0.076	0.0762	0.0762
	0.019	228	619	0.088	27	147	5741	115	27	481	4724	0.076	0.0762	0.0762
	0.019	238	679	0.048	30	307	2754	159	30	1039	4724	0.076	0.0762	0.0762
	0.019	248	731	0.027	34	596	1412	213	34	2088	4724	0.076	0.0762	0.0762
	0.019	258	778	0.016	37	1086	766	276	37	3940	4724	0.076	0.0762	0.0762
	0.019	268	819	0.010	39	1877	437	348	39	7034	4724	0.076	0.0762	0.0762
	0.019	278	854	0.007	42	3092	260	428	42	11961	4724	0.076	0.0762	0.0762
	0.019	288	885	0.004	44	4885	161	515	44	19479	4724	0.076	0.0762	0.0762
	0.019	298	911	0.003	46	7437	103	608	46	30529	4724	0.076	0.0762	0.0762
	0.019	308	933	0.002	48	10953	67	704	48	46244	4724	0.076	0.0762	0.0762
	0.019	318	950	0.002	49	15668	45	803	49	67946	4724	0.076	0.0762	0.0762
	0.019	328	963	0.001	50	21835	31	901	50	97151	4724	0.076	0.0762	0.0762
	0.019	338	971	0.001	51	29726	22	998	51	135550	4724	0.076	0.0762	0.0762
	0.019	348	975	0.001	52	39635	16	1091	52	185030	4724	0.076	0.0762	0.0762
Longer condenser, Increases the viscous limit	0.019	198	396	0.800	16	9	86906	33	17	27	4724	0.076	0.0762	0.1016
	0.019	208	477	0.359	20	26	31799	52	21	79	4724	0.076	0.0762	0.1016
	0.019	218	552	0.172	23	65	12921	79	25	205	4724	0.076	0.0762	0.1016
	0.019	228	620	0.088	27	147	5741	115	29	481	4724	0.076	0.0762	0.1016
	0.019	238	680	0.048	30	307	2754	159	33	1039	4724	0.076	0.0762	0.1016
	0.019	248	733	0.027	34	596	1412	213	36	2088	4724	0.076	0.0762	0.1016
	0.019	258	780	0.016	37	1086	766	276	40	3940	4724	0.076	0.0762	0.1016
	0.019	268	822	0.010	39	1877	437	348	43	7034	4724	0.076	0.0762	0.1016
	0.019	278	858	0.007	42	3092	260	428	45	11961	4724	0.076	0.0762	0.1016
	0.019	288	889	0.004	44	4885	161	515	48	19479	4724	0.076	0.0762	0.1016
	0.019	298	916	0.003	46	7437	103	608	50	30529	4724	0.076	0.0762	0.1016
	0.019	308	939	0.002	48	10953	67	704	52	46244	4724	0.076	0.0762	0.1016
	0.019	318	957	0.002	50	15668	45	803	54	67946	4724	0.076	0.0762	0.1016
	0.019	328	970	0.001	51	21835	31	901	55	97151	4724	0.076	0.0762	0.1016
	0.019	338	979	0.001	52	29726	22	998	56	135550	4724	0.076	0.0762	0.1016

	0.019	348	984	0.001	52	39635	16	1091	57	185030	4724	0.076	0.0762	0.1016
Longer condenser, Increases the viscous limit	0.019	198	396	0.800	16	9	86906	33	18	27	4724	0.076	0.0762	0.127
	0.019	208	477	0.359	20	26	31799	52	23	79	4724	0.076	0.0762	0.127
	0.019	218	552	0.173	23	65	12921	79	27	205	4724	0.076	0.0762	0.127
	0.019	228	620	0.088	27	147	5741	115	31	481	4724	0.076	0.0762	0.127
	0.019	238	681	0.048	30	307	2754	159	36	1039	4724	0.076	0.0762	0.127
	0.019	248	735	0.027	34	596	1412	213	39	2088	4724	0.076	0.0762	0.127
	0.019	258	782	0.016	37	1086	766	276	43	3940	4724	0.076	0.0762	0.127
	0.019	268	824	0.010	40	1877	437	348	46	7034	4724	0.076	0.0762	0.127
	0.019	278	861	0.007	42	3092	260	428	49	11961	4724	0.076	0.0762	0.127
	0.019	288	893	0.004	44	4885	161	515	52	19479	4724	0.076	0.0762	0.127
	0.019	298	920	0.003	47	7437	103	608	54	30529	4724	0.076	0.0762	0.127
	0.019	308	943	0.002	48	10953	67	704	56	46244	4724	0.076	0.0762	0.127
	0.019	318	962	0.002	50	15668	45	803	58	67946	4724	0.076	0.0762	0.127
	0.019	328	977	0.001	51	21835	31	901	60	97151	4724	0.076	0.0762	0.127
	0.019	338	986	0.001	52	29726	22	998	61	135550	4724	0.076	0.0762	0.127
	0.019	348	991	0.001	53	39635	16	1091	61	185030	4724	0.076	0.0762	0.127
Longer Adiabatic Section, lowers the capillary limit	0.019	198	347	0.700	14	9	86906	33	18	27	4724	0.076	0.127	0.0762
	0.019	208	417	0.314	17	26	31799	52	23	79	4724	0.076	0.127	0.0762
	0.019	218	483	0.151	20	65	12921	79	27	205	4724	0.076	0.127	0.0762
	0.019	228	543	0.077	24	147	5741	115	31	481	4724	0.076	0.127	0.0762
	0.019	238	596	0.042	27	307	2754	159	36	1039	4724	0.076	0.127	0.0762
	0.019	248	643	0.024	29	596	1412	213	39	2088	4724	0.076	0.127	0.0762
	0.019	258	685	0.014	32	1086	766	276	43	3940	4724	0.076	0.127	0.0762
	0.019	268	721	0.009	35	1877	437	348	46	7034	4724	0.076	0.127	0.0762
	0.019	278	753	0.006	37	3092	260	428	49	11961	4724	0.076	0.127	0.0762
	0.019	288	781	0.004	39	4885	161	515	52	19479	4724	0.0762	0.127	0.0762
	0.019	298	805	0.003	41	7437	103	608	54	30529	4724	0.0762	0.127	0.0762
	0.019	308	826	0.002	42	10953	67	704	56	46244	4724	0.0762	0.127	0.0762
	0.019	318	842	0.001	44	15668	45	803	58	67946	4724	0.0762	0.127	0.0762
	0.019	328	854	0.001	45	21835	31	901	60	97151	4724	0.0762	0.127	0.0762
	0.019	338	863	0.001	46	29726	22	998	61	135550	4724	0.0762	0.127	0.0762
	0.019	348	867	0.001	46	39635	16	1091	61	185030	4724	0.0762	0.127	0.0762
Longer Evaporator Section, lowers the viscous limit	0.019	198	396	0.800	16	9	144843	33	11	27	4724	0.127	0.0762	0.0762
	0.019	208	477	0.359	20	26	52999	52	14	79	4724	0.127	0.0762	0.0762
	0.019	218	552	0.173	23	65	21534	79	16	205	4724	0.127	0.0762	0.0762
	0.019	228	620	0.088	27	147	9569	115	19	481	4724	0.127	0.0762	0.0762
	0.019	238	681	0.048	30	307	4591	159	21	1039	4724	0.127	0.0762	0.0762
	0.019	248	735	0.027	34	596	2353	213	24	2088	4724	0.127	0.0762	0.0762

	0.019	258	782	0.016	37	1086	1277	276	26	3940	4724	0.127	0.0762	0.0762
	0.019	268	824	0.010	40	1877	728	348	28	7034	4724	0.127	0.0762	0.0762
	0.019	278	861	0.007	42	3092	434	428	29	11961	4724	0.127	0.0762	0.0762
	0.019	288	893	0.004	44	4885	268	515	31	19479	4724	0.127	0.0762	0.0762
	0.019	298	920	0.003	47	7437	171	608	33	30529	4724	0.127	0.0762	0.0762
	0.019	308	943	0.002	48	10953	112	704	34	46244	4724	0.127	0.0762	0.0762
	0.019	318	962	0.002	50	15668	76	803	35	67946	4724	0.127	0.0762	0.0762
	0.019	328	977	0.001	51	21835	52	901	36	97151	4724	0.127	0.0762	0.0762
	0.019	338	986	0.001	52	29726	36	998	36	135550	4724	0.127	0.0762	0.0762
	0.019	348	991	0.001	53	39635	26	1091	37	185030	4724	0.127	0.0762	0.0762

Heat Transfer Limits of an Copper Heat Pipe containing Acetone Varying the Section Lengths

	Pipe Diameter [m]	Temperature of HP [K]	Reynolds Number [X]	Mach Number [X]	Capillary Limit [W]	Sonic Limit [W]	Boiling Limit [W]	Entrainment Limit [W]	Viscous Limit [W]	Saturation Pressure [Pa]	Mesh # [1/m]	Evaporator Length [m]	Adiabatic Length [m]	Condenser Length [m]
Equal lengths, 120 Mesh Twice Wrapped	0.019	198	692	1.408	27	9	74923	30	27	27	3937	0.076	0.0762	0.0762
	0.019	208	836	0.633	34	26	27415	49	34	79	3937	0.076	0.0762	0.0762
	0.019	218	969	0.305	41	64	11139	74	41	205	3937	0.076	0.0762	0.0762
	0.019	228	1089	0.156	47	145	4950	107	47	481	3937	0.076	0.0762	0.0762
	0.019	238	1196	0.085	53	303	2375	148	53	1039	3937	0.076	0.0762	0.0762
	0.019	248	1290	0.048	59	588	1217	198	59	2088	3937	0.076	0.0762	0.0762
	0.019	258	1374	0.029	64	1072	661	257	64	3940	3937	0.076	0.0762	0.0762
	0.019	268	1447	0.018	69	1852	377	324	69	7034	3937	0.076	0.0762	0.0762
	0.019	278	1512	0.012	73	3051	224	398	73	11961	3937	0.076	0.0762	0.0762
	0.019	288	1568	0.008	78	4820	139	479	78	19479	3937	0.076	0.0762	0.0762
	0.019	298	1616	0.005	81	7336	89	566	81	30529	3937	0.076	0.0762	0.0762
	0.019	308	1656	0.004	84	10805	58	655	84	46244	3937	0.076	0.0762	0.0762
	0.019	318	1689	0.003	87	15457	39	747	87	67946	3937	0.076	0.0762	0.0762
	0.019	328	1714	0.002	89	21541	27	838	89	97151	3937	0.076	0.0762	0.0762
	0.019	338	1731	0.001	91	29326	19	928	91	135550	3937	0.076	0.0762	0.0762
	0.019	348	1739	0.001	92	39102	13	1015	92	185030	3937	0.076	0.0762	0.0762
Longer condenser, Increases the viscous limit	0.019	198	694	1.412	27	9	74923	30	30	27	3937	0.076	0.0762	0.1016
	0.019	208	839	0.636	34	26	27415	49	37	79	3937	0.076	0.0762	0.1016
	0.019	218	973	0.306	41	64	11139	74	44	205	3937	0.076	0.0762	0.1016
	0.019	228	1094	0.157	47	145	4950	107	51	481	3937	0.076	0.0762	0.1016
	0.019	238	1202	0.085	53	303	2375	148	58	1039	3937	0.076	0.0762	0.1016
	0.019	248	1298	0.049	59	588	1217	198	64	2088	3937	0.076	0.0762	0.1016

	0.019	258	1382	0.029	64	1072	661	257	70	3940	3937	0.076	0.0762	0.1016
	0.019	268	1457	0.018	69	1852	377	324	75	7034	3937	0.076	0.0762	0.1016
	0.019	278	1522	0.012	74	3051	224	398	80	11961	3937	0.076	0.0762	0.1016
	0.019	288	1580	0.008	78	4820	139	479	85	19479	3937	0.076	0.0762	0.1016
	0.019	298	1629	0.005	82	7336	89	566	89	30529	3937	0.076	0.0762	0.1016
	0.019	308	1671	0.004	85	10805	58	655	92	46244	3937	0.076	0.0762	0.1016
	0.019	318	1705	0.003	88	15457	39	747	95	67946	3937	0.076	0.0762	0.1016
	0.019	328	1731	0.002	90	21541	27	838	98	97151	3937	0.076	0.0762	0.1016
	0.019	338	1750	0.002	92	29326	19	928	99	135550	3937	0.076	0.0762	0.1016
	0.019	348	1759	0.001	93	39102	13	1015	100	185030	3937	0.076	0.0762	0.1016
Longer condenser, Increases the viscous limit	0.019	198	696	1.416	27	9	74923	30	32	27	3937	0.076	0.0762	0.127
	0.019	208	842	0.638	34	26	27415	49	40	79	3937	0.076	0.0762	0.127
	0.019	218	976	0.307	41	64	11139	74	48	205	3937	0.076	0.0762	0.127
	0.019	228	1098	0.157	47	145	4950	107	55	481	3937	0.076	0.0762	0.127
	0.019	238	1207	0.085	54	303	2375	148	63	1039	3937	0.076	0.0762	0.127
	0.019	248	1304	0.049	59	588	1217	198	69	2088	3937	0.076	0.0762	0.127
	0.019	258	1389	0.029	65	1072	661	257	76	3940	3937	0.076	0.0762	0.127
	0.019	268	1465	0.018	70	1852	377	324	81	7034	3937	0.076	0.0762	0.127
	0.019	278	1532	0.012	74	3051	224	398	87	11961	3937	0.076	0.0762	0.127
	0.019	288	1590	0.008	79	4820	139	479	92	19479	3937	0.076	0.0762	0.127
	0.019	298	1641	0.005	82	7336	89	566	96	30529	3937	0.076	0.0762	0.127
	0.019	308	1684	0.004	86	10805	58	655	100	46244	3937	0.076	0.0762	0.127
	0.019	318	1719	0.003	89	15457	39	747	103	67946	3937	0.076	0.0762	0.127
	0.019	328	1746	0.002	91	21541	27	838	106	97151	3937	0.076	0.0762	0.127
	0.019	338	1766	0.002	93	29326	19	928	108	135550	3937	0.076	0.0762	0.127
	0.019	348	1776	0.001	94	39102	13	1015	109	185030	3937	0.076	0.0762	0.127
Longer Adiabatic Section, lowers the capillary limit	0.019	198	609	1.239	24	9	74923	30	32	27	3937	0.076	0.127	0.0762
	0.019	208	736	0.558	30	26	27415	49	40	79	3937	0.076	0.127	0.0762
	0.019	218	854	0.269	36	64	11139	74	48	205	3937	0.076	0.127	0.0762
	0.019	228	961	0.138	42	145	4950	107	55	481	3937	0.076	0.127	0.0762
	0.019	238	1056	0.075	47	303	2375	148	63	1039	3937	0.076	0.127	0.0762
	0.019	248	1141	0.043	52	588	1217	198	69	2088	3937	0.076	0.127	0.0762
	0.019	258	1216	0.026	57	1072	661	257	76	3940	3937	0.076	0.127	0.0762
	0.019	268	1282	0.016	61	1852	377	324	81	7034	3937	0.076	0.127	0.0762
	0.019	278	1340	0.010	65	3051	224	398	87	11961	3937	0.076	0.127	0.0762
	0.019	288	1391	0.007	69	4820	139	479	92	19479	3937	0.0762	0.127	0.0762
	0.019	298	1436	0.005	72	7336	89	566	96	30529	3937	0.0762	0.127	0.0762
	0.019	308	1473	0.003	75	10805	58	655	100	46244	3937	0.0762	0.127	0.0762
	0.019	318	1504	0.002	77	15457	39	747	103	67946	3937	0.0762	0.127	0.0762

	0.019	328	1528	0.002	79	21541	27	838	106	97151	3937	0.0762	0.127	0.0762
	0.019	338	1545	0.001	81	29326	19	928	108	135550	3937	0.0762	0.127	0.0762
	0.019	348	1554	0.001	82	39102	13	1015	109	185030	3937	0.0762	0.127	0.0762
Longer Evaporator Section, lowers the viscous limit	0.019	198	696	1.416	27	9	124872	30	19	27	3937	0.127	0.0762	0.0762
	0.019	208	842	0.638	34	26	45691	49	24	79	3937	0.127	0.0762	0.0762
	0.019	218	976	0.307	41	64	18566	74	29	205	3937	0.127	0.0762	0.0762
	0.019	228	1098	0.157	47	145	8250	107	33	481	3937	0.127	0.0762	0.0762
	0.019	238	1207	0.085	54	303	3958	148	38	1039	3937	0.127	0.0762	0.0762
	0.019	248	1304	0.049	59	588	2029	198	42	2088	3937	0.127	0.0762	0.0762
	0.019	258	1389	0.029	65	1072	1101	257	45	3940	3937	0.127	0.0762	0.0762
	0.019	268	1465	0.018	70	1852	628	324	49	7034	3937	0.127	0.0762	0.0762
	0.019	278	1532	0.012	74	3051	374	398	52	11961	3937	0.127	0.0762	0.0762
	0.019	288	1590	0.008	79	4820	231	479	55	19479	3937	0.127	0.0762	0.0762
	0.019	298	1641	0.005	82	7336	148	566	58	30529	3937	0.127	0.0762	0.0762
	0.019	308	1684	0.004	86	10805	97	655	60	46244	3937	0.127	0.0762	0.0762
	0.019	318	1719	0.003	89	15457	65	747	62	67946	3937	0.127	0.0762	0.0762
	0.019	328	1746	0.002	91	21541	45	838	64	97151	3937	0.127	0.0762	0.0762
	0.019	338	1766	0.002	93	29326	31	928	65	135550	3937	0.127	0.0762	0.0762
	0.019	348	1776	0.001	94	39102	22	1015	66	185030	3937	0.127	0.0762	0.0762

Heat Transfer Limits of an Copper Heat Pipe containing Methanol Varying the Section Lengths

	Pipe Diameter [m]	Temperature of HP [K]	Reynolds Number [X]	Mach Number [X]	Capillary Limit [W]	Sonic Limit [W]	Boiling Limit [W]	Entrainment Limit [W]	Viscous Limit [W]	Saturation Pressure [Pa]	Mesh # [1/m]	Evaporator Length [m]	Adiabatic Length [m]	Condenser Length [m]
Equal lengths, 120 Mesh Twice Wrapped	0.019	198	159	2.968	16	2	441482	18	16	5	3937	0.076	0.0762	0.0762
	0.019	208	212	1.276	22	8	137199	32	22	16	3937	0.076	0.0762	0.0762
	0.019	218	266	0.580	28	23	47930	52	28	47	3937	0.076	0.0762	0.0762
	0.019	228	322	0.281	35	60	18528	80	35	125	3937	0.076	0.0762	0.0762
	0.019	238	379	0.144	43	142	7822	120	43	307	3937	0.076	0.0762	0.0762
	0.019	248	439	0.078	51	312	3567	172	51	694	3937	0.076	0.0762	0.0762
	0.019	258	501	0.045	60	641	1740	239	60	1466	3937	0.076	0.0762	0.0762
	0.019	268	564	0.027	70	1240	901	321	70	2911	3937	0.076	0.0762	0.0762
	0.019	278	629	0.017	79	2275	492	421	79	5476	3937	0.076	0.0762	0.0762
	0.019	288	694	0.011	90	3980	281	539	90	9816	3937	0.076	0.0762	0.0762
	0.019	298	759	0.007	100	6675	168	674	100	16849	3937	0.076	0.0762	0.0762
	0.019	308	822	0.005	110	10778	104	827	110	27819	3937	0.076	0.0762	0.0762
	0.019	318	885	0.003	121	16815	66	996	121	44348	3937	0.076	0.0762	0.0762

	0.019	328	946	0.002	131	25441	43	1179	131	68495	3937	0.076	0.0762	0.0762
	0.019	338	1004	0.002	140	37433	29	1375	140	102800	3937	0.076	0.0762	0.0762
	0.019	348	1060	0.001	149	53705	20	1579	149	150320	3937	0.076	0.0762	0.0762
Longer condenser, Increases the viscous limit	0.019	198	160	2.983	16	2	441482	18	17	5	3937	0.076	0.0762	0.1016
	0.019	208	213	1.283	22	8	137199	32	24	16	3937	0.076	0.0762	0.1016
	0.019	218	268	0.584	28	23	47930	52	31	47	3937	0.076	0.0762	0.1016
	0.019	228	324	0.282	36	60	18528	80	39	125	3937	0.076	0.0762	0.1016
	0.019	238	382	0.145	43	142	7822	120	47	307	3937	0.076	0.0762	0.1016
	0.019	248	442	0.079	52	312	3567	172	56	694	3937	0.076	0.0762	0.1016
	0.019	258	505	0.045	61	641	1740	239	66	1466	3937	0.076	0.0762	0.1016
	0.019	268	569	0.027	70	1240	901	321	76	2911	3937	0.076	0.0762	0.1016
	0.019	278	634	0.017	80	2275	492	421	87	5476	3937	0.076	0.0762	0.1016
	0.019	288	700	0.011	90	3980	281	539	98	9816	3937	0.076	0.0762	0.1016
	0.019	298	765	0.007	101	6675	168	674	109	16849	3937	0.076	0.0762	0.1016
	0.019	308	830	0.005	111	10778	104	827	121	27819	3937	0.076	0.0762	0.1016
	0.019	318	893	0.003	122	16815	66	996	132	44348	3937	0.076	0.0762	0.1016
	0.019	328	955	0.002	132	25441	43	1179	143	68495	3937	0.076	0.0762	0.1016
	0.019	338	1014	0.002	142	37433	29	1375	154	102800	3937	0.076	0.0762	0.1016
	0.019	348	1071	0.001	151	53705	20	1579	163	150320	3937	0.076	0.0762	0.1016
Longer condenser, Increases the viscous limit	0.019	198	161	2.995	16	2	441482	18	18	5	3937	0.076	0.0762	0.127
	0.019	208	214	1.289	22	8	137199	32	26	16	3937	0.076	0.0762	0.127
	0.019	218	269	0.587	29	23	47930	52	33	47	3937	0.076	0.0762	0.127
	0.019	228	325	0.284	36	60	18528	80	42	125	3937	0.076	0.0762	0.127
	0.019	238	384	0.146	44	142	7822	120	51	307	3937	0.076	0.0762	0.127
	0.019	248	445	0.079	52	312	3567	172	61	694	3937	0.076	0.0762	0.127
	0.019	258	508	0.045	61	641	1740	239	71	1466	3937	0.076	0.0762	0.127
	0.019	268	572	0.027	71	1240	901	321	82	2911	3937	0.076	0.0762	0.127
	0.019	278	638	0.017	81	2275	492	421	94	5476	3937	0.076	0.0762	0.127
	0.019	288	705	0.011	91	3980	281	539	106	9816	3937	0.076	0.0762	0.127
	0.019	298	771	0.007	102	6675	168	674	119	16849	3937	0.076	0.0762	0.127
	0.019	308	836	0.005	112	10778	104	827	131	27819	3937	0.076	0.0762	0.127
	0.019	318	900	0.003	123	16815	66	996	143	44348	3937	0.076	0.0762	0.127
	0.019	328	963	0.002	133	25441	43	1179	155	68495	3937	0.076	0.0762	0.127
	0.019	338	1023	0.002	143	37433	29	1375	167	102800	3937	0.076	0.0762	0.127
	0.019	348	1081	0.001	152	53705	20	1579	178	150320	3937	0.076	0.0762	0.127
Longer Adiabatic Section, lowers the	0.019	198	141	2.621	14	2	441482	18	18	5	3937	0.076	0.127	0.0762
	0.019	208	187	1.128	19	8	137199	32	26	16	3937	0.076	0.127	0.0762
	0.019	218	235	0.513	25	23	47930	52	33	47	3937	0.076	0.127	0.0762
	0.019	228	285	0.248	31	60	18528	80	42	125	3937	0.076	0.127	0.0762

capillary limit	0.019	238	336	0.128	38	142	7822	120	51	307	3937	0.076	0.127	0.0762
	0.019	248	389	0.069	45	312	3567	172	61	694	3937	0.076	0.127	0.0762
	0.019	258	444	0.040	53	641	1740	239	71	1466	3937	0.076	0.127	0.0762
	0.019	268	501	0.024	62	1240	901	321	82	2911	3937	0.076	0.127	0.0762
	0.019	278	558	0.015	71	2275	492	421	94	5476	3937	0.076	0.127	0.0762
	0.019	288	617	0.010	80	3980	281	539	106	9816	3937	0.0762	0.127	0.0762
	0.019	298	675	0.006	89	6675	168	674	119	16849	3937	0.0762	0.127	0.0762
	0.019	308	732	0.004	98	10778	104	827	131	27819	3937	0.0762	0.127	0.0762
	0.019	318	788	0.003	107	16815	66	996	143	44348	3937	0.0762	0.127	0.0762
	0.019	328	842	0.002	116	25441	43	1179	155	68495	3937	0.0762	0.127	0.0762
	0.019	338	895	0.002	125	37433	29	1375	167	102800	3937	0.0762	0.127	0.0762
	0.019	348	946	0.001	133	53705	20	1579	178	150320	3937	0.0762	0.127	0.0762
Longer Evaporator Section, lowers the viscous limit	0.019	198	161	2.995	16	2	735803	18	11	5	3937	0.127	0.0762	0.0762
	0.019	208	214	1.289	22	8	228666	32	15	16	3937	0.127	0.0762	0.0762
	0.019	218	269	0.587	29	23	79884	52	20	47	3937	0.127	0.0762	0.0762
	0.019	228	325	0.284	36	60	30879	80	25	125	3937	0.127	0.0762	0.0762
	0.019	238	384	0.146	44	142	13037	120	30	307	3937	0.127	0.0762	0.0762
	0.019	248	445	0.079	52	312	5945	172	36	694	3937	0.127	0.0762	0.0762
	0.019	258	508	0.045	61	641	2901	239	43	1466	3937	0.127	0.0762	0.0762
	0.019	268	572	0.027	71	1240	1502	321	49	2911	3937	0.127	0.0762	0.0762
	0.019	278	638	0.017	81	2275	820	421	56	5476	3937	0.127	0.0762	0.0762
	0.019	288	705	0.011	91	3980	469	539	64	9816	3937	0.127	0.0762	0.0762
	0.019	298	771	0.007	102	6675	280	674	71	16849	3937	0.127	0.0762	0.0762
	0.019	308	836	0.005	112	10778	173	827	79	27819	3937	0.127	0.0762	0.0762
	0.019	318	900	0.003	123	16815	110	996	86	44348	3937	0.127	0.0762	0.0762
	0.019	328	963	0.002	133	25441	72	1179	93	68495	3937	0.127	0.0762	0.0762
	0.019	338	1023	0.002	143	37433	49	1375	100	102800	3937	0.127	0.0762	0.0762
	0.019	348	1081	0.001	152	53705	34	1579	107	150320	3937	0.127	0.0762	0.0762

Appendix K: Modeling Data: Stress Calculations

Stress on 0.5" Outer Tube Pipe							
Pipe Material	**Pipe Thickness**	**Hoop Stress**	**Hoop Safety Factor**	**Compressive Thermal Stress**	**Compressive Safety Factor**	**Tensile Thermal Stress**	**Tensile Safety Factor**
	[m]	**[Pa]**		**[Pa]**		**[Pa]**	
Copper	0.00109	2.93E+05	239	-2.74E+06	25.6	-2.38E+06	29.4
Copper	0.00140	2.23E+05	314	-2.80E+06	25.0	-2.32E+06	30.2
Copper	0.00160	1.91E+05	366	-2.85E+06	24.6	-2.27E+06	30.8
Copper	0.00267	1.04E+05	676	-3.18E+06	22.0	-1.94E+06	36.1
Copper	0.00318	8.26E+04	847	-3.41E+06	20.5	-1.71E+06	41.0
Aluminum	0.00109	2.93E+05	325	-3.13E+06	30.4	-2.72E+06	34.9
Aluminum	0.00140	2.23E+05	426	-3.20E+06	29.7	-2.65E+06	35.9
Aluminum	0.00160	1.91E+05	497	-3.25E+06	29.2	-2.59E+06	36.6
Aluminum	0.00267	1.04E+05	917	-3.63E+06	26.2	-2.22E+06	42.8
Aluminum	0.00318	8.26E+04	1150	-3.90E+06	24.4	-1.95E+06	48.7
304 SS	0.00109	2.93E+05	1715	-6.20E+06	81.0	-5.40E+06	93.0
304 SS	0.00140	2.23E+05	2253	-6.34E+06	79.1	-5.25E+06	95.5
304 SS	0.00160	1.91E+05	2628	-6.45E+06	77.8	-5.15E+06	97.5
304 SS	0.00267	1.04E+05	4845	-7.20E+06	69.7	-4.40E+06	114.1
304 SS	0.00318	8.26E+04	6076	-7.73E+06	64.9	-3.87E+06	129.8

Stress on 0.75" Outer Tube Pipe

Pipe Material	Pipe Thickness [m]	Hoop Stress [Pa]	Hoop Safety Factor	Compressive Thermal Stress [Pa]	Compressive Safety Factor	Tensile Thermal Stress [Pa]	Tensile Safety Factor
Copper	0.00109	4.53E+05	155	-2.67E+06	26.2	-2.45E+06	28.6
Copper	0.00140	3.48E+05	201	-2.71E+06	25.9	-2.41E+06	29.0
Copper	0.00160	3.00E+05	233	-2.73E+06	25.6	-2.39E+06	29.3
Copper	0.00267	1.69E+05	414	-2.89E+06	24.2	-2.23E+06	31.4
Copper	0.00318	1.38E+05	508	-2.99E+06	23.4	-2.13E+06	32.8
Aluminum	0.00109	4.53E+05	210	-2.78E+06	34.1	-2.55E+06	37.2
Aluminum	0.00140	3.48E+05	273	-2.82E+06	33.7	-2.51E+06	37.8
Aluminum	0.00160	3.00E+05	316	-2.85E+06	33.4	-2.49E+06	38.2
Aluminum	0.00267	1.69E+05	562	-3.01E+06	31.5	-2.32E+06	40.9
Aluminum	0.00318	1.38E+05	690	-3.11E+06	30.5	-2.22E+06	42.7
304 SS	0.00109	4.53E+05	1109	-5.52E+06	90.9	-5.06E+06	99.1
304 SS	0.00140	3.48E+05	1442	-5.60E+06	89.7	-4.99E+06	100.6
304 SS	0.00160	3.00E+05	1672	-5.65E+06	88.9	-4.94E+06	101.7
304 SS	0.00267	1.69E+05	2967	-5.98E+06	84.0	-4.61E+06	109.0
304 SS	0.00318	1.38E+05	3646	-6.18E+06	81.3	-4.41E+06	113.8

Stress on 1" Outer Tube Pipe

Pipe Material	Pipe Thickness [m]	Hoop Stress [Pa]	Hoop Safety Factor	Compressive Thermal Stress [Pa]	Compressive Safety Factor	Tensile Thermal Stress [Pa]	Tensile Safety Factor
Copper	0.00109	6.13E+05	114	-2.64E+06	26.5	-2.48E+06	28.2
Copper	0.00140	4.73E+05	148	-2.66E+06	26.3	-2.45E+06	28.5
Copper	0.00160	4.10E+05	171	-2.68E+06	26.1	-2.44E+06	28.7
Copper	0.00267	2.35E+05	298	-2.79E+06	25.1	-2.33E+06	30.0
Copper	0.00318	1.93E+05	363	-2.84E+06	24.6	-2.28E+06	30.8
Aluminum	0.00109	6.13E+05	155	-2.49E+06	38.2	-2.34E+06	40.6
Aluminum	0.00140	4.73E+05	201	-2.51E+06	37.8	-2.31E+06	41.1
Aluminum	0.00160	4.10E+05	232	-2.53E+06	37.6	-2.30E+06	41.4
Aluminum	0.00267	2.35E+05	405	-2.63E+06	36.2	-2.20E+06	43.2
Aluminum	0.00318	1.93E+05	493	-2.68E+06	35.4	-2.14E+06	44.3
304 SS	0.00109	6.13E+05	819	-4.94E+06	101.7	-4.64E+06	108.2
304 SS	0.00140	4.73E+05	1061	-4.99E+06	100.7	-4.59E+06	109.4
304 SS	0.00160	4.10E+05	1226	-5.02E+06	100.0	-4.56E+06	110.1
304 SS	0.00267	2.35E+05	2138	-5.21E+06	96.3	-4.36E+06	115.0
304 SS	0.00318	1.93E+05	2604	-5.32E+06	94.4	-4.26E+06	118.0

Stress on 2" Outer Tube Pipe

Pipe Material	Pipe Thickness [m]	Hoop Stress [Pa]	Hoop Safety Factor	Compressive Thermal Stress [Pa]	Compressive Safety Factor	Tensile Thermal Stress [Pa]	Tensile Safety Factor
Copper	0.00109	1.25E+06	56	-2.60E+06	26.9	-2.52E+06	27.8
Copper	0.00140	9.74E+05	72	-2.61E+06	26.8	-2.51E+06	27.9
Copper	0.00160	8.47E+05	83	-2.62E+06	26.7	-2.50E+06	28.0
Copper	0.00267	4.97E+05	141	-2.66E+06	26.3	-2.46E+06	28.5
Copper	0.00318	4.13E+05	169	-2.68E+06	26.1	-2.44E+06	28.7
Aluminum	0.00109	1.25E+06	76	-2.32E+06	41.0	-2.25E+06	42.2
Aluminum	0.00140	9.74E+05	98	-2.33E+06	40.8	-2.24E+06	42.4
Aluminum	0.00160	8.47E+05	112	-2.34E+06	40.7	-2.23E+06	42.5
Aluminum	0.00267	4.97E+05	191	-2.37E+06	40.0	-2.20E+06	43.3
Aluminum	0.00318	4.13E+05	230	-2.39E+06	39.7	-2.18E+06	43.7
304 SS	0.00109	1.25E+06	401	-4.60E+06	109.1	-4.47E+06	112.4
304 SS	0.00140	9.74E+05	515	-4.62E+06	108.6	-4.45E+06	112.9
304 SS	0.00160	8.47E+05	593	-4.64E+06	108.3	-4.43E+06	113.2
304 SS	0.00267	4.97E+05	1010	-4.71E+06	106.5	-4.36E+06	115.2
304 SS	0.00318	4.13E+05	1215	-4.75E+06	105.7	-4.32E+06	116.2

Stress on 0.187" Fill Tube

Pipe Material	Pipe Thickness [m]	Hoop Stress [Pa]	Hoop Safety Factor	Compressive Thermal Stress [Pa]	Compressive Safety Factor	Tensile Thermal Stress [Pa]	Tensile Safety Factor
Copper	0.00079	1.38E+05	508	-2.99E+06	23.4	-2.13E+06	32.8
Aluminum	0.00079	1.38E+05	508	-2.60E+06	26.9	-1.86E+06	37.7

Appendix L: Heat Pipe Engineering Drawings

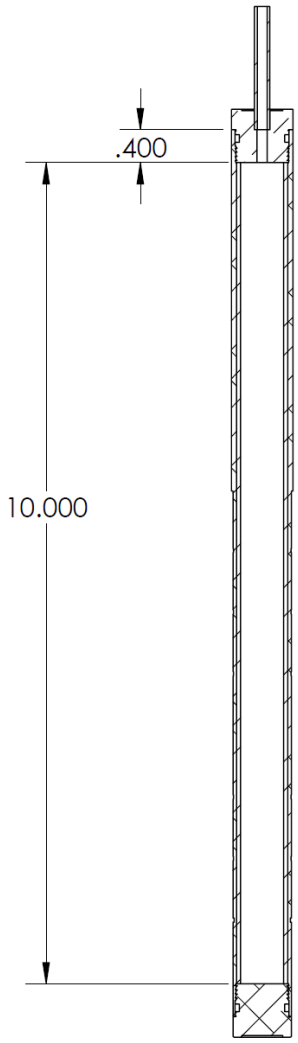

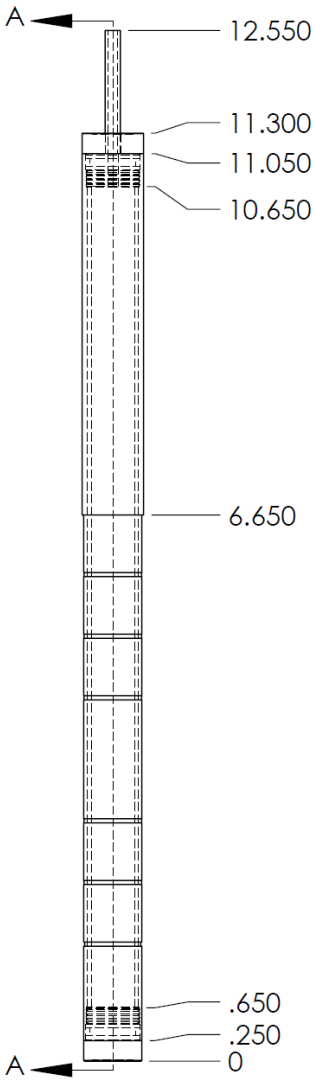

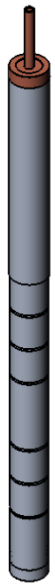

SECTION A-A

SOLIDWORKS Student Edition.
For Academic Use Only.

JANA STRAIN 21/10/16

UNLESS OTHERWISE SPECIFIED:
DIMENSIONS ARE IN INCHES
TOLERANCES:
FRACTIONAL ±0.003
ONE PLACE DECIMAL ±0.015
TWO PLACE DECIMAL ±0.010
THREE PLACE DECIMAL ±0.003

TITLE:

ASSEMBLY

	MATERIAL:	REV
	3 X AL 6061-T6 **4 X COPPER**	**8**
SCALE: 1:2	**QUANTITY: 7**	SHEET 1 OF 6

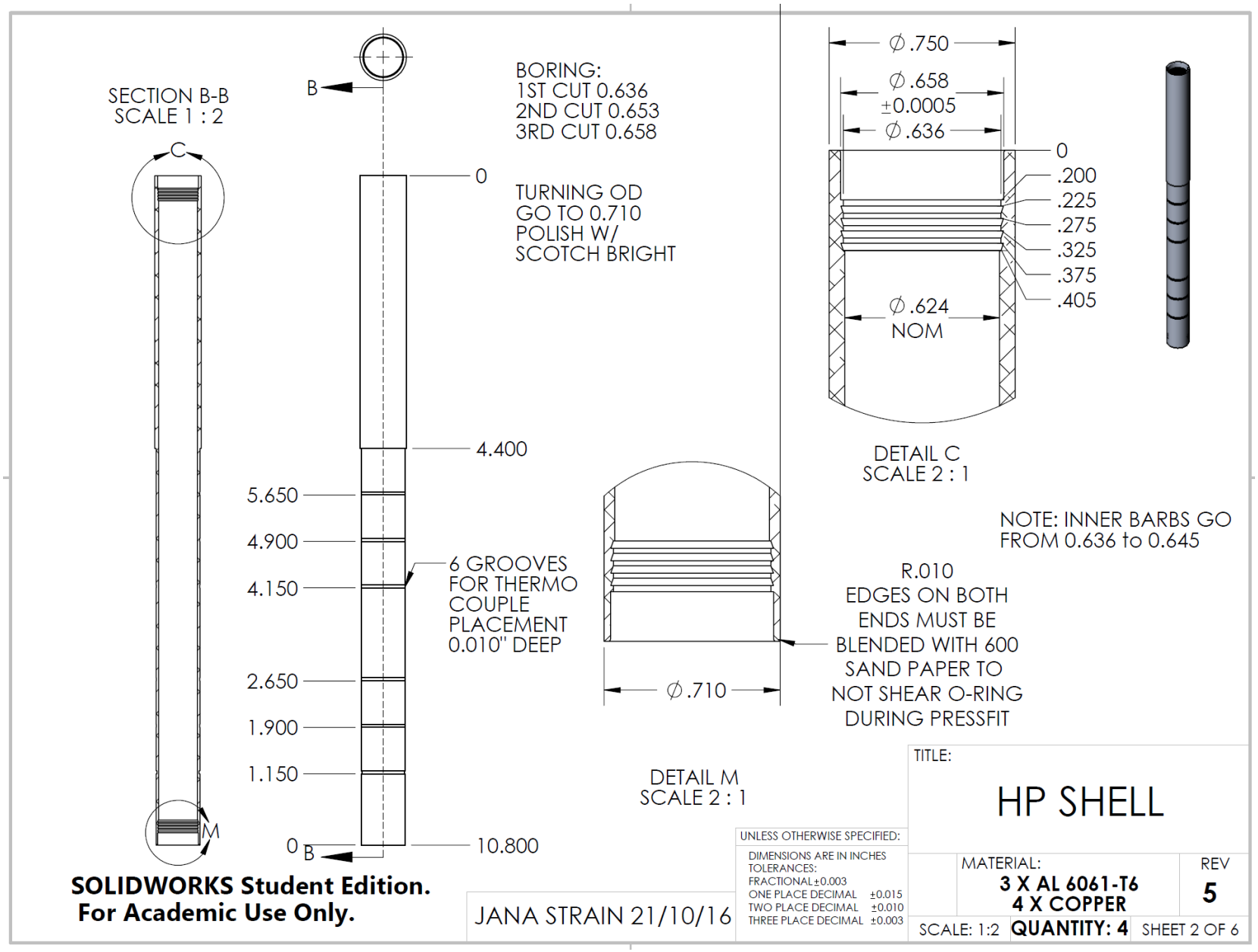
SECTION B-B
SCALE 1 : 2
B
C
M
0
4.400
5.650
4.900
4.150
2.650
1.900
1.150
0
B
10.800
6 GROOVES FOR THERMO COUPLE PLACEMENT 0.010" DEEP
BORING:
1ST CUT 0.636
2ND CUT 0.653
3RD CUT 0.658
TURNING OD
GO TO 0.710
POLISH W/
SCOTCH BRIGHT
Ø.710
DETAIL M
SCALE 2 : 1
R.010
EDGES ON BOTH
ENDS MUST BE
BLENDED WITH 600
SAND PAPER TO
NOT SHEAR O-RING
DURING PRESSFIT
Ø.750
Ø.658
±0.0005
Ø.636
0
.200
.225
.275
.325
.375
.405
Ø.624
NOM
DETAIL C
SCALE 2 : 1
NOTE: INNER BARBS GO
FROM 0.636 to 0.645
SOLIDWORKS Student Edition.
For Academic Use Only.
JANA STRAIN 21/10/16
UNLESS OTHERWISE SPECIFIED:
DIMENSIONS ARE IN INCHES
TOLERANCES:
FRACTIONAL ±0.003
ONE PLACE DECIMAL ±0.015
TWO PLACE DECIMAL ±0.010
THREE PLACE DECIMAL ±0.003
TITLE:
HP SHELL
MATERIAL:
3 X AL 6061-T6
4 X COPPER
REV
5
SCALE: 1:2
QUANTITY: 4
SHEET 2 OF 6

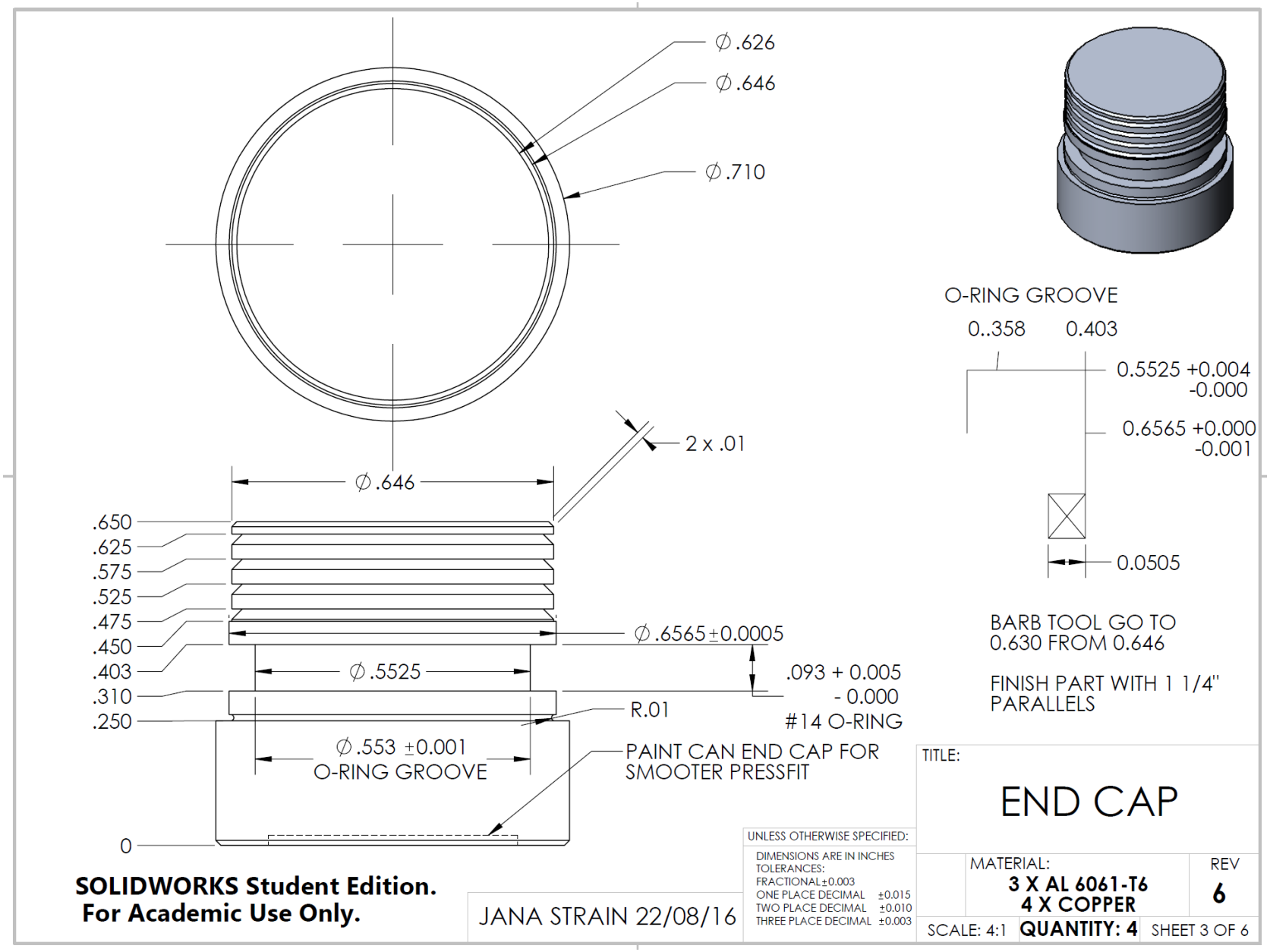
Ø.626
Ø.646
Ø.710
2 x .01
Ø.646
.650
.625
.575
.525
.475
.450
.403
.310
.250
0
Ø.6565±0.0005
Ø.5525
.093 + 0.005
- 0.000
#14 O-RING
R.01
Ø.553 ±0.001
O-RING GROOVE
PAINT CAN END CAP FOR
SMOOTER PRESSFIT
O-RING GROOVE
0..358
0.403
0.5525 +0.004
-0.000
0.6565 +0.000
-0.001
0.0505
BARB TOOL GO TO
0.630 FROM 0.646
FINISH PART WITH 1 1/4"
PARALLELS
SOLIDWORKS Student Edition.
For Academic Use Only.
JANA STRAIN 22/08/16
UNLESS OTHERWISE SPECIFIED:
DIMENSIONS ARE IN INCHES
TOLERANCES:
FRACTIONAL ±0.003
ONE PLACE DECIMAL ±0.015
TWO PLACE DECIMAL ±0.010
THREE PLACE DECIMAL ±0.003
TITLE:
END CAP
MATERIAL:
3 X AL 6061-T6
4 X COPPER
REV
6
SCALE: 4:1
QUANTITY: 4
SHEET 3 OF 6

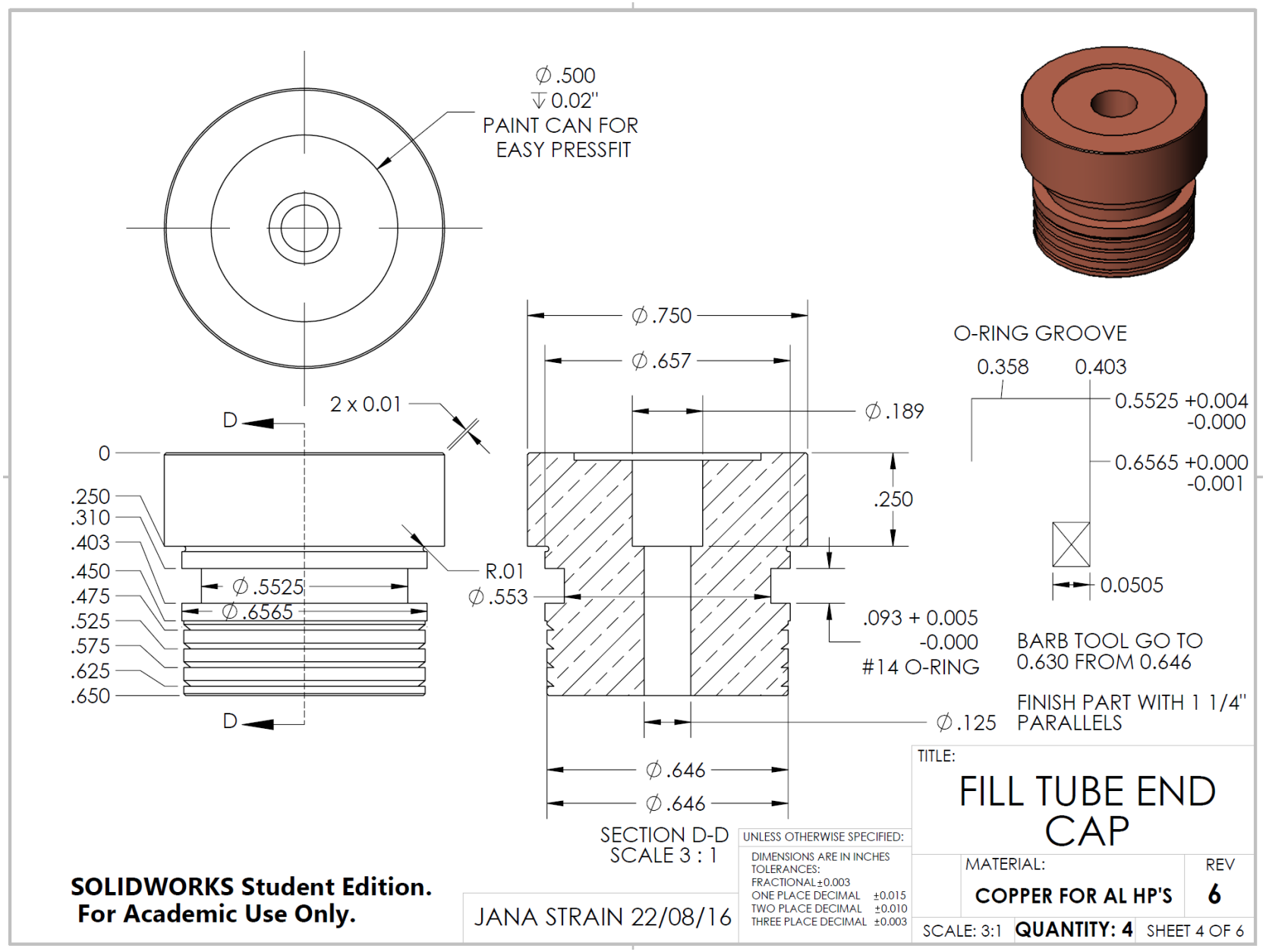
⌀.500
↧0.02"
PAINT CAN FOR
EASY PRESSFIT
2 x 0.01
D
0
.250
.310
.403
.450
.475
.525
.575
.625
.650
⌀.5525
⌀.6565
D
⌀.750
⌀.657
⌀.189
.250
R.01
⌀.553
.093 + 0.005
-0.000
#14 O-RING
⌀.125
⌀.646
⌀.646
SECTION D-D
SCALE 3 : 1
O-RING GROOVE
0.358
0.403
0.5525 +0.004
-0.000
0.6565 +0.000
-0.001
0.0505
BARB TOOL GO TO
0.630 FROM 0.646
FINISH PART WITH 1 1/4"
PARALLELS
UNLESS OTHERWISE SPECIFIED:
DIMENSIONS ARE IN INCHES
TOLERANCES:
FRACTIONAL ±0.003
ONE PLACE DECIMAL ±0.015
TWO PLACE DECIMAL ±0.010
THREE PLACE DECIMAL ±0.003
TITLE:
FILL TUBE END CAP
MATERIAL:
COPPER FOR AL HP'S
REV
6
SCALE: 3:1
QUANTITY: 4
SHEET 4 OF 6
SOLIDWORKS Student Edition.
For Academic Use Only.
JANA STRAIN 22/08/16

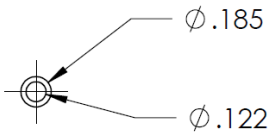

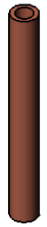

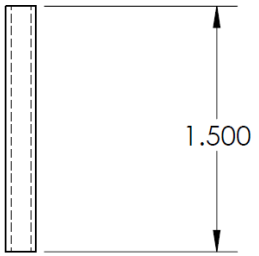

SOLIDWORKS Student Edition.
For Academic Use Only.

JANA STRAIN 27/06/16

UNLESS OTHERWISE SPECIFIED:
DIMENSIONS ARE IN INCHES
TOLERANCES:
FRACTIONAL ±0.003
ONE PLACE DECIMAL ±0.015
TWO PLACE DECIMAL ±0.010
THREE PLACE DECIMAL ±0.003

TITLE:
FILL TUBE END CAP

MATERIAL:	REV
COPPER	**4**

SCALE: 1:1 | **QUANTITY: 5** | SHEET 5 OF 6

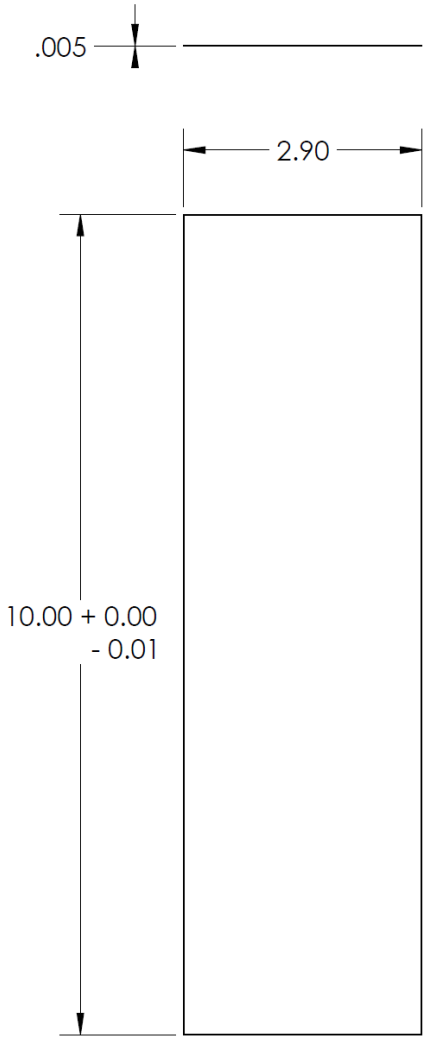

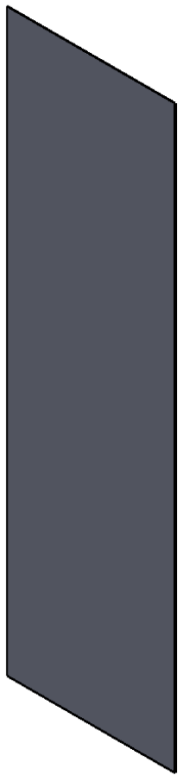

SOLIDWORKS Student Edition.
For Academic Use Only.

JANA STRAIN 06/11/16

UNLESS OTHERWISE SPECIFIED:
DIMENSIONS ARE IN INCHES
TOLERANCES:
FRACTIONAL ±0.003
ONE PLACE DECIMAL ±0.015
TWO PLACE DECIMAL ±0.010
THREE PLACE DECIMAL ±0.003

TITLE:
MESH SCREEN

MATERIAL: **4 COPPER, 3 AL**

REV **1**

SCALE: 1:2 **QUANTITY: 7** SHEET 6 OF 6

Appendix M: HP Testing Apparatus Engineering Drawings

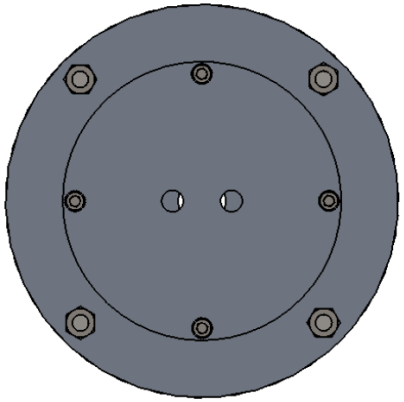

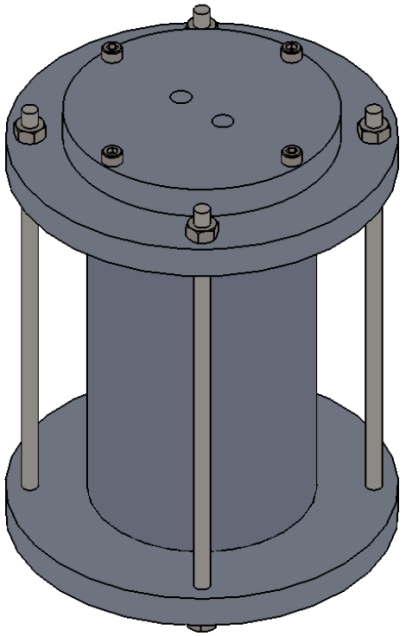

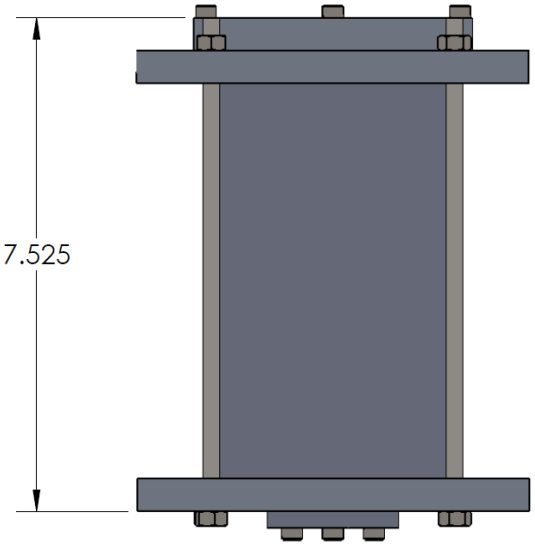

SolidWorks Student Edition.
For Academic Use Only.

JANA STRAIN 25/10/16

UNLESS OTHERWISE SPECIFIED:
DIMENSIONS ARE IN INCHES
TOLERANCES:
FRACTIONAL ±0.003
ONE PLACE DECIMAL ±0.015
TWO PLACE DECIMAL ±0.010
THREE PLACE DECIMAL ±0.003

TITLE:
LIQUID HOLDER ASSEMBLY

MATERIAL:	REV
6061 T6	**3**

SCALE: 1:2.5 **QUANTITY: 1** SHEET 1 OF 10

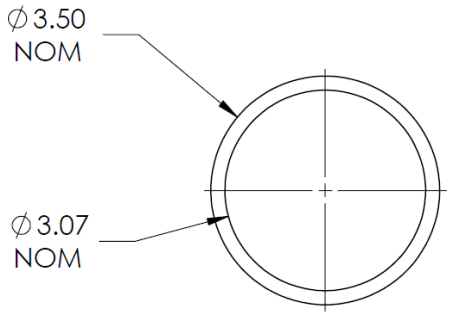

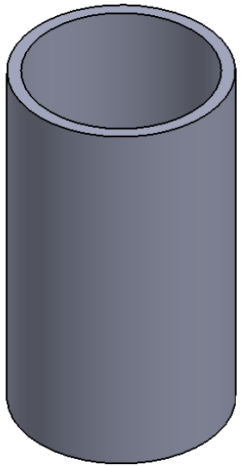

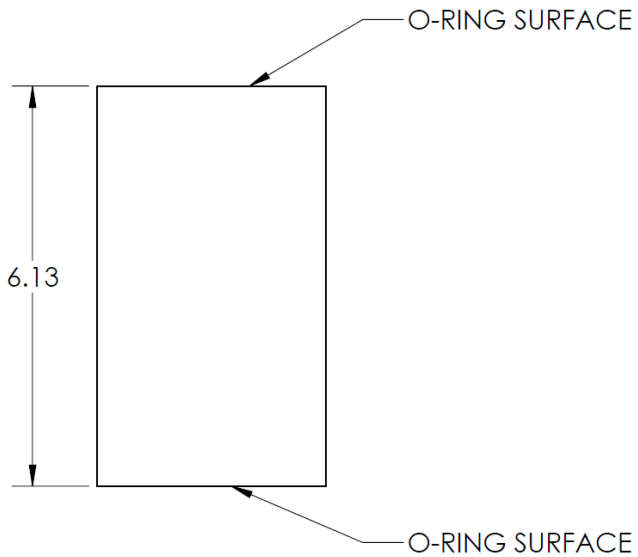

SolidWorks Student Edition.
For Academic Use Only.

JANA STRAIN 25/10/16

UNLESS OTHERWISE SPECIFIED:
DIMENSIONS ARE IN INCHES
TOLERANCES:
FRACTIONAL ±0.003
ONE PLACE DECIMAL ±0.015
TWO PLACE DECIMAL ±0.010
THREE PLACE DECIMAL ±0.003

TITLE:
CENTER TUBE

MATERIAL:	REV
6061 T6	**1**

SCALE: 1:2.5 **QUANTITY: 1** SHEET 2 OF 10

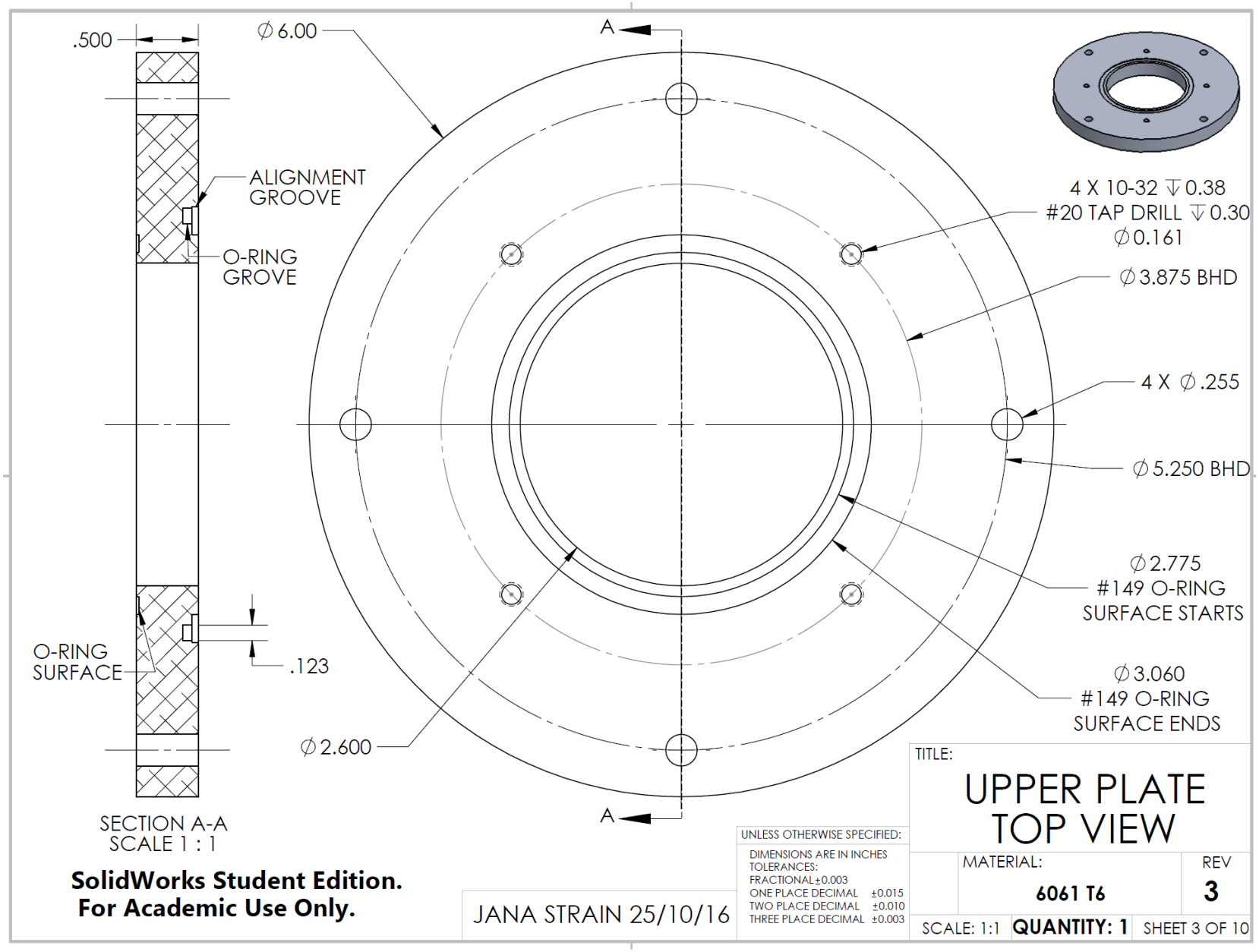
.500
ALIGNMENT GROOVE
O-RING GROVE
O-RING SURFACE
.123
SECTION A-A
SCALE 1 : 1
∅6.00
A
A
∅2.600
4 X 10-32 ↧0.38
#20 TAP DRILL ↧0.30
∅0.161
∅3.875 BHD
4 X ∅.255
∅5.250 BHD
∅2.775
#149 O-RING
SURFACE STARTS
∅3.060
#149 O-RING
SURFACE ENDS
SolidWorks Student Edition.
For Academic Use Only.
JANA STRAIN 25/10/16
UNLESS OTHERWISE SPECIFIED:
DIMENSIONS ARE IN INCHES
TOLERANCES:
FRACTIONAL ±0.003
ONE PLACE DECIMAL ±0.015
TWO PLACE DECIMAL ±0.010
THREE PLACE DECIMAL ±0.003
TITLE:
UPPER PLATE
TOP VIEW
MATERIAL:
6061 T6
REV
3
SCALE: 1:1
QUANTITY: 1
SHEET 3 OF 10

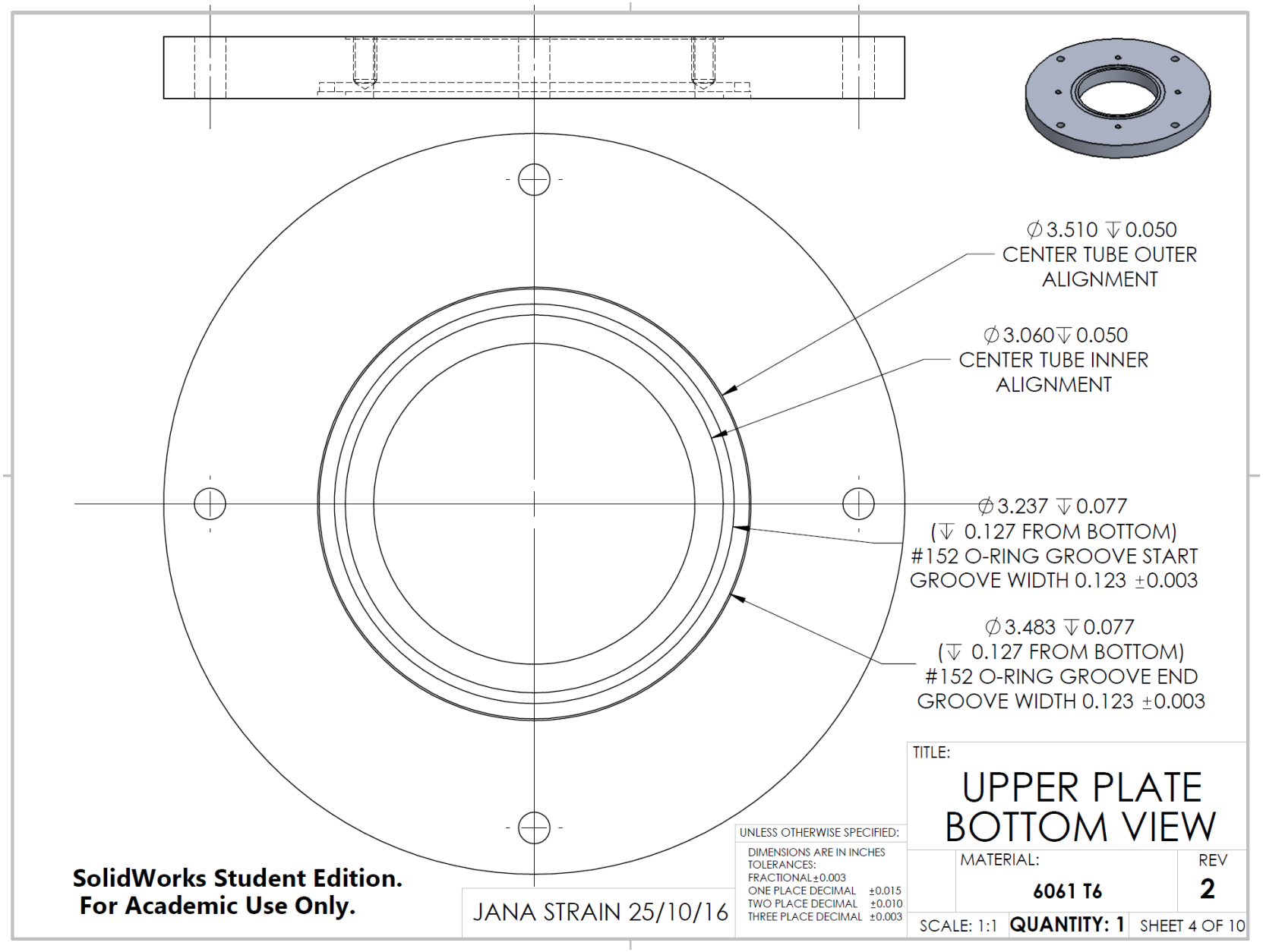
⌀3.510 ↧0.050
CENTER TUBE OUTER
ALIGNMENT
⌀3.060↧0.050
CENTER TUBE INNER
ALIGNMENT
⌀3.237 ↧0.077
(↧ 0.127 FROM BOTTOM)
#152 O-RING GROOVE START
GROOVE WIDTH 0.123 ±0.003
⌀3.483 ↧0.077
(↧ 0.127 FROM BOTTOM)
#152 O-RING GROOVE END
GROOVE WIDTH 0.123 ±0.003
SolidWorks Student Edition.
For Academic Use Only.
JANA STRAIN 25/10/16
UNLESS OTHERWISE SPECIFIED:
DIMENSIONS ARE IN INCHES
TOLERANCES:
FRACTIONAL ±0.003
ONE PLACE DECIMAL ±0.015
TWO PLACE DECIMAL ±0.010
THREE PLACE DECIMAL ±0.003
TITLE:
UPPER PLATE
BOTTOM VIEW
MATERIAL:
6061 T6
REV
2
SCALE: 1:1
QUANTITY: 1
SHEET 4 OF 10

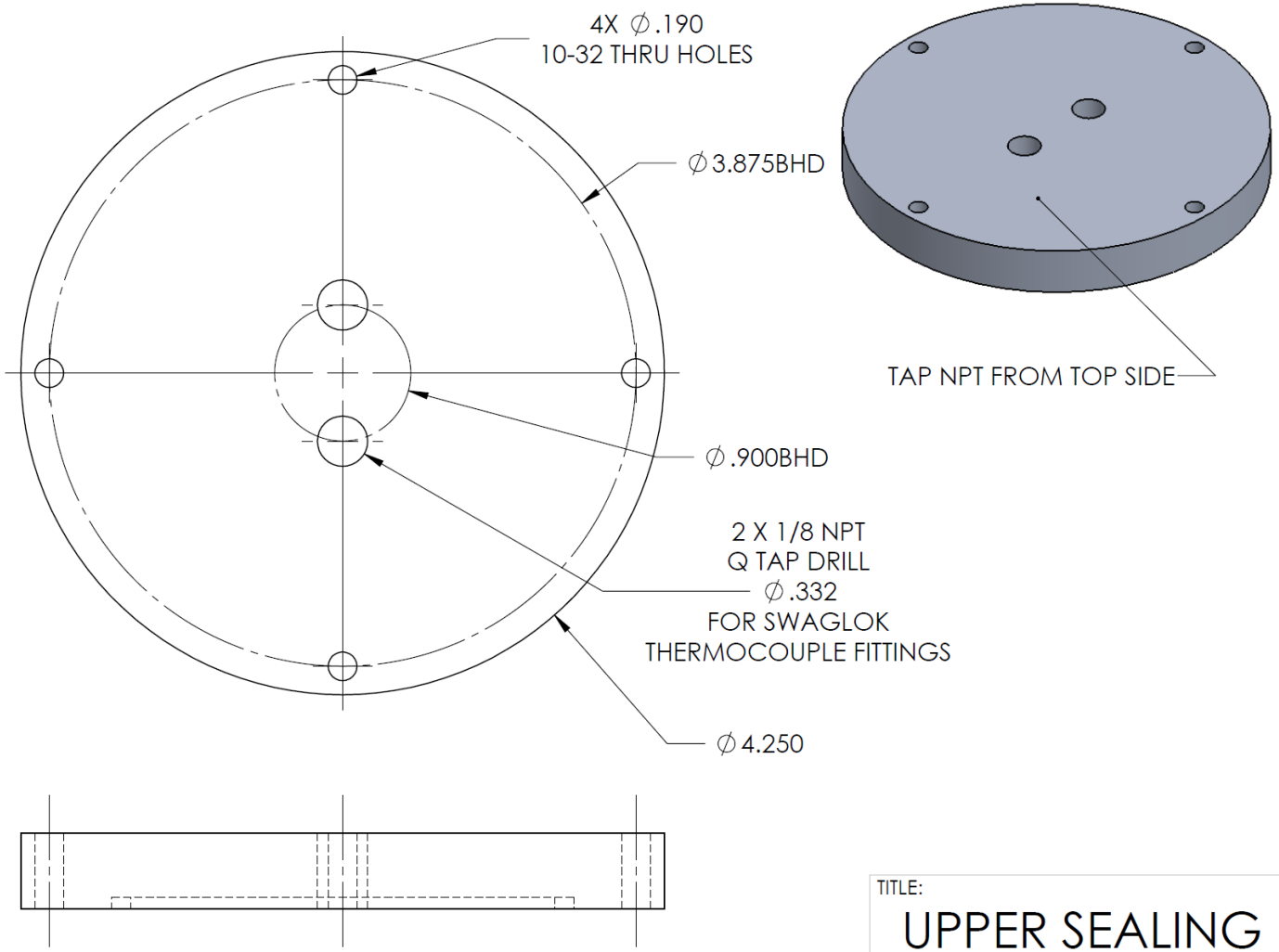

SolidWorks Student Edition.
For Academic Use Only.

JANA STRAIN 25/10/16

UNLESS OTHERWISE SPECIFIED:
DIMENSIONS ARE IN INCHES
TOLERANCES:
FRACTIONAL ±0.003
ONE PLACE DECIMAL ±0.015
TWO PLACE DECIMAL ±0.010
THREE PLACE DECIMAL ±0.003

TITLE:
UPPER SEALING PLATE TOP VIEW

MATERIAL:	REV
6061 T6	1

SCALE: 1:1 | **QUANTITY: 1** | SHEET 5 OF 10

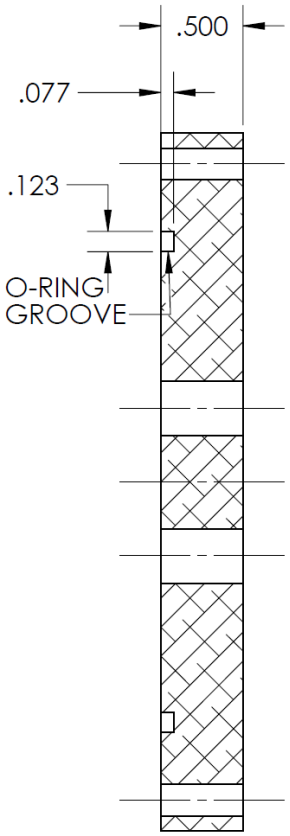

SECTION B-B
SCALE 1 : 1

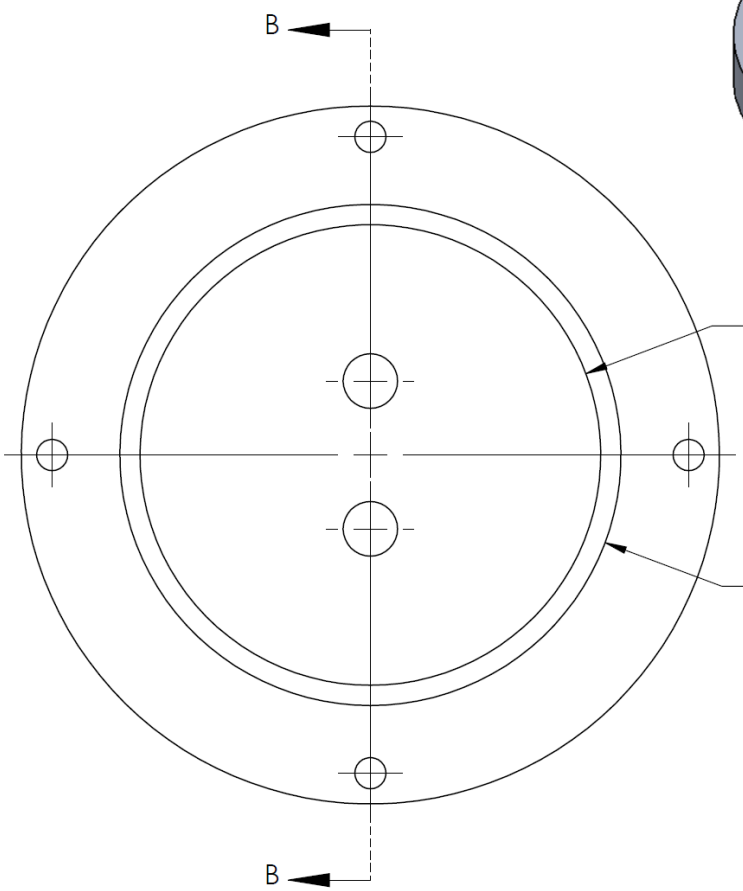

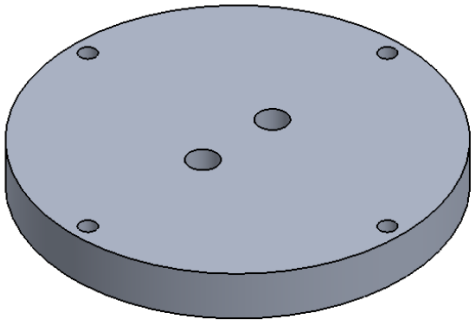

⌀2.805↧0.077
#149 O-RING GROOVE START
GROOVE WIDTH 0.123 ±0.003

⌀3.051↧0.077
#149 O-RING GROOVE END
GROOVE WIDTH 0.123 ±0.003

SolidWorks Student Edition.
For Academic Use Only.

JANA STRAIN 25/10/16

UNLESS OTHERWISE SPECIFIED:
DIMENSIONS ARE IN INCHES
TOLERANCES:
FRACTIONAL ±0.003
ONE PLACE DECIMAL ±0.015
TWO PLACE DECIMAL ±0.010
THREE PLACE DECIMAL ±0.003

TITLE:
UPPER SEALING PLATE BOTTOM

MATERIAL:	REV
6061 T6	**2**

SCALE: 1:1 | **QUANTITY: 1** | SHEET 6 OF 10

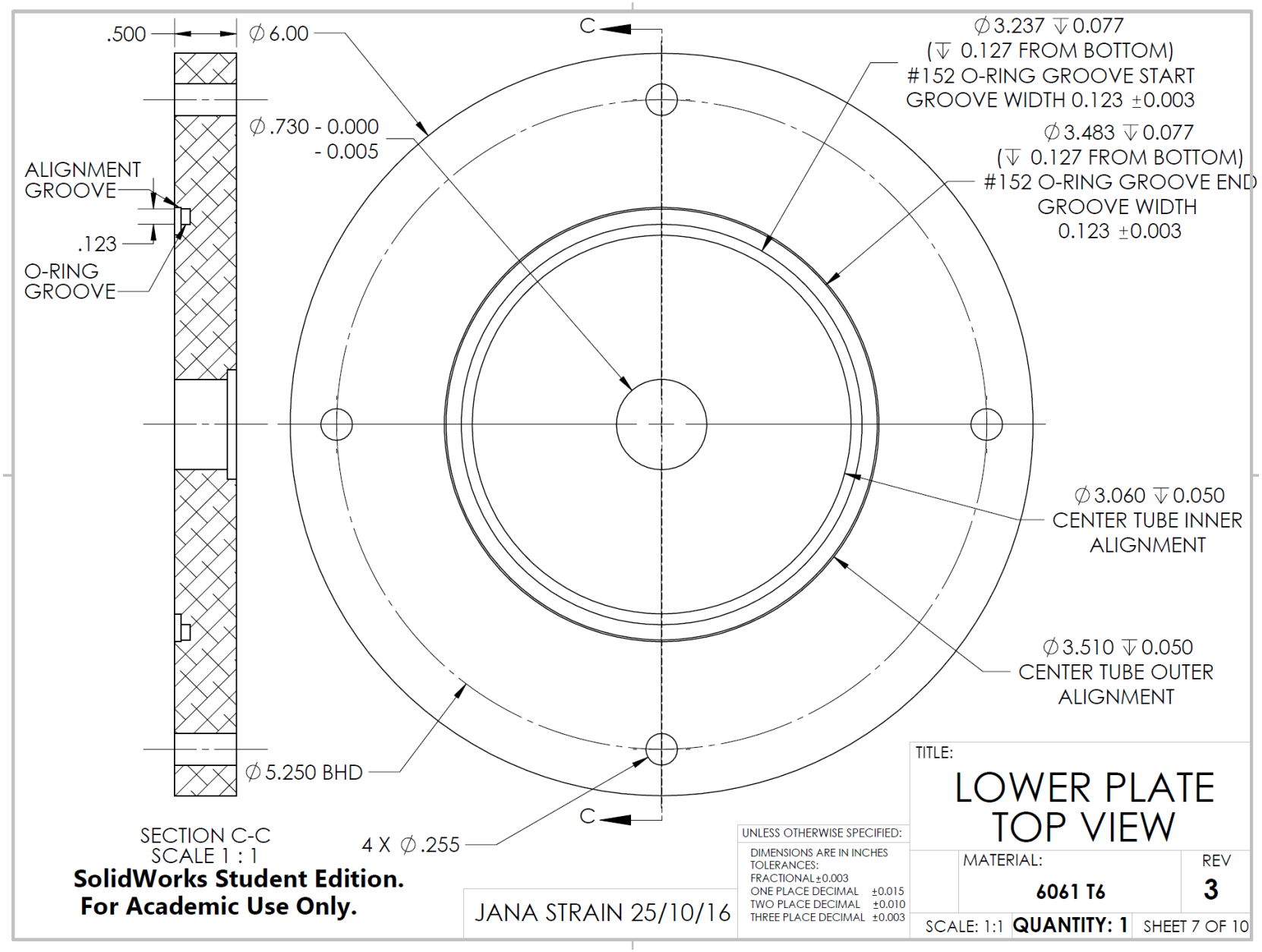
.500
∅6.00
C
∅3.237 ↧0.077
(↧ 0.127 FROM BOTTOM)
#152 O-RING GROOVE START
GROOVE WIDTH 0.123 ±0.003
∅.730 - 0.000
- 0.005
∅3.483 ↧0.077
(↧ 0.127 FROM BOTTOM)
#152 O-RING GROOVE END
GROOVE WIDTH
0.123 ±0.003
ALIGNMENT
GROOVE
.123
O-RING
GROOVE
∅3.060 ↧0.050
CENTER TUBE INNER
ALIGNMENT
∅3.510 ↧0.050
CENTER TUBE OUTER
ALIGNMENT
∅5.250 BHD
C
SECTION C-C
SCALE 1 : 1
4 X ∅.255
SolidWorks Student Edition.
For Academic Use Only.
JANA STRAIN 25/10/16
UNLESS OTHERWISE SPECIFIED:
DIMENSIONS ARE IN INCHES
TOLERANCES:
FRACTIONAL ±0.003
ONE PLACE DECIMAL ±0.015
TWO PLACE DECIMAL ±0.010
THREE PLACE DECIMAL ±0.003
TITLE:
LOWER PLATE
TOP VIEW
MATERIAL:
6061 T6
REV
3
SCALE: 1:1
QUANTITY: 1
SHEET 7 OF 10

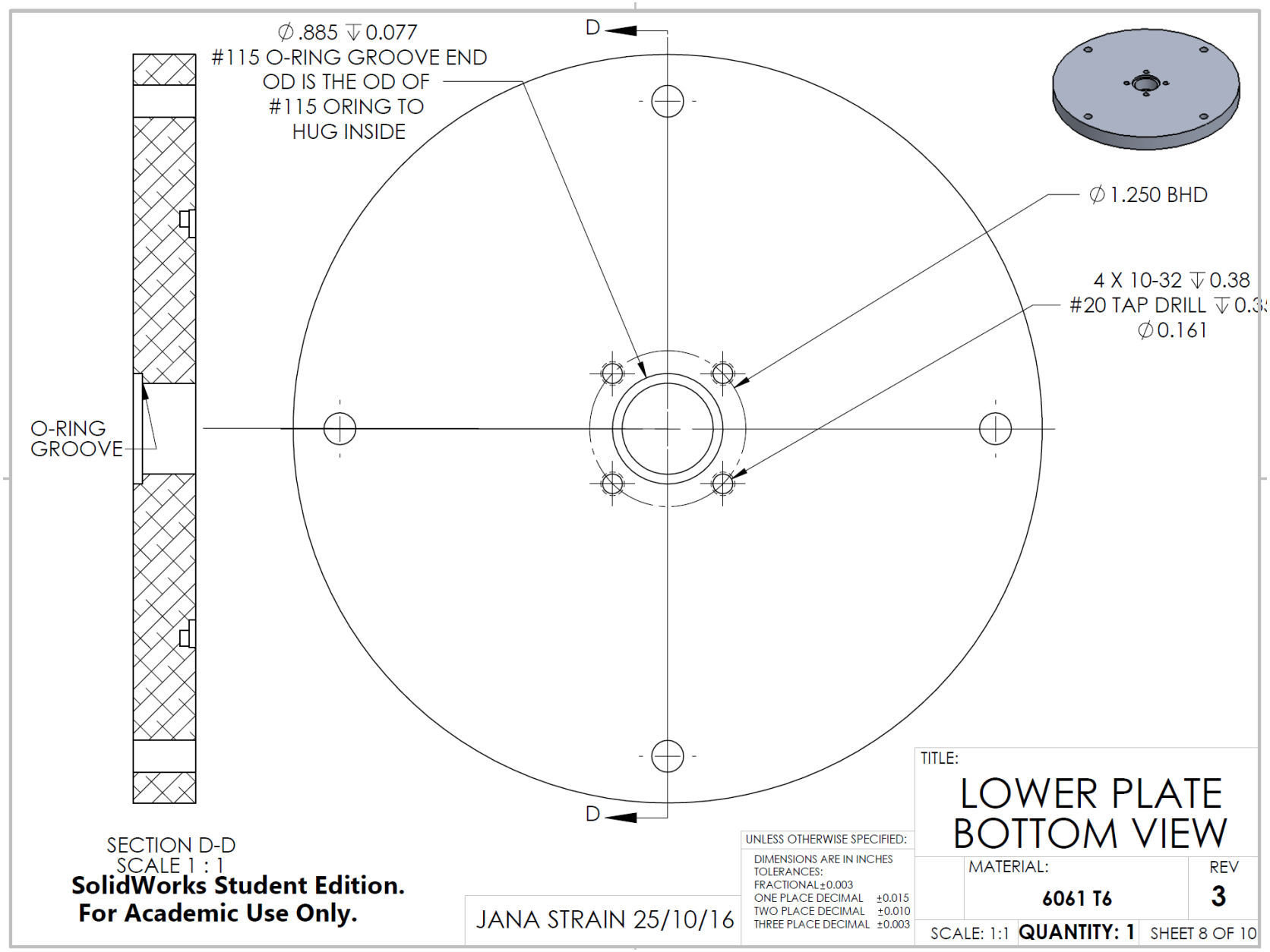
∅.885 ↧0.077
#115 O-RING GROOVE END
OD IS THE OD OF
#115 ORING TO
HUG INSIDE
D
∅1.250 BHD
4 X 10-32 ↧0.38
#20 TAP DRILL ↧0.3
∅0.161
O-RING
GROOVE
D
SECTION D-D
SCALE 1 : 1
SolidWorks Student Edition.
For Academic Use Only.
JANA STRAIN 25/10/16
UNLESS OTHERWISE SPECIFIED:
DIMENSIONS ARE IN INCHES
TOLERANCES:
FRACTIONAL ±0.003
ONE PLACE DECIMAL ±0.015
TWO PLACE DECIMAL ±0.010
THREE PLACE DECIMAL ±0.003
TITLE:
LOWER PLATE
BOTTOM VIEW
MATERIAL:
6061 T6
REV
3
SCALE: 1:1
QUANTITY: 1
SHEET 8 OF 10

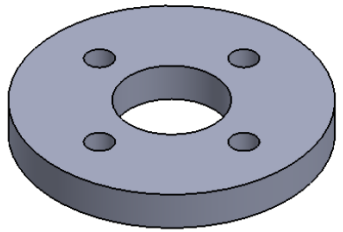

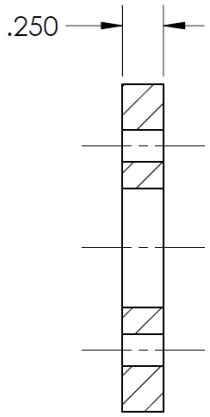

SECTION E-E
SCALE 1 : 1

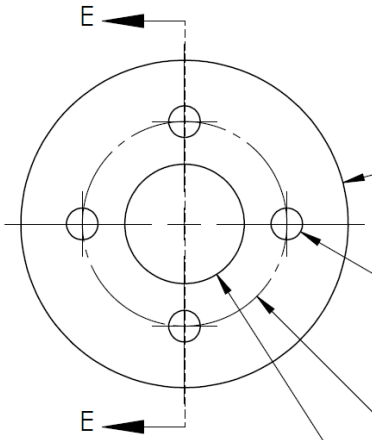

∅2.00

4X ∅.193
10-32 THRU HOLES

∅1.250 BHD
O-RING SURFACE
BETWEEN 0.715 & BHD

∅.730 - 0.000
+ 0.005

SolidWorks Student Edition.
For Academic Use Only.

JANA STRAIN 25/10/16

UNLESS OTHERWISE SPECIFIED:
DIMENSIONS ARE IN INCHES
TOLERANCES:
FRACTIONAL ±0.003
ONE PLACE DECIMAL ±0.015
TWO PLACE DECIMAL ±0.010
THREE PLACE DECIMAL ±0.003

TITLE:
LOWER O-RING PLATE

MATERIAL:	REV
6061 T6	**2**

SCALE: 1:1 | **QUANTITY: 1** | SHEET 9 OF 10

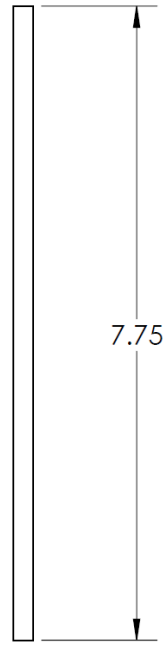

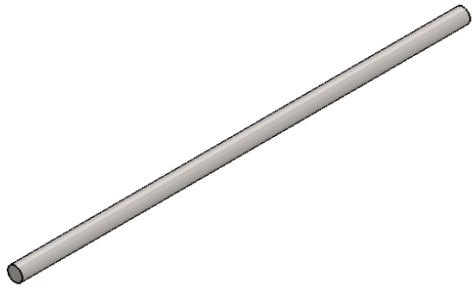

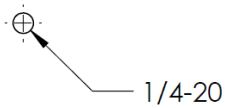

TITLE:

READY ROD

	MATERIAL: SS	REV 2

UNLESS OTHERWISE SPECIFIED:

DIMENSIONS ARE IN INCHES
TOLERANCES:
FRACTIONAL ±0.003
ONE PLACE DECIMAL ±0.015
TWO PLACE DECIMAL ±0.010
THREE PLACE DECIMAL ±0.003

JANA STRAIN 25/10/16

SCALE: 1:2 **QUANTITY: 4** SHEET 10 OF 10

Appendix N: Apparatus Insulation Engineering Drawings

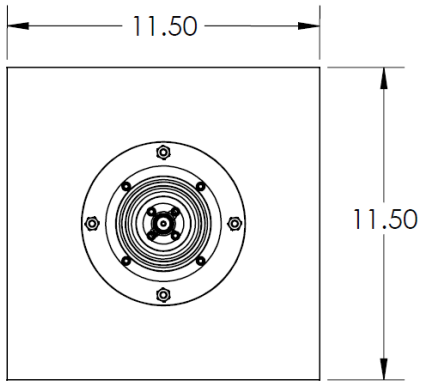

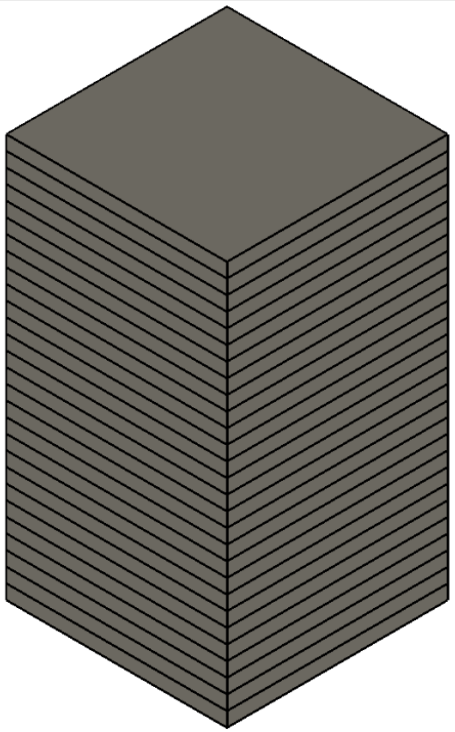

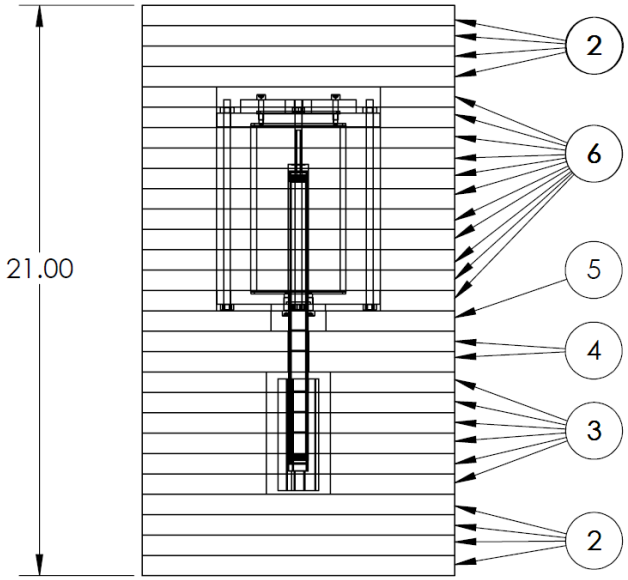

SolidWorks Student Edition.
For Academic Use Only.

JANA STRAIN 23/11/16

UNLESS OTHERWISE SPECIFIED:
DIMENSIONS ARE IN INCHES
TOLERANCES:
FRACTIONAL ±0.003
ONE PLACE DECIMAL ±0.015
TWO PLACE DECIMAL ±0.010
THREE PLACE DECIMAL ±0.003

TITLE:

ASSEMBLY

MATERIAL: **POLYETHYLENE**

REV **2**

SCALE: 1:3 **QUANTITY: 1** SHEET 1 OF 6

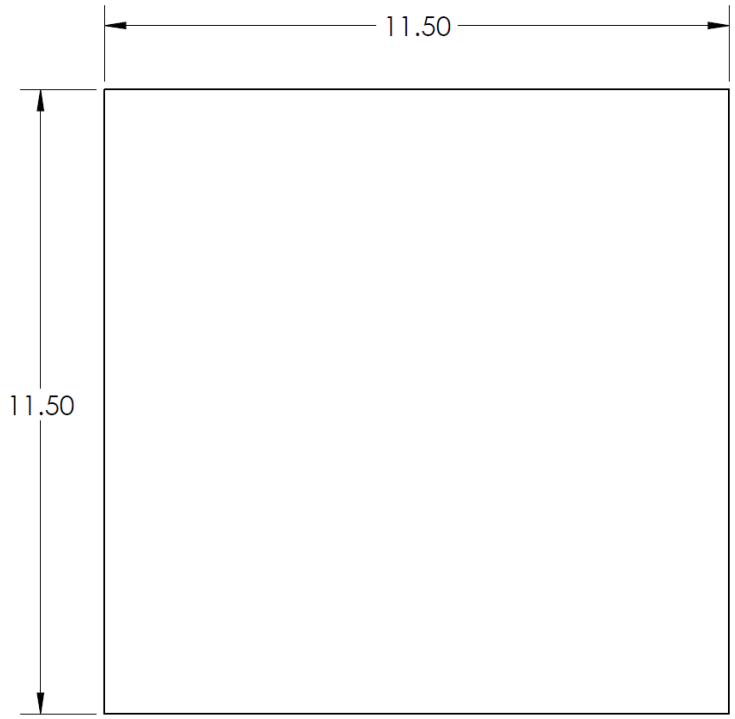

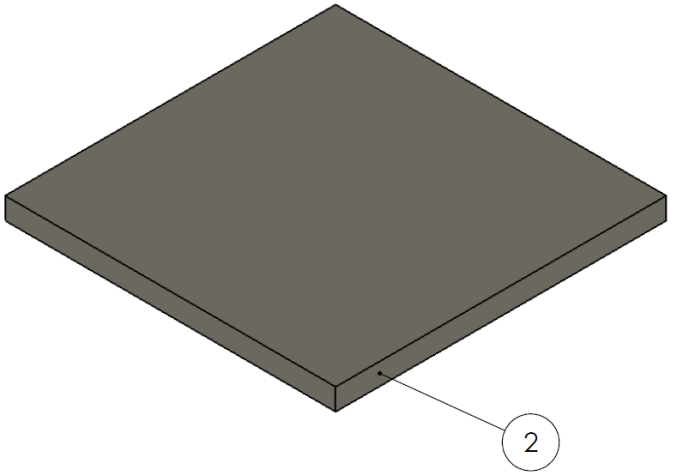

FOUR WHOLE PEICES ON THE TOP AND FOUR ON THE BOTTOM

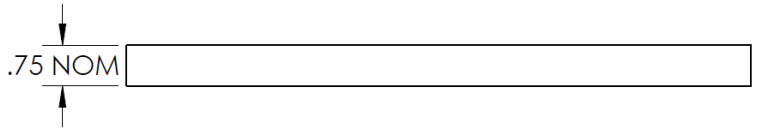

SolidWorks Student Edition.
For Academic Use Only.

JANA STRAIN 01/11/16

UNLESS OTHERWISE SPECIFIED:
DIMENSIONS ARE IN INCHES
TOLERANCES:
FRACTIONAL ±0.003
ONE PLACE DECIMAL ±0.015
TWO PLACE DECIMAL ±0.010
THREE PLACE DECIMAL ±0.003

TITLE:

WHOLE SHEETS

MATERIAL:	REV
POLYETHYLENE	**1**

SCALE: 1:3 | **QUANTITY: 8** | SHEET 2 OF 6

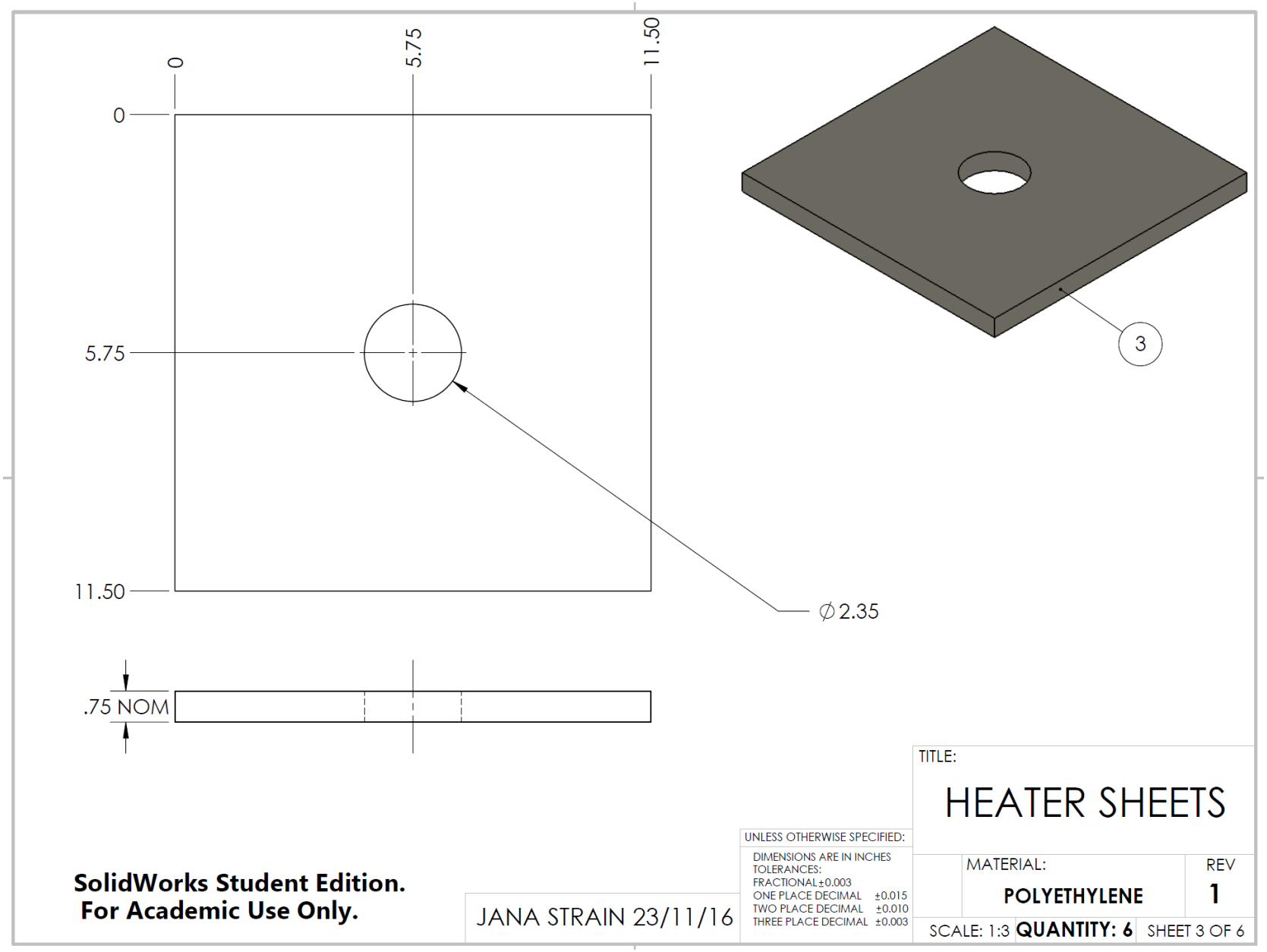
0
5.75
11.50
0
5.75
11.50
∅2.35
.75 NOM
3
SolidWorks Student Edition.
For Academic Use Only.
JANA STRAIN 23/11/16
UNLESS OTHERWISE SPECIFIED:
DIMENSIONS ARE IN INCHES
TOLERANCES:
FRACTIONAL ±0.003
ONE PLACE DECIMAL ±0.015
TWO PLACE DECIMAL ±0.010
THREE PLACE DECIMAL ±0.003
TITLE:
HEATER SHEETS
MATERIAL:
POLYETHYLENE
REV
1
SCALE: 1:3
QUANTITY: 6
SHEET 3 OF 6

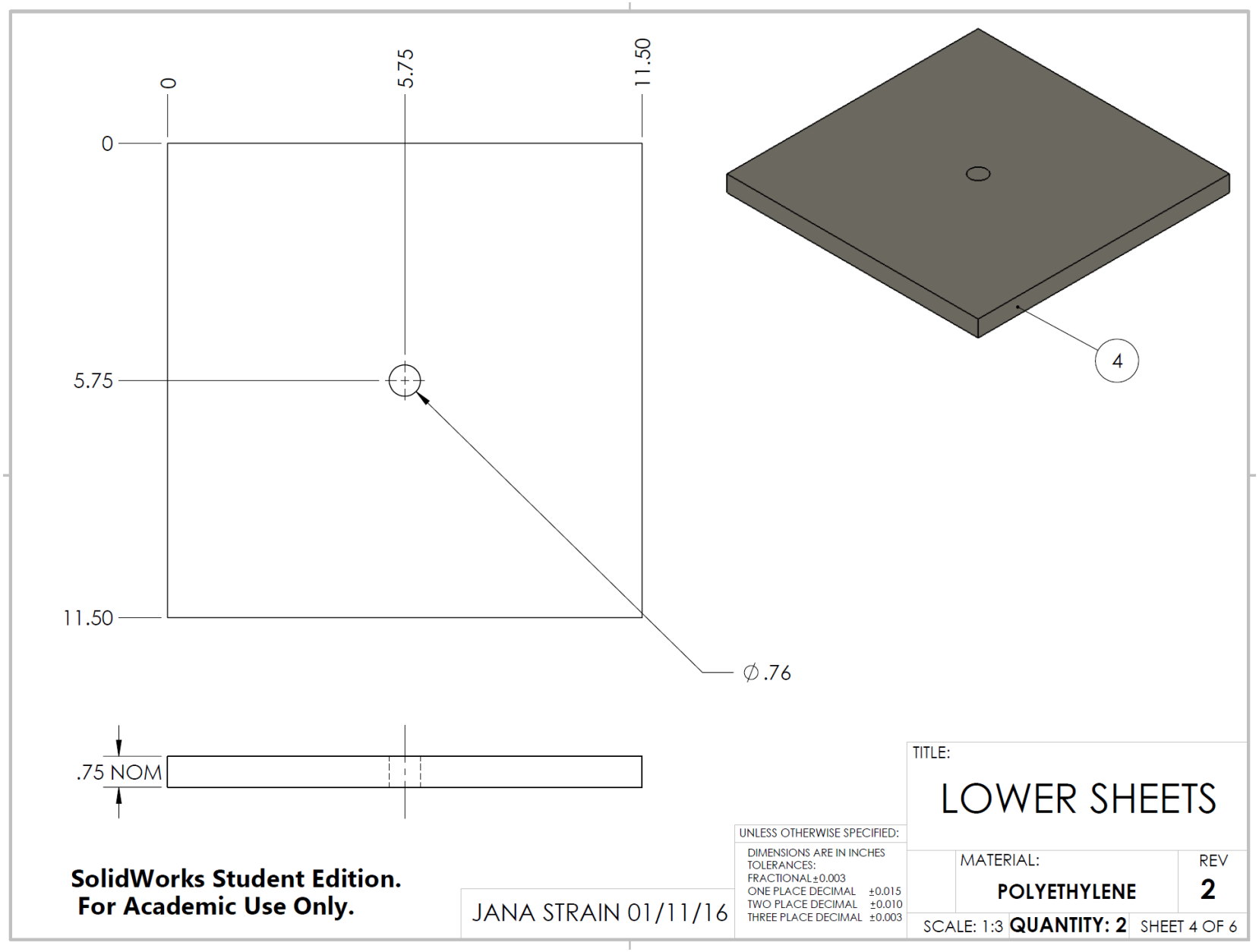
0
5.75
11.50
0
5.75
11.50
∅.76
.75 NOM
4
SolidWorks Student Edition.
For Academic Use Only.
JANA STRAIN 01/11/16
UNLESS OTHERWISE SPECIFIED:
DIMENSIONS ARE IN INCHES
TOLERANCES:
FRACTIONAL ±0.003
ONE PLACE DECIMAL ±0.015
TWO PLACE DECIMAL ±0.010
THREE PLACE DECIMAL ±0.003
TITLE:
LOWER SHEETS
MATERIAL:
POLYETHYLENE
REV
2
SCALE: 1:3
QUANTITY: 2
SHEET 4 OF 6

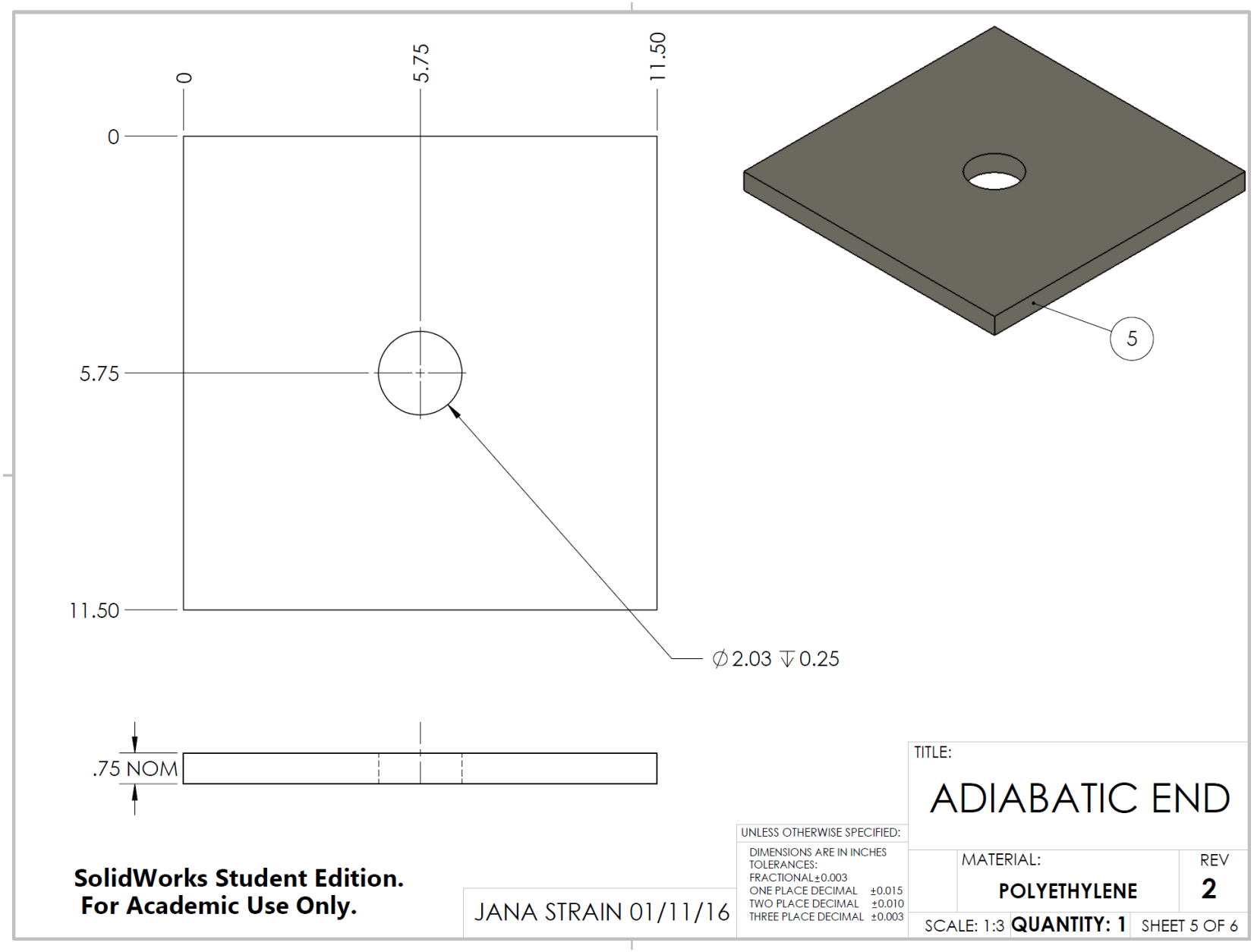
0
5.75
11.50
0
5.75
11.50
∅2.03 ↧0.25
.75 NOM
5
SolidWorks Student Edition.
For Academic Use Only.
JANA STRAIN 01/11/16
UNLESS OTHERWISE SPECIFIED:
DIMENSIONS ARE IN INCHES
TOLERANCES:
FRACTIONAL ±0.003
ONE PLACE DECIMAL ±0.015
TWO PLACE DECIMAL ±0.010
THREE PLACE DECIMAL ±0.003
TITLE:
ADIABATIC END
MATERIAL:
POLYETHYLENE
REV
2
SCALE: 1:3
QUANTITY: 1
SHEET 5 OF 6

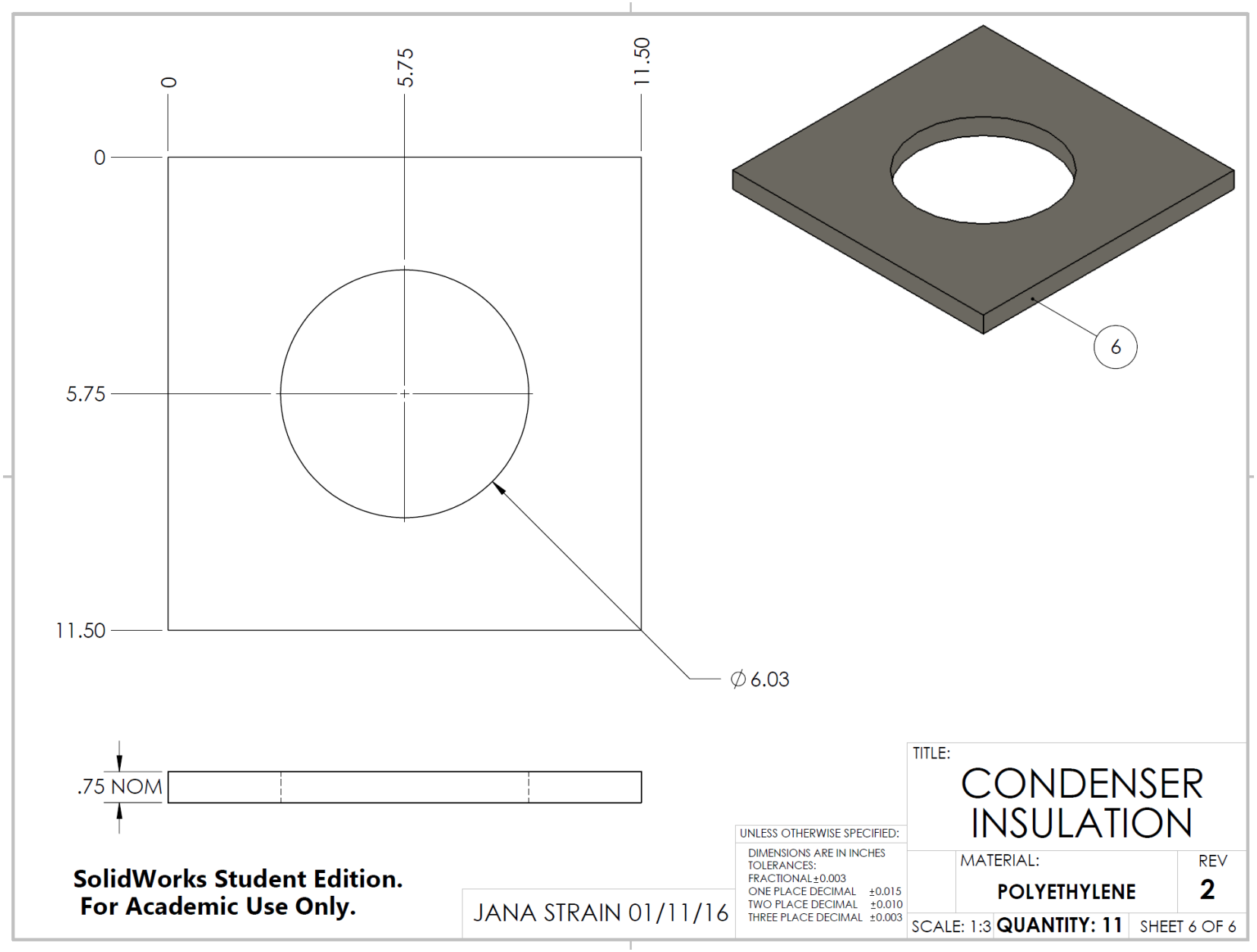
0
5.75
11.50
0
5.75
11.50
∅6.03
6
.75 NOM
SolidWorks Student Edition.
For Academic Use Only.
JANA STRAIN 01/11/16
UNLESS OTHERWISE SPECIFIED:
DIMENSIONS ARE IN INCHES
TOLERANCES:
FRACTIONAL ±0.003
ONE PLACE DECIMAL ±0.015
TWO PLACE DECIMAL ±0.010
THREE PLACE DECIMAL ±0.003
TITLE:
CONDENSER INSULATION
MATERIAL:
POLYETHYLENE
REV
2
SCALE: 1:3
QUANTITY: 11
SHEET 6 OF 6

Appendix O: Vacuum System Engineering Drawings

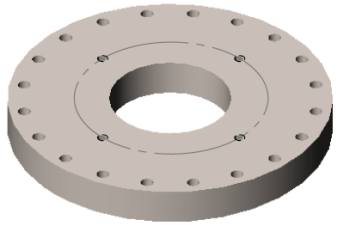

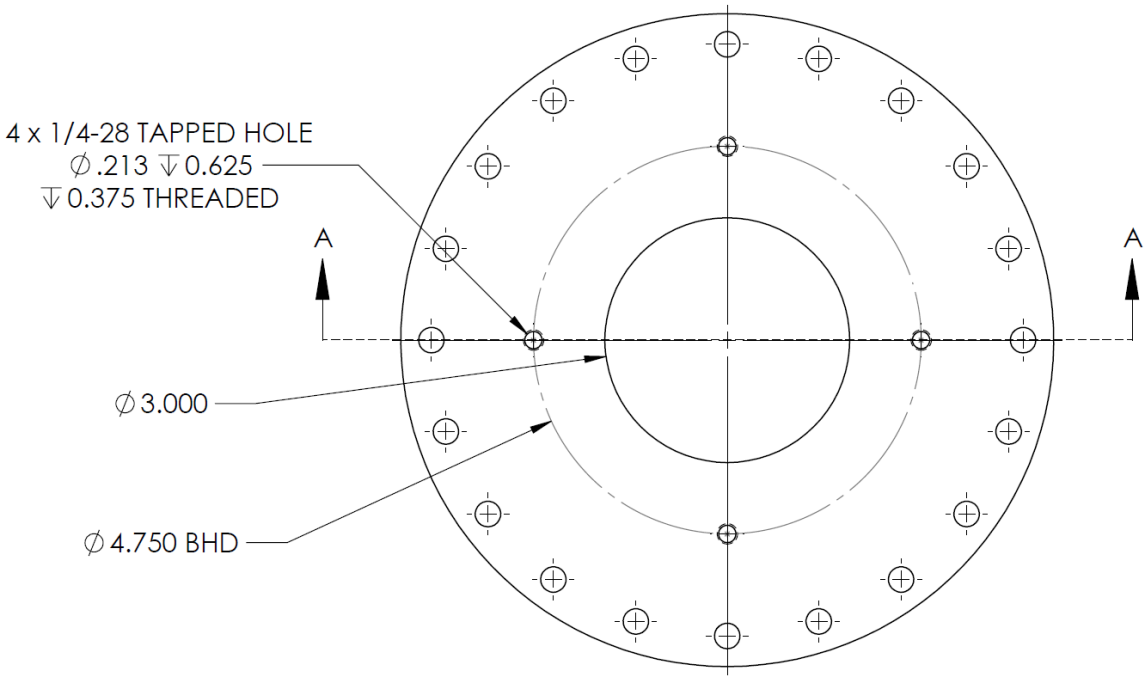

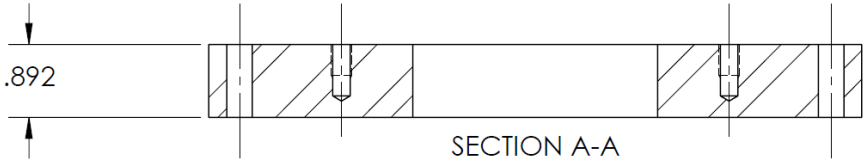

THE 20 OUTER HOLES CAME ALREADY IN THE FLANGE.

SolidWorks Student Edition.
For Academic Use Only.

JANA STRAIN 27/06/16

UNLESS OTHERWISE SPECIFIED:
DIMENSIONS ARE IN INCHES
TOLERANCES:
FRACTIONAL ±0.003
ONE PLACE DECIMAL ±0.015
TWO PLACE DECIMAL ±0.010
THREE PLACE DECIMAL ±0.003

TITLE:

FLANGE

MATERIAL:	REV
SS	**2**

SCALE: 1:2 | **QUANTITY: 1** | SHEET 1 OF 7

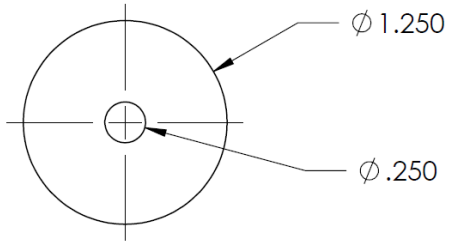

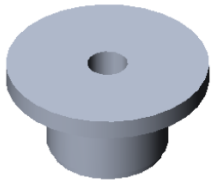

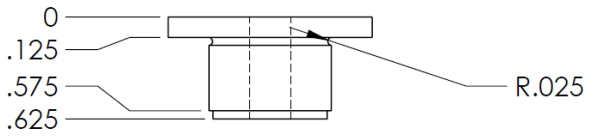

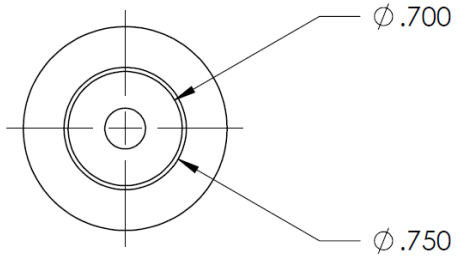

SolidWorks Student Edition.
For Academic Use Only.

JANA STRAIN 27/06/16

UNLESS OTHERWISE SPECIFIED:
DIMENSIONS ARE IN INCHES
TOLERANCES:
FRACTIONAL ±0.003
ONE PLACE DECIMAL ±0.015
TWO PLACE DECIMAL ±0.010
THREE PLACE DECIMAL ±0.003

TITLE:
WASHER

MATERIAL: **AL 6061-T6**
REV **1**
SCALE: 1:1 **QUANTITY: 4** SHEET 2 OF 7

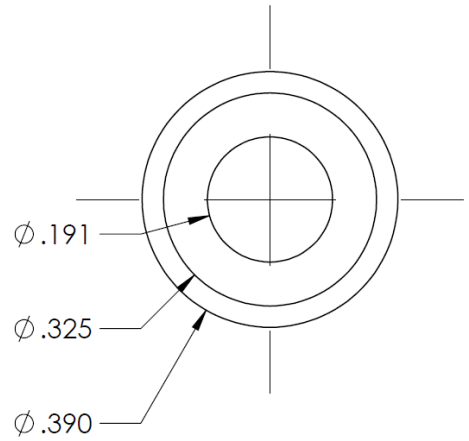

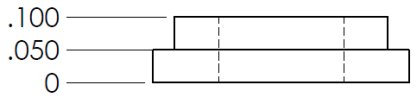

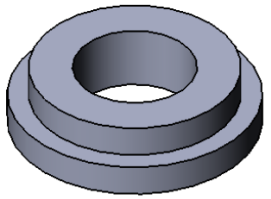

FOR USE INSIDE A 1/4" SWAGLOK FITTING TO CONNECT THE HP TO THE VACUUM SYSTEM. THIS IS USED TO COMPRESS AN O-RING.

TITLE:

FERRULE

	MATERIAL:	REV
	DELRIN	**1**
SCALE: 1:2	**QUANTITY: 1**	SHEET 3 OF 7

UNLESS OTHERWISE SPECIFIED:
DIMENSIONS ARE IN INCHES
TOLERANCES:
FRACTIONAL ±0.003
ONE PLACE DECIMAL ±0.015
TWO PLACE DECIMAL ±0.010
THREE PLACE DECIMAL ±0.003

JANA STRAIN 18/07/16

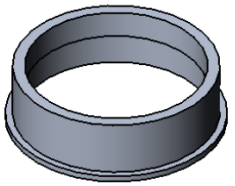

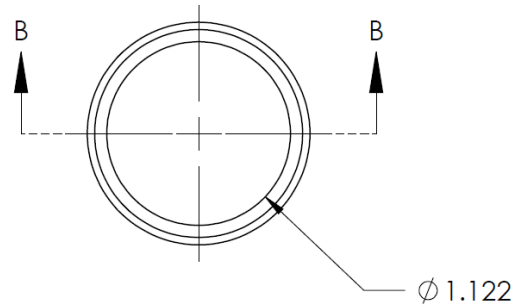

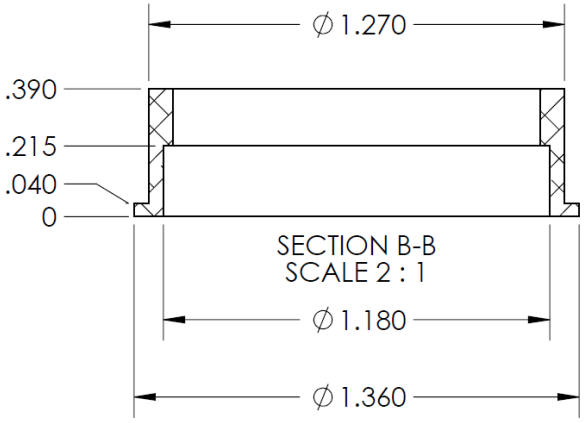

USED TO HOLD KF TYPE VACUUM PARTS IN A LATHE. THIS WAY THE OPPOSING SIDE CAN HAVE THE O-RING SURFACE REFINISHED.

SolidWorks Student Edition.
For Academic Use Only.

JANA STRAIN 19/07/16

UNLESS OTHERWISE SPECIFIED:
DIMENSIONS ARE IN INCHES
TOLERANCES:
FRACTIONAL ±0.003
ONE PLACE DECIMAL ±0.015
TWO PLACE DECIMAL ±0.010
THREE PLACE DECIMAL ±0.003

TITLE:
SM KF VACUUM LATHE FIXTURE

MATERIAL:	REV
AL 6061-T6	**1**

SCALE: 1:1 | **QUANTITY: 1** | SHEET 4 OF 7

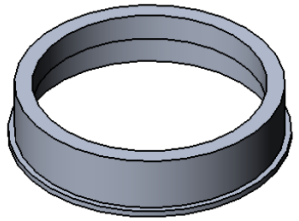

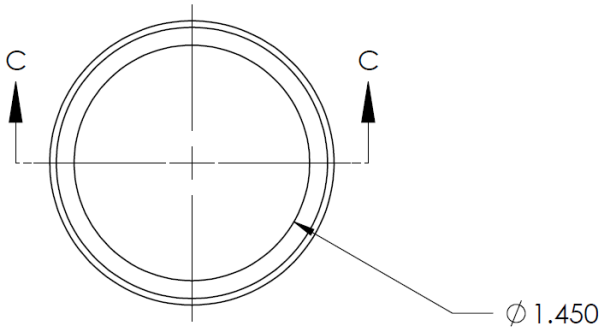

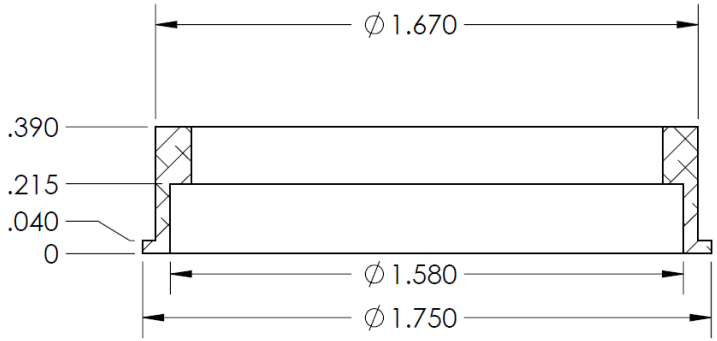

SECTION C-C
SCALE 2 : 1

USED TO HOLD KF TYPE VACUUM PARTS IN A LATHE. THIS WAY THE OPPOSING SIDE CAN HAVE THE O-RING SURFACE REFINISHED.

SolidWorks Student Edition.
For Academic Use Only.

JANA STRAIN 19/07/16

UNLESS OTHERWISE SPECIFIED:
DIMENSIONS ARE IN INCHES
TOLERANCES:
FRACTIONAL ±0.003
ONE PLACE DECIMAL ±0.015
TWO PLACE DECIMAL ±0.010
THREE PLACE DECIMAL ±0.003

TITLE:
LG KF VACUUM LATHE FIXTURE

MATERIAL:	REV
AL 6061-T6	**1**

SCALE: 1:1 | **QUANTITY: 1** | SHEET 5 OF 7

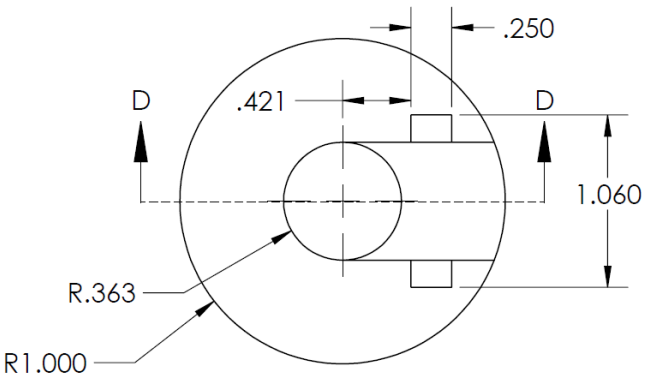

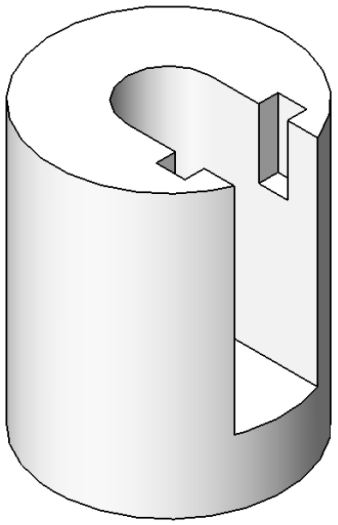

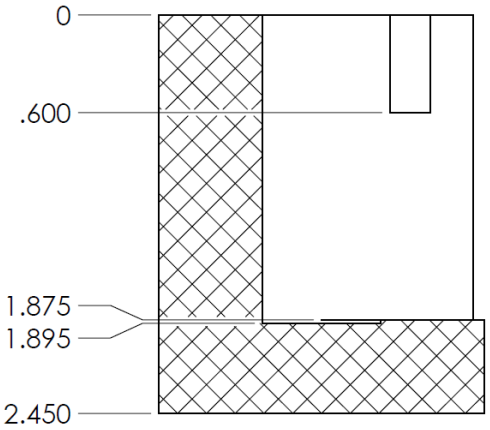

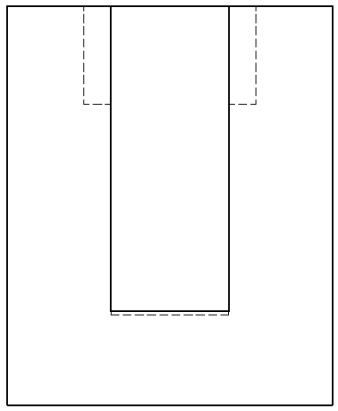

SECTION D-D
SCALE 1 : 1

HEAT PIPE GOES IN THE CENTER THEN A SMALL PIECE OF PLASTIC SLIDES INTO THE SLOT TO KEEP THE HP IN ONE PLACE.

TITLE:

HP STAND

	MATERIAL: **ABS**	REV **1**
SCALE: 1:1	**QUANTITY: 1**	SHEET 6 OF 7

UNLESS OTHERWISE SPECIFIED:

DIMENSIONS ARE IN INCHES
TOLERANCES:
FRACTIONAL ±0.003
ONE PLACE DECIMAL ±0.015
TWO PLACE DECIMAL ±0.010
THREE PLACE DECIMAL ±0.003

JANA STRAIN 19/07/16

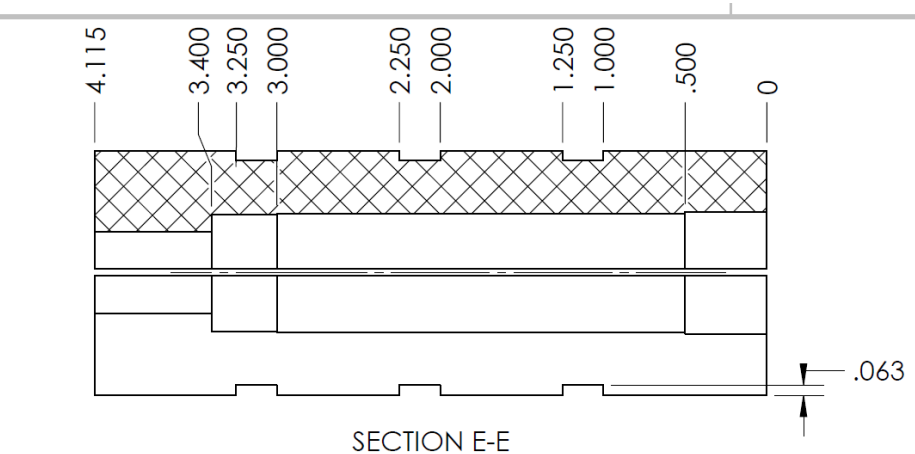

SECTION E-E

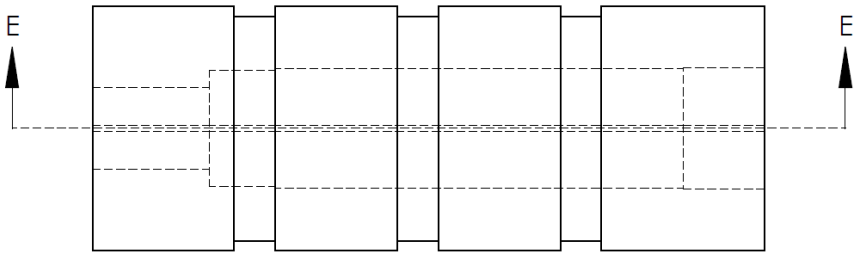

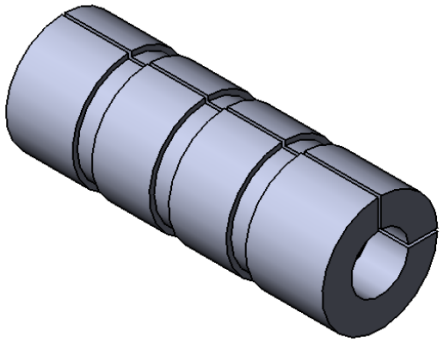

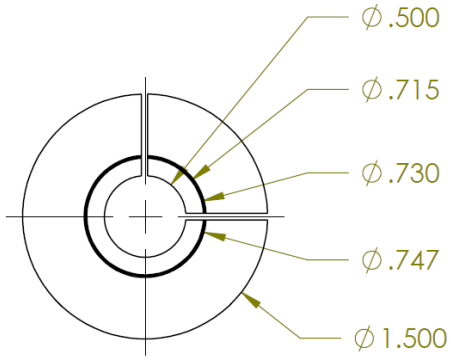

AFTER THE FIXTURE IS COMPLETED, CUT VERTICALLY APPROXIMATELY 1/4 OF THE CIRCLE. SHOULD COVER THERMOCOUPLE WIDTH.

TITLE:

HEATER FIXTURE

UNLESS OTHERWISE SPECIFIED:
DIMENSIONS ARE IN INCHES
TOLERANCES:
FRACTIONAL ±0.003
ONE PLACE DECIMAL ±0.015
TWO PLACE DECIMAL ±0.010
THREE PLACE DECIMAL ±0.003

MATERIAL: **DELRIN**

REV **2**

SCALE: 1:1 **QUANTITY: 1** SHEET 7 OF 7

JANA STRAIN 21/11/16

SolidWorks Student Edition.
For Academic Use Only.

Appendix P: Vacuum System Setup

FIGURE 58: PROCESS OF SETTING UP THE EVACUATION AND FILLING RIG. 1. NEW VACUUM PUMP. 2. TOP VIEW OF VACUUM PUMP. 3. MACHINING VACUUM FLANGE. 4. ASSEMBLING VACUUM SYSTEM. 5. ASSEMBLY CONTINUES. 6. COMPLETED EVACUATION AND FILLING RIG.

Appendix Q: Experimental Evacuation and Charging Results

Pipe #	Material	Type	Initial Mass [g]	Fluid	Density [kg/m^3]	Vacuum Pressure [Pa] 1 hr	Vacuum Pressure [Pa] 22 hr	Fill Time [s]	Final Mass [g]	Final w solder [g]	Fill Mass [g]	Solder Mass [g]	Fill Volume [ml]	Charge Fill [ml]	Filling Losses [ml]	Ideal Fill [ml]	Error [%]	Filling Ratio [%]
B1	Cu	HP	264.5	M	762	7.3E-03	1.1E-02	22	270.4	270.6	5.9	0.24	7.73	10.70	2.97	6.10	26.7	14.0
B2	Cu	TS	244.5	M	770	5.2E-01	4.4E-01	20	259.8	260.0	15.3	0.25	19.81	25.30	5.49	20.00	-0.9	35.8
1	Cu	HP	252.8	M	757	9.1E-03	1.1E-03	7	255.9	256.2	3.1	0.31	4.06	9.60	5.54	6.06	-33.0	7.3
2	Cu	TS	240.2	M	774	5.2E-02	5.7E-02	24	253.4	254.2	13.2	0.74	17.10	24.60	7.50	18.23	-6.2	30.9
3	Cu	HP	251.4	M	776	1.9E-01	6.9E-03	9	256.1	256.7	4.8	0.59	6.14	11.57	5.43	6.06	1.4	11.1
4	Cu	HP	251.5	A	782	1.5E-01	7.3E-03	8	256.5	256.9	4.9	0.44	6.33	11.57	5.24	6.06	4.4	11.4
5	Al	HP	101.5	A	773	3.3E-01	1.2E-02	18	105.7	107.2	4.2	1.44	5.44	11.50	6.06	6.06	-10.2	9.8
6	Al	TS	97.8	A	772	1.7E-01	2.0E-02	18	112.8	113.9	15.0	1.10	19.40	25.73	6.33	18.23	6.4	35.1

Appendix R: Experimental Evacuation Data

July 12th, 10:25am start no Heat					
	ConvecTorr Gauge	Cold Cathode Gauge			Cold Cathode Gauge
Time Past	Pressure	Pressure	Pump Speed	Time Past	Pressure
(min)	(pascal)	(pascal)	(rpm)	(h)	(pascal)
1	2.4E+00		5k	1	7.3E-03
2	8.4E-01		14k	2	4.7E-03
3	5.7E-01		28k	3	3.6E-03
4	2.8E-01	5.6E-02	38k	4	3.1E-03
5	1.3E-02	4.9E-02	42k	5	2.8E-03
10		3.5E-02	42k	6	2.5E-03
15		2.5E-02	42k	7	2.3E-03
20		2.0E-02	42k	26	9.3E-04
30		1.1E-02	42k		
40		9.3E-03	42k		
60		7.3E-03	42k		

Heated Test July 13, 2:35pm					
	ConvecTorr	Cold Cathode			Cold Cathode
Time	Pressure	Pressure	Pump Speed	Time	Converted Pressure
(min)	(pascal)	(pascal)	(rpm)	(h)	(pascal)
1	3.5E+00		5k	1	5.9E-03
2	9.6E-01		14k	4	1.6E-03
3	2.9E-01		28k	19	9.1E-04
4	1.3E-02		38k	24	1.0E-03
5	1.3E-02	2.8E-01	42k		
10		1.0E-01	42k		
15		4.4E-02	42k		
20		2.8E-02	42k		
30		2.9E-02	42k		
40		1.3E-02	42k		
60		5.9E-03	42k		

November 9th, 13:40 start Methanol HP 2nd Generation Beta #1					
	ConvecTorr Gauge	Cold Cathode Gauge			Cold Cathode Gauge
Time Past	Pressure	Pressure	Pump Speed	Time Past	Pressure
(min)	(pascal)	(pascal)	(rpm)	(h)	(pascal)
1	4.5E+00		5k	17	1.1E-03
2	2.4E+00		14k	19.5	1.1E-03
3	2.0E+00		28k	22	1.1E-03
4	2.0E+00	9.7E-02	38k		
5	2.0E+00	7.5E-02	42k		
10		6.8E-02	42k		
15		4.7E-02	42k		
20		2.8E-02	42k		
30		2.0E-02	42k		
40		1.3E-02	42k		
60		9.1E-03	42k		

November 9th, 13:40 start Methanol TS2nd Generation Beta #2					
	ConvecTorr Gauge	Cold Cathode Gauge			Cold Cathode Gauge
Time Past	Pressure	Pressure	Pump Speed	Time Past	Pressure
(min)	(pascal)	(pascal)	(rpm)	(h)	(pascal)
1	1.3E+01		5k	72	5.7E-02
2	2.4E+01		14k		
3	2.7E+01		28k		
4			38k		
5	5.3E+00		42k		
10		5.3E-01	42k		
15		2.9E-01	42k		
20		2.3E-01	42k		
30		1.7E-01	42k		
40		1.2E-01	42k		
60		5.2E-02	42k		

November 14th, 8:40 start Methanol HP 2nd Generation Beta #3					
	ConvecTorr Gauge	Cold Cathode Gauge			Cold Cathode Gauge
Time Past	Pressure	Pressure	Pump Speed	Time Past	Pressure
(min)	(pascal)	(pascal)	(rpm)	(h)	(pascal)
1	1.1E+02		5k	3.5	2.4E-02
2	3.2E+01		14k	21.75	7.0E-03
3	3.3E+00		28k	22.25	6.9E-03
4	3.1E+00		38k		
5	4.0E-01		42k		
10	1.3E-02	7.2E-01	42k		
15		5.6E-01	42k		
20		4.4E-01	42k		
30		3.2E-01	42k		
40		2.7E-01	42k		
60		1.9E-01	42k		

November 15th, 9:20 start Acetone HP 2nd Generation Beta #4					
	ConvecTorr Gauge	Cold Cathode Gauge			Cold Cathode Gauge
Time Past	Pressure	Pressure	Pump Speed	Time Past	Pressure
(min)	(pascal)	(pascal)	(rpm)	(h)	(pascal)
1	2.1E+01		5k	3	2.6E-02
2	3.1E+01		14k	5	1.3E-02
3	5.8E+00		28k	23	7.2E-03
4	5.4E+00		38k		
5	5.2E+00		42k		
10	4.0E+00		42k		
15	1.4E+00	7.7E-01	42k		
20	6.2E-01	3.8E-01	42k		
30	4.3E-01	3.0E-01	42k		
40	2.8E-01	1.9E-01	42k		
60	1.5E-01	1.5E-01	42k		

November 15th, 10:42 start Aluminum Acetone HP 2nd Generation Beta #5					
	ConvecTorr Gauge	Cold Cathode Gauge			Cold Cathode Gauge
Time Past	Pressure	Pressure	Pump Speed	Time Past	Pressure
(min)	(pascal)	(pascal)	(rpm)	(h)	(pascal)
1	2.1E+01		5k	4.75	4.2E-02
2	1.1E+01		14k	6	3.5E-02
3			28k	20.5	1.3E-02
4	7.4E+00		38k	22.25	1.2E-02
5	6.3E+00		42k		
10	4.0E+00		42k		
15	2.6E+00		42k		
20	2.0E+00	9.8E-01	42k		
30	1.3E+00	6.9E-01	42k		
40	9.8E-01	5.0E-01	42k		
60	6.3E-01	3.3E-01	42k		

November 17th, 10:53 start Aluminum Acetone TS 2nd Generation Beta #6					
	ConvecTorr Gauge	Cold Cathode Gauge			Cold Cathode Gauge
Time Past	Pressure	Pressure	Pump Speed	Time Past	Pressure
(min)	(pascal)	(pascal)	(rpm)	(h)	(pascal)
1	2.9E+01		5k	21	2.1E-02
2			14k	22	2.0E-02
3			28k		
4	7.5E+00		38k		
5	6.6E+00		42k		
12	3.2E+00	7.9E-01	42k		
15	2.7E+00	6.9E-01	42k		
20	2.0E+00	5.9E-01	42k		
30	1.4E+00	4.3E-01	42k		
40	1.0E+00	3.0E-01	42k		
60	6.7E-01	1.7E-01	42k		

Appendix S: Experimental Density and Charging Data

Density calculation of Methanol

Volume [ml]	Mass [g]	Density [kg/m^3]
1	0.720	720.0
2	1.486	743.0
3	2.281	760.3
4	3.042	760.5
5	3.857	771.4
6	4.601	766.8
7	5.403	771.9
8	6.176	772.0
9	6.961	773.4
10	7.752	775.2
Average:		**761.5**
Median:		**769.1**

Copper Heat Pipe Filled with Methanol Beta #1

Actual Fill

	Mass [g]	Volume [ml]
Ideal Charge		6.08
Fill Charge	8.17	10.73
Actual Charge	5.89	7.73
Filling Delta	2.29	3.00
Over fill %		27.1%

Heat Pipe Losses

Best	4.444
Average	4.66
Worst	4.996

Heat Pipe Filling Mass Determination

Charge [ml]	Charge [g]	Losses Var [ml]	Loss Var [g]	Total Fill Req [ml]	Total Fill Req[g]	Subtract Best	Subtract average	Subtract Worst
5.53	4.211	4.444	3.384	9.974	7.595	5.53	5.314	4.978
5.53	4.211	4.66	3.548	10.19	7.759	5.746	5.53	5.194
5.53	4.211	4.996	3.804	10.526	8.015	6.082	5.866	5.53
6.08	4.630	4.419	3.365	10.499	7.995	6.055	5.839	5.503
6.08	4.630	4.633	3.528	10.713	8.157	6.269	6.053	5.717
6.08	4.630	4.967	3.782	11.047	8.412	6.603	6.387	6.051
6.64	5.056	4.419	3.365	11.059	8.421	6.615	6.399	6.063
6.64	5.056	4.633	3.528	11.273	8.584	6.829	6.613	6.277
6.64	5.056	4.967	3.782	11.607	8.838	7.163	6.947	6.611

Copper Thermosyphon Filled with Methanol Beta #2

Density calculation of Methanol

Volume [ml]	Mass [g]	Density [kg/m^3]
1	0.753	753.0
2	1.528	764.0
3	2.269	756.3
4	3.092	773.0
5	3.836	767.2
6	4.643	773.8
7	5.431	775.9
8	6.209	776.1
9	7.020	780.0
10	7.819	781.9
Average:		**770.1**
Median:		**773.4**

Actual Fill

	Mass [g]	Volume [ml]
Ideal Charge		20.00
Fill Charge	19.45	25.25
Actual Charge	15.26	19.81
Filling Delta	4.19	5.44
Over fill %		35.8%

Thermocouple Filling Loses

Best	4.816
Average	5.042
Worst	5.269

Charge [ml]	Charge [g]	Losses Var [ml]	Loss Var [g]	Total Fill Req [ml]	Total Fill Req[g]	Subtract Best	Subtract average	Subtract Worst
20	15.402	4.816	3.709	24.816	19.111	20	19.774	19.547
20	15.402	5.042	3.883	25.042	19.285	20.226	20	19.773
20	15.402	5.269	4.058	25.269	19.460	20.453	20.227	20
22	16.943	4.816	3.709	26.816	20.652	22	21.774	21.547
22	16.943	5.042	3.883	27.042	20.826	22.226	22	21.773
22	16.943	5.269	4.058	27.269	21.001	22.453	22.227	22
24	18.483	4.816	3.709	28.816	22.192	24	23.774	23.547
24	18.483	5.042	3.883	29.042	22.366	24.226	24	23.773
24	18.483	5.269	4.058	29.269	22.541	24.453	24.227	24

Copper Heat Pipe Filled with Methanol 2nd Generation Beta #1

Density calculation of Methanol

Volume [ml]	Mass [g]	Density [kg/m^3]
1	0.682	682
2	1.438	719
3	2.251	750.3333333
4	3.048	762
5	3.842	768.4
6	4.616	769.3333333
7	5.435	776.4285714
8	6.236	779.5
9	7.030	781.1111111
10	7.847	784.7
Average:		**757.2806349**
Median:		**768.8666667**

Actual Fill

	Mass [g]	Volume [ml]
Ideal Charge		6.06
Fill Charge	7.25	9.57
Actual Charge	3.07	4.06
Filling Delta	4.17	5.51
Over fill %		-33.1%

Heat Pipe Filling Losses

Best	4.444
Average	4.66
Worst	4.996

Heat Pipe Filling Mass Determination

Charge [ml]	Charge [g]	Losses Var [ml]	Loss Var [g]	Total Fill Req [ml]	Total Fill Req[g]	Subtract Best	Subtract average	Subtract Worst
5.511	4.173	3	2.272	8.511	6.445	5.511	4.067	3.851
5.511	4.173	4.444	3.365	9.955	7.539	6.955	5.511	5.295
5.511	4.173	4.66	3.529	10.171	7.702	7.171	5.727	5.511
6.062	4.591	3	2.272	9.062	6.862	6.062	4.618	4.402
6.062	4.591	3.5	2.650	9.562	7.241	6.562	5.118	4.902
6.062	4.591	4.444	3.365	10.506	7.956	7.506	6.062	5.846
6.062	4.591	4.66	3.529	10.722	8.120	7.722	6.278	6.062
6.613	5.008	3	2.272	9.613	7.280	6.613	5.169	4.953
6.613	5.008	4.444	3.365	11.057	8.373	8.057	6.613	6.397
6.613	5.008	4.66	3.529	11.273	8.537	8.273	6.829	6.613

Copper Thermosyphon Filled with Methanol 2nd Generation Beta #2

Density calculation of Methanol

Volume [ml]	Mass [g]	Density [kg/m^3]
1	0.692	692.0
2	1.560	780.0
3	2.333	777.7
4	3.095	773.8
5	3.899	779.8
6	4.704	784.0
7	5.494	784.9
8	6.303	787.9
9	7.114	790.4
10	7.908	790.8
Average:		**774.1**
Median:		**782.0**

Actual Fill

	Mass [g]	Volume [ml]
Ideal Charge		18.10
Fill Charge	19.04	24.60
Actual Charge	13.24	17.10
Filling Delta	5.80	7.50
Over fill %		34.3%

Thermosyphon Filling Loses

Best	4.816
Average	5.042
Worst	5.269

Thermosyphon Filling Mass Determination

Charge [ml]	Charge [g]	Losses Var [ml]	Loss Var [g]	Total Fill Req [ml]	Total Fill Req[g]	Subtract Best	Subtract average	Subtract Worst
18.23	14.112	4.816	3.728	23.046	17.840	18.23	18.004	17.777
18.23	14.112	5.042	3.903	23.272	18.015	18.456	18.23	18.003
18.23	14.112	5.269	4.079	23.499	18.191	18.683	18.457	18.23
19.1	14.786	5.5	4.258	24.6	19.043	19.784	19.558	19.331
20.05	15.521	4.816	3.728	24.866	19.249	20.05	19.824	19.597
20.05	15.521	5.042	3.903	25.092	19.424	20.276	20.05	19.823
20.05	15.521	5.269	4.079	25.319	19.600	20.503	20.277	20.05
21.88	16.938	4.816	3.728	26.696	20.666	21.88	21.654	21.427
21.88	16.938	5.042	3.903	26.922	20.841	22.106	21.88	21.653
21.88	16.938	5.269	4.079	27.149	21.017	22.333	22.107	21.88

Copper Heat Pipe Filled with Methanol 2nd Generation Beta #3

Density calculation of Methanol

Volume [ml]	Mass [g]	Density [kg/m^3]
1	0.709	709.0
2	1.504	752.0
3	2.342	780.7
4	3.130	782.5
5	3.917	783.4
6	4.733	788.8
7	5.513	787.6
8	6.323	790.4
9	7.142	793.6
10	7.956	795.6
Average:		**776.4**
Median:		**785.5**

	Actual Fill Mass [g]	Volume [ml]
Ideal Charge		6.06
Fill Charge	8.98	11.57
Actual Charge	4.77	6.14
Filling Delta	4.21	5.43
Over fill %		1.3%

Heat Pipe Filling Losses	
Best	4.444
Average	4.66
Worst	5.5

Heat Pipe Filling Mass Determination

Charge [ml]	Charge [g]	Losses Var [ml]	Loss Var [g]	Total Fill Req [ml]	Total Fill Req[g]	Subtract Best	Subtract average	Subtract Worst
5.511	4.278	4.444	3.450	9.955	7.729	5.511	5.295	4.455
5.511	4.278	4.66	3.618	10.171	7.896	5.727	5.511	4.671
5.511	4.278	5.5	4.270	11.011	8.548	6.567	6.351	5.511
6.062	4.706	4.444	3.450	10.506	8.156	6.062	5.846	5.006
6.062	4.706	4.66	3.618	10.722	8.324	6.278	6.062	5.222
6.062	4.706	5.5	4.270	11.562	8.976	7.118	6.902	6.062
6.062	4.706	6	4.658	12.062	9.364	7.618	7.402	6.562
6.613	5.134	4.444	3.450	11.057	8.584	6.613	6.397	5.557
6.613	5.134	4.66	3.618	11.273	8.752	6.829	6.613	5.773
6.613	5.134	5.5	4.270	12.113	9.404	7.669	7.453	6.613

Copper Heat Pipe Filled with Acetone 2nd Generation Beta #4

Density calculation of Acetone

Volume [ml]	Mass [g]	Density [kg/m^3]
1	0.685	
2	1.528	764.0
3	2.306	768.7
4	3.115	778.8
5	3.912	782.4
6	4.701	783.5
7	5.520	788.6
8	6.312	789.0
9	7.128	792.0
10	7.924	792.4
Average:		**782.1**
Median:		**783.5**

	Actual Fill Mass [g]	Volume [ml]
Ideal Charge		6.06
Fill Charge	9.05	11.57
Actual Charge	4.95	6.33
Filling Delta	4.10	5.24
Over fill %		4.4%

Heat Pipe Filling Losses

Best	4.444
Average	4.66
Worst	5.5

Heat Pipe Filling Mass Determination

Charge [ml]	Charge [g]	Losses Var [ml]	Loss Var [g]	Total Fill Req [ml]	Total Fill Req[g]	Subtract Best	Subtract average	Subtract Worst
5.511	4.310	4.444	3.476	9.955	7.786	5.511	5.295	4.455
5.511	4.310	4.66	3.645	10.171	7.955	5.727	5.511	4.671
5.511	4.310	5.5	4.302	11.011	8.612	6.567	6.351	5.511
6.062	4.741	4.444	3.476	10.506	8.217	6.062	5.846	5.006
6.062	4.741	4.66	3.645	10.722	8.386	6.278	6.062	5.222
6.062	4.741	5.5	4.302	11.562	9.043	7.118	6.902	6.062
6.613	5.172	4.444	3.476	11.057	8.648	6.613	6.397	5.557
6.613	5.172	4.66	3.645	11.273	8.817	6.829	6.613	5.773
6.613	5.172	5.5	4.302	12.113	9.474	7.669	7.453	6.613

Aluminum Heat Pipe Filled with Acetone 2nd Generation Beta #5

Density calculation of Acetone

Volume [ml]	Mass [g]	Density [kg/m^3]
1	0.726	726.0
2	1.488	744.0
3	2.307	769.0
4	3.114	778.5
5	3.904	780.8
6	4.691	781.8
7	5.490	784.3
8	6.282	785.3
9	7.096	788.4
10	7.890	789.0
Average:		**772.7**
Median:		**781.3**

	Actual Fill Mass [g]	Volume [ml]
Ideal Charge		6.06
Fill Charge	8.88	11.50
Actual Charge	4.21	5.44
Filling Delta	4.68	6.05
Over fill %		-10.2%

Heat Pipe Filling Losses	
Best	5.24
Average	5.43
Worst	5.5

Heat Pipe Filling Mass Determination

Charge [ml]	Charge [g]	Losses Var [ml]	Loss Var [g]	Total Fill Req [ml]	Total Fill Req[g]	Subtract Best	Subtract average	Subtract Worst
5.511	4.258	5.24	4.049	10.751	8.307	5.511	5.321	5.251
5.511	4.258	5.43	4.196	10.941	8.454	5.701	5.511	5.441
5.511	4.258	5.5	4.250	11.011	8.508	5.771	5.581	5.511
6.062	4.684	5.24	4.049	11.302	8.733	6.062	5.872	5.802
6.062	4.684	5.43	4.196	11.492	8.880	6.252	6.062	5.992
6.062	4.684	5.5	4.250	11.562	8.934	6.322	6.132	6.062
6.613	5.110	5.24	4.049	11.853	9.159	6.613	6.423	6.353
6.613	5.110	5.43	4.196	12.043	9.306	6.803	6.613	6.543
6.613	5.110	5.5	4.250	12.113	9.360	6.873	6.683	6.613

Aluminum Thermosyphon Filled with Acetone 2nd Generation Beta #6

Density calculation of Methanol

Volume [ml]	Mass [g]	Density [kg/m^3]
1	0.714	714.0
2	1.500	750.0
3	2.299	766.3
4	3.089	772.3
5	3.893	778.6
6	4.694	782.3
7	5.527	789.6
8	6.309	788.6
9	7.106	789.6
10	7.893	789.3
Average:		**772.1**
Median:		**780.5**

Actual Fill

	Mass [g]	Volume [ml]
Ideal Charge		18.10
Fill Charge	19.87	25.73
Actual Charge	14.98	19.40
Filling Delta	4.89	6.33
Over fill %		39.0%

Thermosyphon Filling Loses

Best	5.5
Average	6.05
Worst	7.5

Thermosyphon Filling Mass Determination

Charge [ml]	Charge [g]	Losses Var [ml]	Loss Var [g]	Total Fill Req [ml]	Total Fill Req[g]	Subtract Best	Subtract average	Subtract Worst
18.23	14.075	5.5	4.246	23.73	18.321	18.23	17.68	16.23
18.23	14.075	6.05	4.671	24.28	18.746	18.78	18.23	16.78
18.23	14.075	7.5	5.790	25.73	19.865	20.23	19.68	18.23
19.1	14.746	6.05	4.671	25.15	19.417	19.65	19.1	17.65
20.05	15.480	5.5	4.246	25.55	19.726	20.05	19.5	18.05
20.05	15.480	6.05	4.671	26.1	20.151	20.6	20.05	18.6
20.05	15.480	7.5	5.790	27.55	21.270	22.05	21.5	20.05
21.88	16.893	5.5	4.246	27.38	21.139	21.88	21.33	19.88
21.88	16.893	6.05	4.671	27.93	21.564	22.43	21.88	20.43
21.88	16.893	7.5	5.790	29.38	22.683	23.88	23.33	21.88

Appendix T: Experimental Heat Transfer Testing

HP1

R copper methanol	0.8663
R copper Methanol (Conduction)	0.6618

Heat Applied [W]	TE Avg [K]	TC Avg [K]	R Exp [K/W]
1.98			0.0
4.03			0.0
6.08			0.0
7.74			0.0
10.29	243.36	195.41	4.7
20.01	282.54	195.32	4.4
30.24	311.96	195.07	3.9
35.1	323.56	194.96	3.7
37.6	332.77	195.15	3.7
40.47	330.64	195.04	3.4

HP3

R copper methanol	0.8663
R copper Methanol (Conduction)	0.6618

Heat Applied [W]	TE Avg [K]	TC Avg [K]	R Exp [K/W]
1.98	212.6	194.98	8.9
4.03	220.53	194.97	6.3
6.08	228.16	194.97	5.5
7.74	242.18	194.79	6.1
10.29	247.36	195.26	5.1
15.6	265.49	195.2	4.5
20.01	280.25	195.29	4.2
30.24	312.17	195.37	3.9
35.1	318.16	195.31	3.5
40.74	321.31	195.39	3.1
51.23	326.44	195.29	2.6
60.69	331.47	195.3	2.2

HP4

R copper actone	1.0947
R copper acetone (Conduction)	0.7899

Heat Applied [W]	TE Avg [K]	TC Avg [K]	R Exp [K/W]
1.98	218.21	195.31	11.6
4.03	221.2	195.41	6.4
6.08	227.77	195.33	5.3
7.74	243.86	195.25	6.3
10.29	248.42	195.13	5.2
20.01	280.56	195.27	4.3
30.24	315.79	195.59	4.0
35.1	327.86	195.42	3.8
40.74	333	195.11	3.4
49.68	336.07	195.14	2.8
60.69	338.91	195.09	2.4

HP5

R aluminum actone	1.0526
R aluminum acetone (Conduction)	0.874

Heat Applied [W]	TE Avg [K]	TC Avg [K]	R Exp [K/W]
1.98	232.67	198.36	17.3
4.03	242.76	195.28	11.8
6.08	255.6	195.44	9.9
7.74	267.53	195.31	9.3
10.29	281.62	195.4	8.4
20.01	333.25	195.48	6.9
30.24	336.96	195.33	4.7
35.1	338.12	195.34	4.1
40.74	337.83	195.41	3.5
49.68	341.7	195.16	2.9
60.69	340.602	195.28	2.4

TS2

R copper methanol

R copper Methanol (Conduction)

Heat Applied [W]	TE Avg [K]	TC Avg [K]	R Exp [K/W]
1.98	215.04	195.21	10.0
4.03	221.72	195.2	6.6
6.08	229.12	195.22	5.6
7.74	235.57	195.2	5.2
10.29	245.78	195.168	4.9
20.01	270.69	195.25	3.8
30.24	273.78	195.28	2.6
35.1	274.56	195.23	2.3
40.74	275.27	195.22	2.0
51.23	276.52	195.3	1.6
60.69	278.25	195.31	1.4

TS6

R aluminum acetone

R copper acetone (Conduction)

Heat Applied [W]	TE Avg [K]	TC Avg [K]	R Exp [K/W]
1.98	223.2	195.22	14.1
4.03	243.03	195.14	11.9
6.08	252.03	195.26	9.3
7.74	260.22	195.12	8.4
10.29	270.62	195.08	7.3
20.01	316.47	195.21	6.1
30.24	306.19	195.32	3.7
35.1	306.92	195.33	3.2
40.74	308.06	195.02	2.8
51.23	309.79	194.97	2.2
60.69	311.36	195.02	1.9

Copper Rod

R copper rod (Conduction)

Heat Applied [W]	TE Avg [K]	TC Avg [K]	R Exp [K/W]
1.98	213.16	195.41	9.0
4.03	220.85	195.39	6.3
6.08	228.35	195.49	5.4
7.74	235.23	195.58	5.1
10.29	245.22	195.45	4.8
20.01	283.84	195.48	4.4
30.24	318.83	195.54	4.1
40.74	354.39	195.29	3.9
51.23	No Steady State		
60.69	No Steady State		

Copper Rod Second Test

R copper rod (Conduction)

Heat Applied [W]	TE Avg [K]	TC Avg [K]	R Exp [K/W]
10.29	244.42	195.41	4.8
20.01	281.76	195.34	4.3

HP3 Ice Water

R copper methanol	0.8663
R copper Methanol (Conduction)	0.6618

Heat Applied [W]	TE Avg [K]	TC Avg [K]	R Exp [K/W]
1.98	287.35	273.08	7.2
4.03	295.62	273.09	5.6
6.08	303.89	273.12	5.1
7.74	309.87	273.16	4.7
10.29	320.86	273.75	4.6
20.01	342.19	276.55	3.3
30.24	347.12	277.03	2.3
40.74	350.6	282.16	1.7
49.68	353.09	282.74	1.4
60.69	No Steady State		

TS2 Ice Water

R copper methanol	
R copper Methanol (Conduction)	

Heat Applied [W]	TE Avg [K]	TC Avg [K]	R Exp [K/W]
1.98	284.34	273.54	5.5
4.03	291.21	273.4	4.4
6.08	296.11	273.4	3.7
7.74	299.33	273.16	3.4
10.29	291.21	273.45	1.7
20.01	295.59	277.51	0.9
30.24	300.97	283.92	0.6
40.74	304.15	281.88	0.5
51.23	307.89	276.69	0.6
60.69	312.05	282.65	0.5

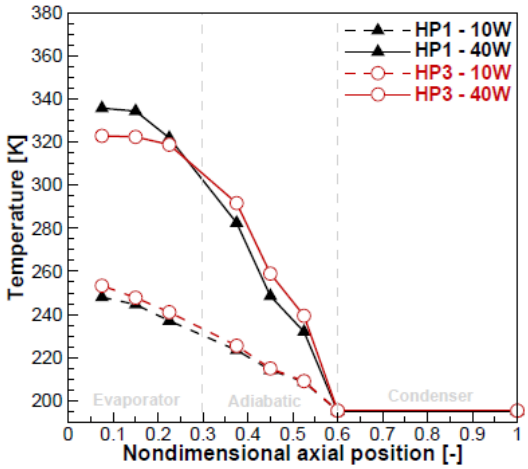

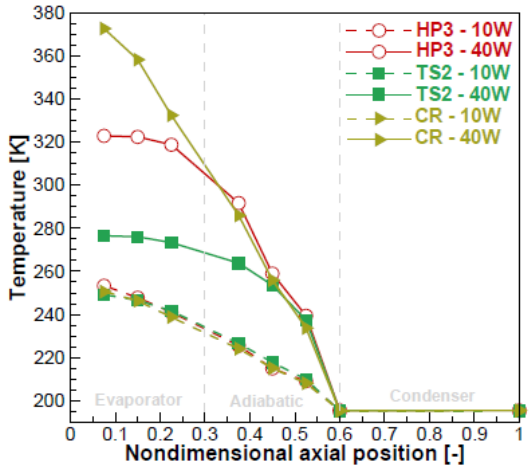

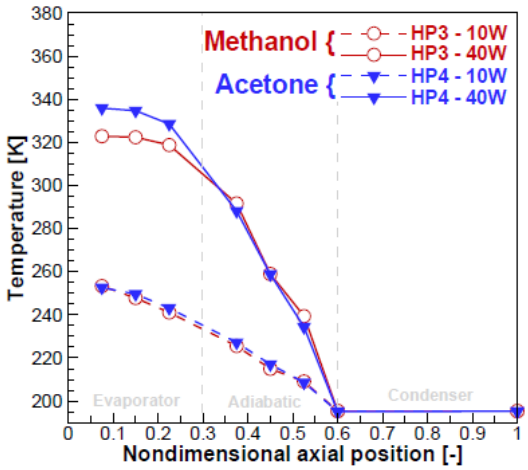

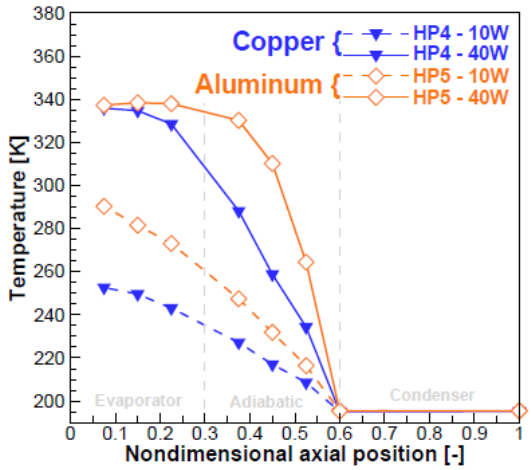

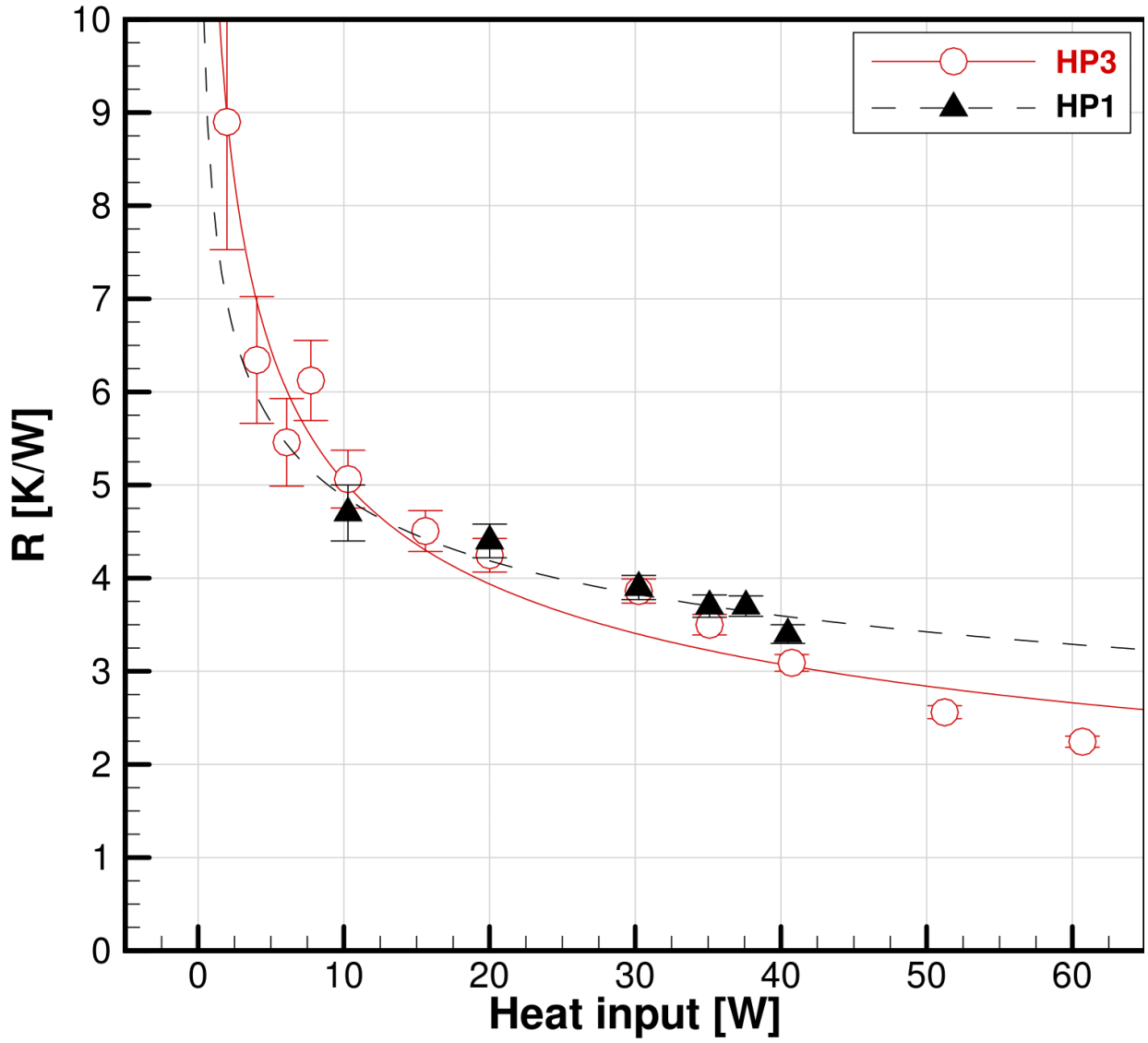

FIGURE 59: COMPARISON OF EXPERIMENTAL RESISTANCE VALUES BETWEEN COPPER AND METHANOL HP1 AND HP3, WITH DIFFERENT WORKING FLUID FILLING RATIOS.

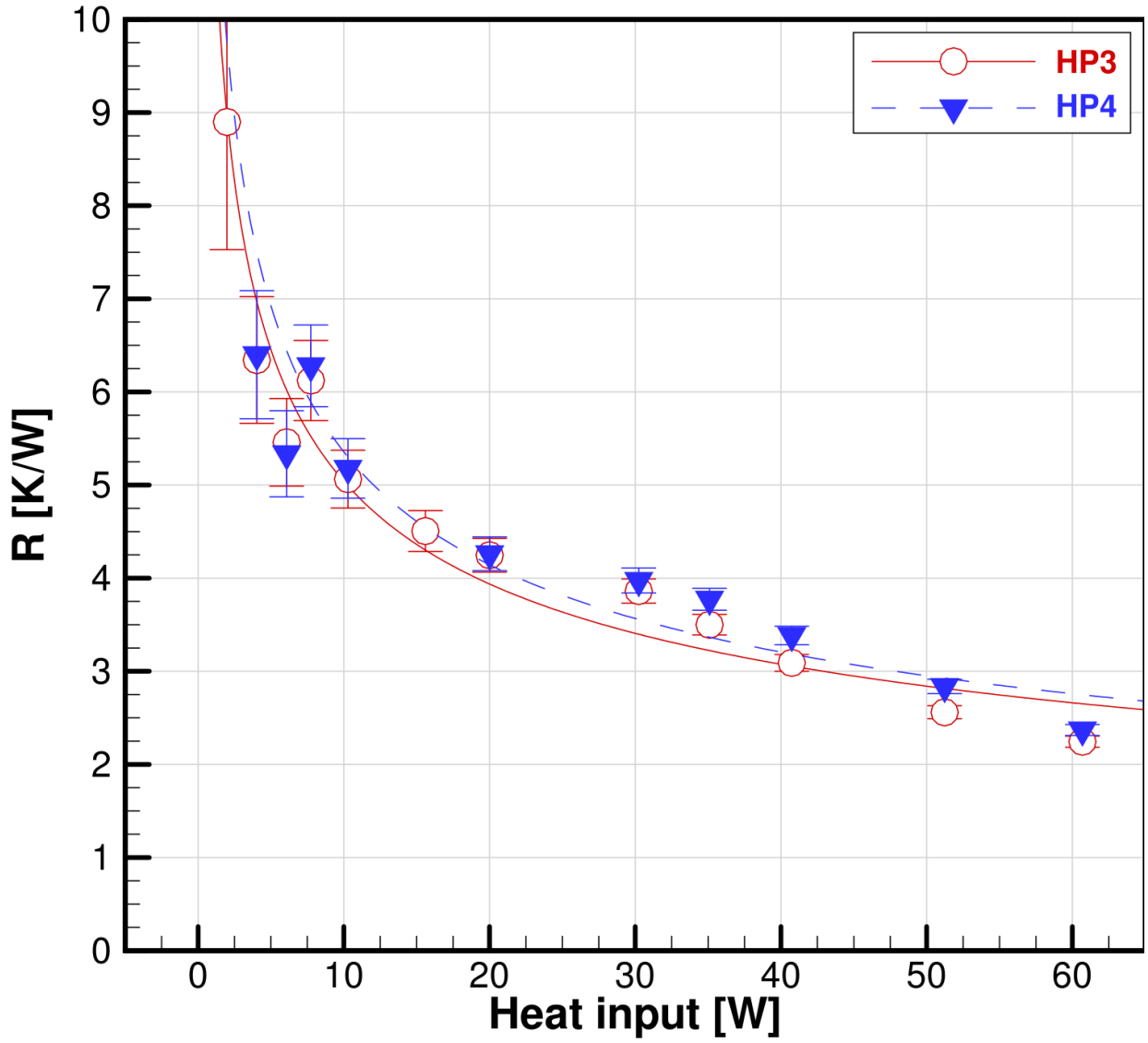

Figure 60: comparison of experimental resistance values between copper HP3 and HP4, with different working fluids. HP3 contains methanol and HP4 contains acetone.

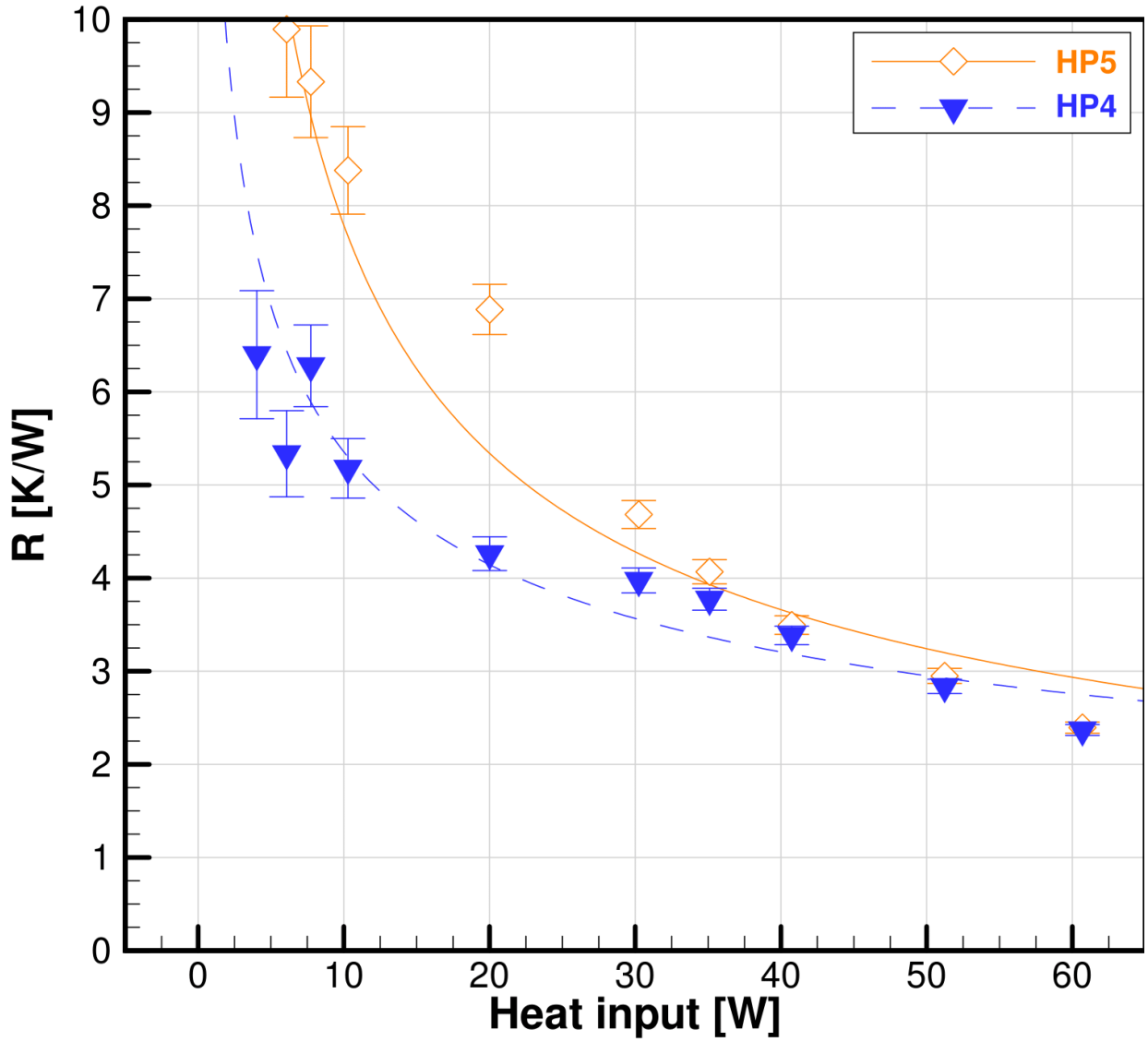

FIGURE 61: COMPARISON OF EXPERIMENTAL RESISTANCE VALUES BETWEEN HP4 AND HP5. BOTH CONTAIN ACETONE, HP4 HAS A COPPER SHELL AND HP5 AN ALUMINUM SHELL.

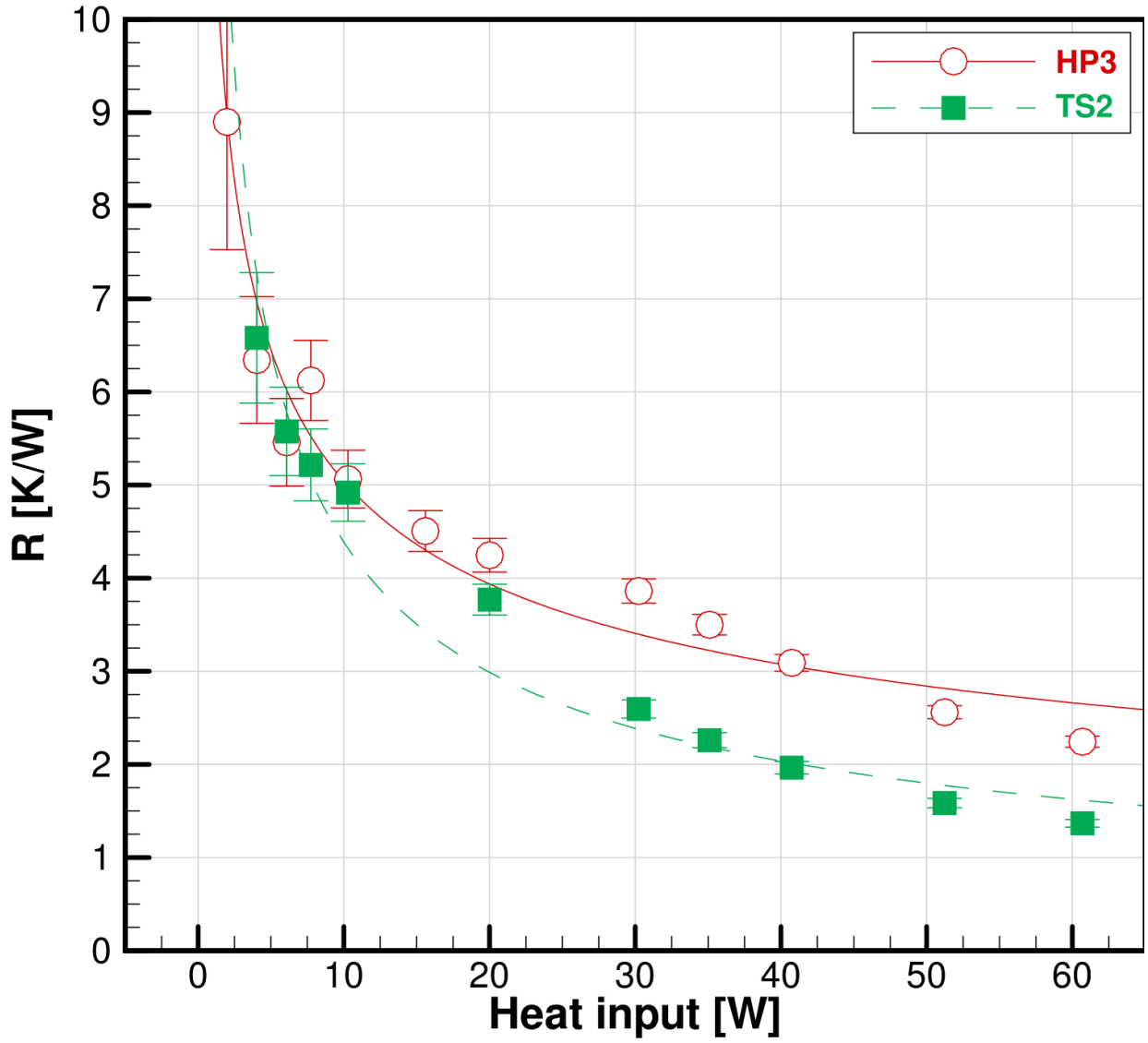

Figure 62: Comparison of experimental resistance values between TS2 and HP3. Both are made of copper with methanol as the working fluid, with different filling ratios.

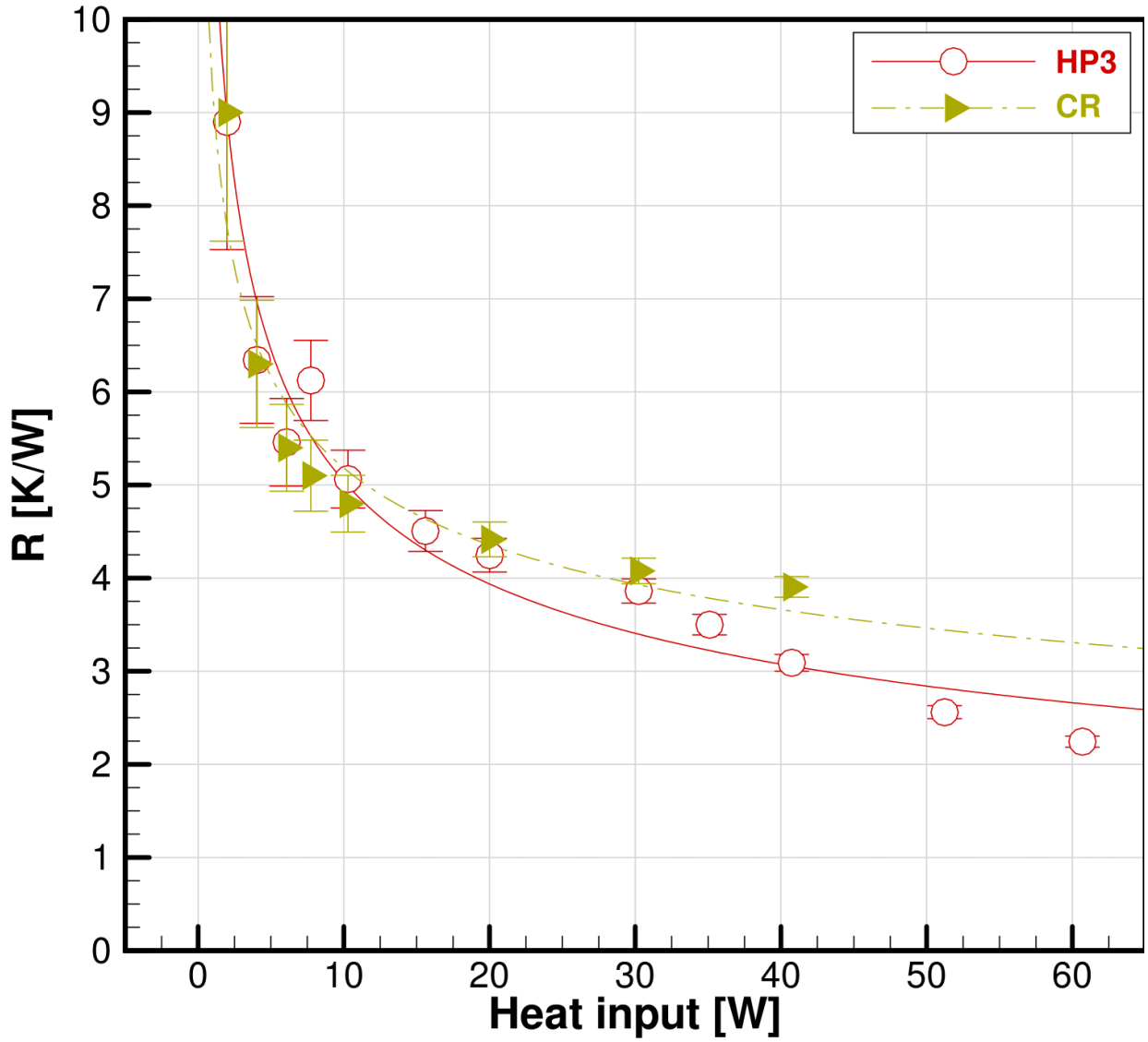

FIGURE 63: COMPARISON OF EXPERIMENTAL RESISTANCE VALUES BETWEEN AN INSULATED COPPER ROD AND HP3. THE HEAT SINK CONTAINS DRY ICE AND ACETONE AND HIGH HEAT LOADS ARE APPLIED.

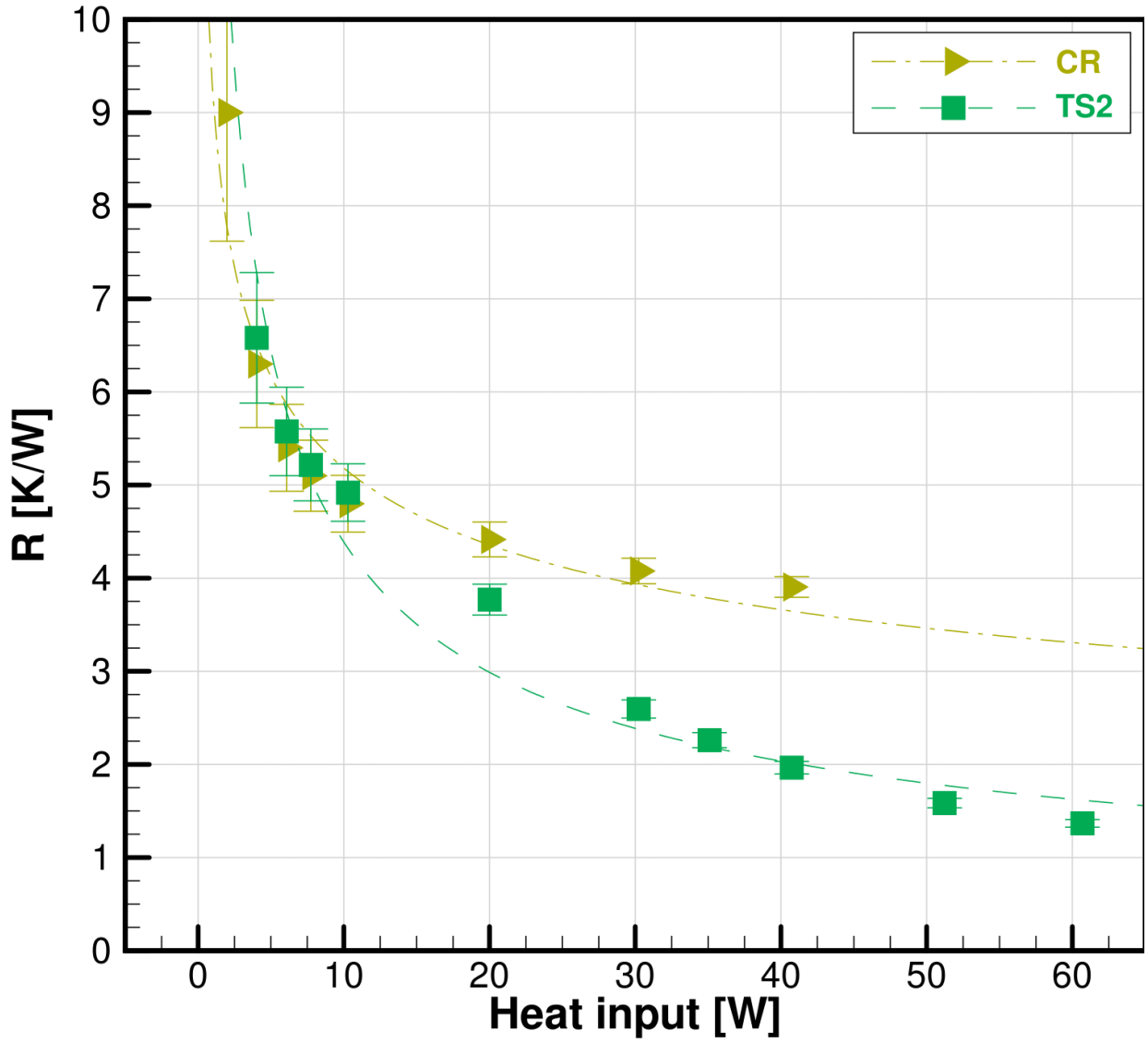

FIGURE 64: COMPARISON OF EXPERIMENTAL RESISTANCE VALUES BETWEEN AN INSULATED COPPER ROD AND TS2. THE HEAT SINK CONTAINS DRY ICE AND ACETONE AND HIGH HEAT LOADS ARE APPLIED.

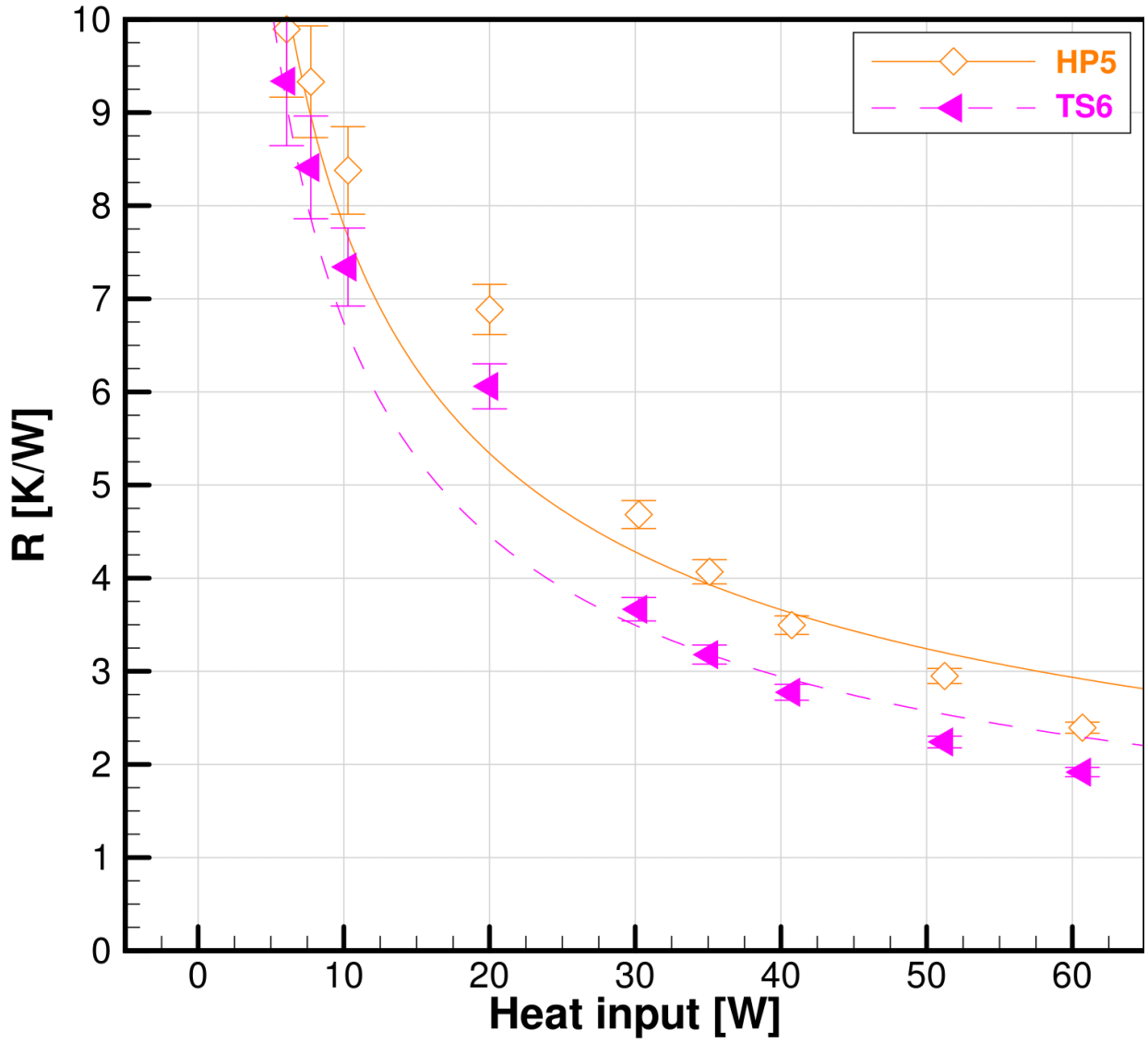

FIGURE 65: COMPARISON OF EXPERIMENTAL RESISTANCE VALUES BETWEEN TS6 AND HP5. BOTH ARE MADE OF ALUMINUM AND CONTAIN ACETONE, WITH DIFFERENT FILLING RATIOS.

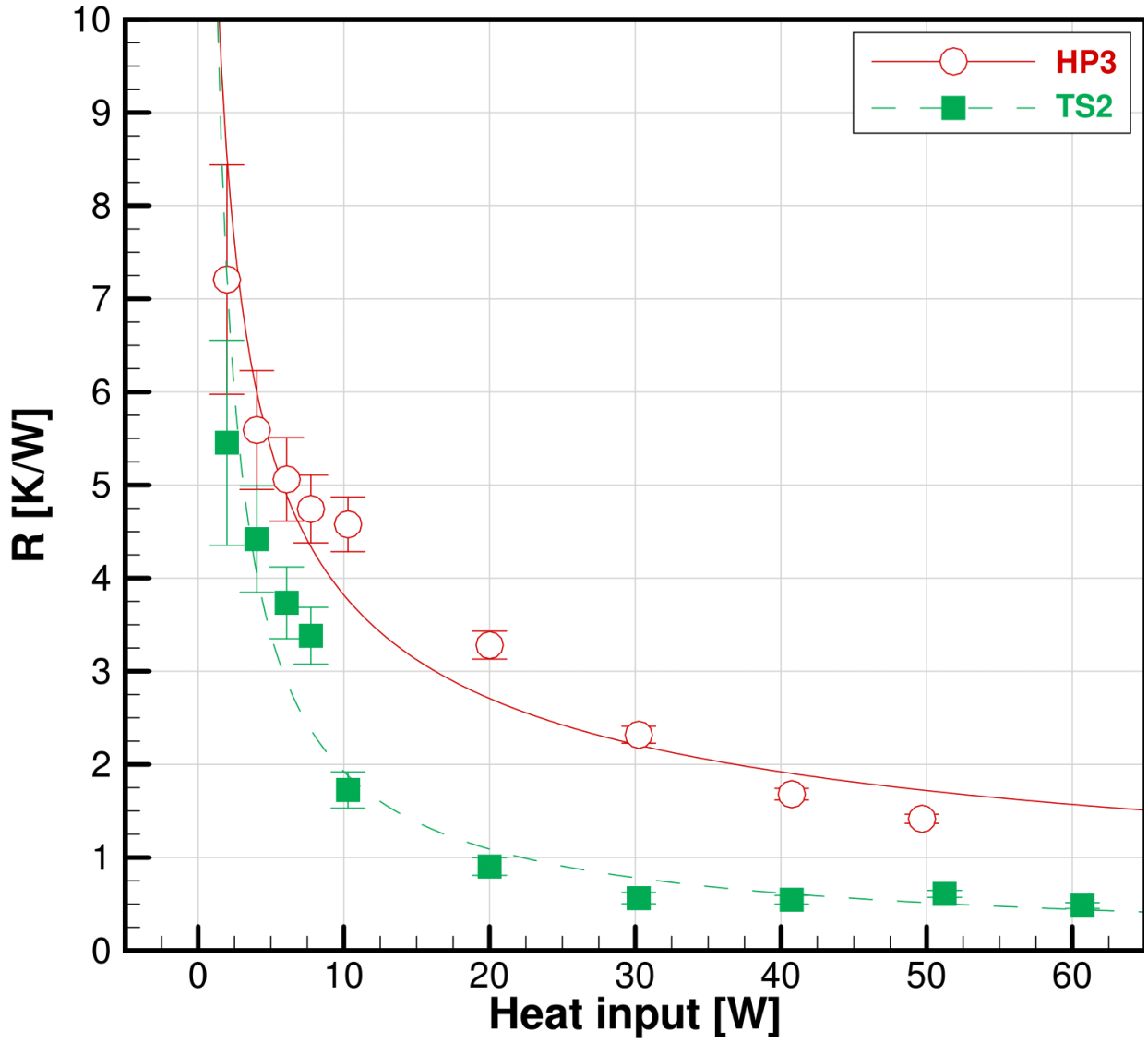

FIGURE 66: COMPARISON OF EXPERIMENTAL RESISTANCE VALUES BETWEEN HP3 AND TS2 WHEN TESTING WITH ICE WATER. BOTH ARE MADE OF COPPER AND CONTAIN METHANOL, WITH DIFFERENT FILLING RATIOS.

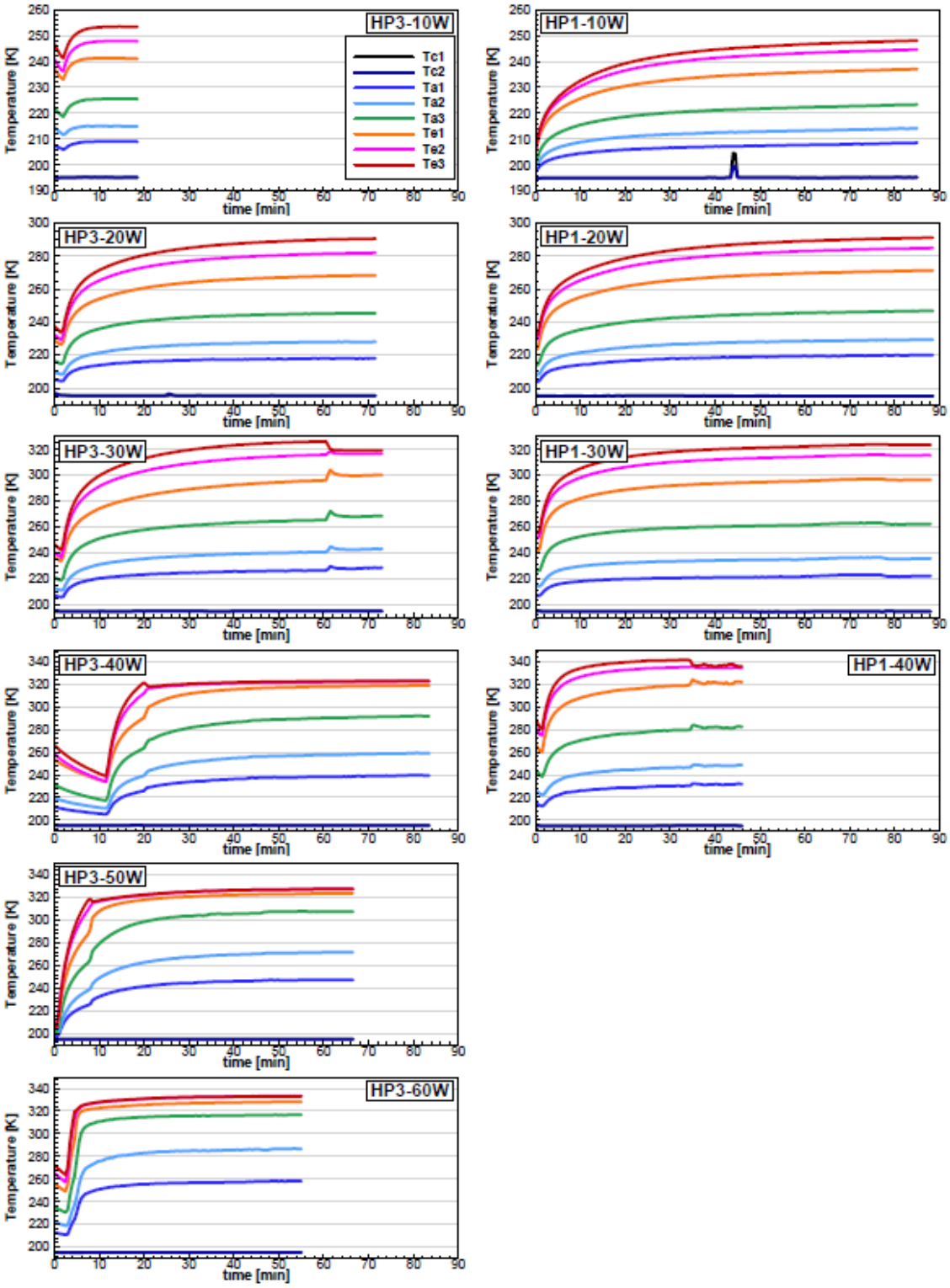

FIGURE 67: TRANSIENT THERMAL RESPONSE COMPARISON OF PERFORMANCE BETWEEN AN UNDERFILLED AND A PERFECTLY FILLED HEAT PIPE. HP1 IS UNDERFILLED. BOTH HEAT PIPES ARE MADE OF COPPER AND CONTAIN METHANOL. THE HEAT SINK CONTAINS DRY ICE AND ACETONE AND HIGH HEAT LOADS ARE APPLIED.

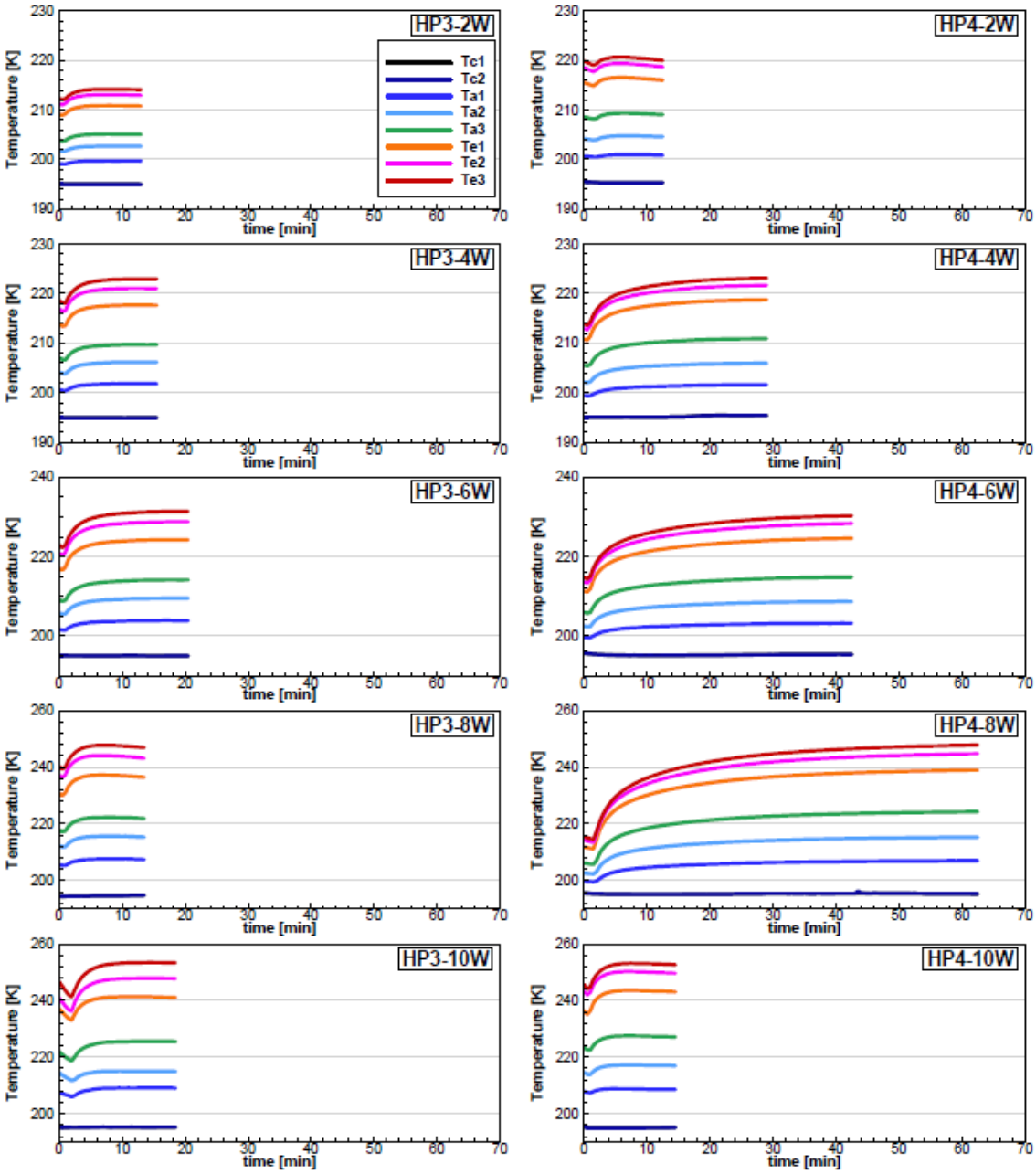

FIGURE 68: TRANSIENT THERMAL RESPONSE COMPARISON OF PERFORMANCE BETWEEN HEAT PIPES WITH WORKING FLUIDS, BOTH ARE ENCASED IN COPPER. HP3 CONTAINS METHANOL AND HP4 CONTAINS ACETONE AS THE WORKING FLUID. THE HEAT SINK CONTAINS DRY ICE AND ACETONE AND LOW HEAT LOADS ARE APPLIED.

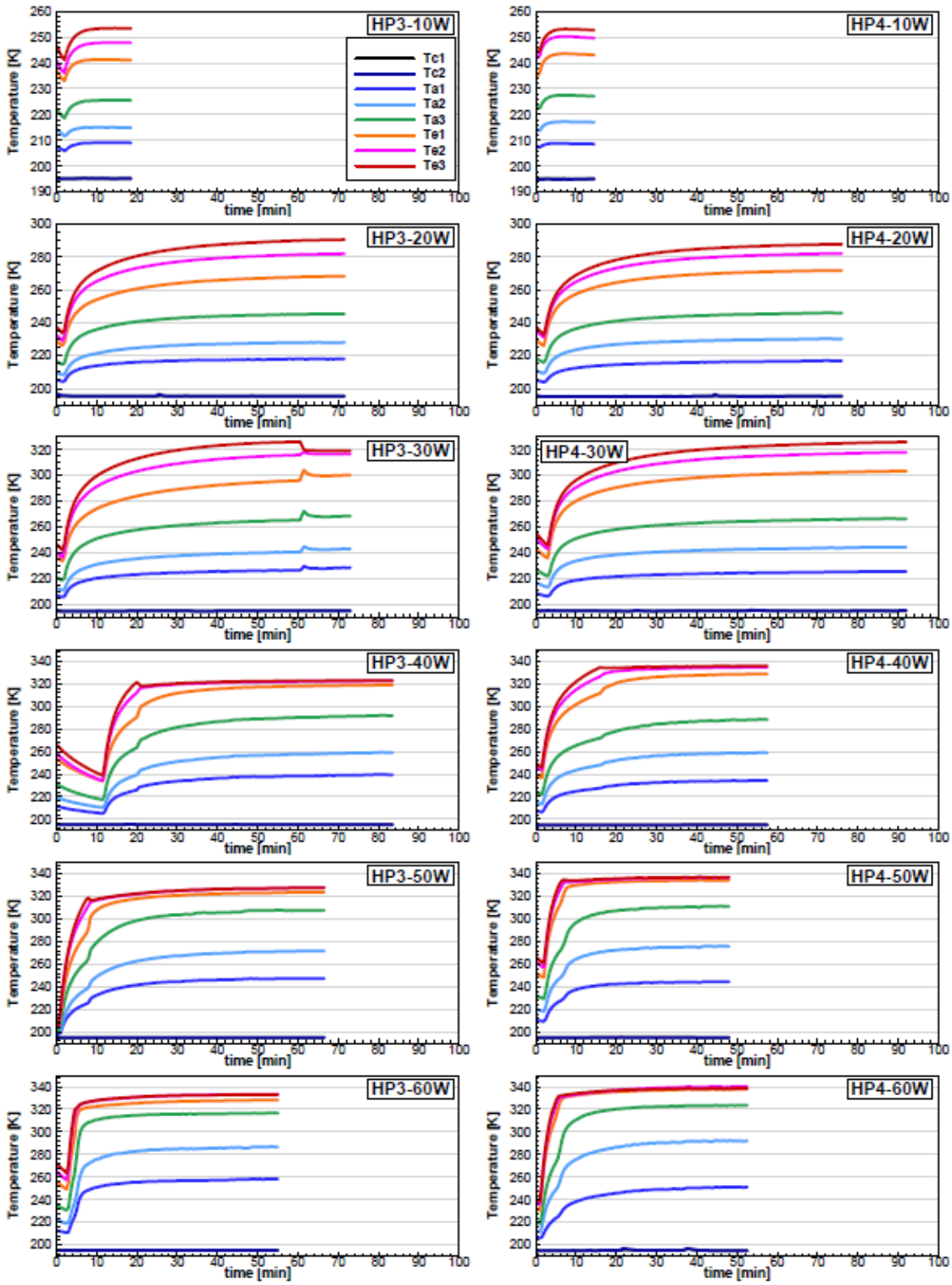

FIGURE 69: TRANSIENT THERMAL RESPONSE COMPARISON OF PERFORMANCE BETWEEN HEAT PIPES WITH WORKING FLUIDS, BOTH ARE ENCASED IN COPPER. HP3 CONTAINS METHANOL AND HP4 CONTAINS ACETONE AS THE WORKING FLUID. THE HEAT SINK CONTAINS DRY ICE AND ACETONE AND HIGH HEAT LOADS ARE APPLIED.

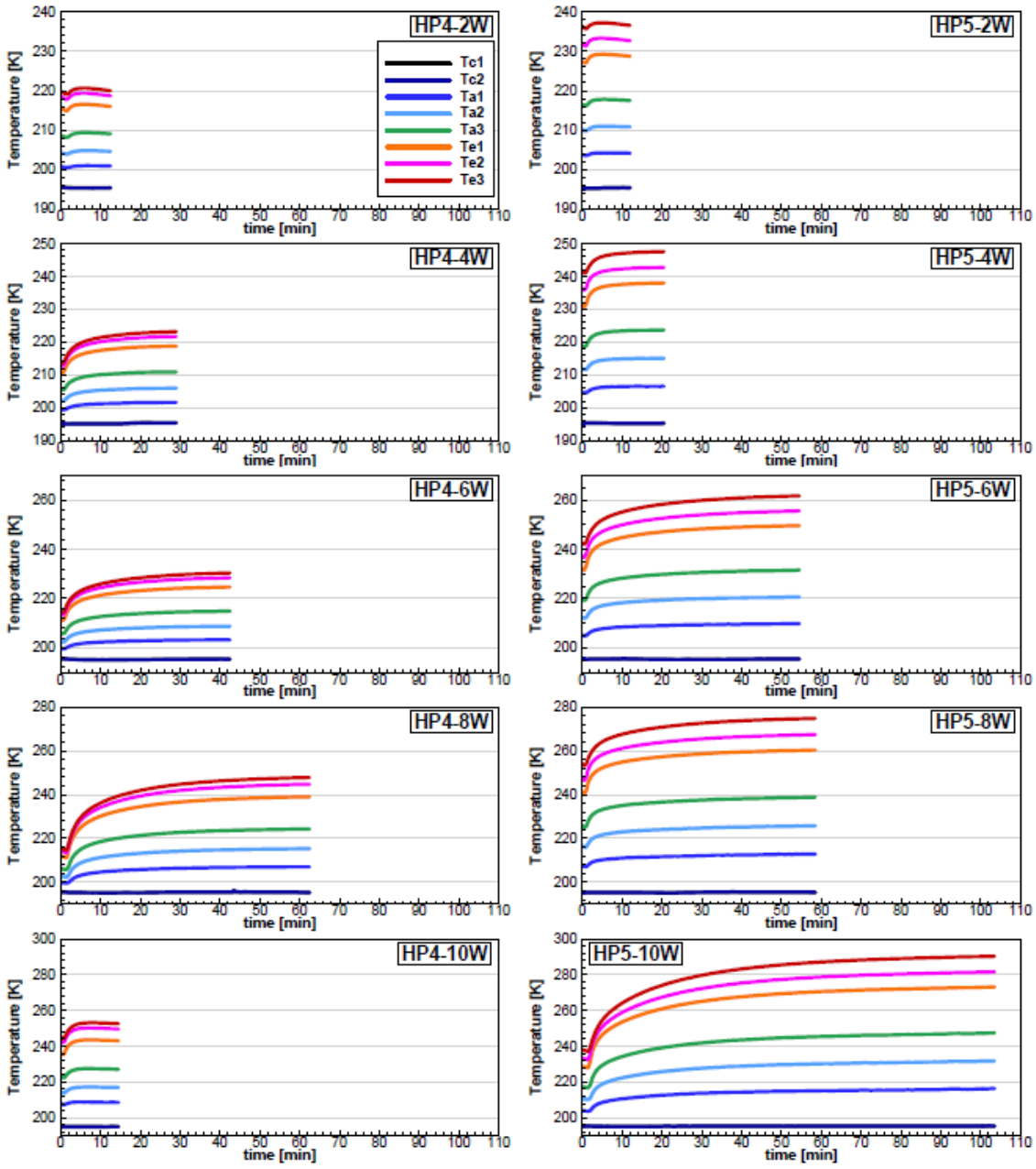

FIGURE 70: TRANSIENT THERMAL RESPONSE COMPARISON OF PERFORMANCE BETWEEN HEAT PIPES WITH DIFFERENT CASE MATERIALS. HP4 IS ENCASED IN COPPER AND HP5 IS ENCASED IN ALUMINUM. BOTH CONTAIN ACETONE AS THE WORKING FLUID. THE HEAT SINK CONTAINS DRY ICE AND ACETONE AND LOW HEAT LOADS ARE APPLIED.

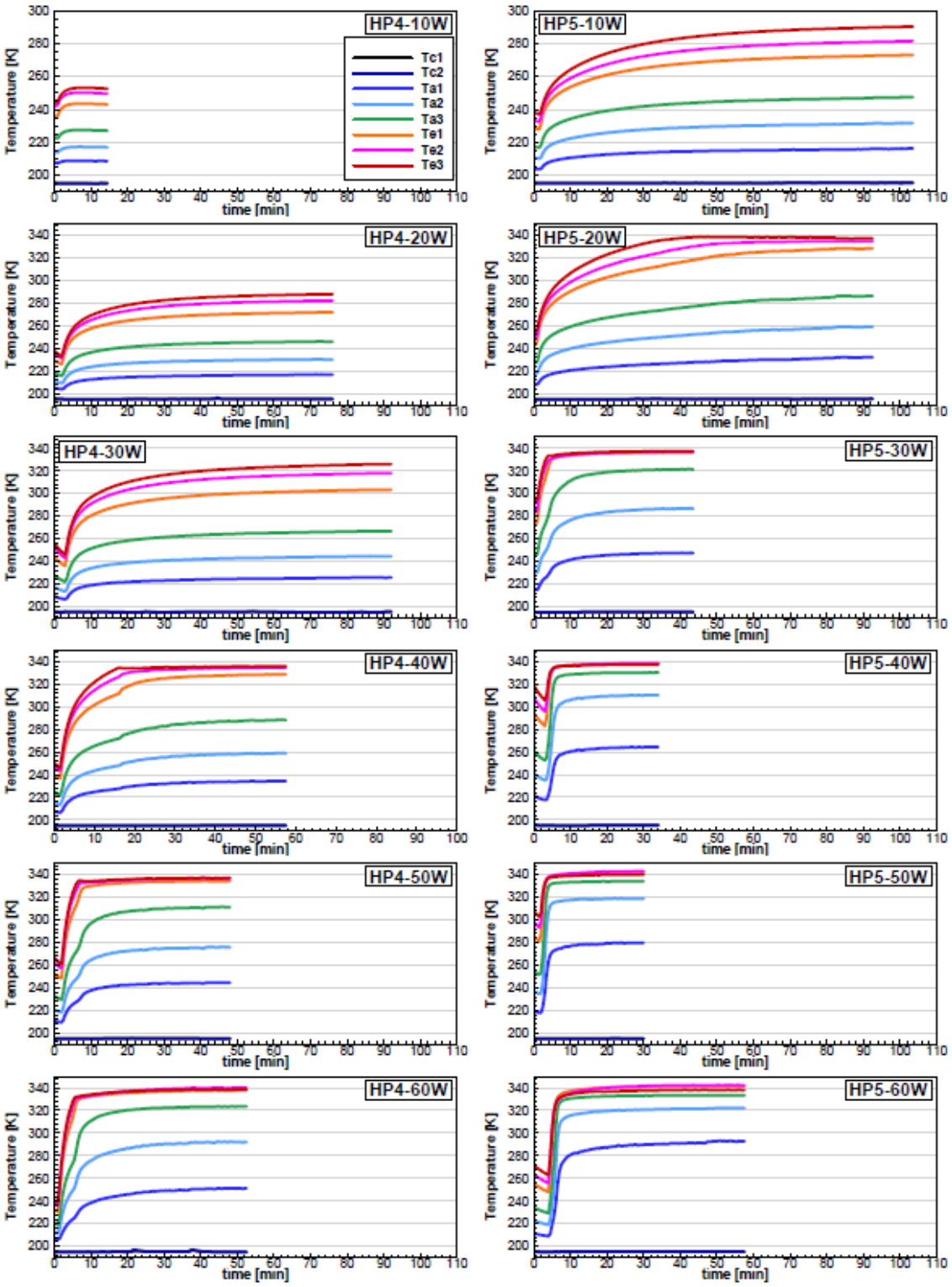

FIGURE 71: TRANSIENT THERMAL RESPONSE COMPARISON OF PERFORMANCE BETWEEN HEAT PIPES WITH DIFFERENT CASE MATERIALS. HP4 IS ENCASED IN COPPER AND HP5 IS ENCASED IN ALUMINUM. BOTH CONTAIN ACETONE AS THE WORKING FLUID. THE HEAT SINK CONTAINS DRY ICE AND ACETONE AND HIGH HEAT LOADS ARE APPLIED.

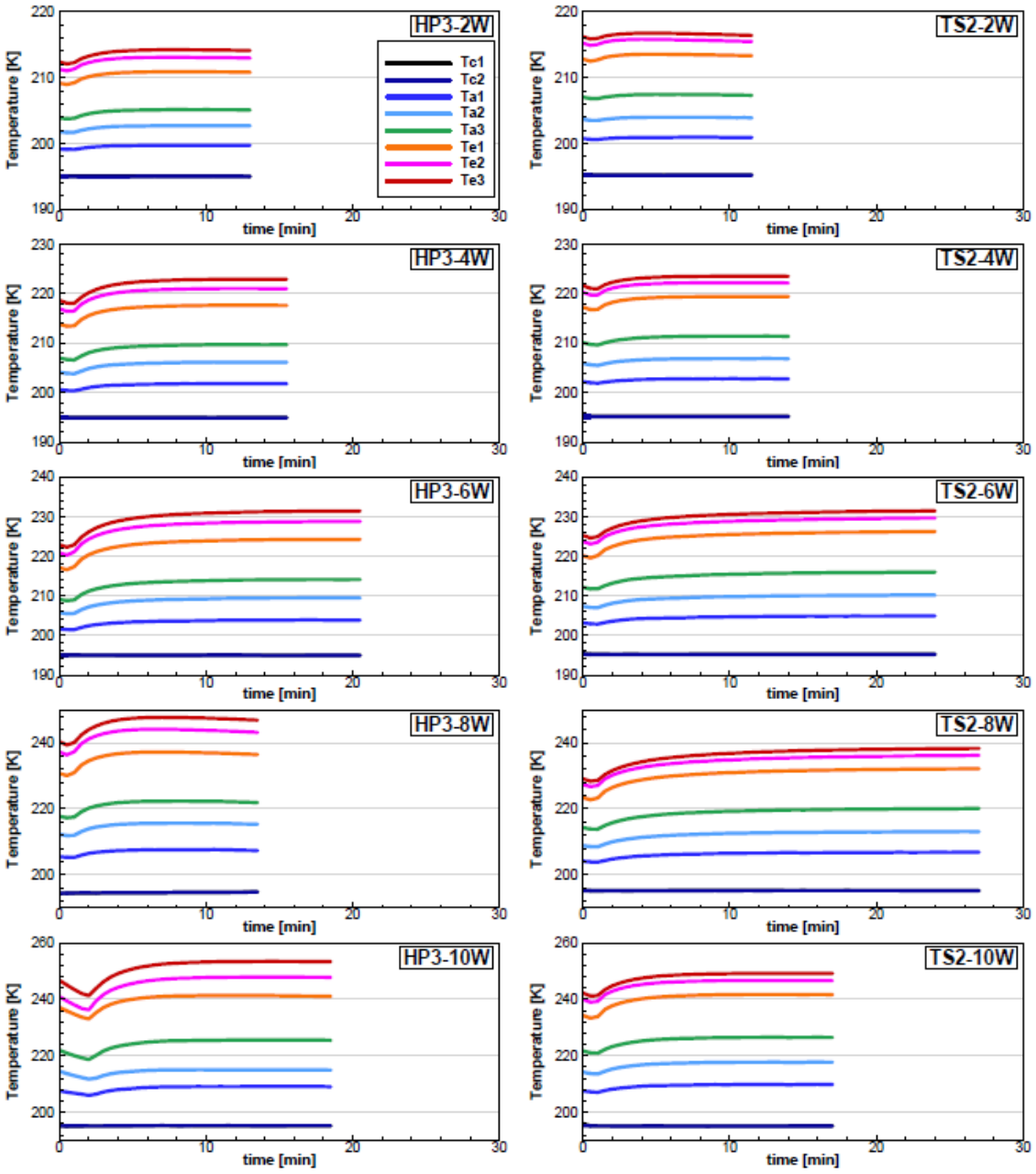

FIGURE 72: TRANSIENT THERMAL RESPONSE COMPARISON OF PERFORMANCE BETWEEN HEAT PIPE AND THERMOSYPHON IN A COPPER CASE WITH METHANOL AS THE WORKING FLUID. THE HEAT SINK CONTAINS DRY ICE AND ACETONE AND LOW HEAT LOADS ARE APPLIED.

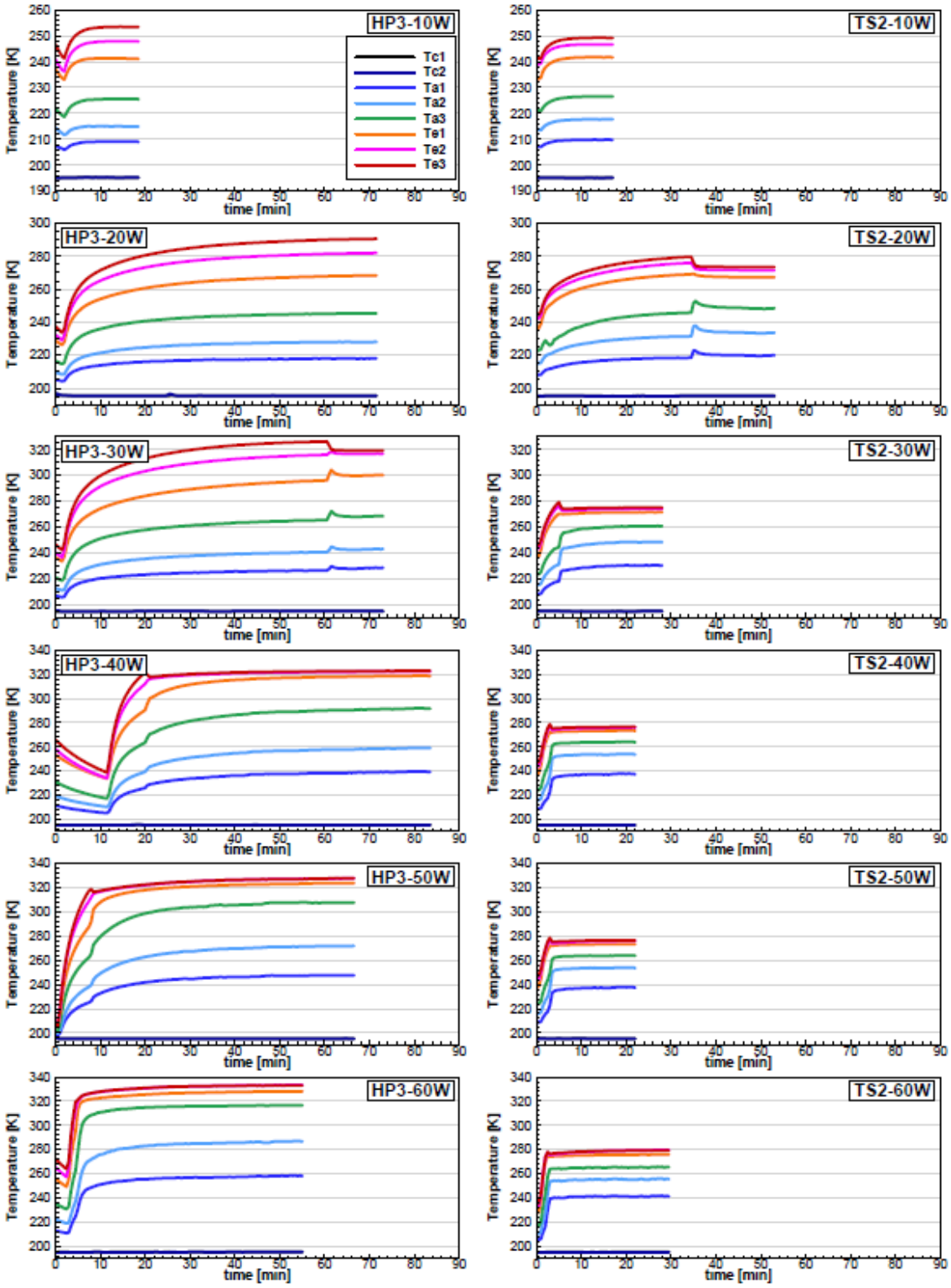

FIGURE 73: TRANSIENT THERMAL RESPONSE COMPARISON OF PERFORMANCE BETWEEN HEAT PIPE AND THERMOSYPHON IN A COPPER CASE WITH METHANOL AS THE WORKING FLUID. THE HEAT SINK CONTAINS DRY ICE AND ACETONE AND HIGH HEAT LOADS ARE APPLIED.

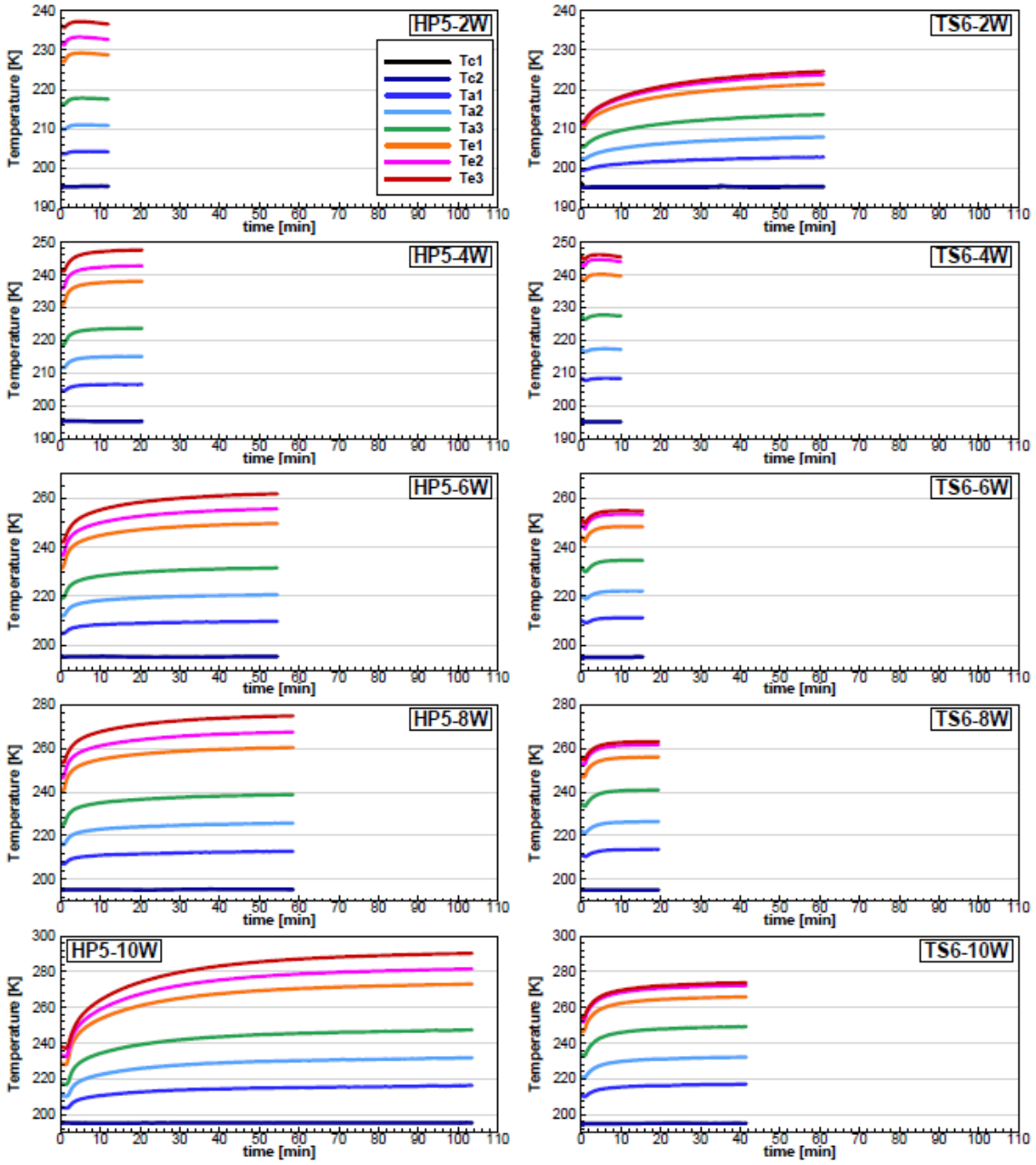

FIGURE 74: TRANSIENT THERMAL RESPONSE COMPARISON OF PERFORMANCE BETWEEN HEAT PIPE AND THERMOSYPHON IN AN ALUMINUM CASE WITH ACETONE AS THE WORKING FLUID. THE HEAT SINK CONTAINS DRY ICE AND ACETONE AND LOW HEAT LOADS ARE APPLIED.

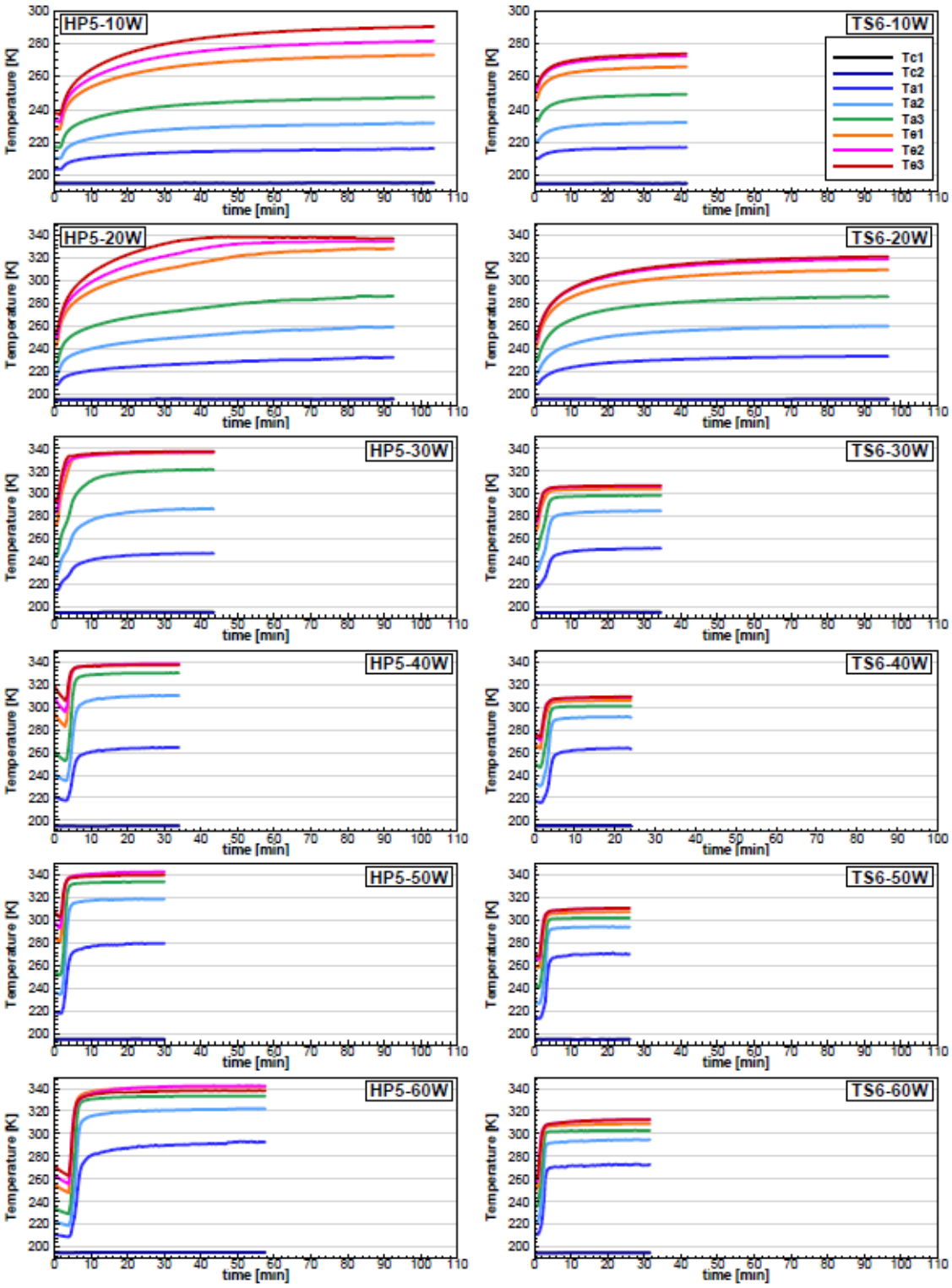

FIGURE 75: TRANSIENT THERMAL RESPONSE COMPARISON OF PERFORMANCE BETWEEN HEAT PIPE AND THERMOSYPHON IN AN ALUMINUM CASE WITH ACETONE AS THE WORKING FLUID. THE HEAT SINK CONTAINS DRY ICE AND ACETONE AND HIGH HEAT LOADS ARE APPLIED.

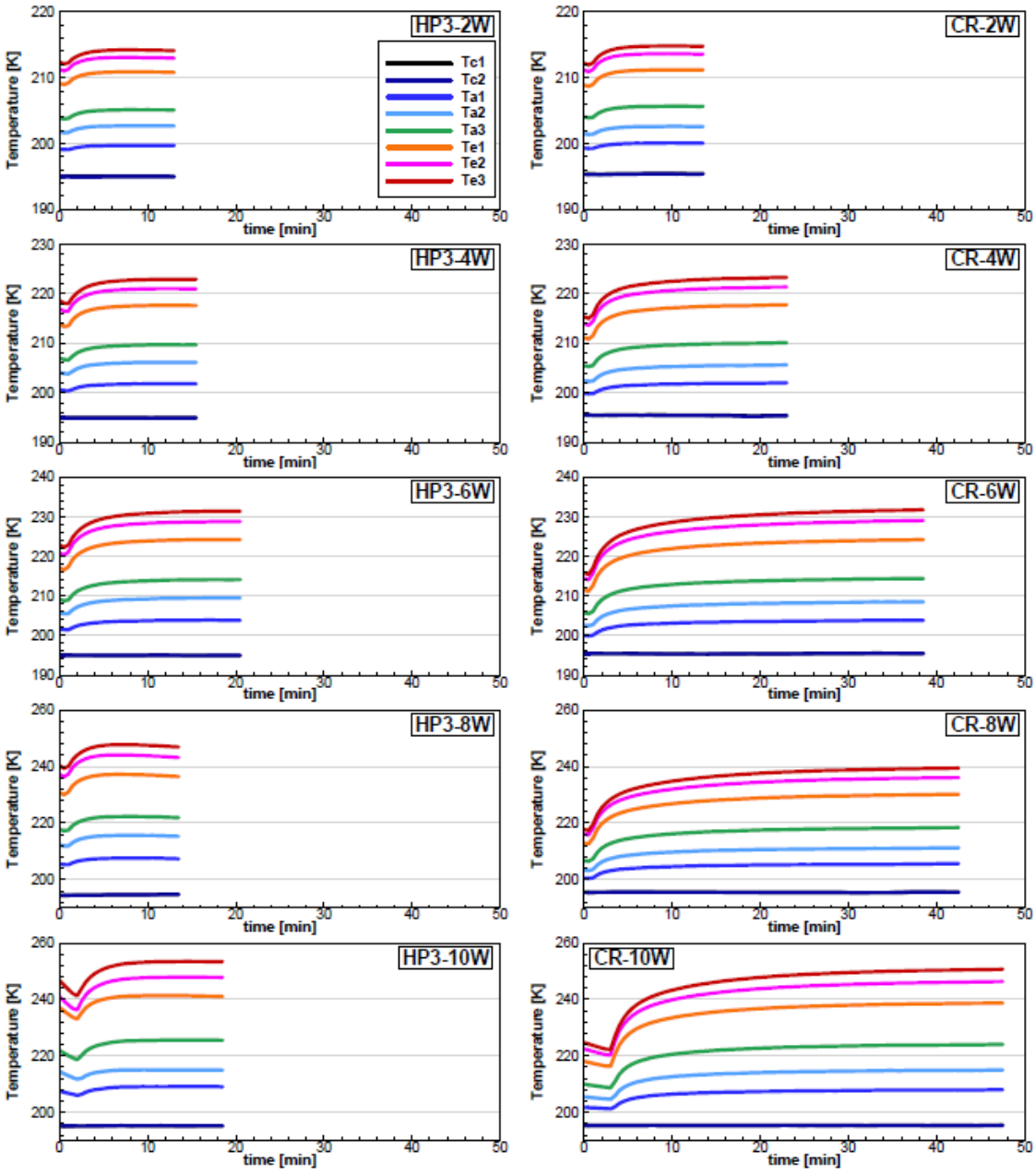

FIGURE 76: TRANSIENT THERMAL RESPONSE COMPARISON OF PERFORMANCE BETWEEN AN INSULATED COPPER ROD AND HP3. THE HEAT SINK CONTAINS DRY ICE AND ACETONE AND LOW HEAT LOADS ARE APPLIED.

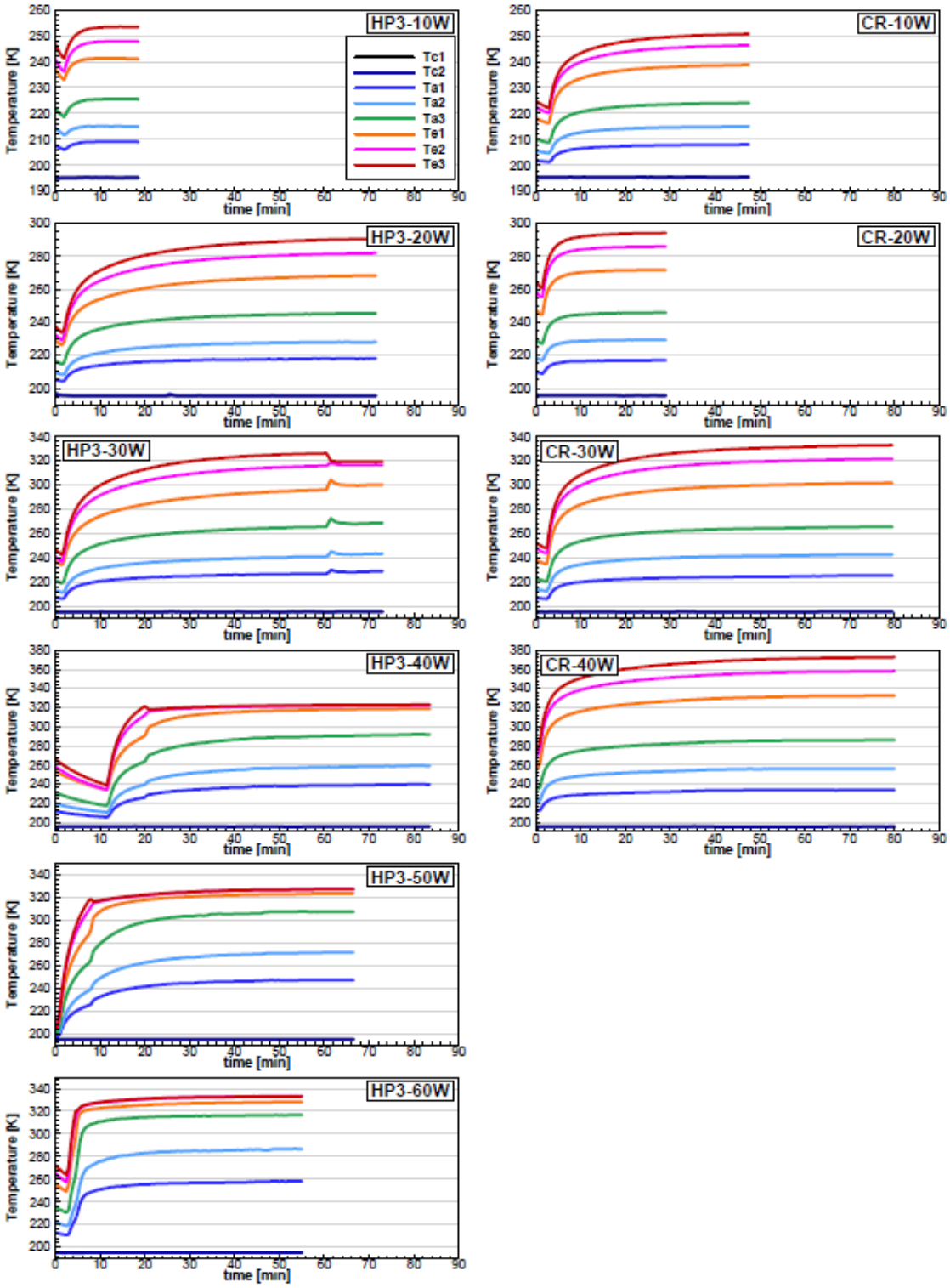

FIGURE 77: TRANSIENT THERMAL RESPONSE COMPARISON OF PERFORMANCE BETWEEN AN INSULATED COPPER ROD AND HP3. THE HEAT SINK CONTAINS DRY ICE AND ACETONE AND HIGH HEAT LOADS ARE APPLIED.

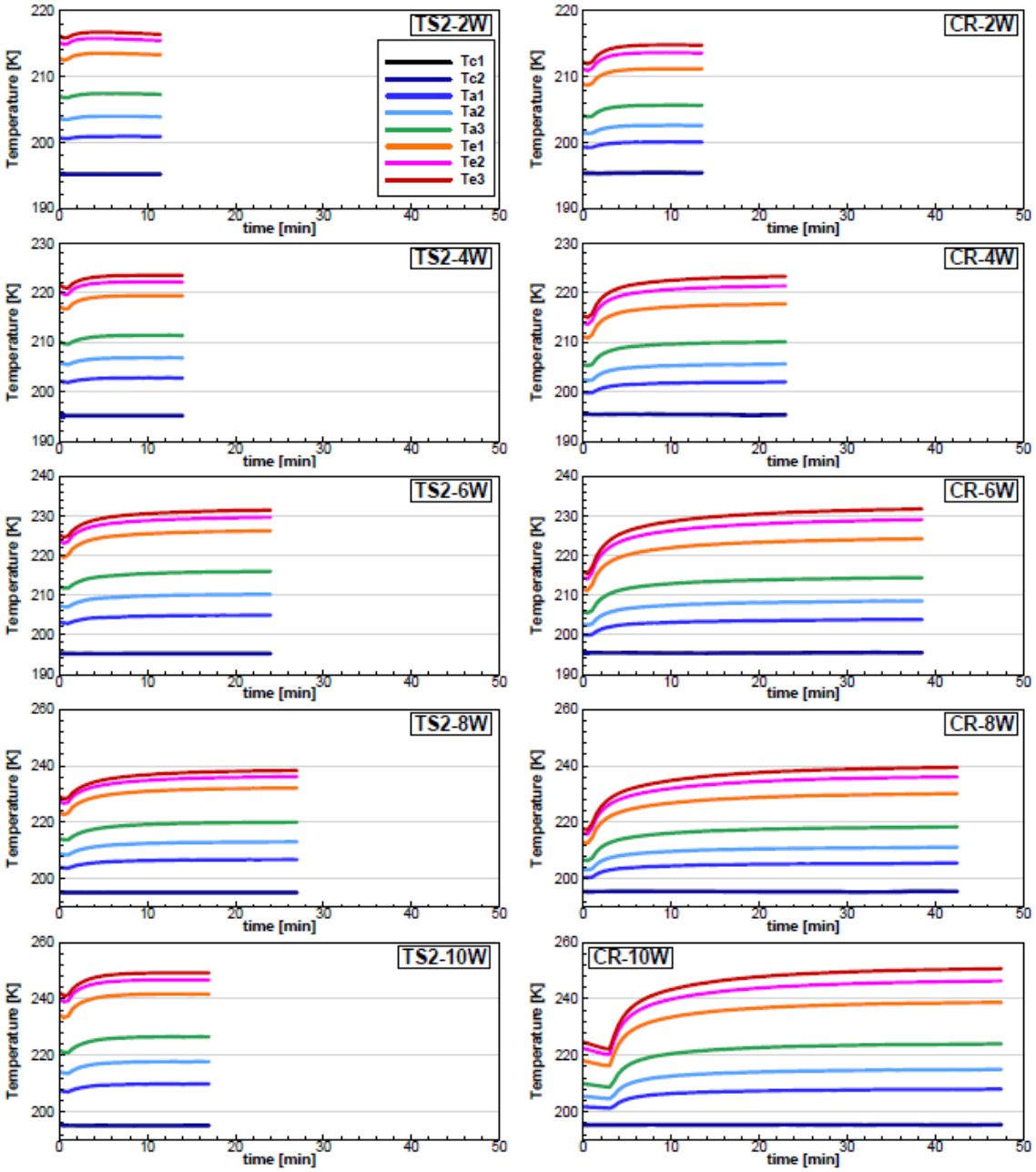

FIGURE 78: TRANSIENT THERMAL RESPONSE COMPARISON OF PERFORMANCE BETWEEN AN INSULATED COPPER ROD AND TS2. THE HEAT SINK CONTAINS DRY ICE AND ACETONE AND LOW HEAT LOADS ARE APPLIED.

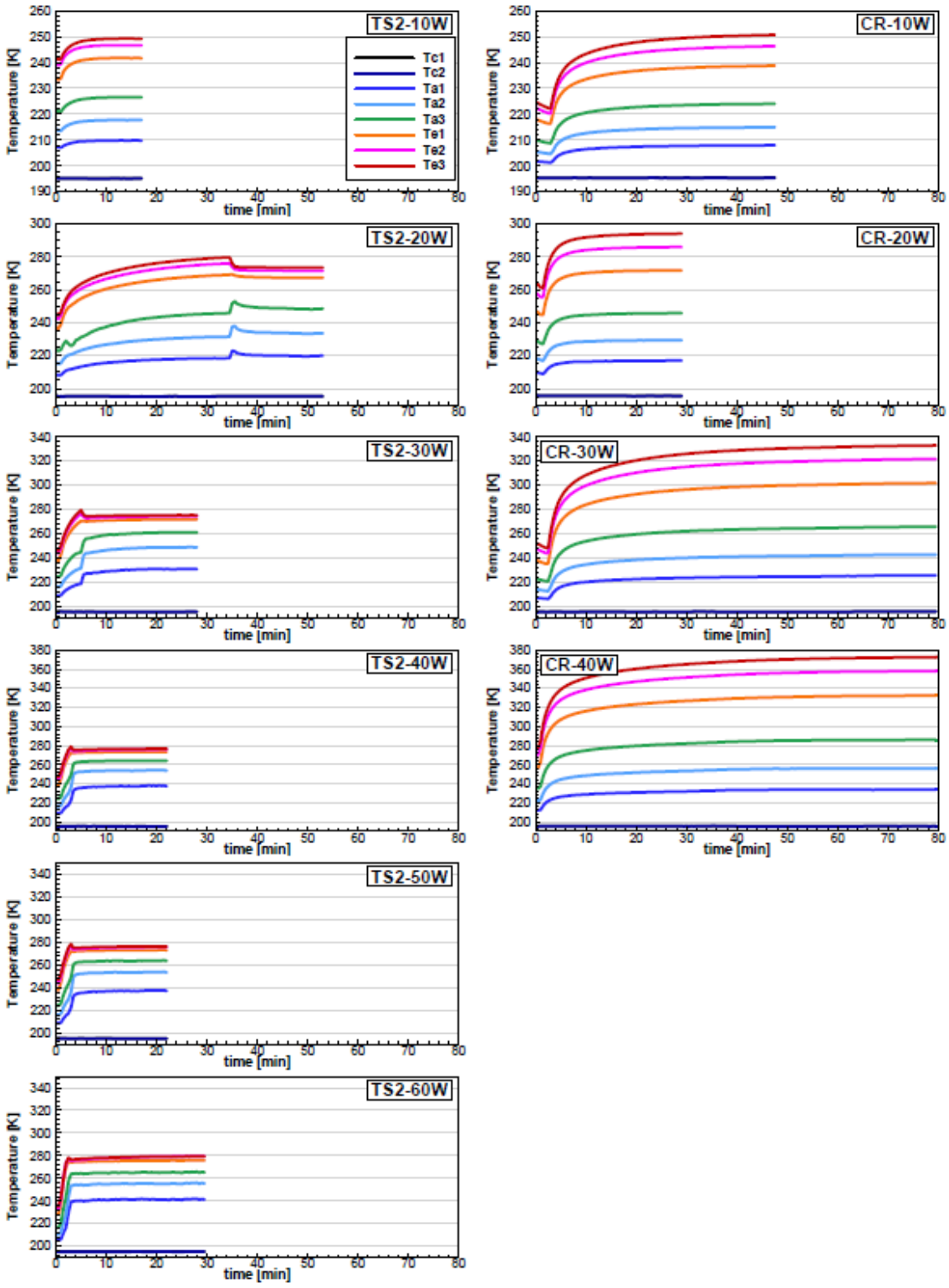

FIGURE 79: TRANSIENT THERMAL RESPONSE COMPARISON OF PERFORMANCE BETWEEN AN INSULATED COPPER ROD AND TS2. THE HEAT SINK CONTAINS DRY ICE AND ACETONE AND HIGH HEAT LOADS ARE APPLIED.

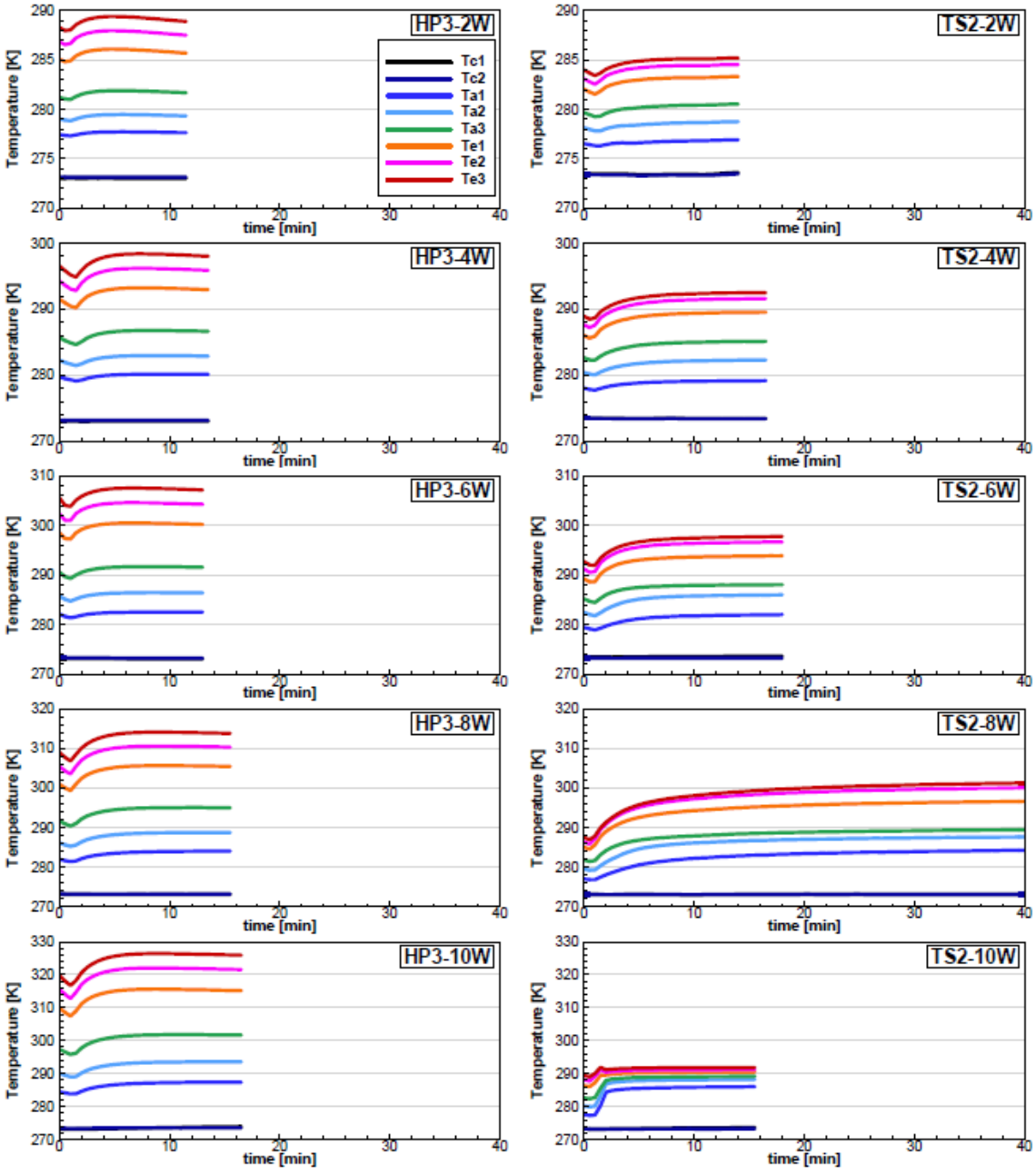

FIGURE 80: COMPARISON OF PERFORMANCE BETWEEN HEAT PIPE AND THERMOSYPHON IN A COPPER CASE WITH METHANOL AS THE WORKING FLUID. THE HEAT SINK CONTAINS ICE WATER AND LOW HEAT LOADS ARE APPLIED.

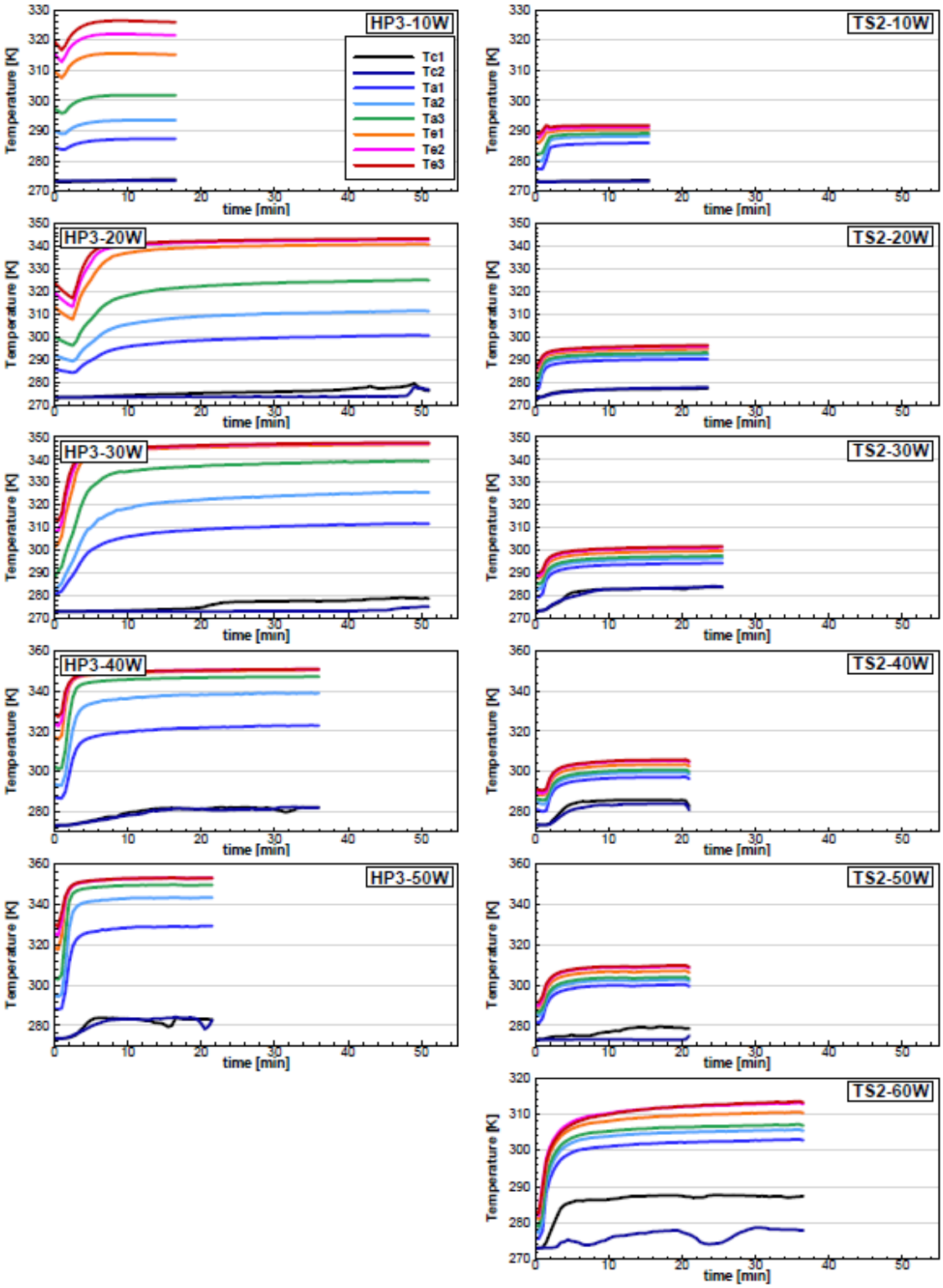

FIGURE 81: COMPARISON OF PERFORMANCE BETWEEN HEAT PIPE AND THERMOSYPHON IN A COPPER CASE WITH METHANOL AS THE WORKING FLUID. THE HEAT SINK CONTAINS ICE WATER AND HIGH HEAT LOADS ARE APPLIED.

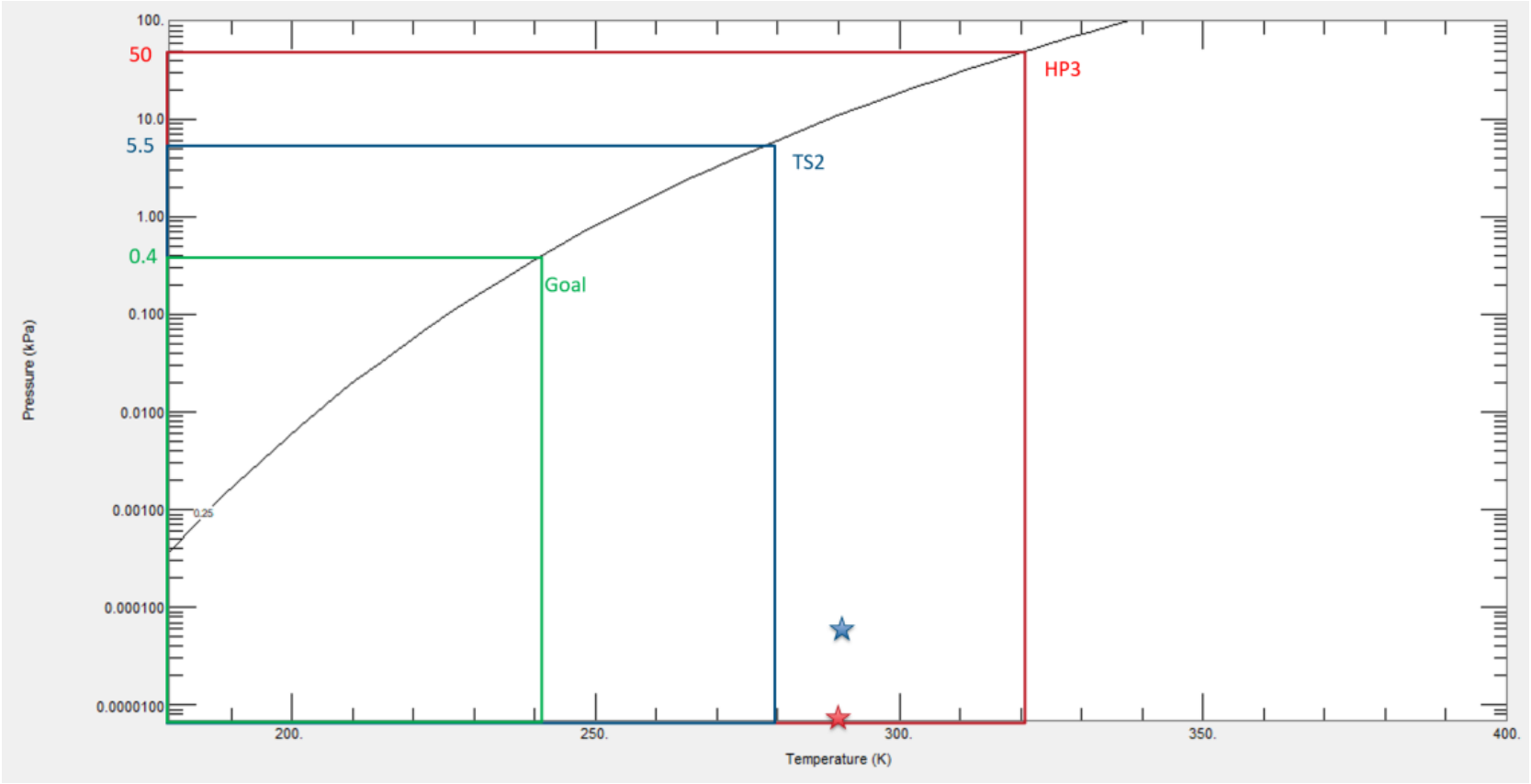

[46]

FIGURE 82: ESTIMATED INTERNAL PRESSURE FOR PROTOTYPES CONTAINING METHANOL, BASED ON EVAPORATOR TEMPERATURE.

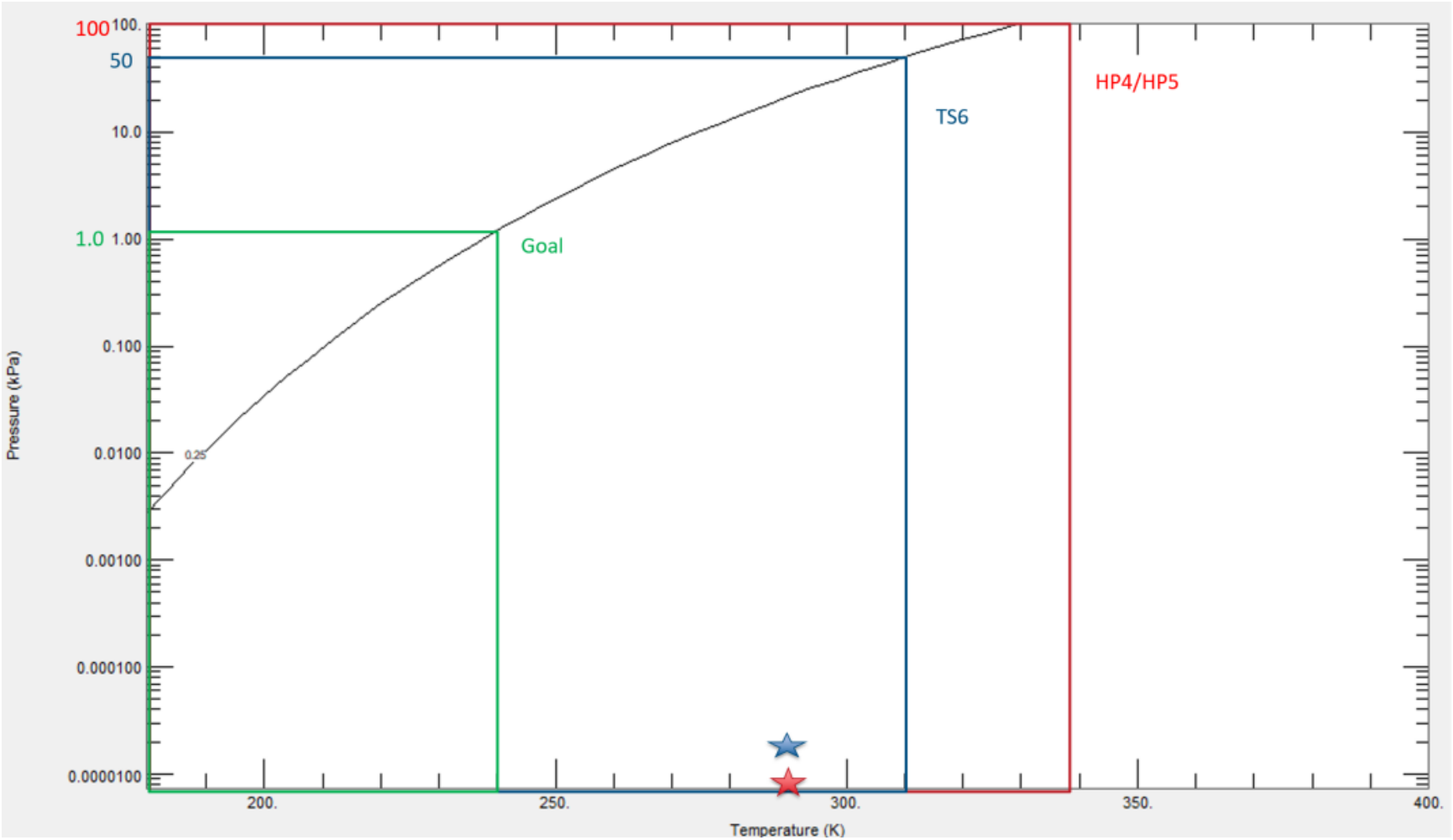

[46]

FIGURE 83: ESTIMATED INTERNAL PRESSURE FOR PROTOTYPES CONTAINING ACETONE, BASED ON EVAPORATOR TEMPERATURE.